



HAL
open science

Satellite characterization of water mass exchange between ocean and continents at interannual to decadal timescales

Alejandro Blazquez

► **To cite this version:**

Alejandro Blazquez. Satellite characterization of water mass exchange between ocean and continents at interannual to decadal timescales. Hydrology. Université Paul Sabatier - Toulouse III, 2020. English. NNT : 2020TOU30074 . tel-03048246v2

HAL Id: tel-03048246

<https://theses.hal.science/tel-03048246v2>

Submitted on 15 Dec 2020

HAL is a multi-disciplinary open access archive for the deposit and dissemination of scientific research documents, whether they are published or not. The documents may come from teaching and research institutions in France or abroad, or from public or private research centers.

L'archive ouverte pluridisciplinaire **HAL**, est destinée au dépôt et à la diffusion de documents scientifiques de niveau recherche, publiés ou non, émanant des établissements d'enseignement et de recherche français ou étrangers, des laboratoires publics ou privés.



Université
de Toulouse

THÈSE

En vue de l'obtention du

DOCTORAT DE L'UNIVERSITÉ DE TOULOUSE

Délivré par : *l'Université Toulouse 3 Paul Sabatier (UT3 Paul Sabatier)*

Présentée et soutenue le *2 Octobre 2020* par :

Alejandro Blazquez

**Caractérisation par satellite des échanges d'eau entre
l'océan et les continents aux échelles interannuelles à
décennales**

JURY

P. EXERTIER	Directeur de recherche	Président du Jury
L. FLEITOUT	Directeur de recherche	Rapporteur
M. HORWAT	Professeur	Rapporteur
L. LONGUEVERGNE	Directeur de recherche	Examineur
B. MEYSSIGNAC	Ingénieur CNES	Directeur de thèse
E. BERTHIER	Directeur de recherche	Co-directeur de thèse

École doctorale et spécialité :

SDU2E : Océan, Atmosphère, Climat

Unité de Recherche :

Laboratoire d'Etudes en Géophysique et Océanographie Spatiales, LEGOS

Directeur(s) de Thèse :

Benoît Meyssignac et Etienne Berthier

Rapporteur :

Voir le jury

Remerciements

Réaliser une thèse dans un cadre comme le mien a été un privilège, tant pour les directeurs de recherche, comme le contexte de la thèse et mon contexte personnel de derniers trois ans.

Tout d'abord, j'ai été encadré par deux grandes personnes : Benoit et Étienne. Merci beaucoup pour vos conseils et support tout au long de ces années. Grâce à vous, j'ai appris que la recherche se fait aussi autour d'un café, d'un thé ou même à vélo. Votre passion pour la Science a été une source de motivation.

Une thèse remarquable a besoin d'un thésard "acceptable", des bons encadrants et surtout des personnes remarquables prêtes à donner son temps et partager sa connaissance comme : Jean Michel Lemoine, Anny Cazenave, Remi Roca, Thomas Filleau, Jean François Cretaux, Fabrice Papa, Sylvain Biancamaria... Je vous remercie !

Je tiens aussi à remercier mes collègues du CNES de m'avoir permis de réaliser cette thèse dans le cadre de mon travail : Philippe Maisongrande, Eric Boussarie et Philippe Cubic.

Cette aventure a été accompagnée et parfois rythmée avec les naissances de mes enfants. La première soumission d'un papier avant la naissance de Sacha. La soumission du manuscrit repoussé par la naissance du Gabriela... Rien de plus effective pour apprendre à gérer un planning que faire une thèse avec deux bébés. Heureusement que Marian était là. Il est plus facile de remonter le courant à deux sur un bateau. Merci pour ta patience, tes mots doux et ta façon de relativiser les problèmes pendant ces longues années de nuits courtes.

Finalement, merci à mes enfants pour m'aider à réapprendre l'importance du sourire.

"A day without laughter is a day wasted"

Charles Chaplin

Satellite characterization of water mass exchange between ocean and continents at interannual to decadal timescales

Abstract:

Over the last decades the Earth's water cycle has changed in response to climate change. Changes have been particularly rapid and intense in the ocean and over land, i.e. in glaciers, ice sheets and land reservoirs. Massive amounts of water have been transferred from land to ocean leading to a significant decrease in freshwater water availability in some regions (like in mountains areas) and to a significant increase of the ocean mass and the sea level. Since 2002, observations from the [Gravity Recovery and Climate Experiment \(GRACE\)](#) satellite mission provide quantitative estimates of these transfers of water-mass from land to the ocean. However, these estimates are uncertain as they show discrepancies when different approaches and different parameters are used to process the [GRACE](#) data. The spread in [GRACE](#)-based estimate for the global water budget is poorly characterized and hampers the accurate estimation of the changes in land water storage and ocean mass leading to an uncertain contribution from ocean mass to sea level rise and an uncertain estimate of the [Earth's Energy Imbalance \(EEI\)](#), when it is estimated through the sea level budget approach.

In my Phd, I revisit the treatment of [GRACE](#) satellite data in order to obtain [GRACE](#)-based estimates of the water mass exchange between ocean and continents, at interannual to decadal timescales, paying a special attention to the different sources of errors and uncertainties. I consider all state-of-the-art data processing of [GRACE](#) data, from which I develop an ensemble of consistent [GRACE](#) solutions to estimate the mass changes in Greenland, Antarctica, the ocean and the rest of the emerged lands including glaciers and [Terrestrial Water Storage \(TWS\)](#). With this ensemble, I document the nature of water mass exchanges between ocean and continents and I estimate the associated uncertainties. The range of the uncertainty explains the spread in previous [GRACE](#)-based estimates of the components of the global water budget. This approach enables also the exploration of the sources of the uncertainties in [GRACE](#) based estimates. I find that the post-processing is responsible for 79% of the uncertainty in the global water budget estimates and that only 21% is due to the differences in the [GRACE](#) data inversion process. The main sources of uncertainties in the [GRACE](#)-based global water budget, at annual to interannual time scales, are the spread in the geocenter corrections and the uncertainty in the [Glacial Isostatic Adjustment \(GIA\)](#) correction, both being applied to [GRACE](#) data. This is particularly true for the ocean mass and glacier and [TWS](#) mass change estimates for which the uncertainty in trends for the period from 2005 to 2015 is ± 0.33 mm SLE/yr.

Regarding the glacier and [TWS](#) mass change at basin scale, I identify glacier leakage as the main source of uncertainty at local scale in regions close to glaciers. I propose a method using non-[GRACE](#)-based mass estimates to reduce the leakage uncertainty on the [GRACE](#)-based local water mass estimate. Accounting for glacier mass changes derived from satellite imagery leads to improved estimates of other hydrological processes affecting the local water cycle.

Regarding the ocean mass, I explore a method in view of improving the estimates of the ocean mass by working in a reference frame centered at the center of mass of the Earth, the goal being to remove the geocenter correction and the associated uncertainty. I analyse the consistency between [GRACE](#)-based ocean mass, altimetry-based sea-level, and ARGO-based steric sea level. This work enables the improvement the estimates of the ocean mass changes. It further leads to a better closure of the sea level budget and a more accurate estimate of the [EEI](#).

Keywords: Global water budget, Ocean mass, Space gravimetry, Climate change, Space Geodesy.

Caractérisation par satellite des échanges d'eau entre l'océan et les continents aux échelles interannuelles à décennales

Résumé:

Au cours des dernières décennies, le cycle global de l'eau a changé en réponse au changement climatique. Les changements ont été particulièrement rapides et intenses dans l'océan et sur les continents. Des quantités très importantes d'eau ont été transférées des continents vers l'océan, entraînant une diminution significative des ressources en eau douce dans certaines régions continentales et une augmentation de la masse de l'océan et du niveau de la mer. Depuis 2002, les observations de la mission spatiale [Gravity Recovery and Climate Experiment \(GRACE\)](#) fournissent des estimations quantitatives de ces échanges d'eau entre l'océan et les continents. Cependant, ces estimations sont incertaines car elles montrent des écarts lorsque différentes approches et différents paramètres sont utilisés pour traiter les données [GRACE](#). L'écart entre les estimations du bilan globale de l'eau basées sur [GRACE](#) est donc mal caractérisé. Ce qui entrave l'estimation précise des changements dans la quantité total d'eau dans les continents et dans la masse de l'océan conduisant à une contribution incertaine de la masse de l'océan à l'élévation du niveau de la mer et à une estimation incertaine du déséquilibre énergétique de la terre, lorsqu'elle est estimée par l'approche bilan globale du niveau de la mer.

Au cours de ma thèse, je revisite le traitement des données satellitaires [GRACE](#) dans le but d'obtenir des estimations du bilan global de l'eau, à des échelles interannuelles à décennales, en accordant une attention particulière aux différentes sources d'erreurs et d'incertitudes. Je prends en compte tous les post-traitements les plus à jour des données [GRACE](#), à partir desquels je développe un ensemble de solutions [GRACE](#) cohérentes pour estimer les changements de masse au Groenland, en Antarctique, dans l'océan et dans le reste des terres émergées y compris les glaciers et les eaux terrestres. Avec cet ensemble, j'analyse la nature des échanges de masse d'eau entre l'océan et les continents, et j'évalue les incertitudes associées. L'amplitude de l'incertitude explique les différences entre les estimations précédentes des composantes du bilan global de l'eau effectuées à partir des données [GRACE](#). Cette approche permet donc d'explorer les sources d'incertitudes dans ces estimations.

J'estime que les différents post-traitements sont responsables de 79% de l'incertitude sur les estimations du bilan global de l'eau, tandis que seulement 21% est dû aux différences entre les processus d'inversion des données [GRACE](#). Les principales sources d'incertitudes dans le bilan global de l'eau basé sur [GRACE](#), à des échelles de temps annuelles à inter-annuelles sont la dispersion dans les corrections du mouvement du géocentre ainsi qu'à l'incertitude dans la correction du rebond post-glaciaire. Cela est particulièrement vrai pour l'estimation de la masse de l'océan et les eaux continentales dont l'incertitude liée à la tendance pour la période 2005 à 2015 est de ± 0.33 mm SLE/yr.

En ce qui concerne les variations de masse des glaciers et des eaux continentales, à l'échelle d'un bassin, j'identifie les fuites spectrales de masse d'eau depuis les glaciers comme étant la principale source d'incertitude dans les régions proches des glaciers. Je propose une méthode utilisant des estimations de masse non basées sur [GRACE](#) afin de réduire l'incertitude liée à ce processus. La prise en compte de ces estimations de masse conduit à une amélioration des estimations d'autres processus hydrologiques affectant le cycle local de l'eau.

En ce qui concerne la masse globale de l'océan, j'explore une méthode pour améliorer les estimations, en travaillant dans un référentiel avec pour origine le centre de masse de la Terre afin de supprimer l'effet venant de l'incertitude de la correction de géocentre. J'analyse la cohérence entre masse de l'océan basée sur [GRACE](#), le niveau de la mer basé sur l'altimétrie et le niveau stérique de la mer basé sur [ARGO](#). Ces travaux permettent d'améliorer les estimations des changements de masse de l'océan et aboutissent ainsi à une meilleure clôture du bilan du niveau de la mer et, finalement, à une estimation plus précise du déséquilibre énergétique de la terre.

Foreword

Climate is changing. This is nowadays a fact that was still under discussion a few decades ago. Great efforts were deployed at the end of the 20th century in order to characterize key variables of the Earth's system (temperature, sea level rise, total amount of CO₂ in the atmosphere, etc.). These efforts revealed that the changes in Earth's climate system were happening at an unprecedented speed during the last decades of the 20th century compared to the previous centuries. In 2007 the [International Panel for Climate Change \(IPCC\)](#) confirmed that climate change was **unequivocal** and stated with a very **high confidence** the anthropogenic origin of this change. This result was confirmed by [IPCC](#) in 2013 and the anthropogenic origin was stated as **extremely likely**. However, these facts are still not fully understood by the non-scientific people. There are a lot of shortcuts and half-trues in the media and in our elected leader's speeches. During this PhD, I realized around me that under the concept of *climate change*, we tend to include the causes and the effects of climate change, as well as several ecological matters as air pollution in the cities, plastic pollution in the seas, lowered biodiversity, etc. Just to clarify this concept, I will try to explain the climate change in plain language.

Earth's climate is driven by the long term response to the energy balance between the input from Sun's radiation and the output from Earth's radiation. Change in this balance is known as [EEI](#). [EEI](#) provokes changes in the Earth's climate. Earth's climate changes also due to natural reasons such as the changes in the orbit of the earth (known as Milankovic cycles¹), volcanic activity, tectonics, or biosphere changes. However, since the industrial era (1850s), the increase of CO₂ in the atmosphere has modified this equilibrium. This extra CO₂ is preventing radiation to escape the Earth's system. The accumulation of this excess of energy leads to changes in the Earth such as the rise of the global-mean temperature (known as global warming), the rise of sea-level, the melting of glaciers, the changes in the global water cycle, etc. This [EEI](#) induced by the increase of CO₂ in the atmosphere is known as the human-induced climate change. Measuring these geophysical consequences is key to understand and quantify climate change.

My work has contributed to characterize the exchange of water between ocean and continents since 2002 using satellite data. This exchange is key to understand the sea level rise as well as to understand the evolution of land water under climate change. The knowledge of this exchange with its uncertainties is necessary to improve the understanding of climate change consequences and to improve the validation of climate models used to predict climate evolution for the 21st century and beyond.

This manuscript is composed of five chapters.

The first chapter introduces the global water budget and sea-level budget. I present the state of the knowledge and the challenges to improve this knowledge. I do not include any own result in this first chapter. At the end, I summarize the main scientific questions addressed in this PhD.

The second chapter focuses on the global water budget estimates from the [GRACE](#) mission which is arguably the most accurate and comprehensive tool to estimate the global water budget. I analyze the limitations and advantages of the [GRACE](#)-based estimates

¹https://en.wikipedia.org/wiki/Milankovitch_cycles

and present the data treatment from [GRACE](#) satellite data to obtain [GRACE](#)-based estimates of the global water budget. I build an ensemble of state-of-the-art solutions to explore the uncertainties of the global water budget at global and regional scale. This chapter is based on the article of Blazquez et al. [2018], attached at the end of the chapter.

In the third chapter, I move to regional scale. I use the ensemble of [GRACE](#) solutions to analyze the uncertainties in the land [GRACE](#)-based estimates at basin scale. I identify the glacier leakage in [GRACE](#) solutions as the main source of uncertainty at local scale in regions close to glaciers. I propose a method using non-[GRACE](#)-based mass estimates to reduce the leakage uncertainty on the [GRACE](#)-based local water mass estimates. I test and validate this method in South Asia, a region where glaciers and lakes are concentrated in small locations. Accounting for their mass changes leads to improved estimates of other hydrological processes affecting the local water cycle. This chapter is based on an article currently in preparation from Blazquez et al. [In prep 2020], attached at the end of the chapter.

In the fourth chapter, I move to the ocean part of the global water budget. On the basis of my ensemble of [GRACE](#) solutions, I focus on the geocenter motion correction and the [GIA](#) correction as the major sources of uncertainty in the ocean mass changes. I explore a method to improve the estimates of the ocean mass by removing the uncertainty in geocenter. This work has implications not only for the ocean mass estimates but also for the sea level budget and for the [EEI](#).

In the fifth chapter, I discuss the conclusions and explore perspectives for the next years in terms of improvement of our knowledge of the global water cycle using [GRACE](#) and the next gravimetry mission measurements

I also include 2 annexes to this manuscript to assist the reader through this work:

- Annex A includes the abstracts of the publications I coauthored without being first author.
- Annex B explains the use of the stokes coefficients for gravity and water mass redistribution.

[Fr] Préface

Le climat change. Aujourd'hui c'est un fait; mais il était encore en discussion il y a quelques années. À la fin du XXème siècle, d'importants efforts ont été déployés dans le but de caractériser les variables clés du système Terre : la température, l'élévation du niveau de la mer, la quantité totale de CO₂ dans l'atmosphère, etc. Ces efforts ont révélé que les changements dans le système climatique terrestre se produisaient à une vitesse sans précédent au cours des dernières décennies du XXème siècle par rapport aux siècles précédents. En 2007, le [IPCC](#) a confirmé que le changement climatique était **sans équivoque**; et il a déclaré avec une **très haute confiance** l'origine anthropique de ce changement. Ce résultat a été confirmé ensuite par [IPCC](#) en 2013 et l'origine anthropique a été déclarée comme **extrêmement probable**. Cependant, ces faits ne sont pas encore pleinement compris par les politiques et le grand public. Il y a encore beaucoup de raccourcis et de demi-vérités dans les médias ainsi que dans les discours de nos élus. Au cours de ma thèse, j'ai remarqué que derrière le concept de *changement climatique*, nous avons tendance à inclure les causes et les effets du changement climatique, ainsi que plusieurs questions écologiques comme la pollution de l'air dans les villes, la pollution plastique dans la mer, la diminution de la biodiversité, etc. Pour clarifier le concept, je vais essayer ici d'expliquer le changement climatique en langage clair.

Le climat de la Terre est régi par la réponse sur le long terme au bilan énergétique entre apport par le rayonnement solaire et perte par le rayonnement terrestre. La modification de cet équilibre est connue sous le nom de déséquilibre énergétique de la Terre ou [EEI](#) en anglais. Le déséquilibre énergétique de la terre provoque des changements dans le climat de la Terre. Mais des changements sont également dus à des raisons naturelles telles que les changements dans l'orbite de la Terre (connus sous le nom de cycles de Milankovic²), l'activité volcanique, la tectonique ou les changements de la biosphère. Cependant depuis l'ère industrielle (environ 1850), l'augmentation de CO₂ dans l'atmosphère a modifié cet équilibre, car le CO₂ supplémentaire empêche le rayonnement de s'échapper du système Terre. L'accumulation de cet excès d'énergie entraîne des changements dans la Terre tels que l'augmentation de la température moyenne mondiale (connue sous le nom de réchauffement climatique), l'élévation du niveau de la mer, la fonte des glaciers, des changements dans le cycle global de l'eau, etc. Ce déséquilibre énergétique de la Terre induit par l'augmentation du CO₂ dans l'atmosphère, est connu sous le nom de changement climatique d'origine anthropique. Mesurer ses conséquences géophysiques est devenu essentiel dans le but de comprendre et quantifier le changement climatique.

Mon travail s'inscrit dans ce domaine et se base essentiellement sur des données satellitaires acquises depuis 2002; il vise à comprendre l'élévation du niveau de la mer ainsi que l'évolution des eaux continentales sous l'effet du changement climatique. La connaissance de cet échange avec ses incertitudes est nécessaire pour améliorer la compréhension des conséquences du changement climatique, valider les modèles climatiques et diminuer si possible les incertitudes dans le but de faire des prévisions sur l'évolution du climat aussi fiables que possible pour les décennies à venir.

J'ai choisi de rédiger Ce manuscrit en anglais mais le résumé, la préface ainsi que les conclusions sont également en français. Le document est composé de cinq chapitres dont

²https://en.wikipedia.org/wiki/Milankovitch_cycles

voici le contenu.

Le premier chapitre présente le bilan global de l'eau et celui du niveau de la mer. Je présente l'état des connaissances et les défis pour les améliorer. Je n'inclus aucun résultat propre dans ce premier chapitre. À la fin, je résume les principales questions scientifiques abordées dans la thèse.

Le deuxième chapitre se concentre sur les estimations du bilan global de l'eau issues de la mission **GRACE**, qui est sans doute l'outil le plus précis et le plus complet pour les estimer. J'analyse les limites et les avantages des estimations basées sur **GRACE** et je présente le traitement des données dans le but d'obtenir des estimations du bilan global de l'eau. Je construis un ensemble de solutions pour explorer les incertitudes aux échelles globale et régionale. Ce chapitre est basé sur l'article de Blazquez et al. [2018], qui est joint à la fin.

Dans le troisième chapitre, je m'intéresse à l'échelle régionale (continentale). J'utilise l'ensemble de mes solutions **GRACE** pour analyser les incertitudes sur les estimations des eaux continentales issues du **GRACE** à l'échelle du bassin. J'identifie la fuite des glaciers dans les solutions **GRACE** comme la principale source d'incertitude à l'échelle locale dans les régions proches des glaciers. Je propose une méthode utilisant des estimations de masse non issues de **GRACE** afin de réduire l'incertitude de fuite sur les estimations locales de masse d'eau basées sur **GRACE**. Je teste et je valide cette méthode en Asie du Sud, une région où les glaciers et les lacs sont concentrés dans de des localisations de faible étendue. La prise en compte de leurs changements de masse permet d'améliorer les estimations d'autres processus hydrologiques affectant le cycle de l'eau local. Ce chapitre est basé sur un article en préparation Blazquez et al. [In prep 2020], qui est joint à la fin du chapitre.

Dans le quatrième chapitre, je m'intéresse à la partie océanique du bilan global de l'eau. Sur la base de mon ensemble de solutions **GRACE**, j'identifie la correction de mouvement du géocentre et la correction **GIA** comme étant les principales sources d'incertitude dans les changements de masse océanique. J'explore une méthode pour améliorer les estimations de la masse océanique en m'affranchissant de l'incertitude sur le géocentre. Ce travail a des implications non seulement pour les estimations de la masse océanique, mais aussi pour le budget du niveau de la mer et pour le déséquilibre énergétique de la Terre.

Dans le cinquième chapitre, je discute les conclusions et explore les perspectives pour les prochaines années en terme d'amélioration de notre connaissance du cycle global de l'eau, en utilisant **GRACE** et les mesures de la prochaine mission de gravimétrie.

J'inclus également 2 annexes à ce manuscrit pour aider le lecteur à travers ce travail:

- L'annexe A comprend les résumés des publications que j'ai co-écrites sans être le premier auteur.
- L'annexe B explique l'utilisation des coefficients de Stokes pour la redistribution de la gravité et des masses d'eau.

Contents

Abstract	i
[Fr] Résumé	ii
Foreword	iii
[FR] Préface	v
1 Introduction: Water cycle and sea level	1
1.1 Water cycle	1
1.2 Land water mass change	3
1.2.1 Greenland and Antarctica	3
1.2.2 Glaciers	6
1.2.3 Terrestrial water storage	8
1.3 Ocean mass change	10
1.3.1 Ocean mass from the global water budget	10
1.3.2 Ocean mass from gravimetry	10
1.3.3 Ocean mass from the sea level budget	11
1.3.3.1 Sea-level change	12
1.3.3.2 Steric sea-level change	14
1.3.3.3 Ocean mass derived from the sea-level budget	15
1.3.4 Ocean mass from the fresh-water budget	15
1.4 Global energy budget and how it relates to the water cycle	16
1.5 Scientific questions associated to the water cycle	17
1.6 Objectives of this PhD	18
2 Evaluating the uncertainty in GRACE-based estimates of the global water budget. Development of an ensemble approach	21
2.1 GRACE and GRACE FO missions	22
2.1.1 Inversion process (From L1 data to L2 products)	23
2.1.2 Post-processing (From L2 products to water mass anomalies)	25
2.2 GRACE Post-processing	26
2.2.1 Geocenter motion	26
2.2.2 Earth's dynamic oblateness	28
2.2.3 Stripes	29
2.2.4 Leakage and Gibbs effect	31
2.2.5 Glacial isostatic Adjustment	33
2.2.6 Pole tide	35
2.2.7 Earthquakes	37
2.3 Applications of the ensemble of GRACE solutions	39
2.3.1 Comparison of the global water budget components with previous studies	39
2.3.2 The global water budget and its uncertainties analyzed with my ensemble of GRACE solutions	39

2.3.3	Article: "Exploring the uncertainty in GRACE estimates of the mass redistributions at the Earth surface: implications for the global water and sea level budgets"	41
2.3.4	Publications using the ensemble of GRACE solutions	59
2.4	Conclusions	61
3	Evaluating the uncertainty in the GRACE-based estimates of land mass changes. Separating glacier and TWS changes	63
3.1	Land leakage correction	65
3.1.1	Land leakage correction method	65
3.1.2	Leakage correction applied to South Asia	66
3.1.3	Article: "Monitoring the changes in terrestrial water storage in South Asia from 2003 to 2015"	69
3.2	Perspective for global land leakage correction	93
3.2.1	Glaciers at global scale	93
3.2.2	Land Water Storage (LWS) at global scale	94
3.3	Conclusion	97
4	Uncertainty in GRACE-based estimates of the ocean mass. Implications for the sea level budget and the estimation of the EEI	99
4.1	Impact of the choice of the reference frame on the ocean mass estimate from GRACE	100
4.2	Implications on the Sea level budget	102
4.2.1	Altimetry sea-level change	102
4.2.2	ARGO-based steric sea-level	103
4.2.3	Consistency in the sea-level budget	105
4.3	Implications for the EEI	108
4.4	Conclusions	109
5	Conclusions and outlook	111
6	[FR] Conclusions and perspectives	117
	Bibliography	120
	Acronyms	135
	List of figures	138
	List of tables	141
	Annex A: Abstracts of the articles not included in the main text	i
	A1: Arctic Sea Level During the Satellite Altimetry Era	i
	A2: Mass Balance of the Antarctic Ice Sheet from 1992 to 2017	ii
	A3: Global Sea-Level Budget 1993–Present	iii
	A4: Measuring Global Ocean Heat Content to Estimate the Earth Energy Imbalance	iv
	A5: Global Ocean Freshening, Ocean Mass Increase and Global Mean Sea Level Rise over 2005–2015	v
	A6: Mass Balance of the Greenland Ice Sheet from 1992 to 2017	vi
	Annex B: Stokes coefficients	vii
	B1: Stokes coefficients description	vii
	B2: Use of Stokes coefficients in GIA models	vii

Chapter 1

Introduction: Water cycle and sea level

1.1 Water cycle

The water cycle refers to the water transformation, transportation and storage in the Earth's system. It is mainly driven by the solar heating which evaporates the water from the ocean and land surfaces and melts the ice from land and from the ocean. The evaporated water condensates and precipitates over land and the ocean. The precipitated water over land may be accumulated or transported back to the ocean closing the cycle.

This water cycle is well characterized at global and annual scale (Fig. 1.1) [Trenberth, 2014]. However, changes at interannual and longer time scales are less well known [Stephens and L'Ecuyer, 2015; Wild et al., 2015; Rodell et al., 2015]. In this PhD, I focus on the interannual to decadal changes in the water cycle.

Earth is a massive planet whose gravity is large enough to prevent the water vapor from escaping through the top of the atmosphere. However it is not big enough to prevent a small loss of hydrogen of about 3 kg/s [Catling and Zahnle, 2009]. This loss of hydrogen represents the main variation of the Earth's mass at annual and longer time scales. The rate of hydrogen loss represents a mass loss of 10^{-7} Gt/yr. As water molecules are made up of hydrogen and oxygen (H_2O), this hydrogen mass loss provoke a water mass loss of $9 \cdot 10^{-7}$ Gt/yr and an increase of oxygen mass in the atmosphere of $8 \cdot 10^{-7}$ Gt/yr¹. In this PhD, I focus on the storage terms of the water cycle and the maximum accuracy I will need in terms of mass is 10^{-1} Gt/yr. So, I assume here the total amount of mass and water in the Earth's system remains constant at interannual to decadal time scales.

Water vapor remains mainly in the lower part of the atmosphere, in the Troposphere essentially. The amount of water vapor in the atmosphere varies very quickly at daily and seasonal time scales and also depending on orography and temperature. At a global scale, the water-holding capacity mainly changes depending on the average temperature (See Clausius-Clapeyron law at Eq. 1.1, where e_s is the water-holding capacity). When

¹2 tons of hydrogen combines with 16 tons of oxygen to create 18 tons of water

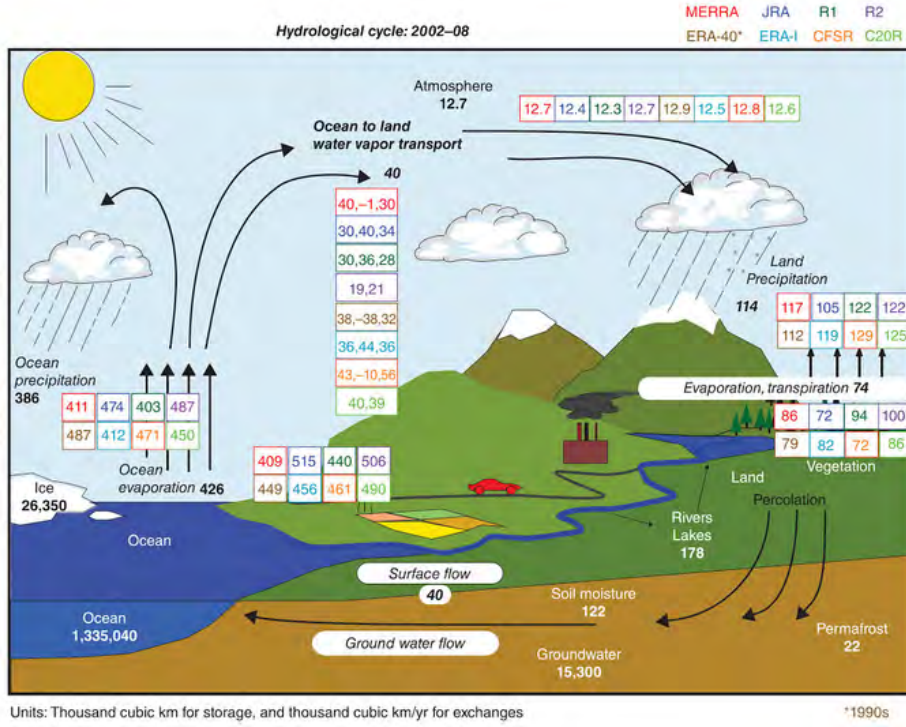


Figure 1.1: Observations (black numbers) and reanalysis (color numbers in the boxes) estimates of the water cycle fluxes in 10^3Gt/yr and storages in 10^3Gt . Excerpt from [Trenberth, 2014].

linearized, the water-holding capacity increases by about 6-7% per extra degree Celsius in global surface temperature (Eq. 1.1).

In the last 60 years surface temperature has increased by 0.72°Celsius in response to climate change [e.g., Hartmann et al., 2013]. Assuming a total water vapor content in the atmosphere of $12.7 \cdot 10^3\text{Gt}$ [Trenberth, 2014], the amount of water in the atmosphere is expected to increase in response to climate change at a rate of 10Gt/yr . This rate is of greater than the maximum accuracy I will need in term of mass (10^{-1}Gt/y) to analyze the changes in the water storage terms of the water cycle. However, as I will show in the next chapters, this accuracy is beyond the actual limits. So I assume atmospheric water mass to remain constant at interannual to decadal time scales.

$$e_s(T) = 6.112 \cdot e^{\frac{17.64T}{T+243.5}}$$

$$\frac{\Delta M_{atm}}{M_{atm}} \simeq 6 - 7\% \Delta T_{\text{dimensional}} \quad (1.1)$$

Under these assumptions, the global water budget may be expressed as the water mass exchange between land and the ocean (Eq.1.2). We analyze the land components of the water cycle in Section 1.2 and the ocean component in Section 1.3.

$$\Delta M_{ocean}(t) + \Delta M_{land}(t) = 0 \quad (1.2)$$

1.2 Land water mass change

Land water mass is composed of ice, snow, soil moisture, water in the biosphere, groundwater and surface water (including rivers, glaciers and lakes). However, as the [International Panel for Climate Change \(IPCC\)](#), we prefer to break down the land storage geographically (Greenland and Antarctica) and by the water state (glaciers and terrestrial water storage), although terrestrial water storage includes solid water from snow, permafrost and ice on lakes and rivers and the ocean includes solid water from sea ice. The global water budget may be expressed as the sum of the ocean, Greenland, Antarctica, glaciers, and [Terrestrial Water Storage \(TWS\)](#) mass changes (Eq. 1.3). Hereafter, I will adopt the following convention: a negative value of the mass change means a land mass loss expressed in Gt and its equivalent ocean mass increase expressed in mm [Sea-Level Equivalent \(SLE\)](#). Note that cubic kilometers, gigatons and mm [SLE](#) are common units used to describe an amount of water mass, usually assuming the density of the water as the density of freshwater

$$1km^3 \sim 1Gt = 10^{12}kg \sim \frac{1}{360}mmSLE$$

$$\Delta M_{ocean}(t) + \Delta M_{Greenland}(t) + \Delta M_{Antarctica}(t) + \Delta M_{glaciers}(t) + \Delta M_{TWS}(t) = 0 \quad (1.3)$$

1.2.1 Greenland and Antarctica

The Greenland and Antarctica ice sheets and peripheral glaciers play a major role in the water cycle at interannual and longer time scales. They are by far the largest reservoirs of freshwater. Antarctica contains $25.71 \cdot 10^6$ Gt (~ 58.3 m [SLE](#)) and Greenland $2.85 \cdot 10^6$ Gt (~ 7.36 m [SLE](#)) [Vaughan et al., 2013]. Nearly at equilibrium until the 90s (Fig. 1.2), they became major contributors to the sea level rise in the last decades [Bamber et al., 2018; Cazenave et al., 2018a].

The mass loss from both ice sheets is estimated by satellite altimetry (since 1991), satellite gravimetry (since 2002), and the [IOM](#) (since 1979).

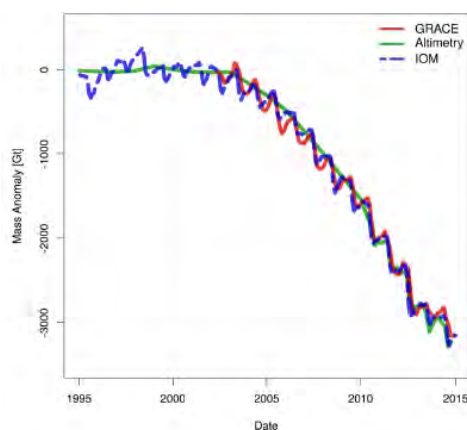
Satellite altimetry includes radar altimetry (since 1993), laser altimetry (only 7 years) and [Synthetic Aperture Radar \(SAR\)](#) (since 2010). Satellite altimetry provides ice sheets elevation anomalies which are converted to mass changes using ice density and firn-layer thickness. The precision of the elevation anomalies relies on modest adjustments to account for sensor drift, changes in the satellite attitude, atmospheric attenuation, and movements of Earth's surface. The conversion from elevation anomalies to mass change remains the main source of uncertainty as it depends on external models of fluctuations in the firn-layer thickness [Shepherd et al., 2012]. This conversion is performed by using a prescribed density model and by allowing for temporal fluctuation in the snowfall. Mass change observation using radar altimetry are continuous since 1991 with: ERS 1 (Jul 1991-Mar 2000), ERS2 (Apr 1995-Jun 2003), Envisat (Mar 2002-Apr 2012) and Sentinel 1 (Apr 2014-present). Laser altimetry from [Ice, Cloud, and land Elevation SATellite](#)

(ICESat) (Jan 2003-Feb 2010) had a fine along-track resolution with high precision but the frequency of observations is reduced. It was used to characterize annual mass balances for 7 years. The use of SAR technique from CryoSat 2 (Apr 2010-present) improves the spatial resolution by including the across-track signal [Helm et al., 2014].

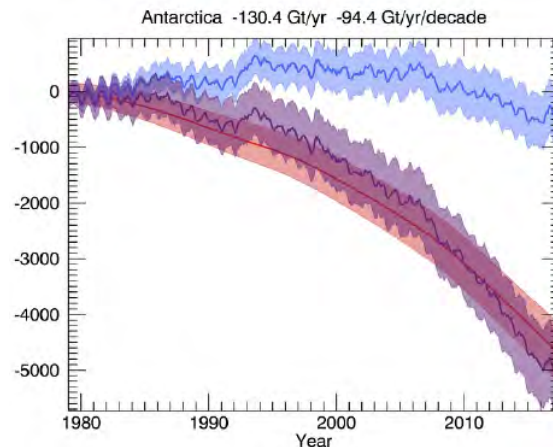
Greenland mass change, including ice sheet and peripheral glaciers, has been measured by satellite altimetry since 1992. It was nearly at equilibrium for the period from 1992 to 2001 with a trend of -16 ± 83 Gt/yr with the uncertainty expressed at 90 % Confidence Level (CL). In the period from 2001 to 2016, it became one of largest contributors with a trend of -266 ± 20 Gt/yr [Bamber et al., 2018]. Antarctica mass change shows clear regional differences between East-Antarctica Ice Sheet (EAIS), West-Antarctica Ice Sheet (WAIS), and Antarctic Peninsula (AP) [Schröder et al., 2019]. Altimetry-based EAIS mass balance trend for the period from 1992 to 2017 is between $[-11$ to $136]$ Gt/yr, WAIS mass balance trend is about $[-97$ to $-25]$ Gt/yr for the same period and AP mass balance trend is about $[-29$ to $3]$ Gt/yr for the same period [Shepherd et al., 2018].

Mass changes using gravimetry are available since 2002 with Gravity Recovery and Climate Experiment (GRACE) (Apr 2002-Jun 2016) and Gravity Recovery and Climate Experiment Follow On (GRACE FO) (Jun 2018 - present). Once corrected for non-water mass anomalies, the gravity field may be converted to water mass anomalies. It complements the local data from altimetry in a monthly time scale and a 300 km spatial resolution. Main sources of uncertainty in the mass estimates based on this technique are: Glacial Isostatic Adjustment (GIA) correction, especially for Antarctica, and land/ocean leakage correction (especially at AP and Greenland) (see chapter 2).

For the period from 2005 to 2015, GRACE-based Greenland mass change trends of -249 ± 23 Gt/yr agrees with altimetry estimates of -235 ± 37 Gt/yr [Shepherd et al.,



(a) Greenland. Excerpt from Bamber et al. [2018]



(b) Antarctica mass balance estimated by the Input-Output Method (IOM) (purple) and its components: surface mass balance (blue) and ice discharge (red). Excerpt from Rignot et al. [2019]

Figure 1.2: Cumulative mass balance for Greenland (a) and Antarctica (b) from different techniques

2019]. Mass balance trends are between [11,107] Gt/yr for [EAIS](#), [-174,-114] Gt/yr for [WAIS](#), and [-39 to -9] for [AP](#) [Shepherd et al., 2018]. Rapid melting in Greenland during summer 2012 and the extreme snow accumulation on winter 2013 explains most of the differences in trends when considering different time spans [Bamber et al., 2018]. Over the period from 2002 to 2015 Greenland mass loss was 265 ± 25 Gt/yr [Wouters et al., 2019].

The [Input-Output Method \(IOM\)](#) consists in quantifying ice discharge into the ocean, and the [Surface Mass Balance \(SMB\)](#). [SMB](#) is the difference between mass gained through snowfall and lost by sublimation at the surface and by melt-water runoff. This method has the advantage of explaining the mass changes in ice sheet and glaciers at drainage basin scale and on monthly basis but its accuracy relies on the models used. The spread in [IOM](#) trend estimates are ± 71 Gt/yr for Greenland mass change and ± 82 Gt/yr for Antarctica mass change, considerably larger than the spread in altimetry and gravimetry mass changes (See [Table 1.1](#)). Recently extended, [IOM](#) provides mass loss estimates for Greenland since 1972 [Mouginot et al., 2019] and for Antarctica since 1979 [Rignot et al., 2019]. These publications use an update drainage inventory, ice thickness, and ice velocity data to calculate the basin grounding line ice discharge.

[IOM](#)-based Greenland mass balance is estimated at -102 ± 20 Gt/yr for the period 1972 to 2018 with clear decadal variations. Greenland mass balance was positive in the 70s with a trend of 47 ± 21 Gt/yr, then it became negative in the 80s with a trend of -51 ± 17 Gt/yr due to an increase of solid ice discharge [Mouginot et al., 2019]. It remained negative in the 90s with a trend of -41 ± 17 Gt/yr. In the decades 2000-2009 and 2010-2019, the Greenland mass loss increased to trends of -187 ± 17 Gt/yr and -286 ± 20 Gt/yr, respectively. It was due to abrupt changes due to a decrease in the [SMB](#) and an increase of solid ice discharge [e.g., Mouginot et al., 2019]. [SMB](#) explains most of the interannual variability, especially the strong negative mass balance in 2012 which was due to an increase in melt-water runoff [van den Broeke et al., 2016]. On the other hand, solid ice discharge and the mass loss of peripheral glaciers mostly contribute to the trend. Most of the mass loss take place in the low elevations (below 2000 m a.s.l.) near the coast (the first 150 km) [van den Broeke et al., 2016].

The total mass balance from Antarctica decreased from -40 ± 9 Gt/yr in the 11-yr time period 1979–1990 and -50 ± 14 Gt/yr in 1989–2000 to -166 ± 18 Gt/yr in 1999–2009, and -252 ± 26 Gt/yr in 2009–2017 [Rignot et al., 2019]. [SMB](#) in Antarctica has been nearly at equilibrium because temperature remains negative except some glaciers in Antarctic peninsula. West Antarctica and Antarctic peninsula mass loss is dominated by the increase in solid ice discharge while solid ice discharge is a minor contribution to the East Antarctica mass balance ([Fig.1.2b](#) and Shepherd et al. [2018]). Compared to the other techniques, Greenland and Antarctica mass loss, estimated by [IOM](#) present higher mass loss rate and not always in agreement ([Table 1.1](#)).

Greenland and Antarctica have become dominant contributors of the global water budget since the beginning of 21st century [Church et al., 2013]. All projections for 21st century foresee that they will remain the main contributor with an expected contribution at the end of 21st century from 0.11 [0.01 to 0.24] m SLE for RCP2.6 to 0.16 [0.01 to 0.33] for RCP8.5 [Church et al., 2013], or even higher values proposed by a structured expert judgment leading to 0.22 [0.05 to 0.51] m SLE for RCP2.6 to 0.49 [0.23 to 1.02]

Table 1.1: Ice sheet mass trends in Gt/yr estimated using the input-output method (IOM), laser altimetry (LA), and gravimetry.

Region	Period	IOM	Altimetry	Gravimetry
Greenland ^a	Jan 2005-Dec 2015	-266 ± 71	-235 ± 37	-249 ± 23
Antarctica ^b	Oct 2003-Dec 2010	-201 ± 82	-43 ± 21	-76 ± 20

^a Extract from Shepherd et al. [2019, Table S4]

^b Extract from Shepherd et al. [2018, Table S4]

for RCP8.5 [Bamber et al., 2019]. The uncertainty in the projections comes mainly from the uncertainty in the Greenland ice sheet SMB response to the changes in north Atlantic weather conditions (0.06 m in RCP2.6 to 0.13 m in RCP8.5) and the Antarctic ice sheet dynamics response (0.17 m in all scenarios). Recently analyzed, marine ice cliff instability may increase Antarctic contribution between 0.26 to 0.58 m and 0.64 to 1.14 m GMSL by 2100, for RCP4.5 and RCP8.5, respectively [DeConto and Pollard, 2016; Kopp et al., 2017; Edwards et al., 2017].

1.2.2 Glaciers

There are around 215 000 glaciers in the last inventory: RGI 6.0 [RGI Consortium, 2017]. They correspond to a water reservoir of $0.158 \pm 41 \cdot 10^6$ Gt ($\sim 0.32 \pm 0.08$ m SLE) [Farinotti et al., 2019]. From the middle of the 19th century (around the end of the little ice age) glacier contribution has dominated the global water budget until the 21st century when Greenland contribution became larger [Leclercq et al., 2014; Marzeion et al., 2017]. Glacier mass changes in response to surface temperature and precipitations changes. Most of the glaciers are losing mass, although a few are nearly at equilibrium or even gaining mass (See South Asia in Fig. 1.3).

Glacier mass loss may be estimated with the same techniques as Greenland and Antarctica ice sheets (altimetry, gravimetry and IOM), but the size of the glacier, their topography, and the large number of glaciers hampers the generalization of these techniques [Marzeion et al., 2017]. Instead, there are specific techniques to estimate glacier mass change based on the glacier length, in situ direct observations (glaciological), and volume change with airborne and high resolution satellite imagery (geodetical) [Cogley et al., 2010].

Gravimetry is used globally and at monthly scale to retrieve glacier mass anomalies as for ice sheets mass changes. Once corrected for the non-water mass anomalies, gravity field is converted to water mass anomalies. However, retrieving glacier mass changes needs to separate hydrological and glacier signals and to reduce the uncertainty due to the spatial resolution. The first attempts to estimate the glacier mass changes by gravimetry assumed the hydrology beneath and around the glacier negligible [Chen et al., 2013; Yi et al., 2015]. Next studies included hydrological models to correct for the hydrological mass changes [Jacob et al., 2012; Gardner et al., 2013; Schrama et al., 2014] and recent studies combine hydrological models for some regions and considered hydrology negligible for other regions [Reager et al., 2016; Rietbroek et al., 2016; Bamber et al., 2018; Wouters et al., 2019]. The other drawback of using gravimetry to retrieve glaciers is the spatial resolution (about

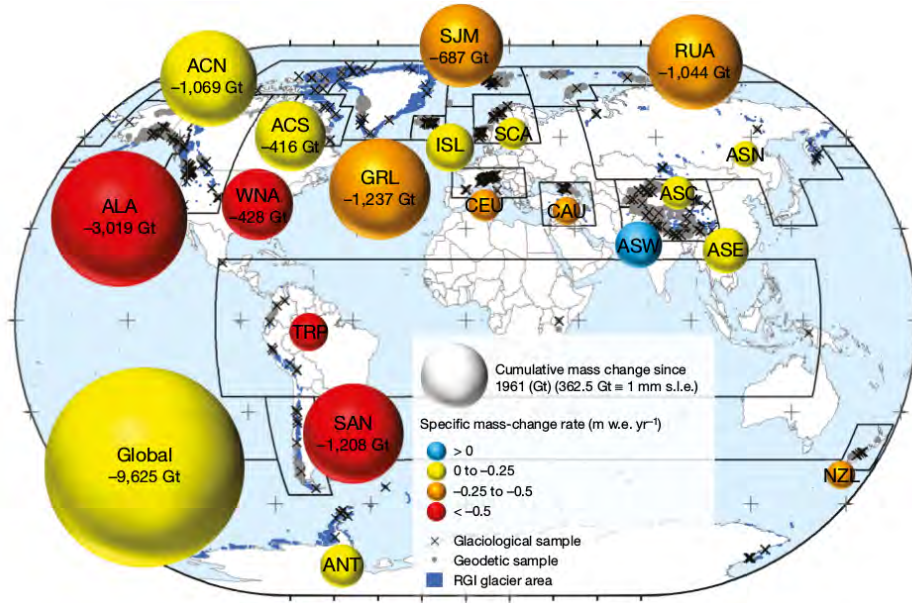


Figure 1.3: Regional glacier contributions to sea-level rise from 1961 to 2016. The cumulative regional and global mass changes (in Gt, represented by the volume of the bubbles) are shown for the 19 regions (outlined with bold black lines from [Randolph’s Glacier Inventory \(RGI\) 6.0](#)). Specific mass-change rates (m water equivalent yr^{-1}) are indicated by the colors of the bubbles. Excerpt from Zemp et al. [2019].

300 km) much larger than glaciers (a few km). There are currently two methods to reduce the uncertainty in the glacier mass estimates: forward modeling [Chen et al., 2013; Yi et al., 2015] and mascons [Jacob et al., 2012; Gardner et al., 2013; Schrama et al., 2014; Rietbroek et al., 2016; Reager et al., 2016; Wouters et al., 2019] although both methods seems to overestimate small glaciers as in Alps or in [High Mountain Asia \(HMA\)](#) [Long et al., 2016]. We discuss the use of gravimetry to estimate glacier mass changes in detail in chapter 3. Globally, gravimetry-based glacier estimate a trend of -183 ± 54 Gt/yr for the period 2003-2009 in glacier mass change, which is smaller than the trends retrieved from other techniques (between -216 and -342 Gt/yr from Table 1.2).

Table 1.2: Global glacier mass trends estimated from different techniques. Values are expressed in Gt/yr. Excerpt from Marzeion et al. [2017] with the addition of estimates from Zemp et al. [2019]

Technique	Reference	2003-2009	1961-2010
Gravimetry-based glacier	[Marzeion et al., 2017]	-183 ± 54^a	
Spatially-weighted in situ mass change observations	[Zemp et al., 2019]	-342^b	-205
Spatially-weighted in situ mass change observations	[Cogley, 2009]	-234 ± 25^b	-194 ± 18
Glacier length change	[Leclercq et al., 2014]	-266 ± 230^b	-209 ± 54
Mass budget from different methods	[Gardner et al., 2013]	-216 ± 25^b	
Glacier modeling	[Marzeion et al., 2017]	-244 ± 54^b	-176 ± 18

^a Averaged over different time periods (2002/2005–2013/2015)

^b Greenland peripheral glaciers removed from Gardner et al. [2013]

Glacier mass change is also estimated through the glacier length observations for some glaciers (i.e. 471 in Leclercq et al. [2014]). A few of these in situ observations are available since mid 1850s. However, to convert the length changes into mass changes, it is necessary

a calibration over a common period against a global glacier mass change from other technique.

For a few glaciers, mass change is directly measured through in situ measurements with stakes and snow pits. These measurements are then extrapolated to the rest of the glaciers [Cogley, 2009; Zemp et al., 2019].

There is also a geodetic technique based on the analyze of multi-temporal-imagery digital elevation models derived from satellite imagery [Berthier et al., 2016]. This technique allows to estimate the volume change which is converted in mass change via the ice density. For the moment this technique has only be applied for some specific regions like High Mountain Asia [Brun et al., 2017] and Patagonia [Dussaillant et al., 2019].

There is a good agreement in estimates of global glacier mass trend for the period from 2003 to 2009 among most of the techniques around -244 ± 33 Gt/yr, except from gravimetry and direct mass change observations. Gravimetry-based estimates are less negative -183 ± 54 Gt/yr while estimates derived from direct observations are more negative -342 Gt/yr (Table 1.2). For the period from 1961 to 2010, glacier mass trend estimated by direct mass observation of -205 Gt/yr shows a better agreement with estimates from the glacier length change.

Glaciers are not included in climate models because the processes that drive their mass changes are too small scale to be resolved by climate models. Instead, climate models outputs are used to force offline glacier models allowing to project future glacier contribution to sea level rise [e.g., Marzeion et al., 2015]. Depending on the scenario, glacier contribution to sea-level rise at the end of the 21st century is 0.10 [0.04 to 0.16] m SLE for RCP2.6 to 0.16 [0.09 to 0.23] for RCP8.5 [Hock et al., 2019]. The uncertainties of ± 0.12 m SLE is smaller than the Greenland and Antarctica contribution uncertainty, and mainly due to the downscaling from climate models [Church et al., 2013]. Glacier contribution is expected to decrease as glaciers retreat to higher mountains and some glaciers are disappearing during the 21st century.

1.2.3 Terrestrial water storage

The **Terrestrial Water Storage (TWS)** includes the water from the emerged land not included in glaciers nor in ice sheets i.e.: ice, snow, soil moisture, water from the biosphere, groundwater and surface water (including rivers, lakes and dams). Groundwater mass down to 4000m is estimated at $15.300 \cdot 10^6$ Gt (~ 42.5 m **SLE**) and the rest of **TWS** is estimated at $0.32 \cdot 10^6$ Gt (~ 0.88 m **SLE**)[Trenberth, 2014]. **TWS** is responsible for most of the ocean mass variability at annual and interannual scale e.g.[Wada et al., 2016]. Changes in **TWS** happens in response to natural variability (e.g. El Niño, **North Atlantic Oscillation (NAO)**, volcanoes, etc.) and to direct human-induced effects (dams, irrigation, water pumping, etc.) [Scanlon et al., 2018]. Climate change induced effects on **TWS** changes have not been yet detected in the last decades because of the large uncertainties in **TWS** changes and the large natural variability [Fasullo et al., 2016a; Kusche et al., 2016].

Due to the large surface of continents, it is very difficult to get a global measurement of the mass changes in **TWS**. Some authors focus in one component like: snow [Biancamaria

et al., 2011], groundwater measured by wells [Asoka et al., 2017], surface water from dams [Wada et al., 2016] or lakes [Cretaux et al., 2016]. Other authors focus on specific regions like Mississippi basin [Rodell et al., 2004]. Seasonal and interannual **TWS** mass changes dominate the **TWS** mass changes at basin scale while trends are at least one order of magnitude smaller [Scanlon et al., 2019]. Spatially, there are also great differences from one basin to another depending on the topography, on local precipitations, on human activities, on policies, etc. [Scanlon et al., 2018]. The differences in order of magnitude and spatial variability hamper trend and interannual variability extrapolation from one basin to another.

The only observing system that provides global **TWS** mass change estimates is **GRACE** but there are great discrepancies among the **TWS** estimates. Based on the 200 main basins (around 60% of the **TWS** surface), some authors suggests a water mass accumulation in continents for the period 2002-2014 between 118 Gt/yr [Reager et al., 2016] and 77 [71 to 82] Gt/yr [Scanlon et al., 2018]. While others authors suggests a mass loss of -79 ± 93 Gt/yr for the same period [Rietbroek et al., 2016].

Mass trends for the same period based on hydrological models are negative -118 ± 64 Gt/yr [Dieng et al., 2017] or $[-450 \text{ to } -12]$ Gt/yr [Scanlon et al., 2018]. Differences are partially explained by some mismodeling in the hydrological models, especially the lack of surface water and groundwater terms or the lack of direct human-induced effects in

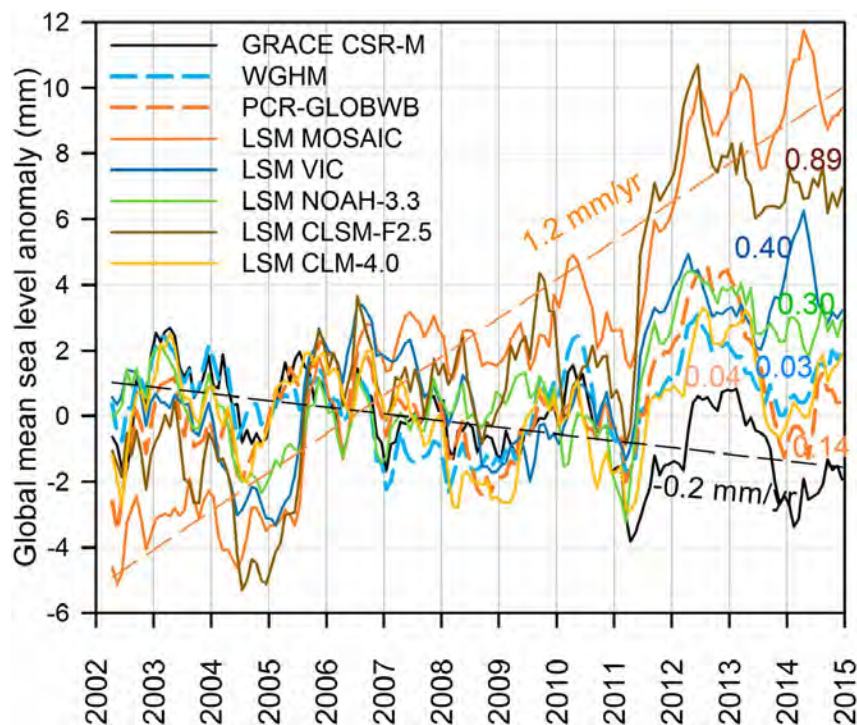


Figure 1.4: GRACE-based **TWS** contribution to the sea-level (black lines), global hydrological and water resources models (PCR-GLOBWB and WGHM) and land surface models (MOSAIC, VIC, NOAH-3.3, CLSM-F2.5, and CLM-4.0). Numbers in the figure corresponds to trends for the period from 2002 to 2015. Note that in the figure positive numbers means positive contribution to sea-level and negative mass balance for the **TWS**. Excerpt from [Scanlon et al., 2018]

most land surface models (LSM in Fig.1.4). However, the analysis of the uncertainty in GRACE-based TWS estimates was still to be addressed and this was one of the motivations for my PhD. We will discuss in detail this point in chapters 2 and 3.

There are few projections of the TWS mass change for the 21st century and the impact of the scenarios is not yet considered. Only projections of the direct human-induced effects are available to date. They lead to a small contribution to the sea-level rise at the end of 21st century of 0.04 [-0.01,0.09] mSLE due to an increase of water consumption per inhabitant and an increase of the total number of inhabitants.

1.3 Ocean mass change

The ocean represents the largest reservoir of water containing 97.5% of the total amount of water mass and covering 70% of the Earth's surface. Observing the ocean is key to understand the changes in the global water cycle because it integrates changes in land ice and land water. The ocean mass is the sum of land mass contributions and as such it can be estimated by adding together the independent estimates of each land mass change (Eq. 1.3). It can also be estimated directly through gravimetry from GRACE, and indirectly via the sea level budget and the ocean freshwater budget. We discuss each method and their estimates in the next subsections.

1.3.1 Ocean mass from the global water budget

Ocean mass estimated via the global water budget is computed as the sum of land mass contributions (Eq.1.3). In this way, the uncertainty in this estimate relies on the uncertainty of each land contribution. The uncertainty is important because of the lack of TWS mass change observations (Section 1.2.3). The 20th century ocean mass trend is estimated via the global water budget at 0.58 [0.41 to 0.73] mm SLE/yr for the period from 1900 to 1991 [Church et al., 2013]. Based on this approach, the ocean mass trend for the period from 1958 to 2014 has been reconstructed to 0.74 ± 0.10 mm SLE/yr [Frederikse et al., 2017].

Ocean mass projections for the 21st century are also estimated via the global water budget between 0.25 [0.04 to 0.49] m SLE in RCP2.6 to 0.36 [0.09 to 0.65] m SLE in RCP8.5 [Church et al., 2013]. Under the assumption that the uncertainties of the different land contributions are not correlated, the uncertainty is estimated as the squared sum of the uncertainties of each contribution (detailed in Section 1.2). Following this calculation, the uncertainty in the projections is mainly due to the uncertainty in the Greenland and Antarctica contributions, and more specifically in the Antarctic rapid ice sheet dynamics' contribution (uncertainty of ± 0.17 m SLE).

1.3.2 Ocean mass from gravimetry

There are two main methods to retrieve ocean mass from gravimetry: (1) Quantifying ocean mass change using an ocean basin mask (also called kernel) which excludes coastal

1.3. OCEAN MASS CHANGE

Table 1.3: Published trends of the global water budget (Eq 1.3) in mm SLE/yr. Ocean mass and land contributions from Greenland, Antarctica, glaciers and TWS. Note that the periods are slightly different for each publication and all uncertainties are expressed at 90 %CL.

Source	Period	Ocean mass	Greenland	Antarctica	Glacier	TWS
[Reager et al., 2016]	Apr 2002-Dec 2014	1.58 ± 0.43^a	0.77 ± 0.13	0.49 ± 0.53	0.65 ± 0.09	-0.33 ± 0.12
[Rietbroek et al., 2016]	Apr 2002-Jun 2014	1.08 ± 0.30^a	0.73 ± 0.03	0.26 ± 0.07	0.38 ± 0.07	0.22 ± 0.26
[Yi et al., 2015]	Jan 2005- Jul 2014	2.03 ± 0.22^a	0.77 ± 0.05	0.60 ± 0.18	0.58 ± 0.03	0.07 ± 0.11
[Dieng et al., 2017]	Jan 2004-Dec 2015	2.24 ± 0.16^b	0.82 ± 0.10	0.33 ± 0.10	0.58 ± 0.10	0.33 ± 0.18
[Chambers et al., 2017]	Jan 2005-Dec 2015	2.11 ± 0.36^a				
[Chen et al., 2018]	Jan 2005-Dec 2016	2.70 ± 0.16^a				
[Chen et al., 2018]	Jan 2005-Dec 2016	2.75 ± 0.18^b				
[Cazenave et al., 2018a]	Jan 2005-Dec 2016	2.40 ± 0.40^b	0.76 ± 0.16	0.42 ± 0.16	0.74 ± 0.16	-0.27 ± 0.24
[Blazquez et al., 2018]	Jan 2005-Dec 2015	1.63 ± 0.27^a	0.80 ± 0.04	0.63 ± 0.15	0.20 ± 0.31^c	
[Uebbing et al., 2019]	Aug 2002-Jul 2016	1.75^a				
[Llovel et al., 2019]	Jan 2005-Dec 2015	1.55 ± 1.20^d				

^a Ocean mass from gravimetry.

^b Ocean mass from the sea-level budget.

^c Glacier and TWS.

^d Ocean mass from the freshwater budget.

areas [e.g., Chambers, 2006a; Chambers and Bonin, 2012] or (2) direct averaging over the whole ocean of a post processed solution that is corrected for leakage [e.g., Rietbroek et al., 2016; Yi et al., 2015; Chen et al., 2018; Reager et al., 2016]. In the kernel approach, coastal ocean areas within certain distance (e.g., 300 or 500 km) from the coast are excluded, in order to minimize leakage signal from land into the ocean and the spatial resolution is degraded to 500 km to reduce the noise. On the contrary, in the direct average over a post-processed GRACE solution, mass changes on land and over ocean are solved at the same time via forward modeling method [e.g., Chen et al., 2018; Yi et al., 2015], joint inversion with altimetry [e.g., Rietbroek et al., 2016] or mass concentration (mascon) method [e.g., Reager et al., 2016]. Both approaches relies on the correction of non-water mass anomalies that affect the gravity field as earthquakes and **Glacial Isostatic Adjustment (GIA)**. Being **GIA** the solid-Earth response to the melting of the continental ice sheets since the last glacial maximum (further details in Section 2.2.5). Ocean mass trends estimates for the last decade ranges from 1.08 ± 0.30 mm SLE/yr [Rietbroek et al., 2016] to 2.11 ± 0.36 mm SLE/yr [Chambers et al., 2017] and even 2.70 ± 0.16 mm SLE/yr [Chen et al., 2018] (Table 1.3). This large uncertainty of ± 1 mm/yr is one of today's largest uncertainty in the global water budget. The characterization of the uncertainties in the ocean mass is one of the main motivations of my PhD. I will analyze the sources of this uncertainty in the trend estimates by rigorously analyzing all the GRACE post processing (See Chapter 2 for more details).

1.3.3 Ocean mass from the sea level budget

The water mass loss from continents run off to the ocean, increasing the ocean mass. As the mass reaches the ocean, it propagates in the ocean leading to an uniform barystatic sea-level rise after 2 to 3 weeks [Lorbacher et al., 2010]. Barystatic sea-level rise (h_b) is related with the ocean mass (ΔM_{Ocean} from Eq. 1.3) via the surface (A_{ocean}) and the

density of the ocean ($\rho_{ocean} \sim 1030 \text{kg/m}^3$) following the equation 1.4,

$$h_b = \frac{\Delta M_{Ocean}}{\rho_{ocean} A_{ocean}} \quad (1.4)$$

This barystatic sea-level rise together with the thermal expansion (global-mean thermosteric sea-level rise or h_θ) are responsible for the **Global-mean sea-level rise (GMSLR)** as in the sea level equation (Eq. 1.5 and Fig. 1.5).

$$GMSLR = h_\theta + h_b \quad (\text{Sea level budget}) \quad (1.5)$$

1.3.3.1 Sea-level change

GMSLR cannot be directly measured; Instead, **GMSLR** is computed as the sum of **Global-mean geocentric sea-level rise (GMGSLR)** measured with respect to the **International Terrestrial Reference Frame (ITRF)** and the sea floor changes estimated with respect to the **ITRF**. These sea floor changes include the sea-floor viscous adjustment caused by past changes in land ice known as **GIA** correction (h_{GIA}) and contemporary

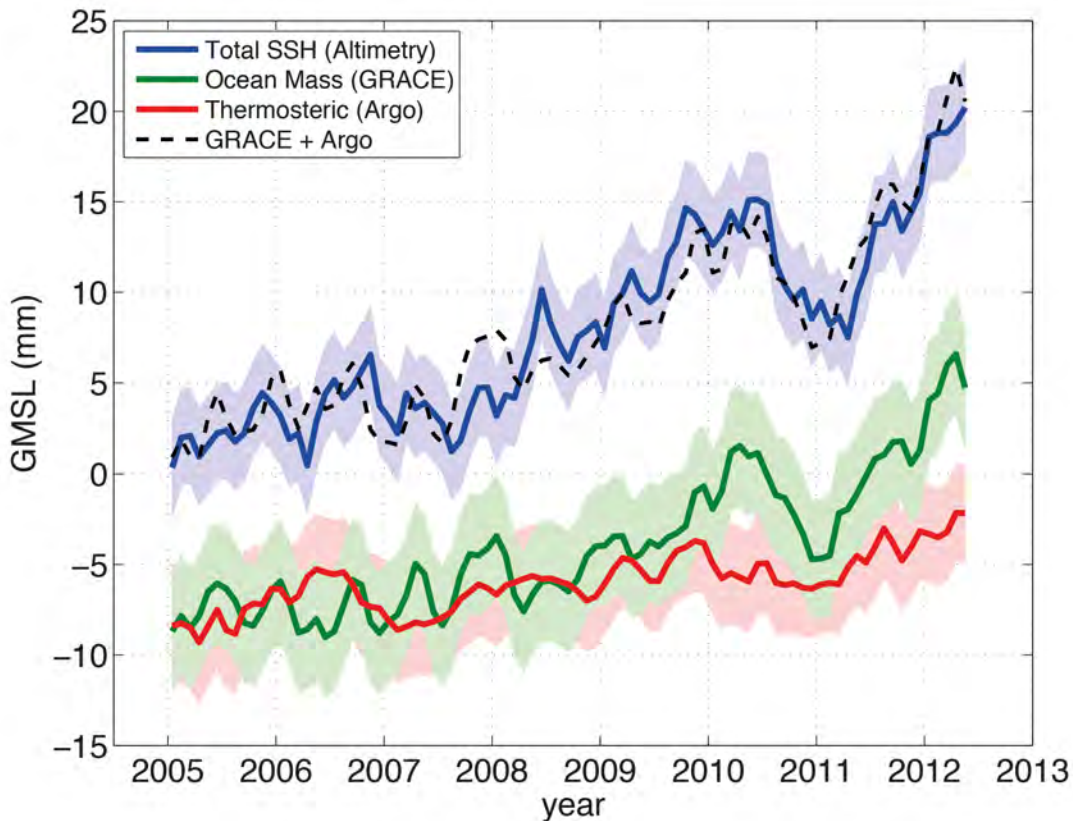


Figure 1.5: global-mean sea-level rise (Total SSH, Altimetry in the figure), barystatic sea-level rise (Ocean mass in the figure), global-mean thermosteric rise (Thermosteric, ARGO in the figure) and GMSLR (the sum of GRACE + Argo in the figure). Figure excerpt from IPCC AR5 Fig 13-6 [Church et al., 2013]

Earth Gravity, Earth Rotation and viscoelastic solid-Earth Deformation (GRD) (h_p) which accounts for sea-floor elastic adjustment to the ongoing changes in the water transport.

$$GMSLR = GMGSLR - h_{GIA} - h_p \quad (\text{Eq.58 from Gregory et al. [2019]}) \quad (1.6)$$

GMGSLR is accurately measured (cm resolution every 10 days every 100 km) with satellite altimeters constellation [Legeais et al., 2018]. Altimeters measure the range between the satellite and the sea surface via the time between the emission and the reception of the radar echo. This range and the satellite position allow to estimate the sea surface height with respect to a geocentric reference ellipsoid. In order to retrieve the sea surface height this measure is corrected for a number of delays in the round travel of the radar echo. The most important delays include the wet Troposphere delay and the ionospheric effect (Further details in Escudier et al. [2017]).

The family of satellite altimeters provides a sea level record of more than 25-year including the records from TOPEX/Poseidon (Aug 1992-Jan 2006), Jason-1 (Dec 2001 – Jun 2013), Jason-2 (Jul 2008 -present), Jason-3 (Jan 2016 -present), as well as those from ERS 1 (Jul 1991-Mar 2000), ERS2 (Apr 1995-Jun 2003), Envisat (Mar 2002 –Apr 2010), SARAL/Altika (Feb 2013- present), Cryosat-2 (Apr 2010-present), HY-2A (Aug 2011-present), Sentinel-3a (Feb 2016-present) and Sentinel-3b (Apr 2018 - present).

The **GIA** correction (h_{GIA}) is mainly due to the changes in geoid. **GIA** affects in many other ways: (1) the three-dimensional displacements of the Earth’s surface both in the near and in the far field of the former ice sheets, (2) the loading- and un-loading-induced stress variations in the crust and the mantle, and (3) the fluctuations of the Earth’s rotation axis, involving lateral movements of the pole or true polar wander and changes in the length of day (Further details in Spada [2017]; Tamisiea [2011]). All these effects must be accounted to estimate the **GIA** correction applied to altimetry (h_{GIA}) which contributes about -0.3 mm/yr [Tamisiea, 2011] to the **GMSLR**. To compute this value, global **GIA** models need to account for the change in the barystatic sea-level change since **Last glacial maximum (LGM)** and its effect on the geoid. There are few **GIA** models which deliver this term, leading to a global **GIA** correction of -0.37 ± 0.05 mm/yr [Stuhne and Peltier, 2015; Peltier et al., 2017]. We will discuss in details this issue in Section 2.2.5.

Contemporary **GRD** accounts for sea-floor adjustment due to the ongoing changes in the continental water mass. The continental water mass changes cause instantaneous vertical land movement and changes in the geoid due to the elastic deformation of the solid-Earth. As contemporary **GRD** and barystatic sea-level are both proportional to the ocean mass (ΔM_{Ocean}), the sum of both effects has been known in the literature as ocean fingerprints. Global mean contemporary **GRD** reduces global mean sea level rise by about 8% of the barystatic sea-level rise [Frederikse et al., 2017].

GMGSLR has increased with at a rate of 2.8 ± 0.3 mm/yr for the period from 1993 to 2017. Once corrected for **GIA** (-0.3 mm/yr from Peltier [2004]) and contemporary **GRD** (-0.1 mm/yr from Frederikse et al. [2017]), **GMSLR** trend is 3.2 ± 0.3 mm/yr for the same period (Fig 1.5). This result is corroborated by an estimation done with tide-gauges along the coast which indicates a trend in **GMSLR** of 3.2 ± 0.40 mm/yr [Ablain et al., 2015;

Mitchum et al., 2010; Watson et al., 2015]. In the last decades, **GMSLR** has accelerated [Cazenave et al., 2018b; Fasullo et al., 2016b; Nerem et al., 2018]. This acceleration is the result of an increase in Greenland and Antarctica mass loss of 30% since 2010, an increase in the thermosteric change and **TWS** interannual variability due to el Niño 2012 [Yi et al., 2015; Dieng et al., 2017].

Uncertainties has been estimated tracking down errors in the data process (from instrument and from corrections). Main contributors to the **GMGSLR** trend uncertainty are the orbit determination (± 0.20 mm SLE /yr), the "wet troposphere correction" (± 0.17 mm SLE/yr) and the bias calibration between satellites [Ablain et al., 2015, 2017, 2019]. The bias calibration is estimated with the data from the overlapping period and a drift analysis of altimetry-based and tide-gauges-based **GMGSLR**. Uncertainties in the tide-gauges 10-yr trend estimates are ± 0.40 mm SLE/yr the period from 1995 to 2005, mainly due to the uncertainties in the vertical land motion near the tide gauges [Ablain et al., 2018]. The bias calibration induce a temporal correlation in the uncertainty of the trend. Uncertainty in the trend varies from ± 0.40 mm SLE/yr for the period from 2002 to 2017 to ± 0.35 mm SLE/yr for the period from 1998 to 2018 [Ablain et al., 2019, Figure 5]. Altimetry and tidegauges estimates agrees within 0.07 mm SLE/yr [Ablain et al., 2018]. The agreement between both methods gives high confidence in the uncertainty of **GMSLR** trend.

Projections of sea-level rise for the 21st century are the sum of the projected thermosteric sea-level rise and the projected ocean mass (computed through the land mass contributions). They are very dependent on the scenario, varying from 0.44 [0.28 to 0.61] m SLE in RCP2.6 to 0.74 [0.52 to 0.98] m SLE in RCP8.5 [Church et al., 2013]. The uncertainty in the estimates of about [0.33 to 0.46] m SLE comes mainly from the uncertainty in the ocean mass [0.25 to 0.34] m SLE and in particular from the uncertainty in the ice sheet contributions, and to a lesser extent the uncertainty in the thermosteric sea level change [0.10 to 0.11] m SLE.

1.3.3.2 Steric sea-level change

Steric sea-level changes are a combination of the thermosteric changes (due to the thermal expansion) and the halosteric changes (due to the changes in salinity). Temperature and salinity data rely on in-situ measurements and to a lesser extent on satellite sea-surface temperature. Since 2000s, the international ARGO program (<http://www.argo.ucsd.edu>, Roemmich et al. [2009]), has coordinated the profilers deployment in a joint effort with buoys, gliders, MBT, and XBT. In 2005, ARGO achieved a quasi global coverage (60°S-60°N latitude), down to 2000 m depth with a monthly resolution and a spatial resolution of $3^\circ \times 3^\circ$ [Roemmich et al., 2009]. Temperature and salinity products are delivered by different research groups: IAP, IFREMER, IPRC, ECCO, Ishii, JAMSTEC, Met Office (EN), SCRIPPS, NOAA, and ECMWF (ORA S5). Differences among these products are due to the different strategies adopted for data editing, the temporal and spatial data gap filing and the instrument bias corrections [Cazenave et al., 2018a].

When freshwater enters the ocean, it modifies the ocean salinity due to the dilution of sea water. However, at global scale and at first order, halosteric changes are negligible

compared to global-mean thermosteric sea-level rise ($h_H \ll h_\theta$) [Gregory and Lowe, 2000]. Thus, we can assume that global-mean steric sea-level is equivalent to global-mean thermosteric sea-level rise. Global-mean thermosteric sea-level rise (h_θ) has increased for the last decades at a rate of 1.49 [0.97 to 2.02] mm/yr for the period from 1993 to 2010 [Church et al., 2013] and 1.3 ± 0.4 mm/yr for the period from 1993 to 2017 [Cazenave et al., 2018a]).

Uncertainties in the steric sea-level change are difficult to estimate because the data relies on a multitude of instruments, each one built and aging in different ways. At global scale, global-mean thermosteric sea-level rise uncertainty is usually estimated as the spread of the thermosteric estimates from the different solutions from the research groups. This uncertainty in trend amounts ± 0.4 mm/yr for the period from 2005 to 2015 [Cazenave et al., 2018a, Table 12]. It is likely biased low because of the sparse density of in situ measurements in critical areas like marginal seas, seasonally ice covered regions and the layers between 2000 m and 6000 m depth.

Thermosteric sea-level rise projections for the 21st century are very sensitive to the scenario from 0.14[0.10 to 0.18] m SLE in RCP2.6 to 0.27[0.21 to 0.33] m SLE in RCP8.5 [Church et al., 2013]. Uncertainty in the estimates is mainly due to the spread in climate models in the radiative forcing (30%), the climate sensitivity, and the ocean heat uptake efficiency [Melet and Meyssignac, 2015].

1.3.3.3 Ocean mass derived from the sea-level budget

Ocean mass can be estimated from the barystatic sea-level (Eq. 1.4) where barystatic sea-level is derived from the difference between GMSLR and global-mean thermosteric sea-level rise (Eq.1.6). Assuming no deep ocean contribution and neglecting the influence of regions where steric sea-level is poorly resolved (e.g. the marginal seas, seasonally ice covered regions), ocean mass trend is estimated at 1.9 ± 0.36 mm SLE/yr for the period from January 1993 to December 2017 and 2.4 ± 0.4 mm SLE/yr for the period from 2005 to 2015 [Cazenave et al., 2018a].

1.3.4 Ocean mass from the fresh-water budget

The increase of freshwater in the ocean, modifies the ocean salinity without modifying the total amount of salt in the ocean (Section 1.3.3.2). Thus, measuring ocean salinity changes from in situ data allows to estimate this freshwater increase (Eq. 1.7). This freshwater comes from the melting of floating ice, including ice shelves, (ΔM_{SeaIce}) and the continental freshwater which is related to the ocean mass (ΔM_{Ocean} from Eq. 1.3). See [Munk, 2003; Llovel et al., 2019].

$$\Delta M_{Ocean} + \Delta M_{SeaIce} = 36.7 \cdot \rho_{ocean} \cdot A_{ocean} \cdot h_H \quad (Freshwaterbudget) \quad (1.7)$$

The ocean salinity is well determined thanks to ARGO program except in marginal seas, seasonally ice covered regions and the layers between 2000 m and 6000 m depth.

Global mean halosteric sea-level is estimated at 0.079 ± 0.032 mm SLE/yr [Llovel et al., 2019]. Sea ice volume is estimated through the ice coverage, well determined by satellite imagery and the ice thickness based on satellite altimetry and in situ measurements. Most of the uncertainty in sea ice volume change comes from the thickness estimation. Sea ice volume change for the period from 2005 to 2015 is estimated at 0.550 ± 0.106 Gt/yr [Guerreiro et al., 2016; Schweiger et al., 2011] which is equivalent to an increase of 1.36 ± 0.26 mm SLE/yr. Based on this approach, The salinity provides an independent estimate on the ocean mass trend of 1.55 ± 1.20 mm SLE/yr for the period from 2005 to 2015 [Llovel et al., 2019].

1.4 Global energy budget and how it relates to the water cycle

The global budget of the Earth's system is composed of the input from Sun's radiation, the output through Earth's radiation, and the difference between both which is known as **Earth's Energy Imbalance (EEI)**. Because of **EEI**, the climate system stores energy. 93% of this energy warms the the ocean warming increasing the **Ocean Heat Content (OHC)**, while the remaining 7% is responsible for the warming of the atmosphere and continents and ice melting [Levitus et al., 2012] (Fig. 1.6 top). **EEI** is responsible of the climate related changes in the Earth's system, like the rise of the global-mean temperature (known as global warming), the rise of sea-level, the melting of glaciers, the changes in the global water cycle, etc. (Fig 1.6 bottom).

EEI can be estimated via: (1) direct measures by satellite using the **Clouds and the Earth's Radiant Energy System (CERES)** instruments, (2) direct **OHC** estimation, via the temperature measurements in the ocean from ARGO, and (3) indirect **OHC** estimation via the steric sea-level deduced from the **GMSLR** and the ocean mass through the sea level budget (Eq. 1.5).

The **CERES** instruments enable to retrieve **EEI** variations from weekly to decadal timescales accurately with an uncertainty of $\pm 0.1 \text{ Wm}^{-2}$ but the time-mean **EEI** is measured with an accuracy of 3.0 Wm^{-2} because of calibration issues [Loeb et al., 2012]. **EEI** estimate is $0.71 \pm 0.11 \text{ Wm}^{-2}$ for the period 2006 to 2015 [Meyssignac et al., 2019].

OHC deduced from ARGO data is computed from the ocean heat changes due to changes in temperature at each position and depth, integrated over the whole ocean. **EEI** based on ARGO is $0.67 \pm 0.17 \text{ Wm}^{-2}$ for the period from 2006 to 2015 [Meyssignac et al., 2019]. This uncertainty is underestimated because it is estimated from the spread between the different solutions and do not include the sparseness of insitu data in critical areas as marginal seas, seasonally ice-covered regions and down to 6000 m depth [Meyssignac et al., 2019].

Indirect **OHC** deduced from the sea level budget presents the advantages of a global spatial coverage and integration over the whole column of water (from surface to sea floor). **OHC** derived from sea-level budget rely on sea-level, ocean mass and the expansion efficiency of heat (**EEH**) via Eq. 1.8. The expansion efficiency of heat is estimated about $0.12mYJ^{-1}$ [Levitus et al., 2012]. Sea-level budget **EEI** is estimated at $0.69 \pm 0.62 \text{ Wm}'^{-2}$

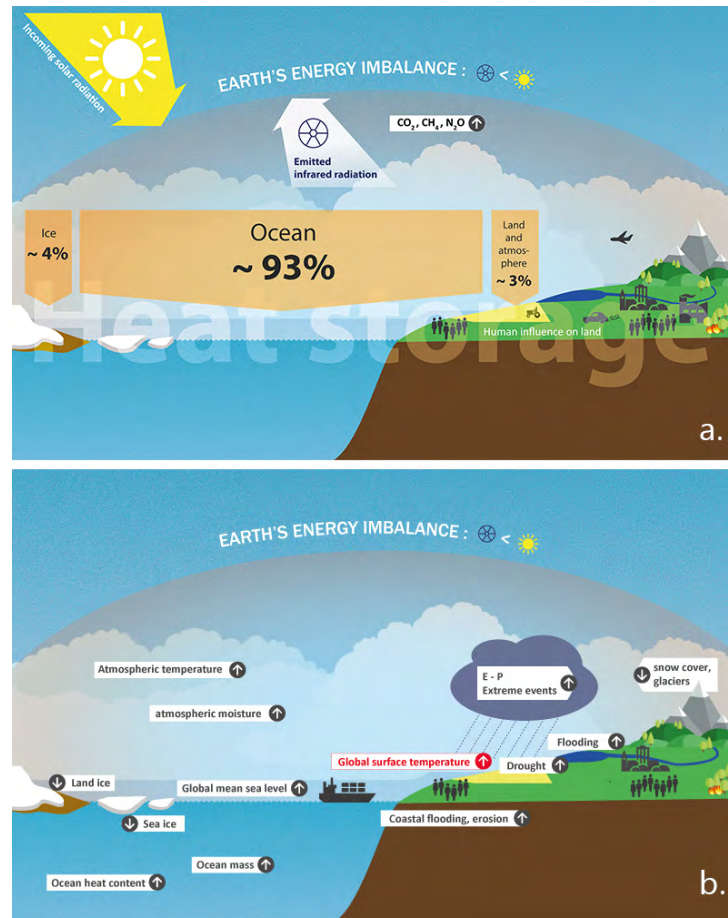


Figure 1.6: Schematic representations of the flow and storage of energy in the Earth's climate system (top), and main consequences of the EEI in the Earth's climate system (bottom)

[Llovel et al., 2014] and $0.48 \pm 0.47 \text{ Wm}^{-2}$ [Meyssignac et al., 2019]. Uncertainty in EEI estimated though the sea level budget is mainly due to the uncertainty in the ocean mass [Meyssignac et al., 2019].

$$OHC = EEH \cdot GMSSLR = EEH \cdot \left(GMSSLR - \frac{\Delta M_{ocean}}{\rho_{ocean} \cdot A_{ocean}} \right) \quad (1.8)$$

EEI and the water cycle are related through the ocean mass via the sea-level budget and the OHC. We discuss the implications of the uncertainty in the ocean mass trends in the estimate of EEI and its uncertainties in detail in Chapter 4.

1.5 Scientific questions associated to the water cycle

In summary, thanks to an unprecedented effort in the development of the observing systems in the last decades, the uncertainty in the estimation of the water cycle, the sea

level budget and the energy budget have decreased significantly [Cazenave et al., 2018a; Chambers et al., 2017; Meyssignac et al., 2019]. However, some research remains to be done to improve the estimates of the global water budget and its individual components and try to close the global water budget. In particular, there is room to improve the accuracy of the estimates and the confidence in the associated uncertainties. Working in these directions should provide new insights on recent science questions, which are still open. I summarize here some of these questions and I present then how my work on the uncertainty in the water cycle components provide new insight on these questions

Scientific questions related to the water budget

1. What is the uncertainty in the global water budget and can we close the water budget at all timescales from annual to decadal within the uncertainties?
2. Are the uncertainty in the different components of the global water budget correlated when assessed with GRACE-based estimates?
3. Given the current uncertainty, can observed global water budget constraint climate models to reduce the spread in the 21st projections?
4. Given the current uncertainty, Are the causes of the recent acceleration in ocean mass increase significant and what is the cause?
5. Given the current uncertainty, has [TWS](#) increased or reduced the sea-level rise in the first decades of the 21th century? Why GRACE-based and model-based [TWS](#) trends have opposite sign?
6. Given the current uncertainty, how is [TWS](#) changing under climate change?
7. Can we separate the glacier and the hydrology signals in space gravimetry signal?

Scientific questions related to the sea level budget

8. Can we close the sea level budget at annual and longer timescales under climate change, given the current uncertainties?
9. Is the deep ocean heating significant? What is its contribution to the steric sea level and to the [EEI](#)?
10. Can we reduce the uncertainty in the ocean mass estimate through the freshwater budget? Can we provide constraint?
11. Given the level of uncertainties, can we use ocean mass and geocentric sea-level observations with geodetic techniques to constrain [EEI](#) which is responsible for the contemporary climate change?

1.6 Objectives of this PhD

The scientific objectives are: (1) to document the nature of global mass exchanges with estimates and the associated uncertainties, and if we can, (2) explain the differences among

the estimates of the global water budget, (3) reconcile and propose robust estimates with uncertainties, (4) on this basis, reevaluate the estimates and revisit the scientific questions cited before and more specifically numbers 1 and 8.

To reach these scientific questions, I improve in my PhD work the treatment of space gravimetry data from [GRACE](#) to obtain consistent global mass changes with, as exhaustive as possible, associated uncertainties. I decided to use an ensemble approach including all available state-of-the-art post-processing to assess the underlying uncertainties.

The second chapter is focused on the development of an ensemble of GRACE solutions. I explain the state-of-the-art of the GRACE treatment and GRACE post processing. I explain how I developed a consistent ensemble of GRACE solutions that conserves mass at global scale. I explore the reason for differences between different GRACE solutions and provide some insights on the sources of the uncertainties in GRACE estimates of the global water cycle. I include a paper that discuss the uncertainties on the GRACE-based global water cycle [Blazquez et al., 2018]. At the end of the chapter, I compare the global water mass estimates with previous estimates, I explain the reason for the differences in previous estimates and I address questions: 1, 2, and 4.

In the third chapter, I focus on land, and I analyze the uncertainties in the land GRACE-based estimates at basin scale. I propose a method using independent mass estimates to reduce the uncertainties on the GRACE-based local water mass estimates. I test and validate this method in South Asia, a region where glaciers and lakes are concentrated in small locations. Accounting for their mass changes leads to improved estimate for other hydrological processes affecting the local water cycle. I summarize the method and validate the hydrological estimates in Blazquez et al. [2020, In prep], attached at the end. This provides regional insight on the science questions 6 and 7 and show the potential of using independent data to improve GRACE data and potentially respond to questions 5, 6, and 7 at global scale in the future, when the method will be applied to all regions influenced by glaciers and lakes.

In the fourth chapter, I focus on the ocean. I identify the geocenter motion correction and the [GIA](#) correction as the major sources of uncertainty in the ocean mass changes. I explore a method to improve the estimates of the ocean mass by removing the uncertainty in geocenter. I analyze the consistency between the ocean mass, the altimetry sea-level and the steric sea level through the sea-level budget. Thanks to the comparison with CERES-based steric sea-level, I identify the sources of some errors in GRACE-based ocean mass. I address questions 8, 9 and 10.

Chapter 2

Evaluating the uncertainty in GRACE-based estimates of the global water budget. Development of an ensemble approach

The main objective of this PhD is to characterize the global water budget at interannual to decadal timescales and to characterize the associated uncertainties. Only [Gravity Recovery and Climate Experiment \(GRACE\)](#) and [GRACE FO](#) missions allow to estimate at the same time all components of the global water budget at interannual to decadal time scales. A significant advantage of deriving estimates of all components from the same single mission is that all estimates, their errors, and their uncertainties should be consistent with each other by construction. For this reason, GRACE solutions have provided essential and critical observations to analyze and test the closure of the global water budget [Church et al., 2013; Llovel et al., 2014; Yi et al., 2015; Reager et al., 2016; Rietbroek et al., 2016; Dieng et al., 2017]. However, in practice, there are significant differences in the water budget components estimates when different GRACE solutions from different data processing centers are used or when different post-processing are applied to the data. So, each single post-processed GRACE solution provides a self consistent estimate of the global water budget components but this estimate is potentially biased. By self consistent, I mean that they close the global water budget. Thus, if GRACE solutions are considered with the same single post processing, they likely underestimate the true uncertainty in global water budget components.

I propose to estimate the components of the global water budget from GRACE and to evaluate the associated uncertainty using an ensemble of global GRACE solutions and an ensemble of post-processing parameters which includes all state-of-the-art GRACE solutions and post-processing parameters that are available. With this ensemble, I expect to capture most of the relevant state-of-the-art estimates of the global water budget from GRACE data. The range covered by my ensemble should enable to explore the uncertainty and to analyze its sources.

In this chapter, I present GRACE and GRACE FO missions in Section [2.1](#). I discuss the post-processing parameters used to produce GRACE solutions in Section [2.2](#). I present

my ensemble solution including the paper that summarizes the method in Section 2.3.2. This ensemble enable me to explore the uncertainty in GRACE estimates and identify its major sources. Then, I compare my solution with previous studies explaining the differences between previous estimates in Subsection 2.3.1. On the basis of this work I revisit and discuss the scientific questions in the conclusions 2.4

2.1 GRACE and GRACE FO missions

GRACE mission was launched under the joint sponsorship of [National Aeronautics and Space Administration, USA \(NASA\)](#) and [Deutsches Zentrum für Luft und Raumfahrt, Germany \(DLR\)](#) while GRACE FO has been launched under the joint sponsorship of [NASA](#) and [GeoForschungsZentrum, Germany \(GFZ\)](#). They are made up of two twin satellites in low quasi-polar orbits with an initial altitude of 500 km and an inclination of 89° [Tapley et al., 2004]. The missions do not measure the gravity field directly but measure the effect of the gravity on both satellites. More specifically, the missions measure the inter-satellite range and inter-satellite range rates with the [K-Band Range \(KBR\)](#) radar at an accuracy of $1 \mu m$ and $1 \mu m/s$ respectively. The satellites accelerate and decelerate in the along-track movement as a consequence of the mass anomalies below them (See Fig. 2.2). These satellites have no moving parts. The platform was designed to minimize the surface forces with respect to the gravitational forces in order to enhance maneuvers in order to enhance the detection of the mass anomalies.

GRACE fulfilled the nominal mission to monitor the mass changes at seasonal scales in the first years. This technological demonstrator mission was the first to analyze time variable gravity at monthly scale [Tapley et al., 2019]. After a few months of technological validation, nominal data became available from August 2002. In the first year there were maintenance operations (November and December 2002 and May and June 2003, red in Fig. 2.1). Since the altitude of the satellites was left to freely decrease (following the atmospheric drag force) from an initial altitude of 500 km to the final altitude of 340 km, the satellites, in the course of their life time, went through episodes of repeat cycles . In such cases the ground tracks, instead of covering more or less evenly the Earth's surface, were gathered into repeat tracks leaving large longitudinal gaps. This was the case in particular for the months from August to November 2004 (asterisks in Fig. 2.1).

In 2011, after fulfilling the nominal mission, some batteries cells were progressively lost, reducing the energy available for the scientific mission. The temperature control of the accelerometers was degraded and ultimately deactivated. Due to this reduction of energy storage, key instruments of the satellites were switched off for some weeks every year during the longest eclipse periods, provoking gaps in the monthly timeseries (red in Fig. 2.1).

In October 2016, the accelerometer of the second satellite (GRACE B) was turned off for six out of the seven final months of the GRACE mission and its data was replaced by the one of GRACE A, degrading the quality of the monthly solutions. The scientific mission ended in September 2017 with the loss of communications with GRACE B and the mission was definitively decommissioned in October 2017 [Tapley et al., 2019].

Considering the missing months and the quality of the data (Fig. 2.1), we considered

2.1. GRACE AND GRACE FO MISSIONS

three different periods: (1) the period from December 2004 to December 2010 were there is no missing months, (2) the period from January 2003 to December 2015 were there are 16 gaps over 156 months in the period, and (3) the larger available period from August 2002 to June 2017. See Wouters et al. [2014] and Tapley et al. [2019] for more details.

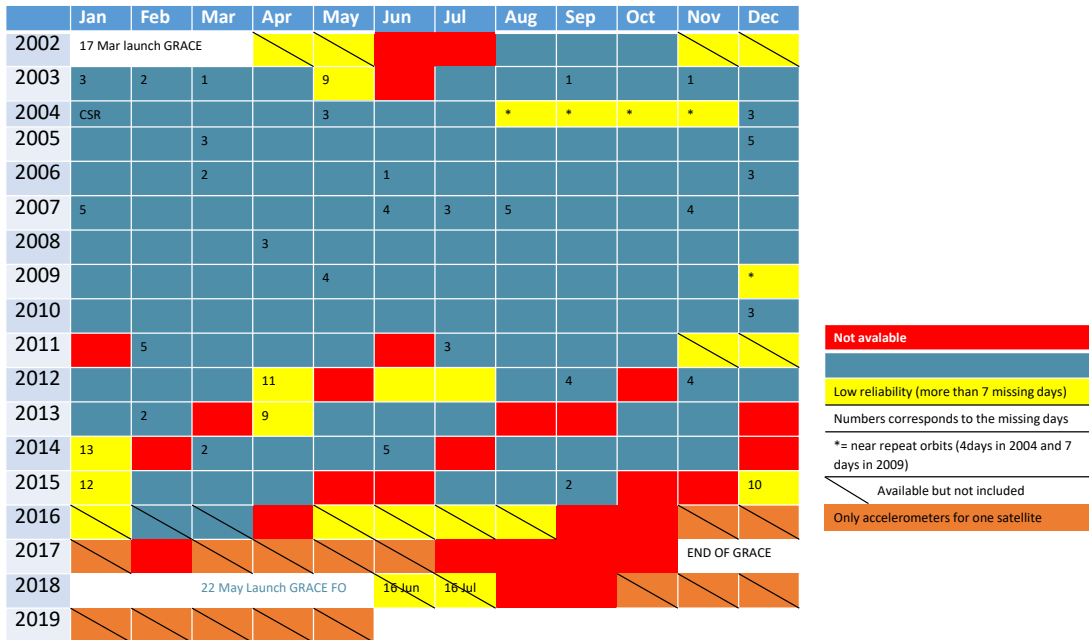


Figure 2.1: GRACE monthly data. Colors corresponds to the reliability and the availability of the data. Numbers expressed the missing days in the months. Asterisks corresponds to the month with repeat cycles.

GRACE FO was launched on May 2018. It produced nominal measurements for almost 4 weeks from 16th June to 17th July until unforeseen reboots disrupted the instrumental platform unit. After several months of tests, the problem was solved using the backup instrumental platform unit. At the same time, there was a degradation of the performances in the accelerometers from the second satellite of **GRACE FO** (**GRACE D**) [Christophe, 2018]. The technique of "accelerometer transplant" used for the last months of **GRACE** mission is since then applied to the **GRACE FO** mission [Bandikova et al., 2019]. **GRACE FO** data is available since June 2018 with a 2-month gap in August-September 2018.

In this PhD I will focus on the period from August 2002 to December 2015 (Fig. 2.1) before the loss of the accelerometer and where there are only a few gaps.

2.1.1 Inversion process (From L1 data to L2 products)

The gravity field cannot be directly observed, instead **GRACE** satellites measure: (1) the inter satellite range and range rates (**KBR**), (2) the forces acting on the satellites via the accelerometers, (3) the satellite attitude via the star trackers and (4) the satellite position and velocities via **Global Positioning System (GPS)** receivers. These on board measurements are known as L1 data. L1 data is used in an inversion process to estimate the gravity field.

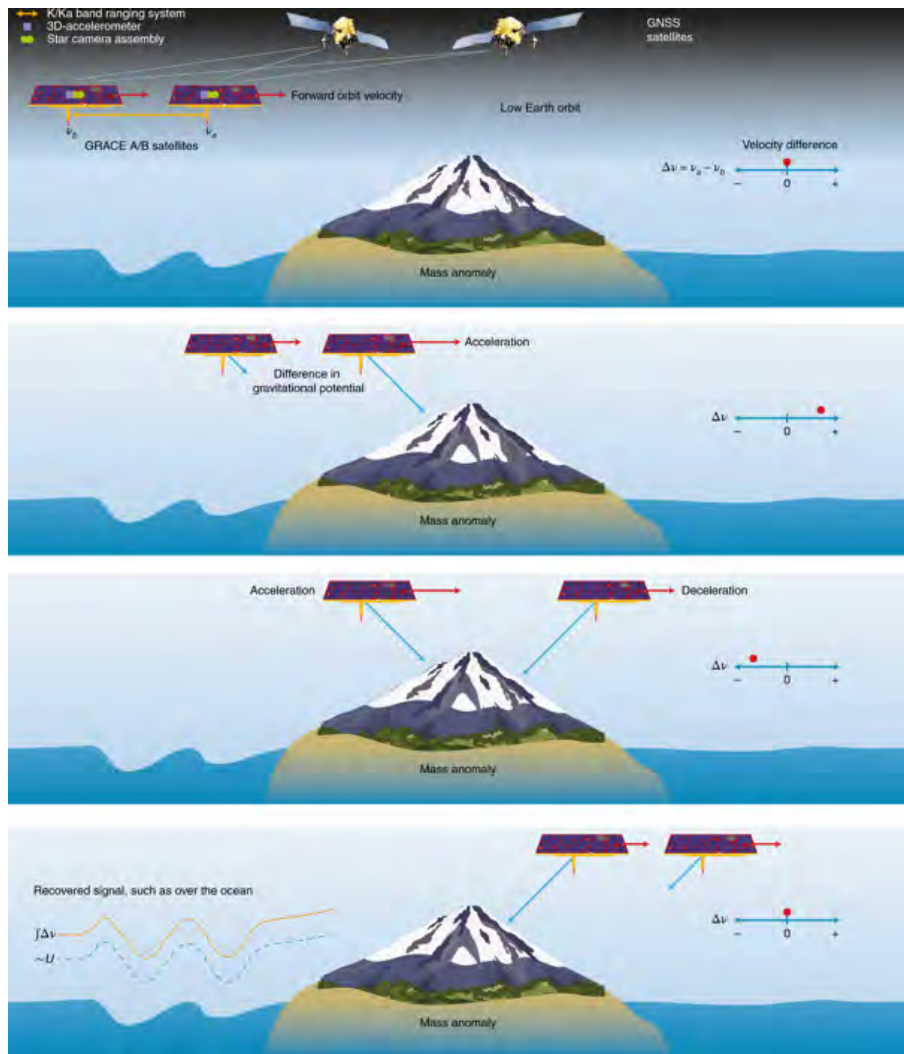


Figure 2.2: GRACE and GRACE-FO measurement is implemented by two identical satellites (GRACE A/B and GRACE C/D respectively) orbiting one behind the other in a near-polar orbit plane. The figure shows the effect on the intersatellite range and inter satellite range rate as a synthetic mass affect their orbits. Excerpt from Tapley et al. [2019]

To perform the inversion, the processing centers use as initial guess an *a priori* model of the gravity field (which can be either a static field or a mean field with time-variable components in the form of drift and periodic terms, based on an earlier release of their monthly solutions). They modify the gravity field to fit the L1 data and to reduce the residuals between the *a priori* gravity field and the retrieved gravity field (L2 products). In order to reduce the noise, they use ocean and atmosphere models (and sometimes hydrological models) to account for sub-month anomalies that would otherwise alias into the gravity solutions. They may also modify the weighting of the GPS and determine the misalignment of the KBR antennas. During the inversion procedure different processing centers use different assumptions, different parameters and different models, which lead to differences among the solutions.

The monthly-mean gravity fields known as L2 products are delivered by each processing

center using the Stokes coefficients ([Farrell, 1972; Wahr et al., 1998] and a mathematical description on the Stokes coefficients in B). There are three official mission centers from Germany and USA: [Center for Spatial Research, USA \(CSR\)](#), [GFZ](#), and [Jet Propulsion Laboratory, USA \(JPL\)](#), as well as several centers and institutions: [Groupe de Recherche de Géodésie Spatiale, France \(GRGS\)](#), [Technische Universität Graz, Austria \(TUG\)](#), [Astronomical Institute of the University of Bern, Switzerland \(AIUB\)](#), Tongji University of Shanghai, PR China, University of Luxembourg, Leibniz University of Hannover, Germany. For more details on the different European solutions, see the [European Gravity Service for Improved Emergency Management \(EGSIEM\)](#) website¹. I decided to include in the ensemble the monthly gravity fields from five processing centers: the three official mission centers ([CSR](#), [GFZ](#), and [JPL](#)), [GRGS](#) which uses different dealiasing models and a different inversion method, and [TUG](#) which applies L1 data filters previous to the inversion showing an improved signal to noise ratio [Klinger, B et al., 2016]. I included the latest updates before GRACE-FO, which are RL05 from [CSR](#), [GFZ](#), and [JPL](#), RL3.2 from [GRGS](#) and ITSG 2018 from [TUG](#).

2.1.2 Post-processing (From L2 products to water mass anomalies)

Gravity fields (L2 products) cannot be directly used to evaluate the global water budget components; they need to be post-processed first [Wahr et al., 1998]. These post-processing steps include improvement of the gravity field to correct L2 data limitations and the removal of solid-Earth changes that affect the gravity but do not cause any water mass changes.

L2 data limitations that are corrected:

- Addition of geocenter motion as it is not observable by GRACE (Detail in [2.2.1](#))
- Improving of the Earth oblateness which is poorly observed by GRACE due to its orbital configuration, known as C_{20} (Detail in [2.2.2](#))
- Filtering of anisotropic noise related to the orbital configuration of GRACE, known as stripes (Detail in [2.2.3](#))
- Correction of Leakage and Gibbs effect due to the low resolution of GRACE measurements (Detail in [2.2.4](#))

Solid-Earth changes that affect gravity:

- [GIA](#) correction (Detail in [2.2.5](#))
- Pole tide correction (Detail in [2.2.6](#))
- Impact of earthquakes (Detail in [2.2.7](#))

There are two widely used in the bibliography choices of post-processing parameters done by the GRACE science team which contributed to the generalization of the use of gravimetry data: The post-processing parameters optimized for land mass change retrieval are dedicated to hydrological studies [Swenson, 2012; Landerer and Swenson, 2012] and the post-processing parameters optimized for ocean mass change retrieval are dedicated to ocean studies [Chambers et al., 2004].

¹www.egsiem.eu

These solutions are widely used for local and regional studies but they cannot be used to estimate all the components of the global water budget in a self consistent way. By consistent I mean that the addition of the different components fulfill the closure of the global water budget. Indeed, their addition do not conserve the total mass from one month to another because of the different post-processing method choices, in particular, the choice of different cut off of the spherical-harmonics degree for land and ocean (60th and 40th respectively), the different gaussian filtering radius (300 km and 500 km, respectively) and the use of a 500 km mask from the coast in the ocean solutions.

Most gravity solutions derived from GRACE are represented in spherical harmonics (Annex B), some are based on mass concentrated (mascon) instead. Mascon solutions present several advantages as they reduce the leakage and the stripes and prevent for the Gibbs effect. However, mascon solutions present the disadvantage that the user cannot choose the post processing parameters. A fixed set of post processing parameters (as GIA correction, C_{20} replacement, geocenter motion, etc.) are embedded in each solution and can not be removed or replaced easily. On top of this, the available mascon solutions: [Goddard Space Flight Center, USA \(GCFC\) v2.3](#) [Luthcke et al., 2013], [CSR RL05.1](#) [Save et al., 2016] and [JPL RL05.1](#) [Watkins et al., 2015] do not conserve the total mass of water from one month to another at a precision smaller than 10^{-1} Gt/yr [Blazquez et al., 2018]. These two problems hamper the use of the mascon solution for my purposes.

In this PdD, I choose to create an ensemble of GRACE solutions including the most up-to-date and the largest number of post-processing parameters with the objective to explore the spread among the GRACE solutions and see if we can explain the spread in GRACE estimates of the water budget components by the spread in the post processing parameters. In my ensemble of solution, I pay a special attention to get solutions that conserve mass with an accuracy smaller than 10^{-1} Gt/yr. This is essential to get consistent estimates of the global water cycle components. In the next section, I review in detail each post processing that is used to correct GRACE solutions. For each parameter, I make a list of all state-of-the-art parameters that is available in the literature and which I used in my ensemble.

2.2 GRACE Post-processing

2.2.1 Geocenter motion

The Earth's [center of mass \(CM\)](#) is the center of the solid Earth and its fluid envelope, and is usually referred as geocenter. The geocenter is used to describe Earth's motion in inertial space and serves as the orbital center for the satellites [Wu et al., 2012]. The Earth's [center of solid Earth \(CE\)](#) is the origin in the geophysical models but its exact position remains unknown. Instead [CE](#) is approximated by [center of figure \(CF\)](#) which is the geometrical center of the Earth's surface. We use the convention that the geocenter motion is the position of the [CM](#) with respect to the [CE](#) (Fig.2.3), although in reality [CM](#) is fixed. The signature of the geocenter motion on the spherical harmonics corresponds to the degree-one via the equations 2.1 [Cretaux et al., 2002]. The differences between both centers are mainly due the fluid envelope including water transfer between ice sheets,

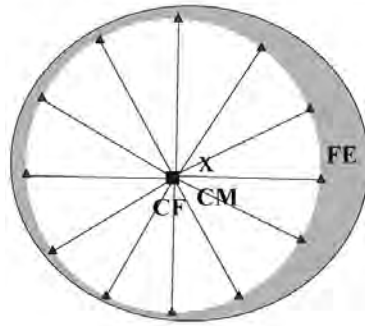


Figure 2.3: Excerpt from Wu et al. [2012]. Simplified illustration of the Center of mass (CM) and center of the figure (CF), including the solid-Earth plus the surface mass system in the fluid envelope (FE).

terrestrial hydrology, ocean, and atmosphere [Wu et al., 2012].

$$\begin{aligned}
 X &= \sqrt{3}R_{Earth} \cdot C_{11} \\
 Y &= \sqrt{3}R_{Earth} \cdot S_{11} \\
 Z &= \sqrt{3}R_{Earth} \cdot C_{10}
 \end{aligned}
 \tag{2.1}$$

GRACE mission cannot observe the degree-one term as both satellites describe orbits around the CM. However, positions on the earth surface are usually given in the CF frame because they are relative to the ground stations or they are retrieved by GPS receivers. The global water budget components measured from in situ data are expressed in the CF frame. Thus, GRACE L2 data needs to be converted from CM frame to CF frame, adding an independent geocenter motion [Swenson et al., 2008; Chambers et al., 2007].

The geocenter motion can be estimated from SLR, GPS, ocean models or joint inversions using a combination of these methods [Wu et al., 2012]. I analyse the most up-to-date estimates of the geocenter motion including: the SLR based estimated from Cheng et al. [2013b], a joint inversion with SLR and GRACE from Lemoine and Reinquin [2017], a joint inversion with GPS and GRACE from Rietbroek et al. [2016] and from Wu et al. [2017] and joint inversion with ocean models and GRACE from Swenson et al. [2008]. The latter is the most widely used in the GRACE community. A recent study based on DORIS data from Jason satellites shows a new technique to estimate the geocenter [Couhert et al., 2018]. DORIS based geocenter estimates is not included in the ensemble as it is only available for Jason 2 orbits (since July 2008).

All solutions compare well in terms of annual cycle but they show important differences in trends (Fig. 2.4 and Blazquez et al. [2018]). In fact, trends are more difficult to retrieve than the annual cycle because they are at the limit of what is achievable with some of the approaches developed so far to estimate the geocentre position [Wu et al., 2012]. Most geocenter solutions lie within the range of uncertainty of others (See Fig.2.4). There is no clear argument today in favor of one of the solution or the other [Wu et al., 2012; Riddell et al., 2017]. So, I choose to include all these state-of-the-art geocenter solutions in the ensemble that covers the GRACE period.

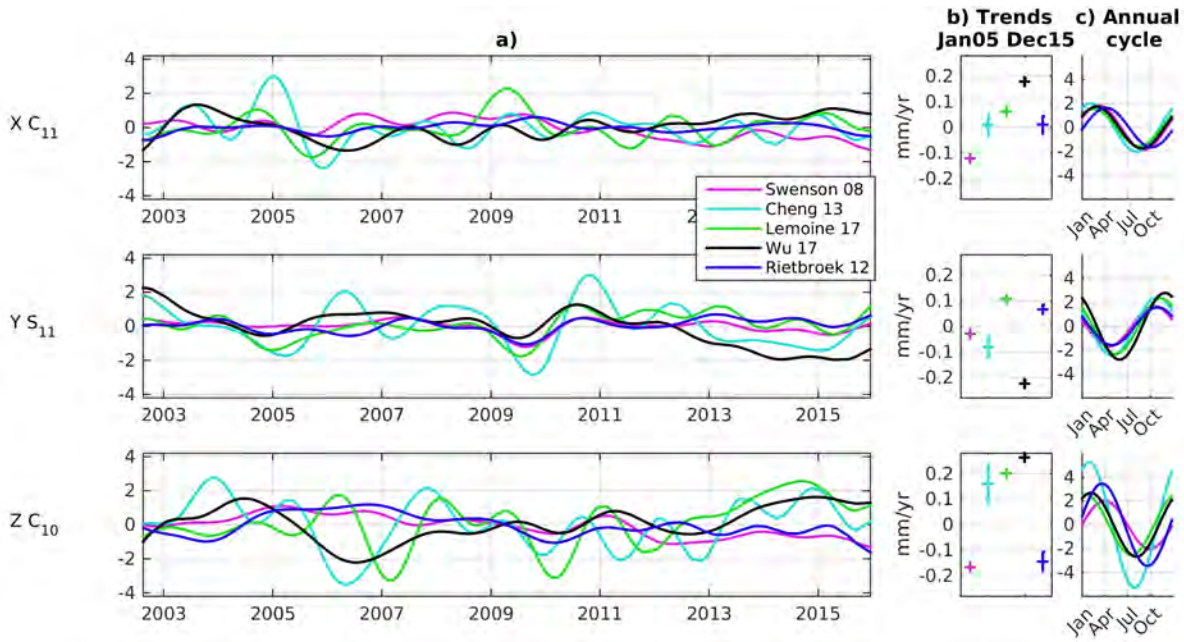


Figure 2.4: Geocenter motion in the X,Y,Z. Time-series in mm (a), associated trends over the period January 2005–December 2015 in mm/yr (b) and annual cycle in mm (c) [Swenson et al., 2008; Rietbroek et al., 2016; Cheng et al., 2013b; Lemoine and Reinquin, 2017; Wu et al., 2017; Couhert et al., 2018] A low-pass filter to remove sub-annual frequencies have been applied to the time-series. The trends are represented by error bars at 90 %CL from the individual errors. Update from Blazquez et al. [2018, Fig.1]

The geocenter correction is particularly important for the estimate of the ocean mass and the sea level budget. In Chapter 4, I discuss in more details the choice of the reference frame for the sea level budget, analyzing the impact of the reference frame in the altimetry-based sea-level change and in the gravimetry-based ocean mass change.

2.2.2 Earth’s dynamic oblateness

Due to the near-polar orbit of [GRACE](#) satellites, the satellite-to-satellite tracking technique is weakly sensitive to the nodal precession acceleration. As a consequence, the estimated Earth’s dynamic oblateness (C_{20}) is poorly retrieved [Wahr et al., 2006]. Estimates from GRACE of C_{20} are replaced by independent estimates based on [Satellite Laser Ranging \(SLR\)](#) [Cheng and Ries, 2017]. The Earth’s dynamic oblateness corresponds to the zonal degree 2 coefficient (C_{20}) also known as J_2 ($J_2 = -\sqrt{5}C_{20}$). There are two timeseries recently available in the literature that are derived from SLR: The solution from Cheng et al. [2013a] and the one from Lemoine and Reinquin [2017]. Each solution is computed considering different dealiasing models and different permanent tide conventions (Lemoine’s solution uses tide-free while Cheng’s solution uses mean tide). The difference in permanent tide conventions causes a constant bias of $42 \cdot 10^{-10}$ between both solutions ². However, in term of trends both solution present similar results for the

²computed through the equation $\Delta C_{20} = 4.228 \cdot 10^{-8} * 0.3146k_{20}$ and considering the number of love for C_{20} ($k_{20}=0.301903$ from IERS2010)

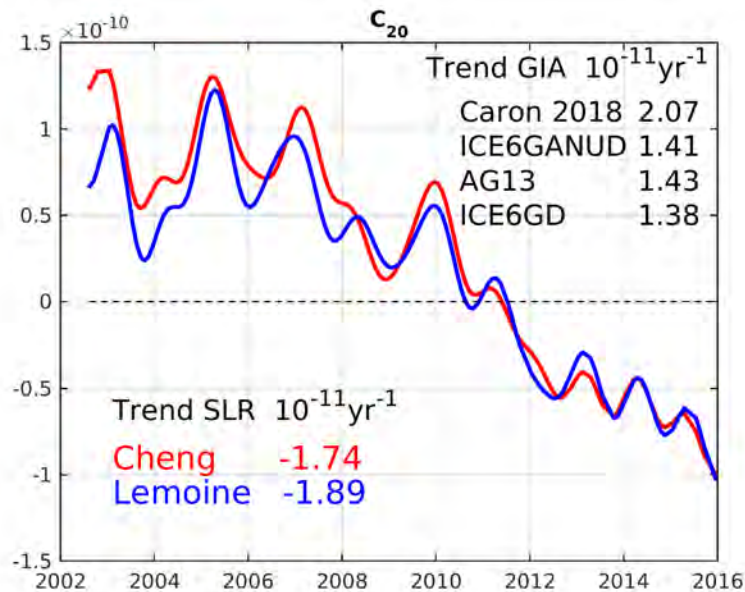


Figure 2.5: Timeseries of the C_{20} coefficient from Cheng et al. [2013a] and Lemoine and Reinquin [2017] expressed in the tide-free convention. Timeseries are centered around $-4841653.22 \cdot 10^{-10}$. Trends are computed for the period from 2002 to 2016. We also include C_{20} trends from GIA models (AG13, Caron18, ICE6G D, ICE6G ANU D) for information. Note that the sign of the trend due to the GIA is opposite to the current sign of the C_{20} trend.

period April 2002 to December 2015, $-1.74 \cdot 10^{-11}$ for Cheng’s solution and $-1.89 \cdot 10^{-11}$ for Lemoine’s solution (Fig. 2.5). We include both series in the ensemble. At the time of the writing of this manuscript, a new solution is being published [Loomis et al., 2019]. The trend in this solution is within the range of Cheng’s and Lemoine’s solutions.

2.2.3 Stripes

GRACE L2 data shows correlated errors in the high degrees (30th degree and over) [Swenson and Wahr, 2006]. This noise propagates into a north–south striping pattern when the spherical harmonics are converted into [Equivalent Water Height \(EWH\)](#). The origin of these stripes lays in the near-polar orbit of GRACE and the associated weak sensitivity of the satellite-to-satellite tracking technique to east–west gravity gradients. Instrument errors, background model inaccuracies and processing errors are minimized in the north–south direction and tend to end up in the east–west gravity gradients where the constraint from observations is weaker. This stripes hamper the retrieval of water storage variations in basins smaller than $200\,000\text{ km}^2$ [Longuevergne et al., 2010].

Before launch, the use of gaussian smoothing [Jekeli, 1981] was already suggested to correct for this problem [Wahr et al., 1998]. After the launch, an intense campaign of research developed by different teams lead to several different global filters: the empirical destriping [Chambers, 2006a; Swenson and Wahr, 2006], the Wiener filtering [Sasgen et al., 2006], the empirical orthogonal function filtering [Schrama et al., 2007], the two-step

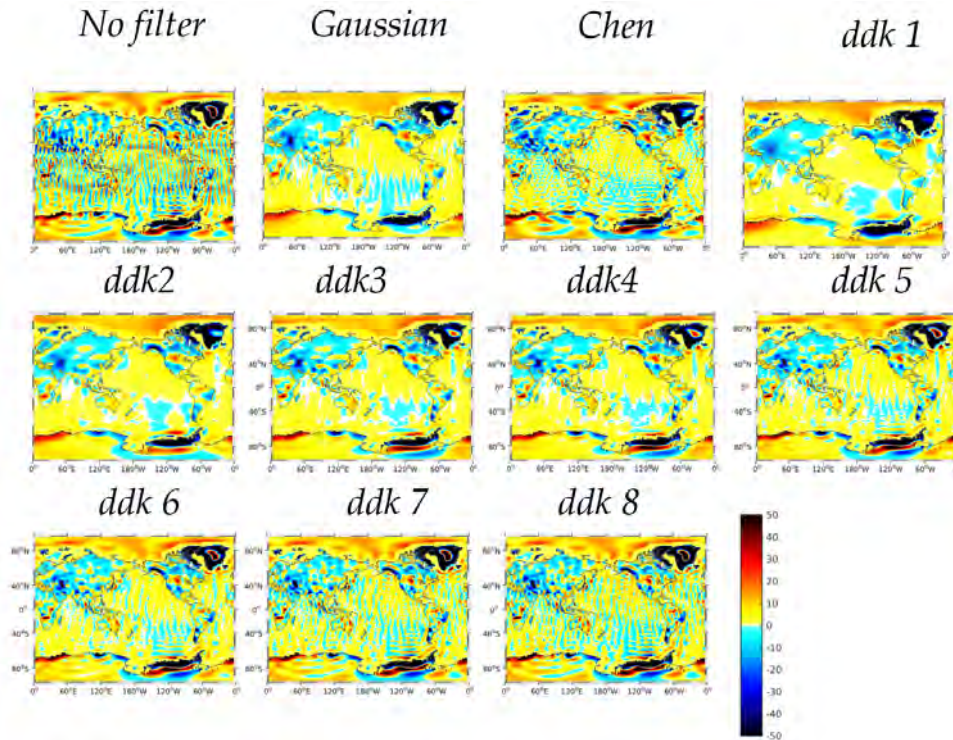


Figure 2.6: Filter comparison excerpt from [Blazquez et al., 2018, Fig S1]. The figures represents the trends for the period from 2005 to 2015

destriping methods [Swenson and Wahr, 2006; Chen et al., 2007; Khaki et al., 2018] and the smoothing with order convolution filters also known as DDK [Kusche et al., 2009]. DDK filters include a family of filters from DDK1 (strongest smoothing) to DDK8 (weakest smoothing)³. The DDK1 filter applies the strongest level of smoothing corresponding to a gaussian smoothing radius of about 530 km along the east–west direction. The level of smoothing decreases to the DDK8 filter, which applies the weakest level of smoothing corresponding to a gaussian radius of 200 km. For a complete review on filtering techniques see Frappart et al. [2016].

GRGS developed a different approach for filtering the noise. Since 2013, they use a truncated single value decomposition scheme for the inversion instead of a classical Choleski inversion. This method reduces drastically the noise but on the other hand the coefficients of high degree where information is scarce are normalized to the mean coefficients [Lemoine et al., 2016]. With this approach, GRGS GRACE solutions are already filtered during the inversion process and therefore they do not need post-processing filtering after the inversion.

In my ensemble of solution, I decide to use DDK3, DDK4, DDK5, and DDK6 (Fig.2.6) because it is a good compromise between the signal to noise ratio in the high order coefficients and the efficiency of the destriping in the ocean (See the coastal ocean around ice sheets in particular in Fig. 2.6). I discarded DDK7 and DDK8 from the ensemble, because the signal/noise is too weak and the destriping is inefficient the ocean (Fig.2.6).

³Visualization of the filter-kernels at http://icgem.gfz-potsdam.de/Visualized_DDKkernels.pdf, provided by Roelof Rietbroek

I also discard DDK1, DDK2, gaussian, and Chen filters because the large smoothing increase the leakage from the ice sheet mass change signal far into the ocean.

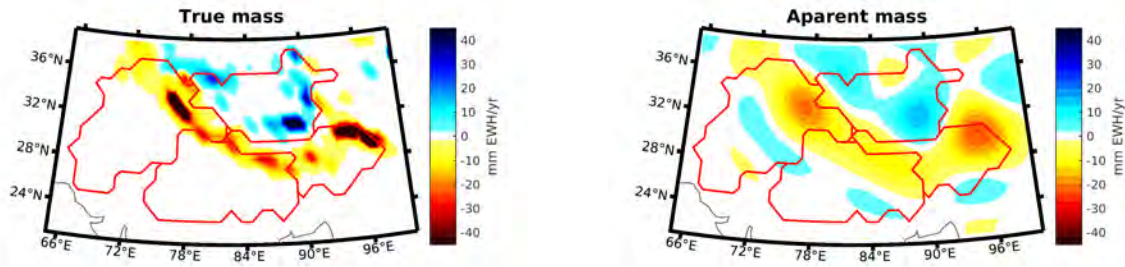
Filtering reduces the stripes by attenuating the noise but the mass change signal is also attenuated, specially at local scale. In order to compensate this attenuation, some authors propose to use scale factors, including external information from hydrological models [Landerer and Swenson, 2012]. This scale factors do not respect the total water conservation as they modify the mass change in certain basins and they are not defined neither for the cryosphere nor for the ocean. I decided not to include any scale factor in the ensemble. However, the inclusion of different filters with different degrees of attenuation in the ensemble allows to explore the sensitivity of the uncertainty to this parameter.

2.2.4 Leakage and Gibbs effect

The noise present in the high degree coefficients of GRACE L2 spherical harmonics hampers the extraction of the small scale variations in mass and thus high degrees are not accurately resolved in GRACE solutions. The lack of high degree coefficients manifests in two different ways: (1) the leak of the strong and sharp signal over the surroundings, known as leakage, and (2) the spatial oscillations of the mass signal before and after a sharp change, known as Gibbs effect. Both effects are important in areas where signal present sharp gradients in small regions as in the coast where land signal is much stronger than ocean signal or in mountains where glaciers loose mass quickly in response to the local warming and the local change in precipitation (See Fig.2.7a). I represent on Figure 2.7a, a synthetic mass change trend over South Asia including glacier mass change and lake mass change. After adding noise in the high degrees to simulate the observability of GRACE, the mass change field over the same region includes leakage around the sharp changes (around 300 km) and Gibbs effect further away (between 300 km and 1000 km) (See Fig. 2.7b).

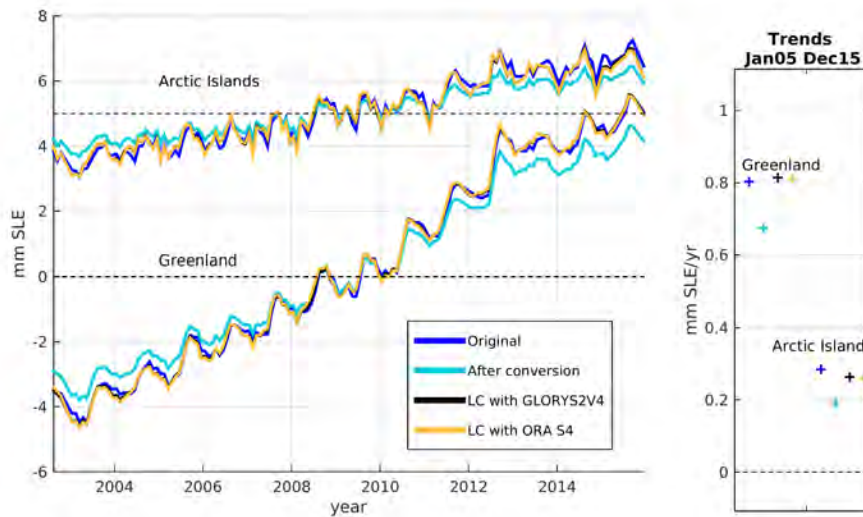
There are several treatments in the literature to reduce the uncertainty due to the leakage and Gibbs effects: the spatial kernels or averaging functions [Velicogna and Wahr, 2006; Rodell et al., 2009], the forward modeling [Chen et al., 2015], and mascons [Luthcke et al., 2013]. Spatial kernels are designed to retrieve local information and it cannot be used at global scale. Forward modeling assumes spatial distribution and it is used to accurately estimate Antarctica and Greenland mass loss, but it tends to overestimate some trends in HMA [Long et al., 2016]. Forward modeling consists in retrieving a synthetic field which fits the observed field when the same cut off of high degrees and filtering is applied.

I decide to develop my own method to reduce land/ocean leakage [Blazquez et al., 2018] based on model comparison to get a method that works at global scale and that ensures mass conservation. I use a model base approach as in Landerer and Swenson [2012]. I correct for the land leakage signal into the ocean by using an independent reference estimate of the ocean mass variations. The reference ocean mass estimate is based on ocean reanalyses: ORA S4 [Balmaseda et al., 2013] and GLORYS2V4 [Garric et al., 2018]. Both reanalysis include altimetry, steric and ocean dynamics in their core. From the reference ocean mass estimate, I compute for each gridpoint in the coastal ocean, monthly mass anomalies (with respect to the local average over 2005–2015). I



(a) Synthetic mass trend field over South Asia including glacier mass change and lake mass change

(b) Apparent mass change field over the same region including leakage and Gibbs effects



(c) Evaluation of the land/ocean leakage correction on a synthetic field. Timeseries and their associated trends over 2005-2015. We represent the original synthetic field, the apparent field (with leakage) and the result of both Leakage Corrections (LC)[Blazquez et al., 2018, Fig.S3]

Figure 2.7: Examples of Leakage and Gibbs effect

assume these monthly mass anomalies from the reanalyses as references and I consider that any difference between these anomalies and GRACE anomalies at the same location is land leakage signal in GRACE solutions. I correct GRACE solutions for this land leakage signal by transferring the signal from the coastal ocean gridpoints to the closest land gridpoint. I apply this correction to all ocean gridpoints located in the coastal ocean. The coastal ocean defined as the ocean within 300 km from the coast. Once corrected, I verify that the new mass distribution conserves the total amount of water at global scale. I assume the spread between both corrected solutions as the uncertainty due to the leakage correction.

I validated this method using a synthetic field over Greenland, the Arctic Islands and the ocean around them (dark blue in Fig. 2.7c). I simulate leakage and Gibbs effect by

converting the synthetic field into a spherical harmonics expansion upto the 256th order and degree and then back to equivalent water height after cutting at the 60th order and degree (light blue in Fig. 2.7c). I applied the land/ocean leakage correction using both ocean reanalyses and I retrieved the original signal with an accuracy smaller than ± 0.1 mm SLE and ± 0.01 mm SLE/yr (black and brown in Fig. 2.7c).

In order to reduce the uncertainties in the land water mass changes, I propose a land leakage correction over the continents based on a similar method, where independent observations of mass changes of glaciers and lakes are used as *a priori* references for mass changes. This method allows to reduce the uncertainties at a local scale and to better disentangle changes in glacier and lake mass and TWS mass. I discuss this method and its implications in Chapter 3.

2.2.5 Glacial isostatic Adjustment

Gravity field is affected by the solid-Earth visco-elastic response to the melting of the continental ice sheets after the **Last glacial maximum (LGM)**, around 21 thousand years ago. This visco-elastic response is known as **Glacial Isostatic Adjustment (GIA)**. In order to retrieve the water mass change, we need to correct for this gravity **GIA** signal [Peltier, 2004]. **GIA** models differs on the rheology of the mantle, the continental ice sheets history and the sea level history since the **LGM** and the spatial coverage (global or regional).

Regional models use improved rheology of the mantle and modify regional deglaciation history to better fit local uplifts obtained by modern geodetic techniques such as GPS measurements. There are regional **GIA** models over Antarctica [Whitehouse et al., 2012] and Greenland [Khan et al., 2016]) among other regions. However, these regional models are not aimed at conserving the total amount of water in the Earth’s system and often they are not defined out of their region of interest. In this work, I will only focus on global models because unlike regional models they assure the conservation of mass at global scale.

Table 2.1: **GIA** corrections for the gravity and altimetry fields. values are expressed as apparent mass in mm SLE/yr. Red values corresponds to the extreme values. First 4 models are compared in Fig 2.8, the rest are listed for comparison.

Product	Reference	Gravity						Altimetry
		Ocean	Green-land	Antarc-tica	Arctic Islands	North America	Rest of land	
ICE6G D	[Peltier et al., 2017]	-0.89	0.01	0.20	0.05	0.42	0.21	-0.37
AG13	[A et al., 2013]	-0.95	0.00	0.32	0.05	0.43	0.15	^a
ICE6G D ANU ^b	[Purcell et al., 2018]	-0.68	0.00	0.18	0.04	0.32	0.14	^a
Caron	[Caron et al., 2018]	-0.84	0.03	0.19	0.04	0.60	-0.03	^a
ICE6G ANU	[Purcell et al., 2016]	-0.72	0.01	0.19	0.04	0.32	0.16	^a
ICE6G C rc	[Stuhne and Peltier, 2015]	-0.92	0.00	0.20	0.06	0.44	0.22	-0.43
ICE6G C	[Stuhne and Peltier, 2015]	-0.92	0.01	0.23	0.05	0.41	0.22	-0.39
W12a	[Whitehouse et al., 2012]	^c	^c	0.12	^c	^c	^c	^c
K16	[Khan et al., 2016]	^c	0.04	^c	^c	^c	^c	^c

^a No value for the change of isopotential of the geode. (Personal communications)

^b Values are slightly different than [Blazquez et al., 2018, Table S1] due to a correction of the degree-one and C_{21}/S_{21}

^c Local model, non defined in this region

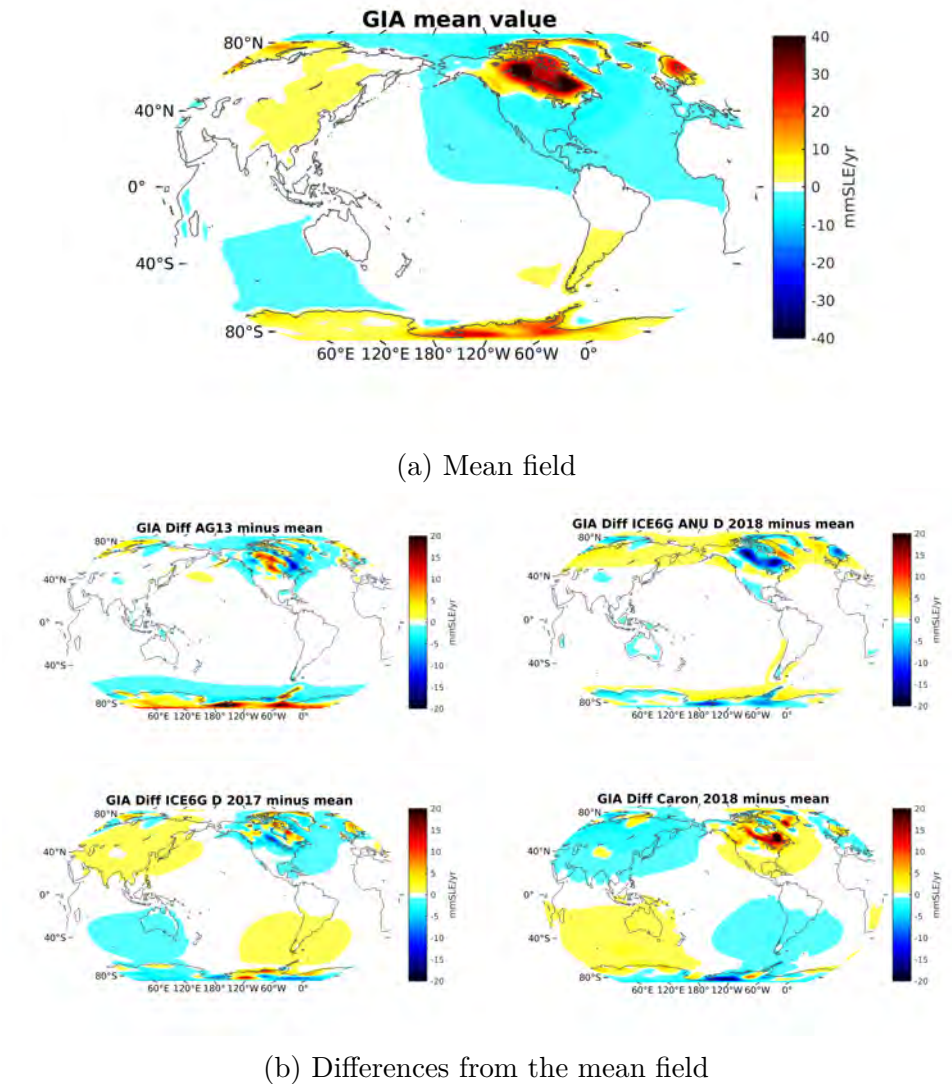


Figure 2.8: Rates of gravitational GIA correction in mm [EWH](#)/yr. Mean field (a) and difference between each product and the mean field (b). Note that there is a scale factor of 2 between bottom and top panels.

GIA models are delivered as Stokes coefficients (See Annex B). These Stokes coefficients are adimensional and they can be used to compute the gravity GIA signal (expressed as apparent mass in mm [EWH](#)/yr or as mm SLE/yr) as well as altimetry GIA correction (see [1.3.3.1](#)). The altimetry GIA correction is computed in a rotating frame (applying a scaling factor of 2.06 to C_{21}/S_{21}) and including the term to the change of isopotential of the geode [Tamisiea, 2011].

The Gravity GIA correction affects mainly the regions that were covered by former large ice sheets in the [LGM](#) like North America (Laurentia), the Baltic region (Fennoscandia) and Antarctica (See gravity mean field in Fig.2.8a). These regions presents also the largest spread among the models (Fig.2.8b). GIA gravity correction in North America is between 0.32 to 0.62 mm SLE/yr while in Antarctica is between 0.18 to 0.32 mm SLE/yr (Table 2.1). These values are even larger ,from 0.08 to 0.32 mm SLE/yr , when including local

models [Martin-Español et al., 2016].

Small differences in the low degrees of the GIA models (C_{20} in Fig. 2.5 and C_{21}/S_{21} in Fig. 2.9b) lead to a large spread in ocean gravity GIA correction (between -0.68 and -0.95 mm SLE/yr from Table 2.1).

Because of the absence of clear argument in favor of one or the other GIA model. I choose to include the most up-to-date GIA model from the literature in the ensemble (ICE 6G D, ICE 6G D ANU and AG13). Caron’s GIA model was not available at the time of the writing of Blazquez et al. [2018]. It is interesting to highlight that most of the publications related to the ocean mass before 2018 use AG13 gravity correction, which gives extreme values for the ocean and Antarctica GIA corrections.

2.2.6 Pole tide

The pole tide is the combination of the solid-Earth pole tide and the oceanic pole tide. The pole tide is the response to polar motion which is the motion of the rotation axis. Polar motion and the associated pole tide, occur mainly at annual and Chandler (14 months) timescales, and at long term variations. Polar motion has been accurately modeled (International Earth rotation and Reference system (IERS) 2003, IERS 2010) at sub-decadal scales. Since we only have accurate data since 1875, long-term movement is not yet fully understood [Wahr et al., 2015].

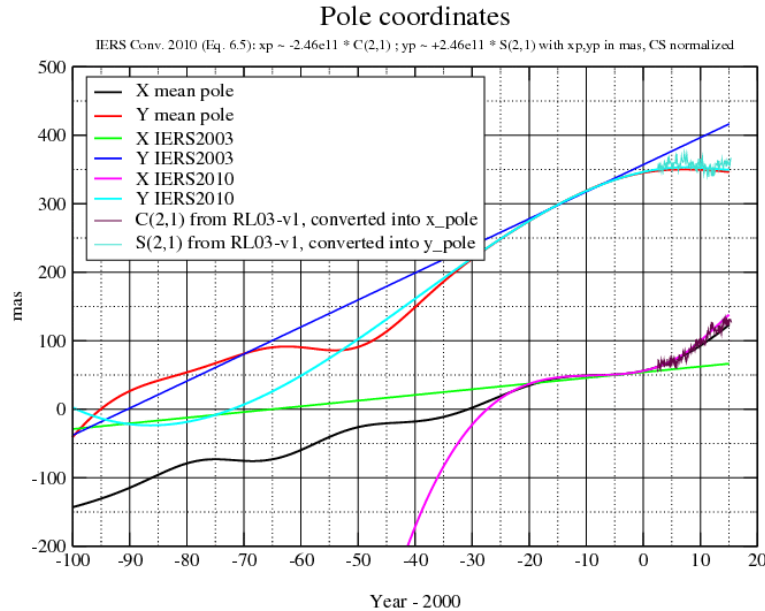


Figure 2.9: X mean pole and Y mean pole extracted from 115 years of observations after removing the Chandler period and annual cycle. IERS 2003 standards, IERS 2010 standards and C_{21}/S_{21} from GRACE GRGS RL03 v1. All values are expressed in mas (milliarcsecond)

Pole tide affects gravity harmonics of degree 2, order 1 (C_{21} , S_{21}) [Gross, 2007]. I repre-

sent in Figure 2.9 the observed mean pole for the last 100 years, the models from IERS2003 and IERS2010, and the timeseries from GRGS GRACE. There are a good agreement between the mean pole, IERS2010 and GRACE C_{21} , S_{21} during the GRACE period. However, there is a disagreement before 1960 between the mean pole and IERS2010. IERS2010 has been recently corrected for the long term pole motion after 2010 [Wahr et al., 2015].

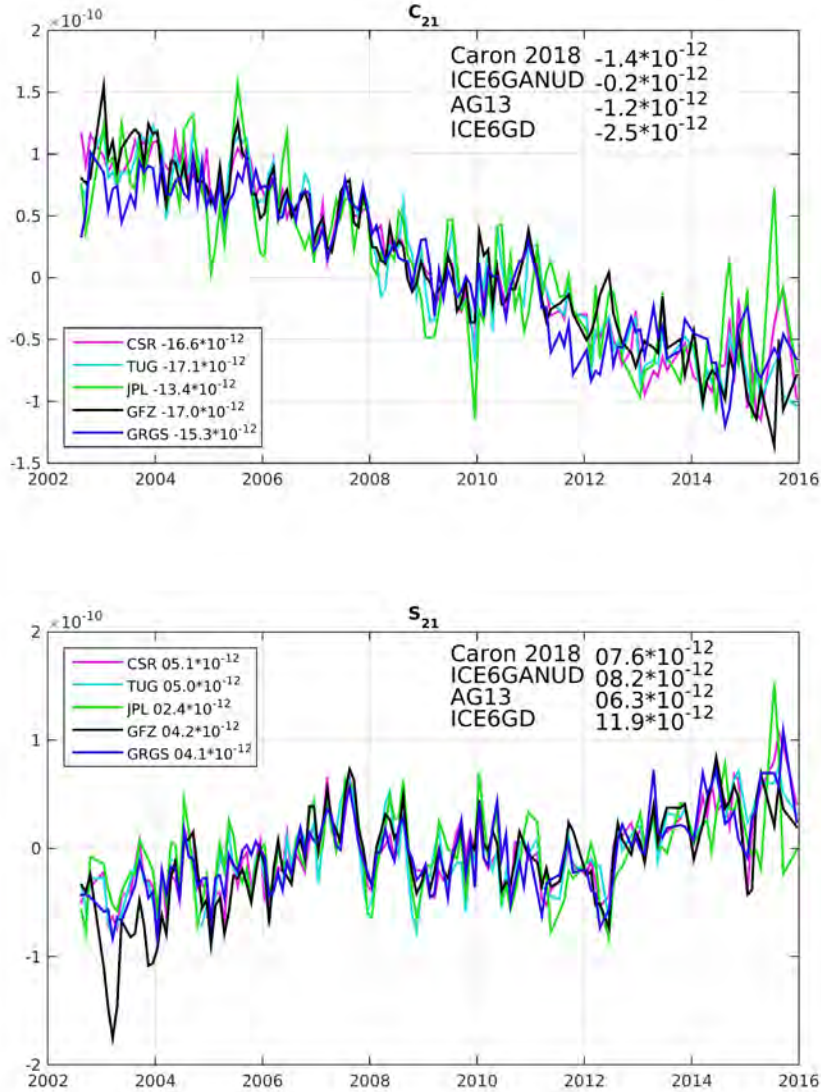


Figure 2.10: Timeseries for C_{21} S_{21} from CSR, GFZ, GRGS, JPL and TUG. Values in the legend and in the box corresponds to the trends for the period 2003-2015

The cause and the sources of this long term motion are still an open question. Some authors suggest that the significant variability in polar motion at periods much longer than a year is caused either by present-day variations in surface loads in response to current ice melt in mountains and ice sheets or by GIA [Wahr et al., 2015].

C_{21} and S_{21} trends for the period 2003 to 2015 from GRACE L2 solutions is $-16.0 \pm$

$2.8 \cdot 10^{-12}$ and $4.2 \pm 1.8 \cdot 10^{-12}$, respectively (See individual trends Fig. 2.10). While C_{21} and S_{21} trends in GIA models is $-1.3 \pm 1.6 \cdot 10^{-12}$ and $8.5 \pm 4.0 \cdot 10^{-12}$, respectively (See individual trends in Fig. 2.10). The difference between the C_{21} and S_{21} observed by GRACE and the pole tide explained by GIA is responsible for a decrease in ocean mass trend of 0.11 mm SLE/yr.

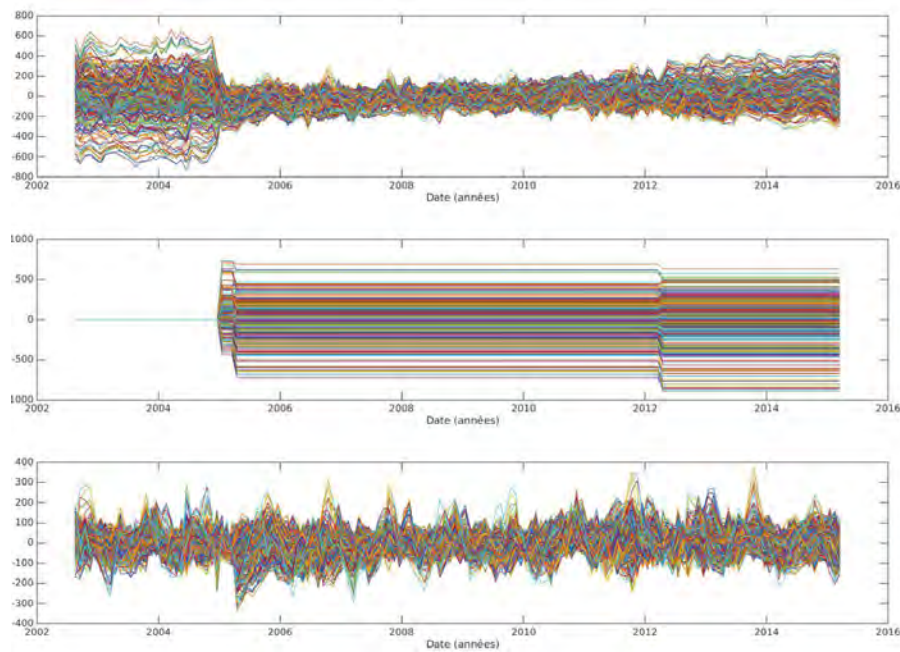
I do not consider pole tide as a post-processing parameter in the ensemble because there are no alternative pole tide correction to the correction from Wahr et al. [2015]. However, I would like to further investigate this post-processing in the future because it could explain part of the disagreement we find between gravimetry, altimetry and steric at regional scale (See Chapter 4 for more details). There is a need to understand the differences in C_{21} and S_{21} among GIA models, among GRACE L2 solutions and between GIA models and GRACE L2 solutions. This is one of the open issues to tackle.

2.2.7 Earthquakes

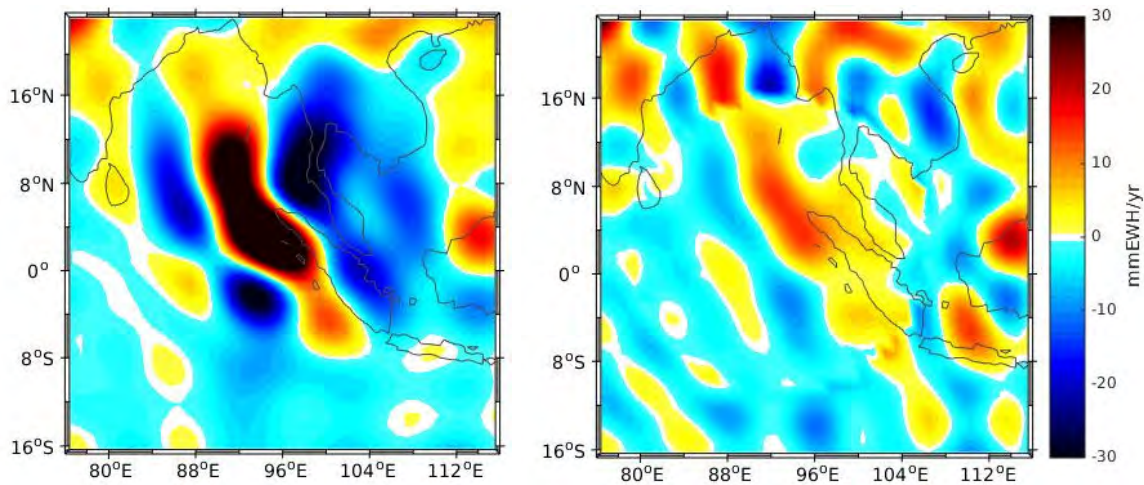
Earthquakes affect the gravity field through two different processes: they displace the density interfaces and they change the density dilatation [Panet et al., 2007]. They present a very local effect and hamper the isolation of the local water long term signals unless they are corrected for with independent models. However at regional and global scales their impact is estimated under 0.2 mm SLE/yr for the period from 2003 to 2015 [Reager et al., 2016].

There is no general consensus on how to separate the gravity field due to the earthquakes and due to the water mass transfers. Most of the studies focus only on one earthquake. Due to the different causes of each earthquake, results are difficult to extrapolate from one case to another [Han et al., 2013; Panet et al., 2018]. During Alexandre Mignucci internship that I supervised, Alexandre and I analysed earthquakes in order to propose a method to extract the gravity signal due to the earthquakes and which conserves the global water mass [Mignucci and Blazquez, 2016, Unpublished, available on demand].

During this internship, Alexandre characterized 4 types of earthquakes depending on the co-seismic jump, the annual signal and the presence of more than one earthquake during the studied period. He was able to propose a preliminary method to remove the earthquake signal for three earthquakes: Sumatra 2004 (Indonesia), Tohoku-Oki 2011 (Japan) and Near Bio Bio 2015 (Chile). I present in Figure 2.11 a synthesis of the method for the Sumatra region which was affected by earthquakes in December 2004, Mars 2005 and April 2012. Figure 2.11a present the equivalent water mass anomalies for every position in 2000 km near the earthquakes, before the correction (top panel), the coseismic jump correction (middle panel) and time series after correction (bottom panel). The correction only includes the coseismic jump with no post seismic relaxation (See large peak in the first months after the 2002 earthquake in Fig 2.11 a bottom panel). However with this preliminary method, we have been able to extract most of the signal and to retrieve the water mass trends (Figure 2.11b). Results were encouraging for these regions, but the method is still to be validated and generalized.



(a) Water mass timeseries in mm EWH near Sumatra before correction (top) Proposed correction including only coseismic jumps for the three earthquakes: December 2004, Mars 2005 and April 2012 (middle) and Water mass timeseries after correction (bottom). Note that scales are different at each panel.



(b) Trend map in mm EWH/yr before (left) and after correction (right)

Figure 2.11: Impact of the Earthquake correction on the Water mass timeseries and trends. Extract from Mignucci’s internal report [Mignucci and Blazquez, 2016]

2.3 Applications of the ensemble of GRACE solutions

2.3.1 Comparison of the global water budget components with previous studies

After analyzing the available post-processing possibilities, I created an ensemble including all solutions using all state-of-the-art post processing parameters. Then, I analyzed the range in GRACE estimates of the water budget components due to the spread in these parameters. I assumed the spread in my ensemble of GRACE solutions to be representative of the uncertainty in GRACE estimates of the water budget components. On this basis, I can explore the uncertainty in GRACE estimates and find the parameters that are responsible for this uncertainty.

Ocean mass, Greenland, Antarctica and Arctic Islands trend estimates from the ensemble are in agreement with previous published estimates, except two ocean mass trend estimates [Yi et al., 2015; Dieng et al., 2017] (Fig.2.12). The general agreement gives confidence in the choice of post-processing parameters.

2.3.2 The global water budget and its uncertainties analyzed with my ensemble of GRACE solutions

With this ensemble, the ocean mass trend for the period from January 2005 to December 2015 is estimated at 1.55 ± 0.33 mm/yr. This uncertainty of ± 0.33 mm/yr is mainly due to the uncertainties in geocenter trends and in GIA gravity corrections.

Greenland is the main contributor to the global water budget with 0.80 ± 0.03 mm/yr for the period from 2005 to 2015, followed by Antarctica with 0.61 ± 0.15 mm/yr (Fig. 2.13). Uncertainty in Antarctica mass balance comes mainly from GIA (Table 2.2). I excerpt the arctic islands contribution from the rest of the glaciers as their are not lumped with TWS. I estimated their trend at 0.27 ± 0.03 mm/yr while the rest of glaciers and TWS contribution is -0.14 ± 0.33 mm/yr. Uncertainty in the glacier and TWS mass trends is correlated with the uncertainty in ocean mass trend as their uncertainty is caused by the same post-processing parameters (geocenter and GIA from Table 2.2)(Scientific question 2).

The interannual variability of glaciers & TWS drives the interannual variability of the ocean mass, while the rest of the contributions are responsible for the trends. The negative trend of glacier and TWS mass is very dependent on the time span because of this interannual variability.

I analyze the acceleration in ocean mass by comparing two 7-years periods: the period from August 2002 to December 2008 and the period from February 2009 to December 2015. I find a trend increase from 0.77 ± 0.73 mm/yr to 1.99 ± 0.39 mm/yr. I found significant acceleration in Greenland mass loss where trend increase from 0.62 ± 0.04 mm/yr to 0.86 ± 0.04 mm/yr for the two periods and a significant acceleration in Antarctica mass loss where trend increase from 0.30 ± 0.18 mm/yr to 0.76 ± 0.15 . There is no significant

increase in trends for the arctic islands mass loss where trends increase from 0.24 ± 0.05 mm/yr to 0.29 ± 0.04 mm/yr. Concerning the glacier & TWS mass loss trends variations are not significant, they vary from -0.17 ± 0.59 to 0.16 ± 0.35 for the two 7 years period. Confirming previous results [Yi et al., 2015], I find that the ocean mass acceleration observed in the last two decades is due to a net increase of Greenland and Antarctica contribution and the effect of the large interannual variability from TWS.

Although acceleration in Greenland in Antarctica mass loss is significant, trends ex-

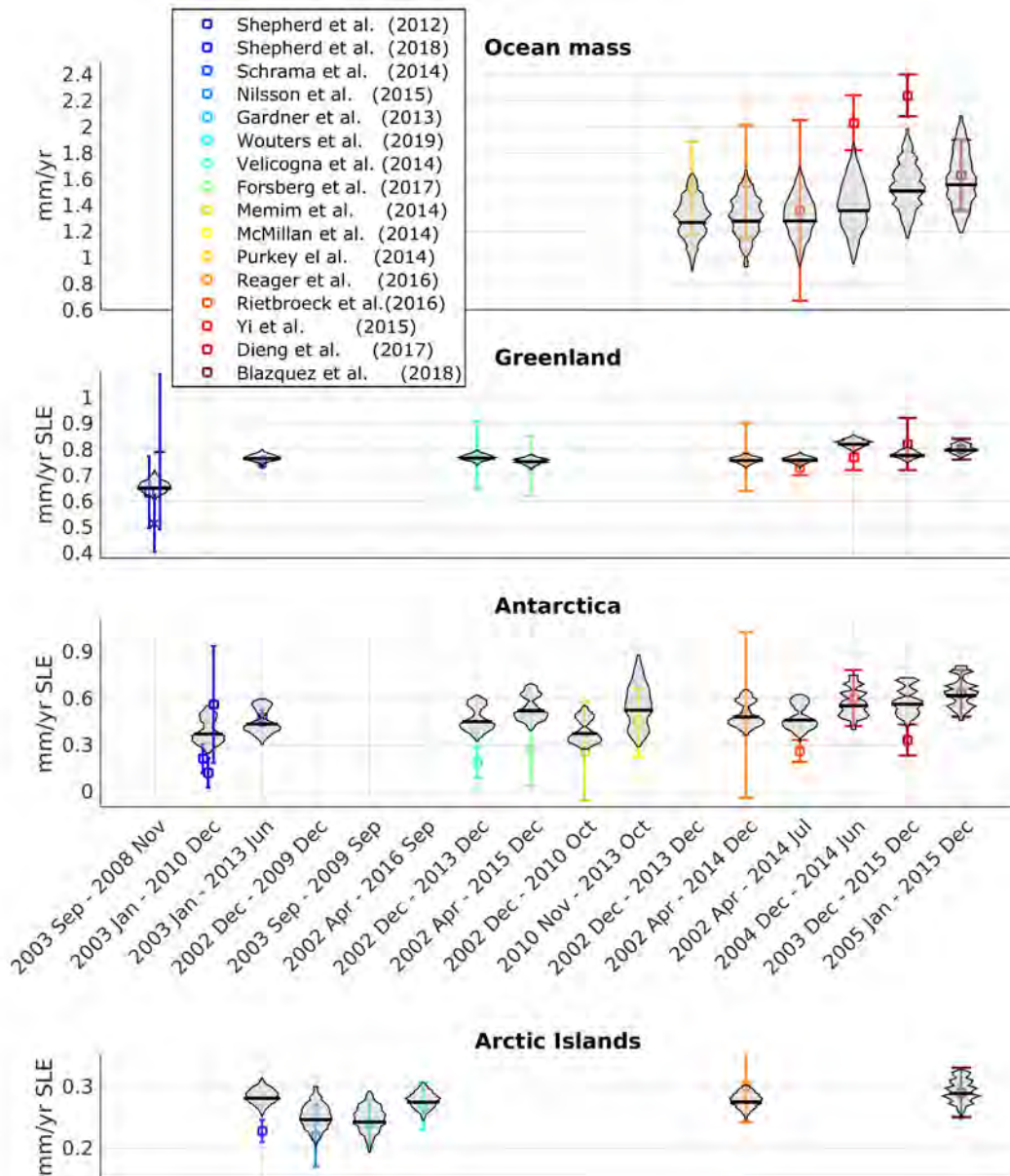


Figure 2.12: Comparison of GRACE LEGOS ensemble V1.1 with previous estimates of some of the water budget components trends. Vertical lines represent 90% CL around the mean values and the grey shaded areas the distribution of trends from GRACE LEGOS V1.1.

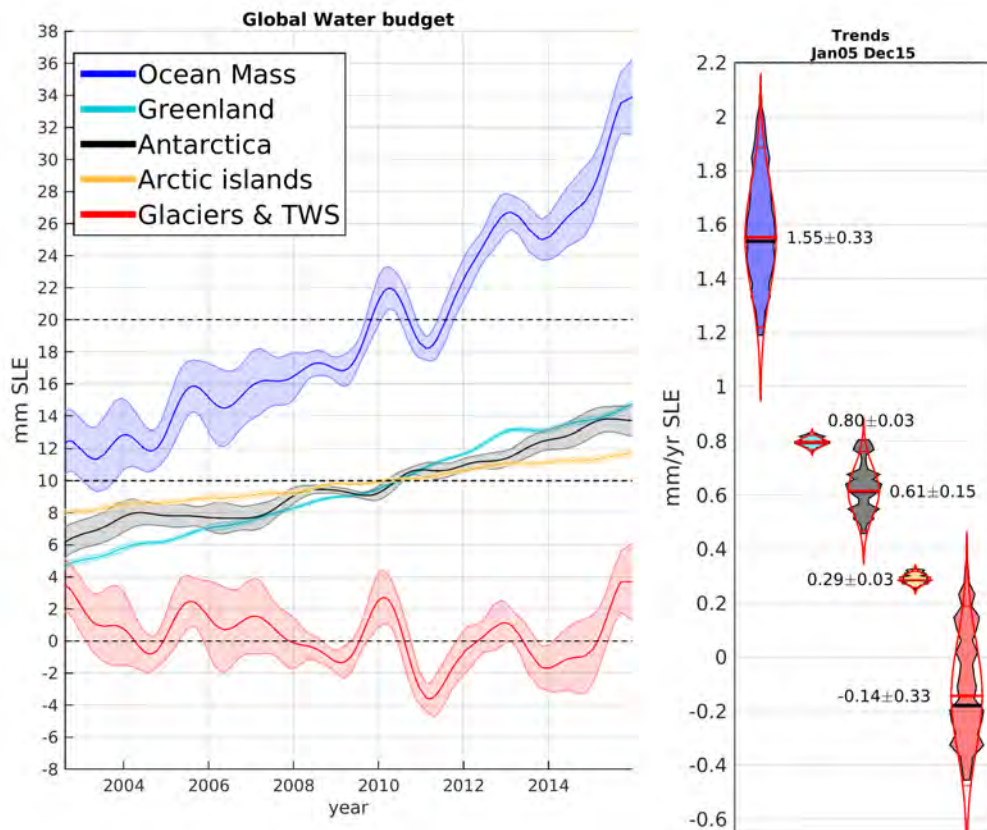


Figure 2.13: Time-series of the global water budget components after applying a low-pass filter to remove sub-annual frequencies (left) and their trends distributions for 2005–2015 (right). In the left panel, the shaded areas correspond to the distribution of the timeseries while the lines correspond to the mean values at each month. In the right-hand panel, the shaded areas indicate the distribution of trends, while the red lines indicate the distribution that would be obtained under the assumption of a Gaussian distribution. Uncertainties are expressed at 90 % CL. For comparison, estimates have been offset in the left-hand panel. Updated from Blazquez et al. [2018, Figure 5] using GRACE LEGOS ensemble 1.1

tracted from time spans of 7 years are not necessarily representative of the long term trend in response to the climate change. This means that although the acceleration is real, I cannot link it to the current climate because the time series are too short (Scientific question 3).

2.3.3 Article: "Exploring the uncertainty in GRACE estimates of the mass redistributions at the Earth surface: implications for the global water and sea level budgets"

I include here the article Blazquez et al. [2018] that summarizes most of the information included in this chapter. Before I include a brief summary of the review process and the

Table 2.2: Trends and uncertainties of GRACE estimates of the global water budget for the period from 2005 to 2015. First two lines correspond to the mean trends and the uncertainty at 90 % CL. The next lines are the uncertainties associated to each post-processing parameters. All numbers are expressed in mm SLE /yr. Updated from Blazquez et al. [2018, Table 1]

	Ocean	Greenland	Antarctica	Arctic Islands	glaciers	TWS
Trends	1.55	0.79	0.61	0.28		-0.14
Uncertainty	0.33	0.02	0.14	0.03		0.33
processing center	0.07	< 0.01	0.04	< 0.01		0.06
geocenter	0.27	0.02	0.08	0.02		0.30
C ₂₀	0.01	< 0.01	0.01	< 0.01		< 0.01
Filtering	< 0.01	0.01	< 0.01	< 0.01		0.02
GIA	0.16	< 0.01	0.11	0.01		0.08
Leakage correction	0.08	< 0.01	< 0.01	< 0.01		0.08

evolution of the geocenter solutions during the past 2 years. The article was judged pertinent and of good quality in all the revisions but it encountered reluctance to the use of several geocenter solutions.

In the first submission, the spread we found in the ocean mass trends of ± 0.30 mm SLE/yr was judged "unrealistic" and the revision focused around the pertinence of including the geocenter solution from Lemoine and Requin [2017] to infer GRACE-based estimates of the global water cycle. Although within the uncertainties of the geocenter trends [Wu et al., 2012], this timeserie was considered an outlier by one reviewer and there was a major revision to remove this timeserie. We decided to support our choice including more geocenter solutions from Rietbroek et al. [2016]; Wu et al. [2017]. The inclusion of these series further increased the large spread in the geocenter Y and Z trends as also suggested in other publications [Wu et al., 2012; Riddell et al., 2017] (see Fig. 2.4). As a consequence, the uncertainty in the ocean mass trend rose to ± 0.55 mm SLE/yr. The uncertainty was even larger than in the previous submission but it was the result of including the state-of-the-art in geocenter solutions. We also decided not to resubmit to the same journal as it appeared that the editor/reviewer would not accept our choice to keep the spread in geocenter trends.

In a new submission, geocenter solutions used were still the main point of the revision. Further, an anonymous reviewer analyzed the geocenter solutions, and suggested improvement in the geocenter solutions. We had to come back to these authors to request corrected time series. All these changes reduced the spread in Z geocenter trend from ± 0.4 mm/yr for the period from Jan2005 to Dec 2015 to ± 0.2 mm/yr, reducing the uncertainty in Ocean mass trend for the same period from ± 0.55 mm SLE /yr to ± 0.27 mm SLE/yr.

Once these updated data were included, the article was finally published in July 2018, almost two years after its initial submission, more than six reviewers and several corrections in the geocenter solutions.

Exploring the uncertainty in GRACE estimates of the mass redistributions at the Earth surface: implications for the global water and sea level budgets

A. Blazquez,^{1,2} B. Meyssignac,^{1,2} J.M. Lemoine,^{2,3,4} E. Berthier,¹ A. Ribes⁵ and A. Cazenave¹

¹LEGOS, Université de Toulouse, CNES, CNRS, UPS, IRD, 31400 Toulouse, France. E-mail: alejandro.blazquez@cnes.fr

²CNES, 31400 Toulouse, France

³GET, Université de Toulouse, CNRS, IRD, UPS, 31400 Toulouse, France

⁴GRGS, 31400 Toulouse, France

⁵CNRM, Météo France – CNRS, 31100 Toulouse, France

Accepted 2018 July 19. Received 2018 July 10; in original form 2017 November 08

SUMMARY

Observations from the Gravity Recovery and Climate Experiment (GRACE) satellite mission provide quantitative estimates of the global water budget components. However, these estimates are uncertain as they show discrepancies when different parameters are used in the processing of the GRACE data. We examine trends in ocean mass, ice loss from Antarctica, Greenland, arctic islands and trends in water storage over land and glaciers from GRACE data (2005–2015) and explore the associated uncertainty. We consider variations in six different GRACE processing parameters, namely the processing centre of the raw GRACE solutions, the geocentre motion, the Earth oblateness, the filtering, the leakage correction and the glacial isostatic adjustment (GIA). Considering all possible combinations of the different processing parameters leads to an ensemble of 1500 post-processed GRACE solutions, which is assumed to cover a significant part of the uncertainty range of GRACE estimates. The ensemble-mean trend in all global water budget components agree within uncertainties with previous estimates based on different sources of observations. The uncertainty in the global water budget is $\pm 0.27 \text{ mm yr}^{-1}$ [at the 90 per cent confidence level (CL)] over 2005–2015. We find that the uncertainty in the geocentre motion and GIA corrections dominate the uncertainty in GRACE estimate of the global water budget. Their contribution to the uncertainty in GRACE estimate is respectively ± 0.21 and $\pm 0.12 \text{ mm yr}^{-1}$ (90 per cent CL). This uncertainty in GRACE estimate implies an uncertainty in the net warming of the ocean and the Earth energy budget of $\pm 0.25 \text{ W m}^{-2}$ (90 per cent CL) when inferred using the sea level budget approach.

Key words: Global change from geodesy; Satellite geodesy; Sea level change; Time variable gravity.

1 INTRODUCTION

The Gravity Recovery and Climate Experiment (GRACE) mission sponsored by the National Aeronautics and Space Administration and the Deutsches Zentrum für Luft- und Raumfahrt has been providing precise, time-varying measurements of the Earth's gravitational field since 2002 (Tapley *et al.* 2004). Changes in the Earth gravitational field are caused by changes in the mass distribution in the solid Earth and at the Earth's surface, i.e. in the ocean, the atmosphere and on land. The solid Earth processes that can cause significant variations in the Earth gravity field at interannual to decadal timescales include essentially the Earth and Ocean-load tides, the solid Earth pole tide, the glacial isostatic adjustment (GIA) and

the earthquakes (at small spatial scale). Once corrected for these effects, the variations in the time-varying gravity field represent the water mass exchanges at the Earth surface within and among the ocean, the atmosphere and the water/snow/ice storage on land. By providing the first global, satellite-based, accurate measurement of these exchanges on a monthly basis, the GRACE mission has given unprecedented insights on the Earth water cycle changes in response to the current climate change (Wouters *et al.* 2014).

In particular GRACE measurements have provided since 2002 estimates of many components of the global water budget. These components are the ice loss from glaciers (Jacob *et al.* 2012; Gardner *et al.* 2013; Schrama *et al.* 2014), ice sheets (Shepherd *et al.* 2012; Velicogna *et al.* 2014), the water storage changes in major river

basins (e.g. Llovel *et al.* 2011; Chen *et al.* 2015a; Reager *et al.* 2016) and the variations of the ocean mass due to transfer of water between continents and the ocean (Chambers 2009; Leuliette & Willis 2011). GRACE estimates further helped in identifying and unraveling the role of each of the global water budget components in the contemporary sea level rise (Yi *et al.* 2015; Dieng *et al.* 2015a; Reager *et al.* 2016; Rietbroek *et al.* 2016).

An interesting feature of GRACE-based estimates of the different components of the global water budget is that they are derived from the same single observing system and thus show a high level of consistency with each other when computed with the same global GRACE solution. For this reason, GRACE solutions have provided essential and critical observations to analyse and test the closure of the global water budget (Church *et al.* 2013; Llovel *et al.* 2014; Yi *et al.* 2015; Reager *et al.* 2016; Rietbroek *et al.* 2016; Dieng *et al.* 2017). However, previous studies have noted significant differences in the water budget components estimates when different GRACE solutions from different data processing centres are used or when different post-processing is applied to the data (e.g. Gardner *et al.* 2013, for glacier mass changes; Barletta *et al.* 2013, Velicogna & Wahr 2013 for ice sheets mass changes; Quinn & Ponte 2010, Chambers & Bonin 2012, for ocean mass changes and Reager *et al.* 2016; for the terrestrial water storage changes). These results indicate that each single post-processed GRACE solution provides consistent estimates of the global water budget components (in the sense that they close the global water budget), but they are potentially biased. Thus if GRACE solutions are considered alone, they likely underestimate the true uncertainty in global water budget components.

In this study, we propose to estimate the components of the global water budget from GRACE in terms of trends over the period of January 2005 to December 2015 and to evaluate the associated uncertainty using an ensemble of global GRACE solutions and an ensemble of post-processing parameters. We break down the uncertainty into uncertainties associated to each post-processing parameter. Here, we consider the different component of the global water budget as global ocean mass, Greenland (ice sheet + peripheral glaciers), Antarctica (ice sheet + peripheral glaciers), glaciers on arctic islands while others glacier are lumped with terrestrial water storage. Glaciers on arctic islands are separated from other glaciers as they represent a coherent component for which several mass change estimates have been published in the recent past.

We analyse five GRACE spherical harmonics solutions from five different processing centres: the Center for Space Research (CSR), the Jet Propulsion Laboratory (JPL), the Deutsches Geo-ForschungsZentrum (GFZ), the Technische Universität Graz (TUG) and the Groupe de Recherche en Géodésie Spatiale (GRGS). These solutions cannot be directly used to evaluate the global water budget components; they need to be post-processed first (Wahr *et al.* 1998). The post-processing parameters include (i) the addition of independent estimates of the geocentre motion as these harmonics are not observable by GRACE (ii) the substitution of the Earth oblateness by independent estimates as this harmonic is poorly observed by GRACE (iii) a filtering for correlated errors that map into characteristic north–south stripes, (iv) a correction for the large land signals (from hydrology, glaciers and ice sheet) that can ‘leak’ into the ocean because of the coarse spatial resolution of GRACE, and (v) a correction for GIA. For each GRACE solution from our ensemble we test a range of post-processing parameters to get a spread of estimates of the ice sheet mass changes, the continental water storage changes and the ocean mass changes. Our selection of GRACE solutions and post-processing parameters is not exhaustive

and thus does not cover the whole range of uncertainty of GRACE. However, because we choose the most up-to-date and the largest possible number of parameters, the spread of our ensemble should approach the real underlying uncertainty. The implications on the closure of the global water budget, the sea level budget and the Earth energy budgets are further analysed.

Previous studies have used a similar ensemble approach based on different GRACE solutions and different post-processing to assess the uncertainty in GRACE estimates but they all focused on a single component of the water budget such as the ocean mass change (Quinn & Ponte 2010; Chambers & Bonin 2012), the ice sheet mass changes (Velicogna & Wahr 2013; Chen *et al.* 2015b) or the glacier mass changes (Gardner *et al.* 2013). Here we analyse all the components together in a consistent way. This novel approach enables us to explore whether the uncertainty in the different components of the global water budget are correlated (or not) when assessed with GRACE measurements. This issue is essential when assessing the closure of the global water budget and the sea level budget (the latter includes all components of the water budget plus the thermal expansion of the ocean).

In the second section of this paper we present the five GRACE spherical harmonic solutions that are used in this study and we briefly explain the main differences among them (Section 2.1). We also describe the range of post-processing parameters that are applied to the GRACE solutions (Sections 2.2–2.5) and the statistical framework used to evaluate the uncertainties (Section 2.6). In Section 3 we present an ensemble of GRACE post-processed solutions based on all possible combinations from the set of post-processing parameters and the set of GRACE solutions. From this ensemble, we compute an estimate of the global water budget components and test its sensitivity to the post-processing parameters and GRACE solutions. In Section 4 we compare the ensemble of solutions with the three mascons solutions available from CSR, JPL and GSFC. We propose a new estimate of the uncertainties associated to the water budget components. We also discuss the implications on the closure of the global water budget and sea level budget and on the indirect estimate of the ocean warming and Earth energy imbalance through the sea level budget approach.

In addition to the spherical harmonic solutions, we analyse three mascons solutions from JPL, CSR and the Goddard Space Flight Center (GSFC). These solutions are already post-processed to add the geocentre and the earth oblateness and to correct for the GIA signal. This set of post-processing parameters is the same for the three mascon solutions. We decided not to add these three mascon solutions to our ensemble because it would have resulted in arbitrary larger weight for this set of post-processing parameters when we compute ensemble means. We prefer to use the mascon solutions for comparison (see Section 4.3).

2 DATA AND METHODS

2.1 GRACE data

We focus on global solutions that are provided to users in the form of spherical harmonic gravity coefficients (Stokes coefficients). Five global solutions are obtained from five different processing centres: CSR, GFZ, GRGS, JPL and TUG. We use the release five of CSR, GFZ and JPL solutions and the release ITSG 2016 of the TUG solution (Klinger *et al.* 2016) from the International center for global Earth models (ICGEM). We use the release 3.3 of the GRGS solution (Lemoine *et al.* 2016). All centres process the same

raw data (level L1) from the GRACE mission which includes the intersatellite range and range rates measured by the K-Band Range (KBR), the range and phase measurements between satellites and the GPS constellation, the accelerometers and the star trackers data. The GRGS centre also uses the satellite laser ranging (SLR) data from LAGEOS1–2, Starlette and Stella in a joint inversion with the GRACE data. To perform the inversion, which yields the gravity field, processing centres use as initial guess an *a priori* model of the gravity field (which is usually a mean field with time-variable components in the form of drift and periodic terms, based on an earlier release of their monthly solutions). In order to reduce the noise, they use ocean and atmosphere models (and sometimes hydrological models) to account for sub-month anomalies that would otherwise alias into the GRACE solutions. They may also modify the weighting of the GPS and the misalignment of the KBR antennas. During the inversion procedure different processing centres use different assumptions, different parameters and different models, which lead to differences among the solutions. Of particular note, the JPL version was considered as a validation product and is by design processed differently than the official CSR and GFZ products. Except for the GRGS product, all processing centres deliver unconstrained solutions, which are not usable without a filtering process (see in Section 2.3). The GRGS product uses an inversion scheme that allows to control the noise of the solutions at small spatial scales (by a normalization of the higher degrees) and therefore does not need any *a posteriori* filtering (Lemoine *et al.* 2016). The TUG product uses an empirical covariance function of the KBR range-rate data in order to better decorrelate the KBR measurements.

For all GRACE solutions we use the spherical harmonic coefficients up to degree 60 for the conversion to gridded mass anomalies. CSR and TUG solutions provide directly a 60-degree solution, which we use here. For the solutions from other centres, we truncate at the degree 60 to keep the comparison consistent among solutions. To account for the full-mass variability estimated by GRACE, the ocean and atmosphere background models (i.e. initial guess *a priori* models of the gravity field) has to be restored to GRACE solutions. Here we are not interested in the atmospheric mass variability so we only restore the ocean background model and the atmospheric load over the ocean (GAD products, Flechtner *et al.* 2015) so that we get a full-mass variability estimated by GRACE without the atmospheric variations over land. Over the ocean, the atmospheric model is restored in order to correct the ocean mass variations for the inverse barometer effect and make it comparable with satellite altimetry (of course, for this purpose we remove the time-variable spatial mean of the atmospheric load over the ocean before restoring the atmospheric model). A problem with such an approach is that the atmospheric and oceanic background models are not the same for every GRACE solution (GRGS uses TUGO for the ocean and ERA Interim for the atmosphere while the other centres use OMCT for the ocean and ECMWF's IFS for the atmosphere). To address this issue we use an alternative approach for the GRGS solution: we first restore its own ocean and atmosphere background models to get the estimate of the full mass variability; then we remove the atmospheric load over land and the mean of the atmospheric load over the ocean using the ECMWF's IFS model.

GRACE solutions must be corrected for the pole tide (the solid Earth and ocean response to the polar motion) to get estimates of the surface mass variations. All processing centres except GFZ, use the International Earth Rotation and Reference System Service (IERS) recommended pole tide correction (Altamimi *et al.* 2016).

But this correction accounts only for the timescales at the Chandler period, since it involves the offset between the instantaneous pole and the mean pole. It does not include the long-period pole tide signals (interannual and longer periods, Wahr *et al.* 2015). To remove these long-period signals that contaminate GRACE surface mass estimates, we apply to all GRACE solutions the correction proposed by Wahr *et al.* (2015). For the GFZ solution we also apply the IERS-recommended pole tide correction (which is not applied *a priori*) to get a full pole tide correction and be consistent with other solutions. The mascon solutions that are additionally used in this study are described in Section 4.3. A time mean over 2005–2015 is removed from all GRACE solutions to compute anomalies.

2.2 Geocentre motion and Earth oblateness

Several corrections need to be made to the GRACE data in order to be usable over land and over the ocean. The first correction is to include estimates of the degree 1 spherical harmonic coefficients. The degree 1 terms are proportional to the position of the geocentre, defined as the position of the centre of mass of the Earth (CM), relative to the centre of figure (CF) of the Earth's outer solid surface (i.e. the Earth surface over land). As the GRACE mission orbits around the CM and measures the intersatellite range and range rates it cannot observe the degree 1 term. Previous studies based on SLR (Watkins & Eanes 1997; Cretaux *et al.* 2002; Cheng *et al.* 2013b; Lemoine & Reinquin 2017), GPS (Fritsche *et al.* 2010; Wu Xiaoping 2010), ocean models (Swenson *et al.* 2008) and joint inversions using GPS, GRACE and models (Rietbroek *et al.* 2012; Wu *et al.* 2017) provide some estimates of the degree 1 correction. In this study, we consider the four most recent estimates of the degree 1 (Rietbroek *et al.* 2012; Cheng *et al.* 2013b; Lemoine & Reinquin 2017; Wu *et al.* 2017) and we consider also the degree 1 correction from Swenson *et al.* (2008) which is widely used in the GRACE community (Fig. 1). Lemoine & Reinquin (2017) and Cheng *et al.* (2013b) estimates are both based on SLR data but they differ in the inversion technique. The Swenson *et al.* (2008) solution is based on a combination of an ocean model with estimates of degree 2 and higher from GRACE. The Rietbroek *et al.* (2012) and the Wu *et al.* (2017) solutions use a combination of observations from GPS and GRACE. All solutions compare well in terms of annual cycle but they show different trends (see Fig. 1). The estimates from Cheng *et al.* (2013b), Lemoine & Reinquin (2017) and Wu *et al.* (2017) show a trend in the Z component that is positive (+0.12, +0.18 and +0.24 mm yr⁻¹, respectively) while estimates from Swenson *et al.* (2008) and Rietbroek *et al.* (2012) show a negative trend (−0.05 and −0.04 mm yr⁻¹, respectively). Past studies have focused on estimating the annual cycle of the geocentre. But here we are interested in the trends. The trends are more difficult to retrieve than the annual cycle because they are at the limit of what is achievable with some of the approaches developed so far to estimate the geocentre position (Wu *et al.* 2012). A recent study from Riddell *et al.* (2017) suggests that the uncertainty in the trend of the geocentre could be up to ±0.21, ±0.28 and ±0.54 mm yr⁻¹ in X, Y and Z, respectively (at 1.65σ level). We adopt here a conservative approach, considering the most recent state-of-the-art published geocentre motions available at the time of writing and use the spread in their trend as an estimate of the uncertainty in the trend. Here, the spread in trend between different geocentre is slightly smaller (±0.30 mm yr⁻¹ on the Z-axis) than in Riddell *et al.* (2017; see Fig. 1).

The second correction consists in including an estimate of the Earth oblateness which corresponds to the degree 2 order 0 zonal

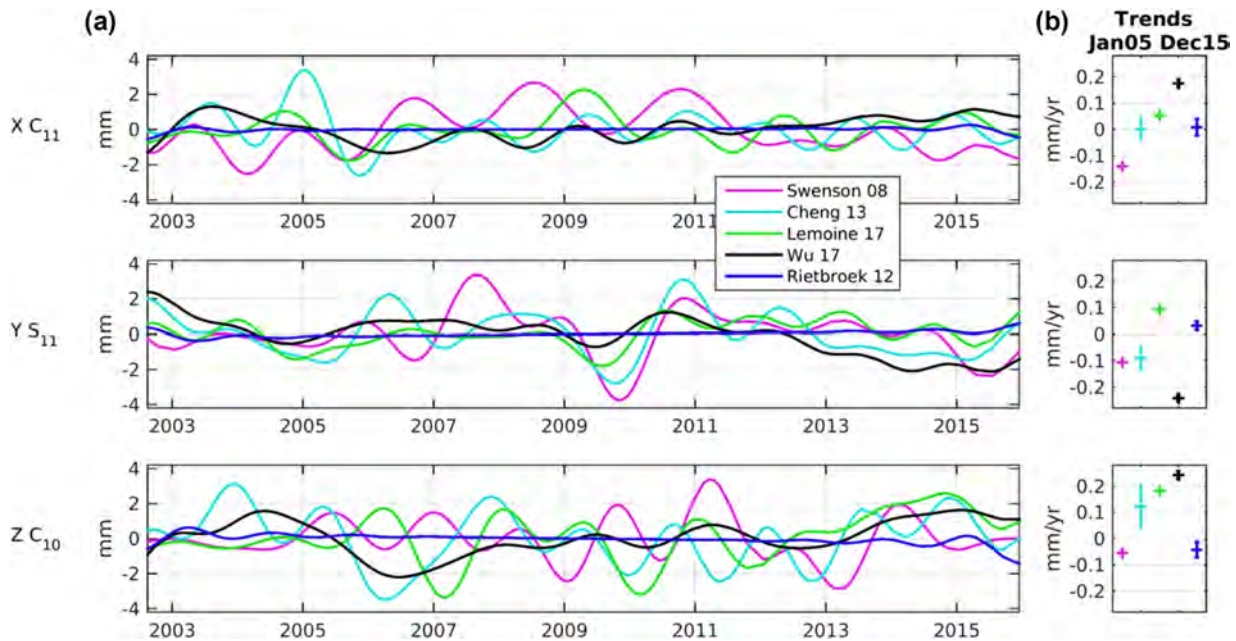


Figure 1. Geocentre motion in the (X,Y,Z). Time-series (a) and associated trends over the period January 2005–December 2015 (b) from Swenson *et al.* (2008), Rietbroek *et al.* (2012), Cheng *et al.* (2013b), Lemoine & Reinquin (2017) and Wu *et al.* (2017). A low-pass filter to remove sub-annual frequencies have been applied to the time-series. The trends are represented by error bars considering the 1.65 std from the individual errors.

spherical harmonic coefficient ($C_{2,0}$). In principle, it can be determined from the nodal precession acceleration of GRACE. But GRACE is in a near-polar orbit which makes the satellite-to-satellite tracking technique weakly sensitive to the nodal precession acceleration. As a consequence GRACE estimates of the $C_{2,0}$ coefficient are inaccurate (Wahr *et al.* 2006; Cheng & Ries 2017), and have to be replaced by estimates based on SLR data (Chambers 2006). In this study we consider two recent estimates of $C_{2,0}$ from Cheng *et al.* (2013a) and Lemoine & Reinquin (2017; see Fig. 2). Cheng *et al.* (2013a) estimate is obtained from the analysis of SLR data only, using five geodetic satellites: LAGEOS 1 and 2, Starlette, Stella and Ajisai. Lemoine & Reinquin (2017) use the same SLR raw data (except the Ajisai data) but obtain the $C_{2,0}$ estimate through a joint inversion of the SLR data with GRACE data. Both $C_{2,0}$ estimates are very close (see Fig. 2) in terms of annual to interannual variability and also in terms of trends over the period 2005–2015. This is because the weighting scheme in the joint inversion of Lemoine & Reinquin (2017) makes the calculation of $C_{2,0}$ heavily dependent on SLR data.

2.3 Filtering

GRACE solutions show correlated errors in the high degrees and orders coefficients (Swenson & Wahr 2006). This noise, which is more pronounced on the sectorial coefficients than on the tesseral and zonal coefficients, propagates into a north–south striping pattern when the spherical harmonics are converted into equivalent water height grids (EWH). The origin of these stripes lays in the near-polar orbit of GRACE and the associated weak sensitivity of the satellite-to-satellite tracking technique to East–West gravity gradients. Instrument errors, background model inaccuracies and processing errors are minimized in the North–South direction and tend to end up in the East–West gravity gradients where the constraint from observations is weaker. These stripes need to be corrected for, if we

want to retrieve accurate estimates of the surface mass variations at small spatial scales (300–500 km). There are several methods to reduce this noise. The most used are the simple Gaussian smoothing of Jekeli (1981) adapted by Wahr *et al.* (1998), the empirical destriping (Chambers 2006; Swenson & Wahr 2006), the Wiener filtering (Sasgen *et al.* 2006), the empirical orthogonal function filtering (Schrama *et al.* 2007), the two-step destriping method (Swenson & Wahr; Chen *et al.* 2007) and the smoothing with order convolution filters (Kusche *et al.* 2009). Every method carries its limitations. Here we choose to test two methods: the two steps method P3M6 from Chen *et al.* (2007) and the order convolution filters from Kusche *et al.* (2009). The P3M6 method consists in smoothing all the coefficients above the sixth order by computing a polynomial fit of order 3 to the odd and even coefficients of a given order. For the order convolution filter, ICGEM provides eight DDK filters with different degrees of smoothing referred to as DDK1 to DDK8. The DDK1 filter applies the strongest level of smoothing approximately corresponding to a Gaussian smoothing radius of 530 km along the East–West direction. The level of smoothing decreases to the DDK8 filter, which applies the weakest level of smoothing corresponding to a Gaussian radius of 200 km (more information on http://icgem.gfz-potsdam.de/Visualized_DDKkernels.pdf). The large smoothing applied by the DDK1, DDK2 filters and Gaussian filter results in an increased leakage of the ice sheet, and coastal glacier signals into the ocean and a dampened signal on land while the weak smoothing of the DDK7 and DDK8 filters make the destriping inefficient in the ocean (see Fig. S1 in the Supporting Information). For these reasons, these DDK filters are discarded here and we only test four DDK filters, namely DDK3, DDK4, DDK5 and DDK6. The filtering is applied to all GRACE solutions except the GRGS solution which does not need a *posteriori* filtering. Indeed, the GRGS centre uses a truncated single value decomposition scheme (leaving out less than 12 per cent of the total variance) for the inversion instead of a classical Choleski inversion. This allows the resolution of the better-determined linear combinations of

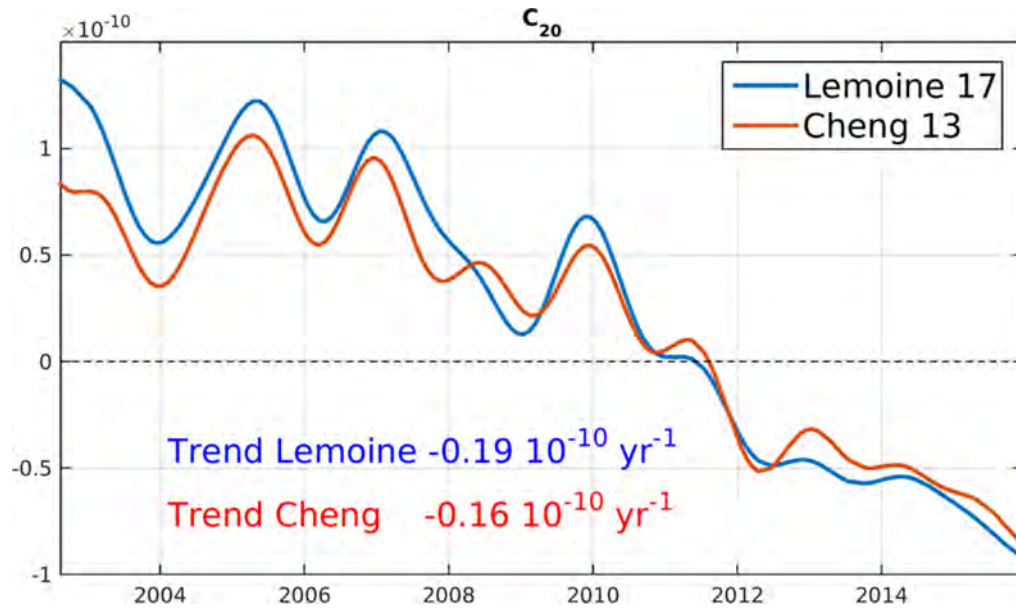


Figure 2. Time-series of the $C_{2,0}$ coefficient from Lemoine & Reinquin (2017) and Cheng *et al.* (2013a). A low-pass filter to remove sub-annual frequencies have been applied to the time-series. Time-series are centred around $-4\ 841\ 653.22 \times 10^{-10}$. The trends are computed for the period January 2005–December 2015. $C_{2,0}$ is adimensional and its trend is expressed in yr^{-1} .

the gravity coefficients and prevents the resolution of the most ill-determined ones, responsible for the stripes in the classical solution.

2.4 Leakage correction

At monthly and longer periods, mass variations are in general much larger over land than over the ocean. Close to the coast the large mass signal from land tends to spread out into the nearby ocean because of the limited GRACE resolution. This effect, called ‘leakage’, generates spurious signal on the coastal ocean and an underestimation of the signal on land in the coastal zone. Based on a model approach (Landerer & Swenson 2012), we correct for this land leakage signal by using an independent reference estimate of the ocean mass variations. The reference ocean mass estimate is based on ocean reanalyses that assimilates observations from satellite altimetry and *in situ* temperature and salinity profiles. From the reference ocean mass estimate, we compute for each gridpoint in the coastal ocean, monthly mass anomalies (with respect to the local mean value over 2005–2015) in EWH. We assume these monthly mass anomalies from the reanalyses as references and we consider that any difference between these anomalies and GRACE anomalies is land leakage signal in GRACE solutions. We correct GRACE solutions for this land leakage signal by transferring it from the coastal ocean gridpoints to the closest land gridpoint. We apply this correction to all ocean gridpoints located in the coastal ocean defined as the ocean within 300 km from the coast. Once corrected, we verify that the new mass distribution is compliant with GRACE raw uncertainty (see Text S1 and Fig. S2 in the Supporting Information for the GRACE raw uncertainty and Text S2, Figs S3 and S4 in the Supporting Information for further details on the leakage correction). This leakage correction depends on the reference ocean mass estimate. We test different values for this parameter.

Two different reference ocean mass estimates are considered. They are computed from two ocean reanalysis namely ORA S4 (Balmaseda *et al.* 2013) and GLORYS2V4 (Garric *et al.* 2018). These estimates cover the whole ocean including high latitudes

and the coastal zones. They assimilate observations from satellite altimetry and temperature and salinity profiles worldwide. The dynamical core of the ORA S4 and GLORYS2V4 models enable to interpolate the temperature and salinity fields in a physical consistent way in regions where observations are scarce like coastal regions.

We tested different methods to allocate the leakage signal on land (distributing the signal on all land gridpoints with an amplitude inversely proportional to the distance instead of distributing the signal on the closest land point) but it did not yield significant differences in the results (not shown). We tested the boundary conditions of the coastal ocean for the leakage correction and we choose 300 km (see Fig. S5 in the Supporting Information). We also tested solutions for which the destriping was not done before the leakage correction. It yields differences in ocean mass trend (and other components of the global water budget) below $0.03\ \text{mm}\ \text{yr}^{-1}$ (see Fig. S1 in the Supporting Information). Another issue is the ‘ringing’ that the truncation of the spherical harmonics generates. Note that the leakage correction does not prevent for this effect. However, although the ringing presents an important local effect it does not affect the global budgets so we neglect this effect here.

2.5 GIA correction

Several solid Earth processes generate significant variations in the Earth gravity field at interannual to decadal timescales and can blur the gravity changes associated with water mass redistributions at the Earth surface. These processes are essentially the solid Earth load tides, the solid Earth pole tides, the earthquakes and the GIA. The solid Earth load tides and pole tides are already corrected for in the solutions provided by the processing centres. Earthquakes generate local mass redistributions on short timescales (over a few days). They can also impact mass redistributions at interannual to multidecadal timescales through long-term post-seismic adjustment. However their effect is local (typically over a few 100 km) and their impact is small at global scale (Reager *et al.* 2016). In this

study we neglect their effect. In contrast, the GIA signal induces significant trends in GRACE solutions that must be removed. The only way to correct for this signal is to use GIA models. GIA models primarily depend on models of the deglaciation history and the mantle viscosity profile. Here we consider three different models namely AG 2013 (Geruo *et al.* 2013), ICE 6G_D 2017 (Peltier *et al.* 2017) and ICE6G_ANU_D 2018 (Purcell *et al.* 2018). AG 2013 is based on the ICE5G deglaciation model and the mantle viscosity is computed numerically via a finite element method considering a viscoelastic profile that varies laterally. ICE6G_D 2017 is an update of ICE5G_C which was developed simultaneously to the deglaciation model (ICE 6 G; Stuhne & Peltier 2015) and the viscosity mantle model (VM5a). ICE6G_ANU_D is an alternative version of ICE6G_D that is corrected for anomalously large uplift signals over regions where ice has been grounded below sea level at or since the Last Glacial Maximum (Purcell *et al.* 2016).

Note that regional GIA models exist to correct GRACE in specific regions. These models often use regionally refined sets of observations of the vertical land movement and refined sets of local proxies of the past ice extent in their inversion scheme. Regional GIA models show results that can be different from global models locally. They yield to significantly different ice mass change estimates when they are used to correct local GRACE solutions in particular in Antarctica (Shepherd *et al.* 2012; Whitehouse *et al.* 2012; Ivins *et al.* 2013; Martín-Español *et al.* 2016) and Greenland (Khan *et al.* 2016). Here we do not use regional GIA models to correct global GRACE solutions as they give spurious estimates of the GIA signal out of the specific regions for which they have been designed (Whitehouse *et al.* 2012). They would lead to inconsistent estimates of mass changes at global scale. We only use two regional GIA models over Antarctica (Whitehouse *et al.* 2012) and over Greenland (Khan *et al.* 2016) as references to quantify the impact of using regionally refined GIA models rather than global GIA models on GRACE mass trends (see Table S1 in the Supporting Information).

2.6 Statistical method to evaluate GRACE uncertainty

Variations in processing and post-processing parameters affect GRACE estimates of the mass redistributions. In order to determine to which extent these variations can bias GRACE estimates, we consider the range of the six processing parameters described in previous sections (i.e. processing centre, geocentre motion, $C_{2,0}$, the filtering parameter, the leakage parameter and the GIA correction) and we compute an ensemble of GRACE post-processed solutions. The range of processing includes five GRACE solutions from five processing centres, five geocentre motion corrections, two $C_{2,0}$ corrections, five filtering techniques, two leakage corrections and three GIA corrections which lead to 1500 possible combinations to generate a post-processed GRACE solution. We thus build an ensemble of 1500 post-processed solutions and use it to estimate the global water budget.

The global water budget is broken down into five components: the ocean mass change, the Antarctica mass change, the Greenland mass change, the arctic islands mass change and remaining glaciers plus terrestrial water storage (TWS) mass change (glaciers & TWS). The ocean component is further broken down into the coastal ocean mass change (within 300 km from the coast, which represents 17 per cent of the ocean surface) and the open ocean mass change because it is essentially the coastal ocean that is affected by variations in

processing techniques (see below). Greenland and Antarctica components include the ice sheet and the peripheral glaciers. Antarctica is defined using the bedmap2 mask (Fretwell *et al.* 2013). The arctic islands component is defined using the version 4.0 of the Randolph glaciers inventory (RGI) from Pfeffer *et al.* (2014). It includes islands in the northern and southern arctic Canada (region 3 and 4 in RGI), in Iceland (region 6 in RGI), in Svalbard (region 7 in RGI) and in the Russian arctic (region 9 in RGI). The glaciers & TWS component includes all other regions on Earth (see Fig. S6 in the Supporting Information). All contributions are expressed in mm Sea Level Equivalent (mm SLE is defined as the mass change of a water budget component normalized by the total global ocean area). Note that because water mass is conserved in the Earth system and in GRACE observations (GRACE solutions do not include any degree 0), GRACE estimate of the ocean mass change is equal to the sum of GRACE estimate of the other water budget components.

In this article, we focus on the trends of the global water budget components over the period January 2005–December 2015. January 2005 corresponds to the full deployment of the ARGO profiling floats in the ocean (Roemmich 2009), increasing the performance of ocean reanalysis. However, the ensemble solution is provided from August 2002, which is the first common month from the five chosen processing centres. Note that all the trends in this study are computed by least-squares fitting a first-order polynomial after removing the annual and semi-annual cycles. This method provides an estimate of the formal error associated to the trend estimate. This formal error is very small ($<0.001 \text{ mm yr}^{-1}$) because we use monthly time-series that cover a decade. We neglect this source of uncertainty.

The ensemble is built with the intent to consider the largest number of state-of-the-art processing parameters as possible. Any processing parameter that has been shown to have deficiencies has been discarded (e.g. the filters ddk1 or ddk2). All the other parameters are weighted equally in the ensemble because we could not find any reason in the literature to favour a parameter over another. With this selection, we expect that our ensemble actually gathers most of the current state-of-the-art GRACE solutions. As such, we expect that the variance of our ensemble can provide insights on GRACE uncertainty in global water budget component trends. That said, we acknowledge that our ensemble is not exhaustive. It builds on prior work to develop and refine the best processing parameters and thus it does not include all GRACE estimates. In addition, it does not account for any unknown systematic error that could affect all GRACE solutions. As such, the spread of our ensemble do certainly not represent the true uncertainty in GRACE. But we believe it gives interesting insights on the sources of uncertainty in state-of-the-art GRACE solutions.

To evaluate the role of the variations in a given processing parameter on GRACE uncertainty, we first average the ensemble across the five other processing parameters. Then we compute the variance of the resulting single-parameter ensemble (see Sections 3.1–3.6). To evaluate the total GRACE uncertainty, we compute the variance of the whole 1500-member ensemble (see Section 3.7). This variance can be expressed as the sum of the variance of each single-parameter ensemble plus an interaction term. This method is similar to the ANalysis Of VAriance procedure – ANOVA e.g. (Fisher 1925) – except that we do not have residual terms here. This method was used by Geoffroy *et al.* (2012) to assess the contribution of different parameters to the variations of climate sensitivity, and we refer to that study for details on the method. To summarize, the total variance of GRACE reconstruction is decomposed as follows:

Eq. (1) computation of the variance as the sum of the variance of each single-parameter ensemble plus an interaction term

$$\begin{aligned}
 & \text{var} (Tr_i (pc, GM, C_{2,0}, Fp, Lp, GIA)) \\
 &= \text{var} \left(\langle Tr_i (pc) \rangle_{GM, C_{2,0}, Fp, Lp, GIA} \right) \\
 &+ \text{var} \left(\langle Tr_i (GM) \rangle_{pc, C_{2,0}, Fp, Lp, GIA} \right) \\
 &+ \text{var} \left(\langle Tr_i (C_{2,0}) \rangle_{pc, GM, Fp, Lp, GIA} \right) \\
 &+ \text{var} \left(\langle Tr_i (Fp) \rangle_{pc, GM, C_{2,0}, Lp, GIA} \right) \\
 &+ \text{var} \left(\langle Tr_i (Lp) \rangle_{pc, GM, C_{2,0}, Fp, GIA} \right) \\
 &+ \text{var} \left(\langle Tr_i (GIA) \rangle_{pc, GM, C_{2,0}, Fp, Lp} \right) \\
 &+ \text{var} (I (pc, GM, C_{2,0}, Fp, Lp, GIA)), \quad (1)
 \end{aligned}$$

where the brackets $\langle \rangle_{p_1, \dots, p_5}$ indicate the mean across the five parameters p_1, \dots, p_5 . Tr_i indicates GRACE estimate of the trend in the i th global water budget component (ocean mass, Greenland, Antarctica, Arctic islands and glaciers & TWS). $pc, GM, C_{2,0}, Fp, Lp, GIA$ indicate the six processing parameters (namely the processing centre, the geocentre motion, the $C_{2,0}$, the filtering parameter, the leakage parameter and the GIA parameter) and I indicates the interaction term. Note that this decomposition of the variance of the ensemble is exact. There is no approximation. The interaction term corresponds to the non-additive interaction of processing parameters in the GRACE post-processed solution (i.e. the Tr_i function) on one or several processing parameters. We evaluate the interaction term in Section 3.7 and discuss the consequences for GRACE uncertainty.

3 RESULTS: UNCERTAINTY IN GRACE ESTIMATE OF THE WATER BUDGET COMPONENTS

3.1 Uncertainty related to the GRACE processing centre

Fig. 3(a) shows the effect of varying the processing centre parameter on GRACE estimates of the global water budget trends for the period 2005–2015. As described in eq. (1), we compute the trend for each water budget component as the mean of the trends of the sub-ensemble defined by the processing centre parameter. For all water budget components, the trend varies by less than 0.20 mm yr^{-1} SLE among the different processing centres. The largest differences are obtained for the open ocean mass and glaciers & TWS trends for which largest differences reach 0.20 mm yr^{-1} SLE. For Antarctica, differences in trends estimates are below 0.09 mm yr^{-1} SLE and for Greenland and the arctic Islands the differences are smaller (0.03 mm yr^{-1} SLE).

3.2 Uncertainty related to the geocentre motion correction

The geocentre motion parameter has a small impact on the estimate of the Greenland and arctic islands mass trends (smaller than 0.03 mm yr^{-1} SLE). The Antarctica mass trend differences are below 0.08 mm yr^{-1} SLE. However ocean and glaciers & TWS mass trends are more sensitive to the geocentre parameter (differences up to 0.42 mm yr^{-1} SLE). The use of Lemoine & Reinquin (2017) or Wu *et al.* (2017) geocentre motion parameters yield similar results. They lead to small ocean mass trend (1.49 – 1.51 mm yr^{-1} SLE) and small glaciers & TWS mass trends (-0.24

and -0.21 mm yr^{-1} SLE). The differences between both solutions are below 0.02 mm yr^{-1} SLE for all components of the global water budget. Using Cheng *et al.* (2013b) or Rietbroek *et al.* (2012) yield also similar results but they lead to a different picture (Fig. 3b) compared to Lemoine & Reinquin (2017) or Wu *et al.* (2017). In the case of Cheng *et al.* (2013b) and Rietbroek *et al.* (2012), the ocean mass and glaciers & TWS trends are both significantly larger (1.63 – 1.68 mm yr^{-1} SLE) than when we consider the Lemoine & Reinquin (2017) and Wu *et al.* (2017) parameter. The use of the Swenson *et al.* (2008) geocentre parameter leads to the largest ocean mass trend ($+1.84 \text{ mm yr}^{-1}$) and the largest glaciers & TWS mass trend ($+0.14 \text{ mm yr}^{-1}$). These large differences in ocean and glaciers & TWS mass trend among GRACE solutions are essentially caused by differences in trends of the Z component of the geocentre motion parameter (see Barletta *et al.* 2013 and Table S2 in the Supporting Information for the impact of the x, y and z component of the geocentre motion parameter on the trends of the global water budget).

3.3 Uncertainty related to the $C_{2,0}$ correction

The use of different $C_{2,0}$ corrections generate small differences in the water budget component trends. These differences are smaller than 0.03 mm yr^{-1} for all components (Fig. 3c). The largest effect is on the ocean and Antarctica mass trends.

3.4 Uncertainty related to the filtering

The filtering parameter has a small effect. This is for three reasons. First, because we selected here only up-to-date state-of-the-art filters and these filters tend to yield similar results. Second, because we consider separately the leakage effect and the filtering (unlike many previous studies). And third, because we only analyse large areas (see Fig. 4a). We probably would find significant differences among filters at basin or glacier scale. Here we find that the differences in the water budget trends generated by the different filtering are below 0.04 mm yr^{-1} SLE for all components and all filters.

3.5 Uncertainty related to the leakage correction

As explained in Section 2.4, the leakage correction is sensitive to the choice of the reference ocean mass used to correct the coastal ocean. Here the two different reference ocean masses used in the leakage correction generates differences in GRACE estimates of the trends in the water budget components that are below 0.11 mm yr^{-1} SLE (see Fig. 4b). Because of the localization of the leakage on the coast, only the coastal ocean mass and land components are affected. The effect of this parameter is important on the glaciers & TWS component. We find that it is small on Greenland, arctic Islands and Antarctica mass trends.

3.6 Uncertainty related to the GIA correction

There is a good agreement between GRACE estimates of Greenland, the arctic islands and glaciers & TWS mass trends when any of the three GIA model is considered. With ICE-6G.D 2017 and ICE6G_ANU.D 2018 models, similar Antarctica mass trends are obtained. However, the ocean mass trends are different by up to 0.08 mm yr^{-1} SLE. When AG 2013 is used, the picture is different with a global ocean mass trend and Antarctica mass trend higher (1.72 and 0.73 mm yr^{-1} SLE) than the two other global GIA models.

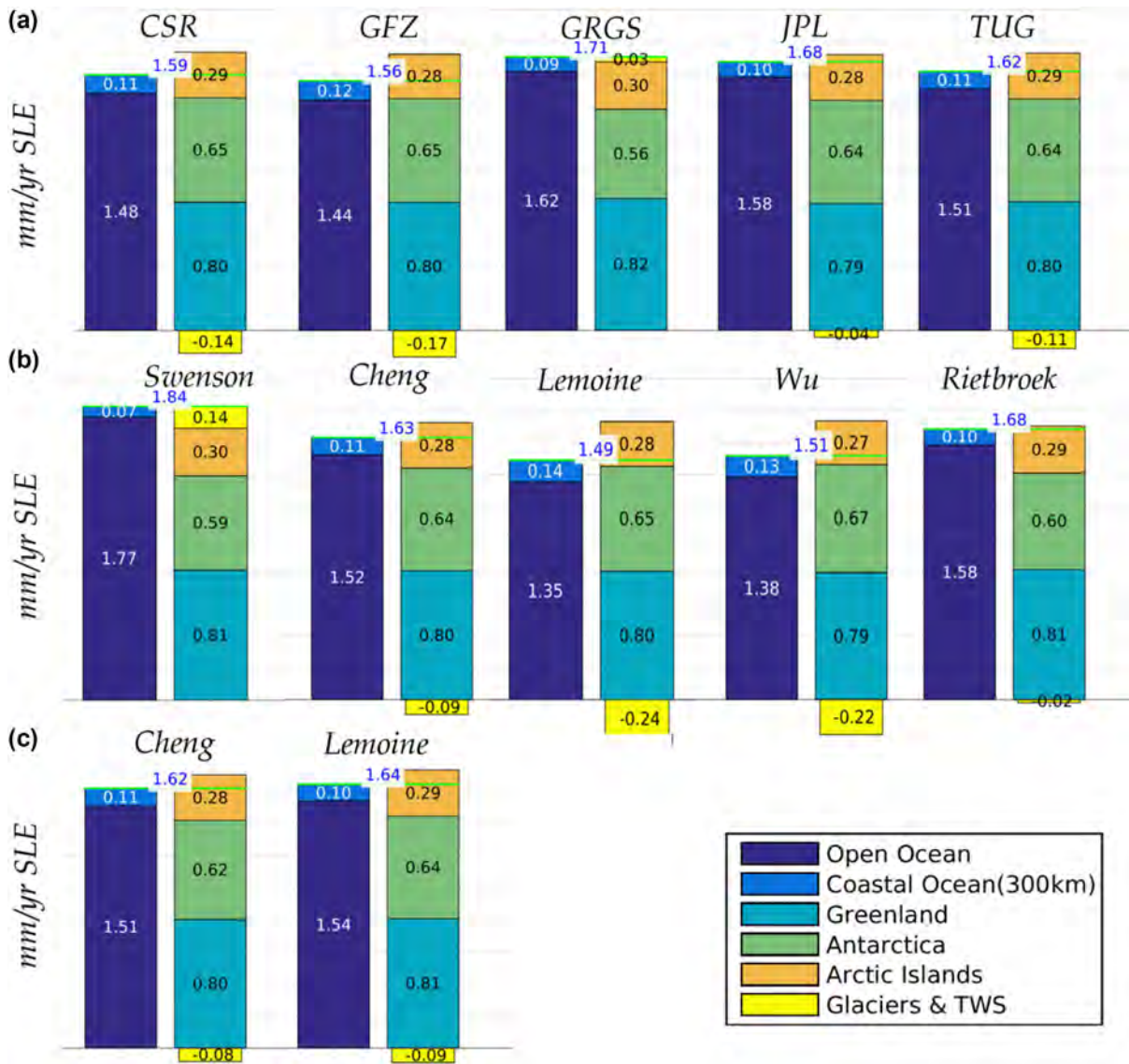


Figure 3. Trends in global mass budget (in mm yr⁻¹ SLE over 2005–2015) for all components of the global water budget. Comparison of the mean values over the sub-ensembles according to (a) processing centre, (b) Geocentre motion and (c) C_{2,0}.

ICE-6G_D 2017 and ICE6G_ANU_D 2018 models lead to similar Antarctica mass trend (Whitehouse *et al.* 2012; Ivins *et al.* 2013) while AG 2013 present the highest value of all GIA models available for Antarctica (Martín-Español *et al.* 2016). The reason of the smaller difference comes from the fact that here two of the three global GIA models have been recently updated considering the same BEDMAP2 bathymetry for the Southern Ocean (Peltier *et al.* 2017; Purcell *et al.* 2018). For Greenland, the regional model of Khan *et al.* (2016) yields to a local GIA apparent mass higher than global models, leading to a Greenland SLE mass loss which is 0.06 mm yr⁻¹ SLE smaller than when using global models (see Table S1 in the Supporting Information).

3.7 Total uncertainty

Table 1 summarizes the sources of uncertainty in GRACE estimate of the global water budget components associated to each processing parameter. The uncertainty is expressed as 1.65 standard deviation of each single-parameter ensemble corresponding to the 90 per cent

confidence level (CL) when assuming a Gaussian distribution. The uncertainty of the whole ensemble of GRACE solutions (referred to as the ‘total uncertainty’) is computed also as the 1.65 standard deviation of the whole ensemble. We find that the total uncertainty in GRACE estimates of the trends in Greenland and arctic islands mass is below 0.04 mm yr⁻¹. It represents respectively 5 and 13 per cent of the mass trend signal in these regions confirming the accuracy of GRACE estimates of the current Greenland and arctic islands mass loss. For the global ocean, Antarctica and glaciers & TWS mass changes, the total GRACE uncertainty is about one order of magnitude larger than for Greenland and the arctic islands. It reaches respectively 0.27 mm yr⁻¹ SLE, 0.15 mm yr⁻¹ SLE and 0.27 mm yr⁻¹ SLE which represent 16, 23 and 300 per cent of the average mass change signal in these regions confirming earlier studies which point out the large uncertainty in GRACE estimates of the current changes in Glaciers & TWS (Yi *et al.* 2015; Reager *et al.* 2016; Rietbroek *et al.* 2016; Dieng *et al.* 2017).

Table 1 also shows the interaction term, which is computed as the difference between the total uncertainty and the quadratic sum

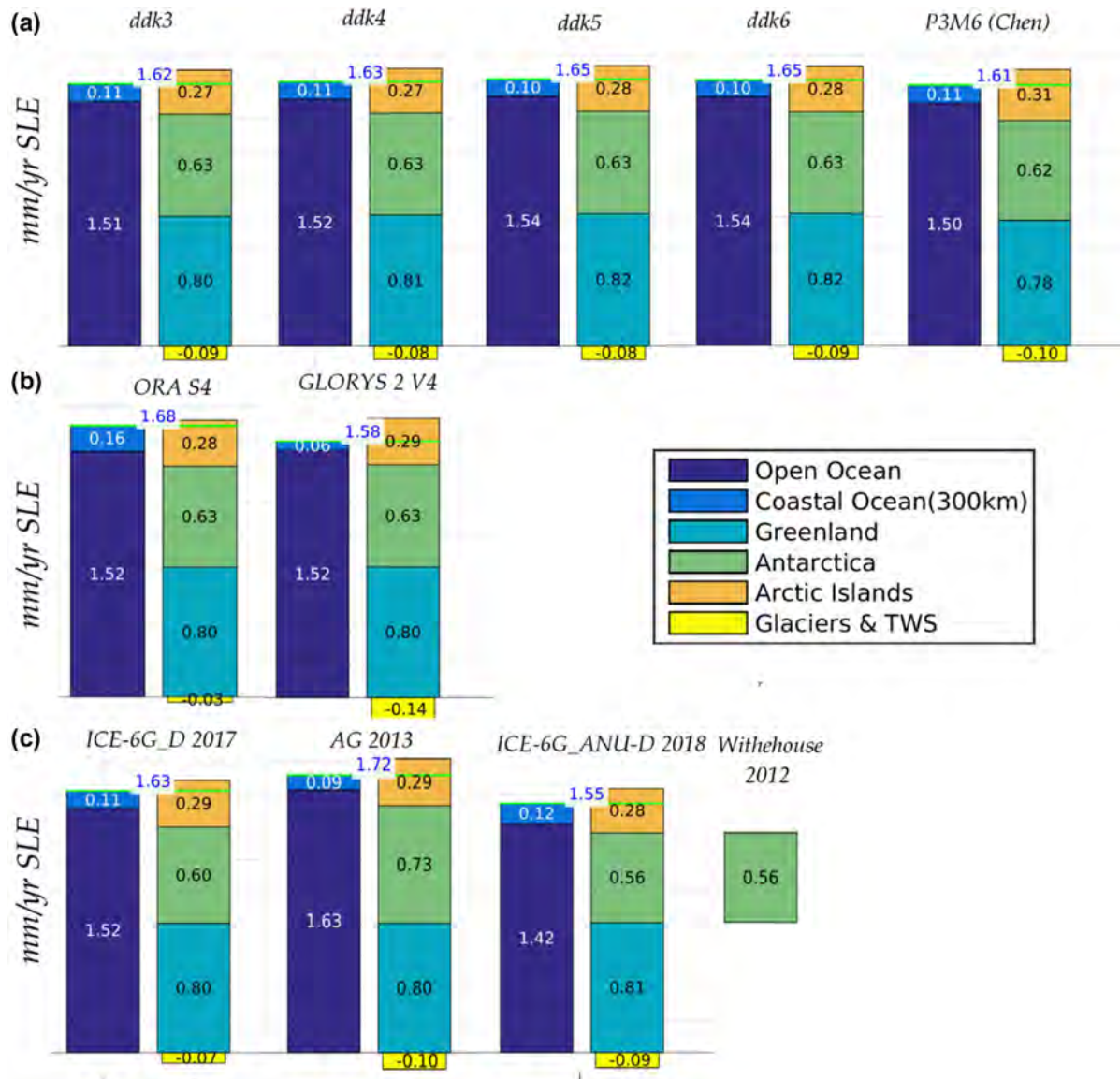


Figure 4. Trends in global mass budget (in mm yr^{-1} SLE over 2005–2015) for all components of the global water budget. Comparison of the mean values over the sub-ensembles according to (a) filtering parameter, (b) leakage correction and (c) GIA correction.

of the uncertainty associated to each single processing parameter. As explained in Section 2.6 the interaction term arises from the non-additive interaction of parameters in the ensemble of GRACE post-processed solutions. Here it represents less than 1 per cent of the total GRACE uncertainty for all global water budget components. The reason for this low interaction term is that here all estimates of the processing parameters are sampled independently and for this reason they are largely uncorrelated. This approach is partly biased because some estimates of the different processing parameters rely on a common reference frame (e.g. estimates of the geocentre motion, $C_{2,0}$ and GIA) that could impact several parameters simultaneously, and thus generate covariance among the processing parameter estimates. So the interaction term here is likely underestimated. However the underestimation is probably small as the biases of the International Terrestrial Reference

are likely small (of the order of a few tenth of mm yr^{-1} ; Altamimi *et al.* 2016).

At interannual timescales, we estimate the uncertainty in GRACE solutions by computing for each year, the standard deviation of the ensemble of all GRACE annual estimates. This uncertainty reaches up to ± 4.23 mm SLE for the most uncertain years (at 1.65σ , i.e. 90 per cent CL assuming a Gaussian distribution).

Fig. 5(c) shows the ensemble-mean time-series of the global water budget components. The uncertainty in glaciers & TWS mass variations at interannual timescales reaches up to ± 4.28 mm SLE (90 per cent CL). The main contributor to this uncertainty is the uncertainty in geocentre motion (Fig. 6b). For Antarctica, the uncertainty in mass variations at interannual timescales reaches up to ± 1.24 mm SLE (90 per cent CL) while for Greenland and arctic islands the uncertainty is smaller (up to ± 0.37 mm SLE).

Table 1. Uncertainties in trend over 2005–2015 of GRACE estimates of the global water budget components (mm yr^{-1}).

(mm yr^{-1} SLE)	Ocean mass		Greenland		Antarctica		Arctic islands		Glacier & TWS	
Mean trend	1.63		0.80		0.63		0.29		−0.09	
Processing centre	0.09	(5 per cent)	0.02	(2 per cent)	0.06	(9 per cent)	0.01	(3 per cent)	0.12	(137 per cent)
Geocentre motion	0.21	(13 per cent)	0.01	(2 per cent)	0.05	(8 per cent)	0.02	(5 per cent)	0.23	(255 per cent)
$C_{2,0}$	0.02	(1 per cent)	<0.01	(<1 per cent)	0.02	(3 per cent)	<0.01	(1 per cent)	<0.01	(6 per cent)
Filtering	0.02	(1 per cent)	0.03	(3 per cent)	0.01	(1 per cent)	0.02	(8 per cent)	<0.01	(10 per cent)
Leakage correction	0.08	(5 per cent)	<0.01	(<1 per cent)	<0.01	(<1 per cent)	<0.01	(1 per cent)	0.09	(103 per cent)
GIA	0.12	(7 per cent)	<0.01	(<1 per cent)	0.12	(19 per cent)	0.01	(4 per cent)	0.03	(30 per cent)
Total uncertainty	0.27		0.04		0.15		0.04		0.27	
Quadratic sum of individual uncertainties	0.27		0.04		0.15		0.04		0.27	
Interaction	<0.01		<0.01		<0.01		<0.01		<0.01	

All uncertainties are given at 1.65σ (i.e. 90 per cent CL assuming a Gaussian distribution). Relative uncertainties are provided in per cent and calculated using the mean trend value. Total uncertainty is computed as the $1.65 \times \text{RMS}$ of the whole ensemble.

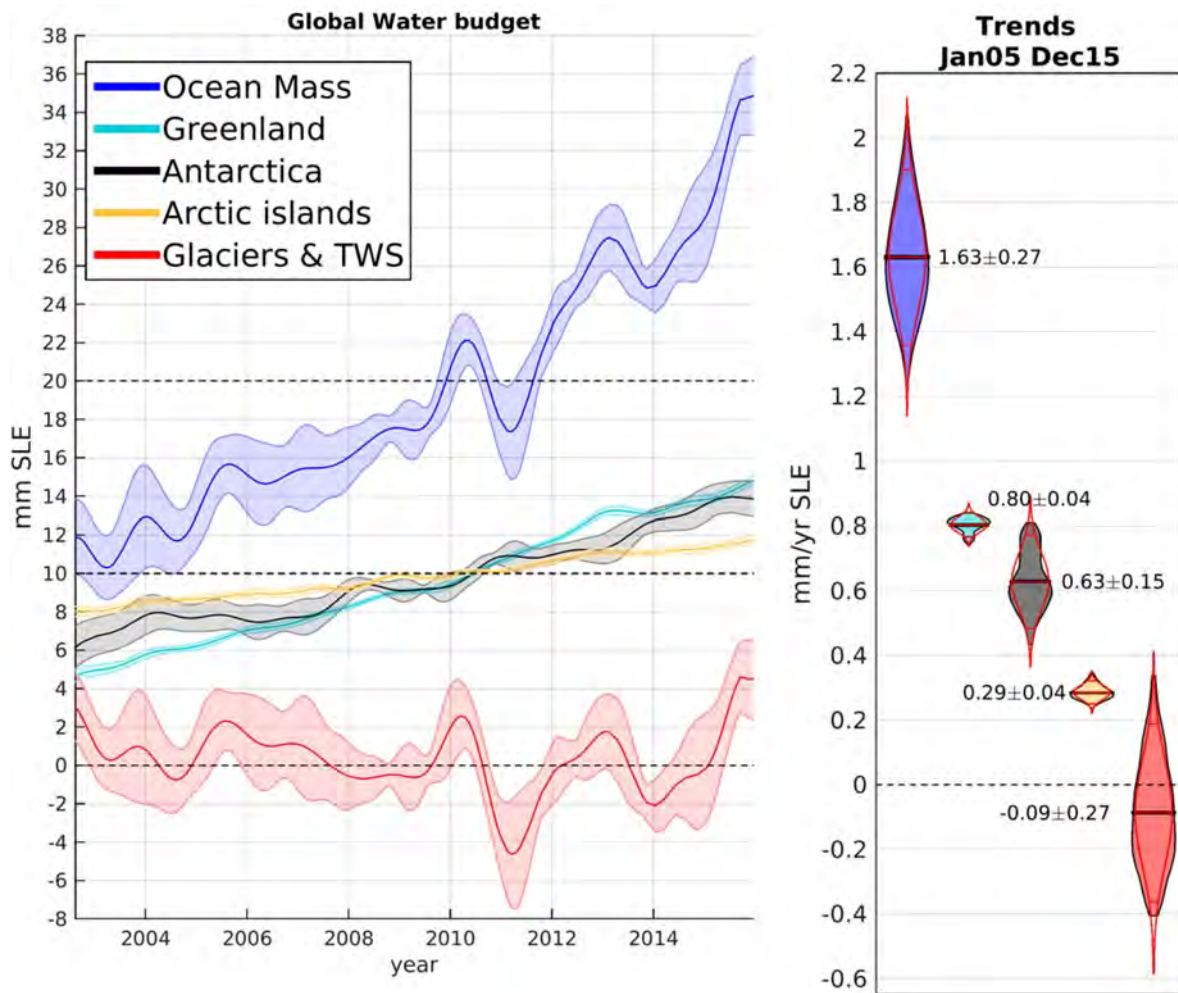


Figure 5. Time-series of the global water budget components after applying a low-pass filter to remove sub-annual frequencies (left) and their trends distributions for 2005–2015 (right). In the right-hand panel, the shaded areas indicate the distribution of trends, while the red lines indicate the distribution that would be obtained under the assumption of a Gaussian distribution. For comparison, estimates have been offset in the left-hand panel.

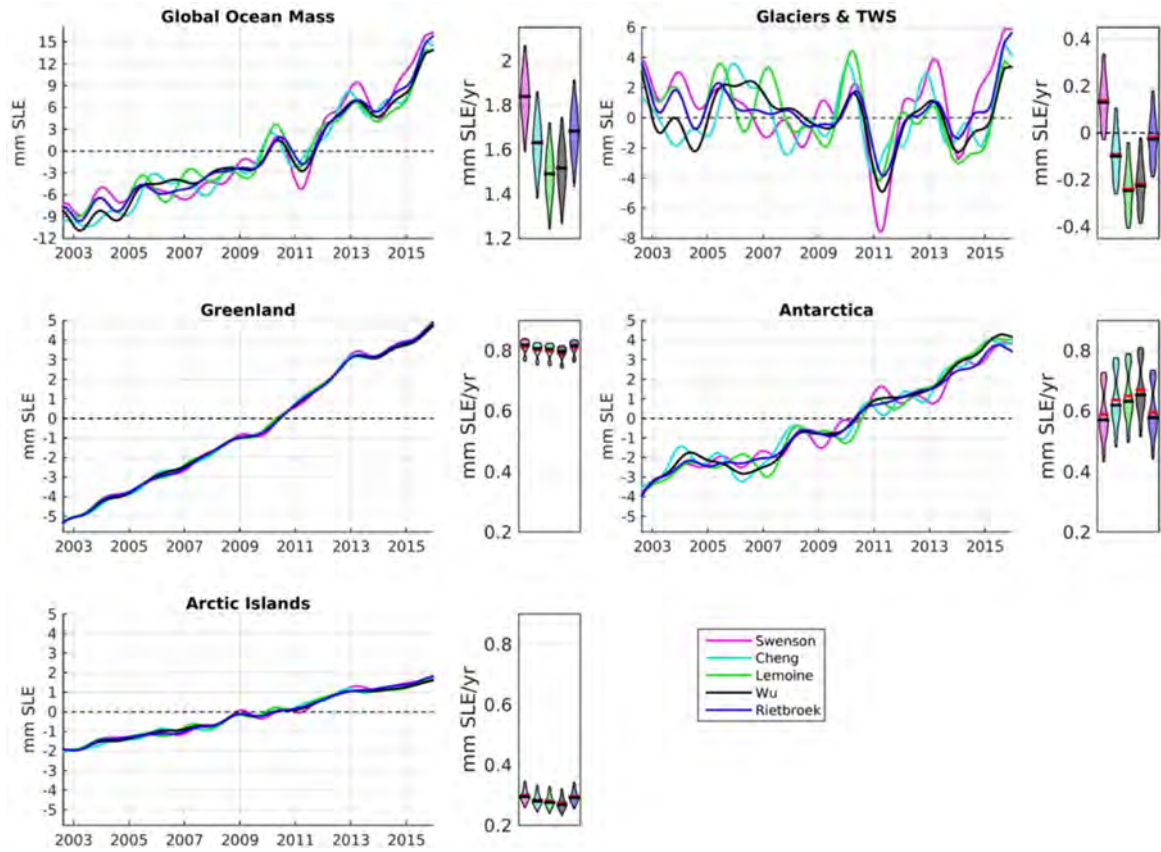


Figure 6. Impact of the geocentre parameter in the components of the global water budget. The small boxes correspond to the distribution of trends of each sub-ensembles for each of the four geocentre series. A low-pass filter to remove sub-annual frequencies have been applied to the time-series.

Table 2. Comparison with previous global water budget estimates in mm yr^{-1} .

Period	Source	Ocean mass (mm yr^{-1} SLE)	Greenland (mm yr^{-1} SLE)	Antarctica (mm yr^{-1} SLer)	Rest of the land (mm yr^{-1} SLE)
Apr 2002–Dec 2014	Reager <i>et al.</i> 2016 ^a	1.58 ± 0.43	0.77 ± 0.13	0.49 ± 0.53	0.32 ± 0.21
Aug 2002–Dec 2014	This study	1.32 ± 0.21	0.77 ± 0.03	0.49 ± 0.13	0.07 ± 0.20
Apr 2002–Jun2014	Rietbroek <i>et al.</i> 2016 ^a	1.36 ± 0.69^b	0.73 ± 0.03	0.26 ± 0.07	0.09 ± 0.27^c
Aug 2002–Jun2014	This study	1.31 ± 0.23	0.77 ± 0.03	0.46 ± 0.13	0.07 ± 0.20
Jan 2005–Jul 2014	(Yi <i>et al.</i> 2015) ^d	2.03 ± 0.21	0.77 ± 0.05	0.60 ± 0.18	0.65 ± 0.28^e
Jan 2005–Jul 2014	This study	1.40 ± 0.22	0.83 ± 0.03	0.57 ± 0.14	0.00 ± 0.21
Jan 2004–Dec 2015	(Dieng <i>et al.</i> 2017) ^a	2.24 ± 0.16^f	0.82 ± 0.10	0.33 ± 0.10	1.03 ± 0.17
–	–	2.35 ± 0.27^b	–	–	–
Jan 2004–Dec 2015	This study	1.57 ± 0.21	0.78 ± 0.03	0.57 ± 0.14	0.21 ± 0.20

^aValues in the article are expressed in 1σ

^bOcean mass computed as altimetry (total) minus steric from the reference

^cRest of land computed as sum of glaciers and hydro from the reference

^dValues in the article are expressed in 1.96σ (95 per cent of CL)

^eRest of land computed as glacier, ice caps and land water from the reference

^fOcean mass is based on Chambers & Bonin (2012)

Our GRACE ensemble starts in August 2002 (and not April 2002) because there are some missing months in one of the processing centres. ‘Rest of the land’ corresponds to the sum of arctic islands and glaciers & TWS from our study. Uncertainty is expressed in 1.65σ (90 per cent of CL). Red values do not overlap within 1.65σ (90 per cent of CL).

4 DISCUSSION

4.1 Impact of the geocentre motion in the global water budget

As shown by previous studies (Barletta *et al.* 2013; Reager *et al.* 2016) most of the GRACE uncertainty related to the geocentre is due to the uncertainty in the geocentre velocity along the Z-axis. We

tested this hypothesis by detrending the z component of geocentre solutions and recomputing GRACE solutions. This experience resulted in a significant reduction of the spread in GRACE estimates of the ocean mass trend confirming previous studies (the spread among the trends dropped from ± 0.35 to $\pm 0.17 \text{ mm yr}^{-1}$ SLE, see Fig. S7 in the Supporting Information). Here the five different estimates of the geocentre motion (Swenson *et al.* 2008; Rietbroek

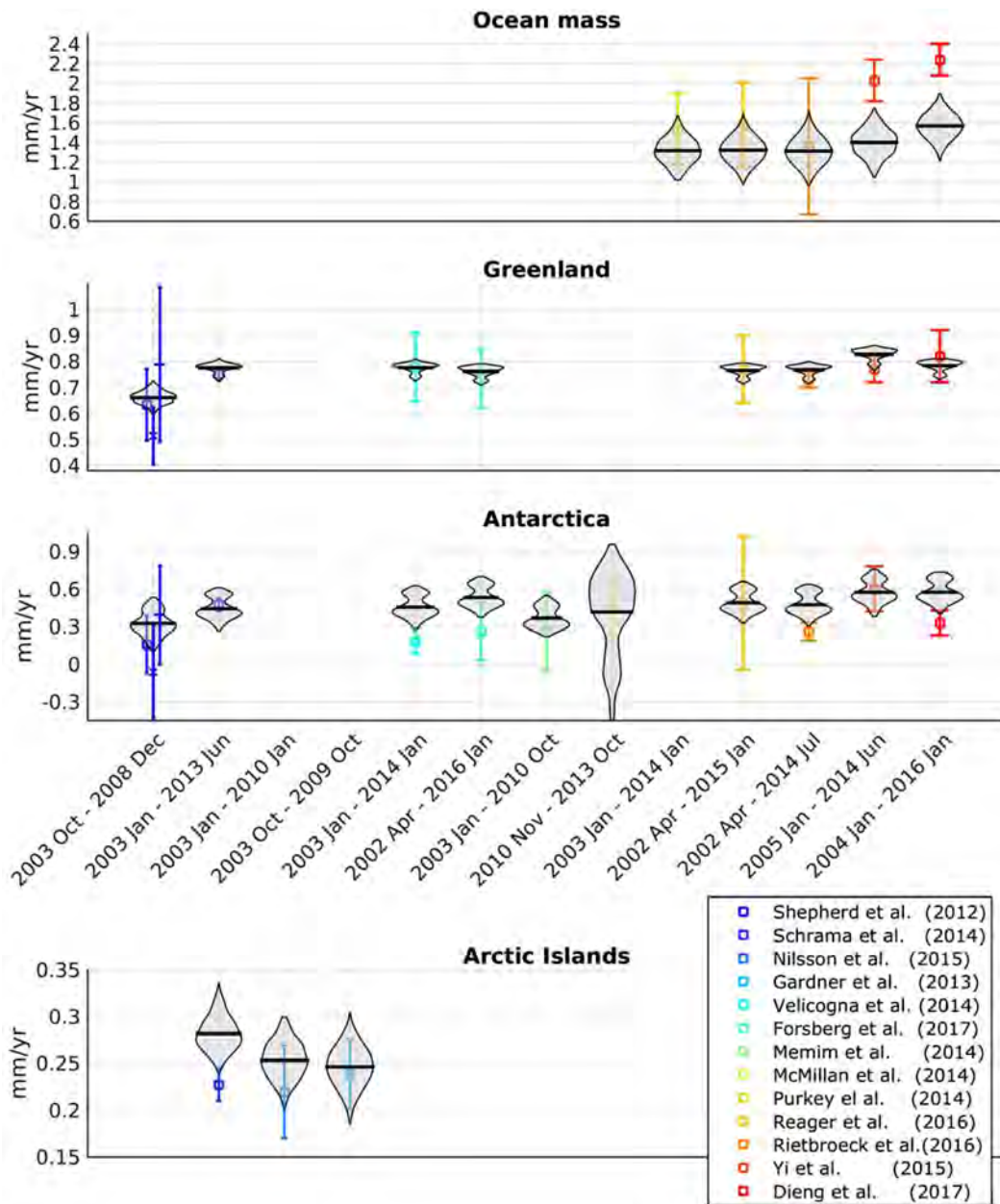


Figure 7. Comparison of our ensemble with previous estimates of some of the water budget components trends. Vertical lines represent ± 1.65 standard deviation around the mean values and the grey shaded areas the distribution of trends from our ensemble. The estimates from Table 2 are included to complete the comparison.

et al. 2012; Cheng *et al.* 2013b; Lemoine & Reinquin 2017; Wu *et al.* 2017) show a geocentre velocity along Z ranging from -0.05 and $+0.24$ mm yr $^{-1}$, and a dispersion around the ensemble mean in general agreement with recent studies (Riddell *et al.* 2017 – shows an uncertainty in the trend of the z component of the geocentre of ± 0.54 mm yr $^{-1}$). However our range may underestimate the real range as it is based on only five geocentre solutions and it does not take into account any potential sources of systematic bias.

4.2 Comparison with previous estimates

Table 2 and Fig. 7 show the comparison of the trends estimates of the global water budget components from our ensemble with previous

estimates over similar time period (Shepherd *et al.* 2012; Gardner *et al.* 2013; McMillan *et al.* 2014; Mémin *et al.* 2014; Purkey *et al.* 2014; Schrama *et al.* 2014; Velicogna *et al.* 2014; Nilsson *et al.* 2015; Yi *et al.* 2015; Reager *et al.* 2016; Rietbroek *et al.* 2016; Dieng *et al.* 2017). Overall, the general agreement (within uncertainties at 1.65σ) of our solution with previous published estimates of the trends in the water budget components gives confidence in the choice of post-processing parameters. There are only two cases for which our estimate significantly differs from previous estimates: the ocean mass and glaciers & TWS trends estimates from Yi *et al.* (2015) and from Dieng *et al.* (2017). Dieng *et al.* (2017), is based on older data sets which tend to be higher than what is estimated here.

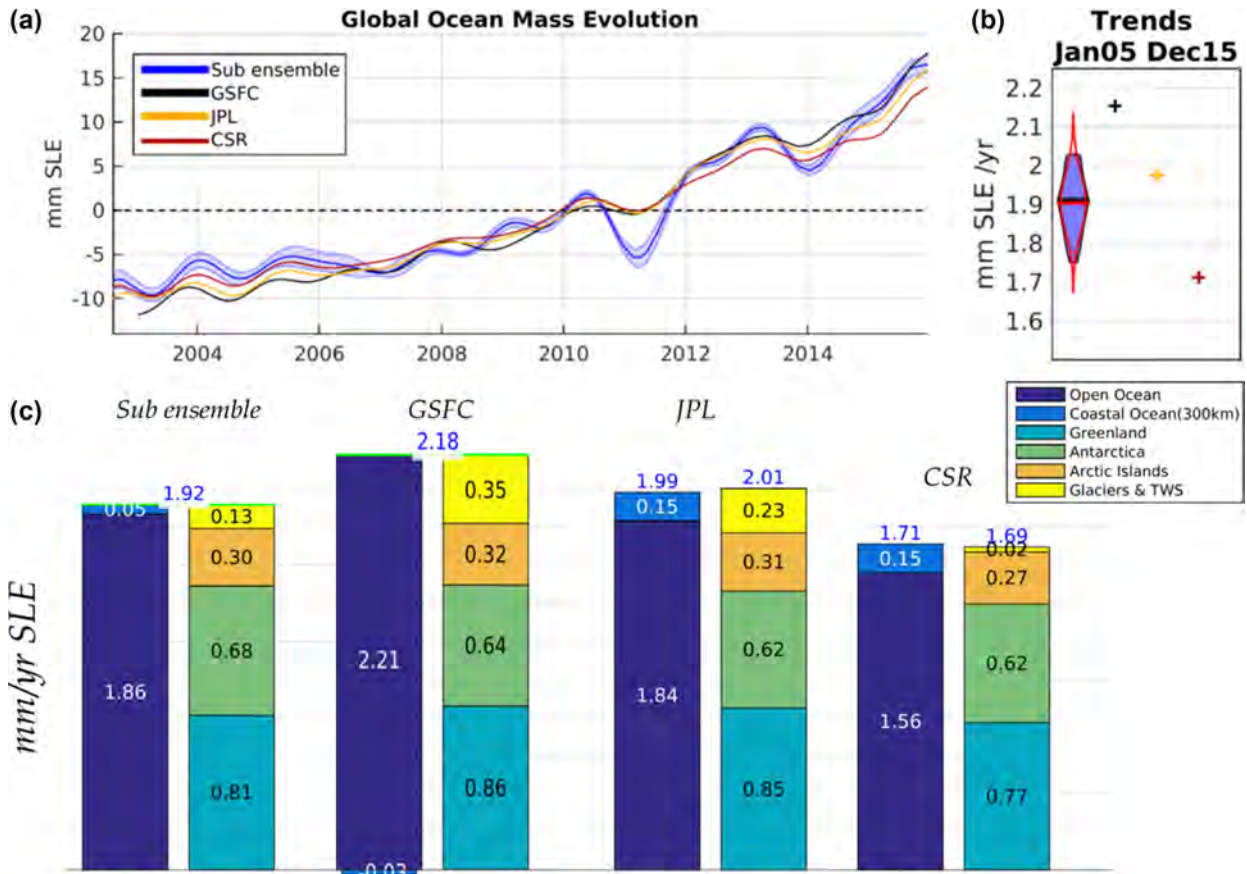


Figure 8. Comparison between mascon solutions and a subset of our ensemble for the (a) global ocean mass evolution, (b) global ocean mass trends for 2005–2015 and (c) trends in global mass budget (in mm yr^{-1} SLE over 2005–2015) for all components of the global water budget. A low-pass filter to remove sub-annual frequencies has been applied to the time-series.

4.3 Comparison with mascons solutions

In this section, we compare our ensemble with the mascon solutions from JPL (RL05M.1.MSCNv02CRIv02 solution with Coastal Regional Improvement filter applied; Watkins *et al.* 2015), CSR (the CSR RL05.Mascons.v01; Save *et al.* 2016) and GSFC (the Global Solution v2.3; Luthcke *et al.* 2013). For a rigorous comparison, we select the subset of our ensemble that is consistent with the mascon solutions in terms of post-processing. The subset includes all solutions that use the Swenson *et al.* (2008) geocentre motion correction, the Cheng *et al.* (2013a) $C_{2,0}$ correction and the Geruo *et al.* (2013) GIA model. JPL and CSR solutions are released with the ocean model and the atmosphere model restored over the ocean. To ensure that these solutions are consistent with the spherical harmonic solution, we restore the mean atmosphere load over the ocean (Landerer, personal communication 2017). We use the land/ocean mask of each mascon centre to compute the trends in the water budget components.

Regarding the trend in global ocean mass (Fig. 8b), there is a good agreement between our subset and the JPL mascon estimate while the CSR mascon estimate is significantly smaller (by 0.09 mm yr^{-1} , 90 per cent CL) and the GSFC estimate is significantly larger (by 0.14 mm yr^{-1} at the 90 per cent CL). At interannual timescales (Fig. 8a), our sub-ensemble is in general agreement with mascons solutions except during La Nina 2011 where it differs significantly from all mascons solutions. Regarding the glaciers & TWS trend

component our sub-ensemble differs with the three mascons solutions but it is not an outlier (0.13 mm yr^{-1} SLE versus 0.35 , 0.23 and 0.02 mm yr^{-1} SLE). Regarding the Antarctica trend our sub-ensemble presents the highest mass loss (0.68 mm yr^{-1} SLE versus 0.64 , 0.64 and 0.62 mm yr^{-1} SLE). In terms of the other global water budget components, there is a good agreement ($\pm 0.05 \text{ mm yr}^{-1}$ SLE). Note that CSR solution do not close the global water budget because of some interpolation issues between the hexagonal computation grid and the final product that is in a rectangular grid (Save, personal communication 2017). The JPL solution closes the mass budget with a precision of 0.01 mm yr^{-1} SLE. The small non-closure of 0.01 mm yr^{-1} probably comes from a residual trend of 0.01 mm yr^{-1} in the atmospheric background model (over land) which has not been restored here.

4.4 Implications for the global water budget, the sea level budget and the Earth energy imbalance

Based on our ensemble, we find a total uncertainty in global ocean mass from GRACE of $\pm 0.27 \text{ mm yr}^{-1}$ over 2005–2015 (SLE at the 90 per cent CL). This uncertainty is comparable to the uncertainty in thermal expansion [$\pm 0.15 \text{ mm yr}^{-1}$, Dieng *et al.* (2017) and $\pm 0.27 \text{ mm yr}^{-1}$, Desbruyères *et al.* (2016)] and the uncertainty in global mean sea level from satellite altimetry over the same period (which is of $\pm 0.33 \text{ mm yr}^{-1}$; Ablain *et al.* 2015).

When GRACE observations of the ocean mass changes are combined with satellite altimetry, it gives an alternative estimate of

the thermal expansion with an uncertainty of $\pm 0.30 \text{ mm yr}^{-1}$ over 2005–2015 (at the 90 per cent CL assuming that the uncertainty from GRACE and satellite altimetry are independent). Assuming a global expansion efficiency of heat of $0.12 \pm 0.01 \text{ m YJ}^{-1}$ (Levitus *et al.* 2012) we find that this uncertainty implies an uncertainty in the net warming of the ocean and the Earth energy budget of $\pm 0.25 \text{ W m}^{-2}$ over 2005–2015 (at 90 per cent CL assuming Gaussian distribution) when inferred using the sea level budget approach.

5 CONCLUSION

We compared trends in GRACE estimates of the global water budget components over 2005–2015 for different set of processing parameters. We considered variations in six different processing parameters namely the processing centre of the raw GRACE solutions, the geocentre motion and $C_{2,0}$ corrections, the filtering, the leakage correction and the GIA correction. With all possible combinations of the different processing parameters we computed an ensemble of 1500 post-processed GRACE solutions from which we evaluated the trends in global water budget components and their associated uncertainty. As an estimate of the uncertainty we consider the spread around the ensemble mean. This approach has limitations and may not reveal the true uncertainty of the GRACE estimates but it gives interesting insights on the sources of GRACE errors as it enables to explore the dependency of GRACE uncertainty to the different processing parameters.

The analysis of the uncertainties associated with GRACE solutions shows that they are dominated by the uncertainty in the geocentre motion correction and the GIA correction. The uncertainty in the geocentre motion generates an uncertainty in GRACE estimates of $\pm 0.21 \text{ mm yr}^{-1}$ on the global ocean mass, $\pm 0.01 \text{ mm yr}^{-1}$ SLE on Greenland mass loss, $\pm 0.05 \text{ mm yr}^{-1}$ SLE on Antarctica mass loss, $\pm 0.02 \text{ mm yr}^{-1}$ SLE on arctic islands mass loss and $\pm 0.23 \text{ mm yr}^{-1}$ SLE on glaciers & TWS changes over 2005–2015 (at 1.65σ , i.e. 90 per cent CL).

The uncertainty in the GIA correction generates an uncertainty in GRACE estimates of $\pm 0.12 \text{ mm yr}^{-1}$ on the global ocean mass, $\pm 0.01 \text{ mm yr}^{-1}$ SLE on the Greenland mass loss, $\pm 0.12 \text{ mm yr}^{-1}$ SLE on the Antarctica mass loss, $\pm 0.01 \text{ mm yr}^{-1}$ SLE on arctic islands mass loss and of $\pm 0.03 \text{ mm yr}^{-1}$ SLE on the glaciers & TWS changes over 2005–2015 (at 1.65σ , i.e. 90 per cent CL). This uncertainty in GIA is likely underestimated because it does not take into account the total uncertainty in the ice history (we only considered here GIA solutions based on the ICE5G and ICE6G models) and two of the three models have updated and converged in the estimate of the Antarctica GIA mass apparent trend with the regional GIA models. This is evidenced in Greenland where the use of a regional GIA model yield a mass trend that is significantly smaller (by 0.06 mm yr^{-1}) than our ensemble estimate.

There are other sources of uncertainty in GRACE solutions that have not been taken into account here like the effect of earthquakes or the uncertainties in the Earth reference frame that are not related to the geocentre motion. But they are likely small compared to the GIA and the geocentre motion effects (Reager *et al.* 2016).

A more general caveat concerning our uncertainty estimate is that our calculations are based on an ensemble of products which is limited (because of a limited available sampling of the parameters), and which does not explore all sources of uncertainties (because some uncertainty sources such as earthquakes, are not represented). These

two characteristics make us think that our uncertainty estimates are likely underestimated.

Compared with mascons solutions, we find a good agreement in terms of interannual variability and trends with JPL solution. However, with the CSR and GSFC solutions, we find significant discrepancies in terms of trends.

Compared to the other GRACE-based studies (listed in Table 2 and Fig. 7), our estimates of the uncertainties are in general agreement for all global water budget components

When the uncertainty on the geocentre motion is included, the total uncertainty of GRACE on the global water and sea level budget is $\pm 0.27 \text{ mm yr}^{-1}$ SLE (at 1.65σ , i.e. 90 per cent CL; Table 1). This uncertainty is similar to the uncertainty in sea level estimate. It fixes a limit on the constraints that the budget approach provides on missing or poorly known contributions to sea level rise (such as the deep ocean contribution; see Dieng *et al.* 2015b) or on related essential climate variable such as the total ocean heat content from which the Earth's energy imbalance can be deduced (Llovel *et al.* 2014; Dieng *et al.* 2015b). These results call for more research to refine our estimates of the geocentre motion and the geoid response to GIA.

ACKNOWLEDGEMENTS

The Grace Level 3 data were obtained from ICGEM (www.icgem.gfz-potsdam.de/ICGEM/) and GRGS (grgs.obs-mip.fr/grace/). Ocean reanalysis data from www.ecmwf.int/en/research/climate-reanalysis/ocean-reanalysis and www.marine.copernicus.eu. We acknowledge support from CNES.

The ensemble of post-processed GRACE solutions created for this study is available online at ftp.legos.obs-mip.fr/pub/soa/gravimetrie/grace_legos

We want to thank Dr A, Dr Chen, Dr Cheng, Dr Li, Dr Rietbroek, Dr Save and Dr Wu for providing data. We also want to thank Dr Chambers, Dr Horwath, Dr Kusche, Dr Landerer and an anonymous reviewer for their constructive remarks, corrections and suggestions that improved this article significantly.

Author contributions: BM and AB designed the study. AB made the data analysis. AB and BM lead the writing of the paper. Others co-authors discussed the results and contributed to the writing. CNES supported the work of BM, AB and EB.

REFERENCES

- Ablain, M. *et al.*, 2015. Improved sea level record over the satellite altimetry era (1993–2010) from the Climate Change Initiative project, *Ocean Sci.*, **11**(1), 67–82.
- Altamimi, Z., Rebischung, P., Métivier, L. & Collilieux, X., 2016. ITRF2014: a new release of the International Terrestrial Reference Frame modeling nonlinear station motions, *J. geophys. Res.*, **121**(8).
- Balmaseda, M.A., Mogensen, K. & Weaver, A.T., 2013. Evaluation of the ECMWF ocean reanalysis system ORAS4, *Q. J. R. Meteorol. Soc.*, **139**(674), 1132–1161.
- Barletta, V.R., Sørensen, L.S. & Forsberg, R., 2013. Scatter of mass changes estimates at basin scale for Greenland and Antarctica, *Cryosphere*, **7**(5), 1411–1432.
- Chambers, D.P., 2006. Evaluation of new GRACE time-variable gravity data over the ocean, *Geophys. Res. Lett.*, **33**(17).
- Chambers, D.P., 2009. Calculating trends from GRACE in the presence of large changes in continental ice storage and ocean mass, *Geophys. J. Int.*, **176**(2), 415–419.

- Chambers, D.P. & Bonin, J.A., 2012. Evaluation of Release-05 GRACE time-variable gravity coefficients over the ocean, *Ocean Sci.*, **8**(5), 859–868.
- Cheng, M. & Ries, J., 2017. The unexpected signal in GRACE estimates of C20, *J. Geod.*, **91**(8), 897–914.
- Cheng, M., Tapley, B.D. & Ries, J.C., 2013a. Deceleration in the Earth's oblateness, *J. geophys. Res.*, **118**(2), 740–747.
- Cheng, M.K., Ries, J.C. & Tapley, B.D., 2013b. Geocenter variations from analysis of SLR data. In *Reference Frames for Applications in Geosciences*, pp. 19–25, eds Altamimi, Z. & Collilieux, X., Springer.
- Chen, J., Famiglietti, J.S., Scanlon, B.R. & Rodell, M., 2015a. Groundwater storage changes: present status from GRACE observations, *Surv. Geophys.*, **37**(2), 397–417.
- Chen, J.L., Wilson, C.R., Li, J. & Zhang, Z., 2015b. Reducing leakage error in GRACE-observed long-term ice mass change: a case study in West Antarctica, *J. Geod.*, **89**(9), 925–940.
- Chen, J.L., Wilson, C.R., Tapley, B.D. & Grand, S., 2007. GRACE detects coseismic and postseismic deformation from the Sumatra-Andaman earthquake, *Geophys. Res. Lett.*, **34**(13), L13302.
- Church, J.A. *et al.*, 2013. Sea level change. In *Climate Change 2013: The Physical Science Basis. Contribution of Working Group I to the Fifth Assessment Report of the Intergovernmental Panel on Climate Change*, eds Stocker, T.F. *et al.* Cambridge University Press.
- Cretaux, J.F., Soudarin, L., Davidson, F.J.M., Gennero, M.C., Berge-Nguyen, M. & Cazenave, A., 2002. Seasonal and interannual geocenter motion from SLR and DORIS measurements: comparison with surface loading data, *J. geophys. Res.*, **107**(B12), ETG 16–1–ETG 16–9.
- Desbruyères, D.G., Purkey, S.G., McDonagh, E.L., Johnson, G.C. & King, B.A., 2016. Deep and abyssal ocean warming from 35 years of repeat hydrography, *Geophys. Res. Lett.*, **43**(19).
- Dieng, H.B., Cazenave, A., Meyssignac, B. & Ablain, M., 2017. New estimate of the current rate of sea level rise from a sea level budget approach, *Geophys. Res. Lett.*, **44**(8).
- Dieng, H.B., Champollion, N., Cazenave, A., Wada, Y., Schrama, E. & Meyssignac, B., 2015a. Total land water storage change over 2003–2013 estimated from a global mass budget approach, *Environ. Res. Lett.*, **10**(12).
- Dieng, H.B., Palanisamy, H., Cazenave, A., Meyssignac, B. & von Schuckmann, K., 2015b. The sea level budget since 2003: inference on the deep ocean heat content, *Surv. Geophys.*, **36**(2), 209–229.
- Fisher, R.A., 1925. *Statistical Methods for Research Workers*, Oliver & Boyd.
- Flechtner, F., Döbslaw, H. & Fagiolini, E., 2015. *AODIB Product Description Document for Product Release 05 Rev4.4 GRACE 327–750*, Geo Forschungszentrum Potsdam, Potsdam, Germany.
- Fretwell, P. *et al.*, 2013. Bedmap2: improved ice bed, surface and thickness datasets for Antarctica, *Cryosphere*, **7**(1), 375–393.
- Fritsche, M., Dietrich, R., Rülke, A., Rothacher, M. & Steigenberger, P., 2010. Low-degree earth deformation from reprocessed GPS observations, *GPS Solutions*, **14**(2), 165–175.
- Gardner, A.S. *et al.*, 2013. A reconciled estimate of glacier contributions to sea level rise: 2003 to, 2009, *Science*, **340**(6134), 852–857.
- Garric, G. *et al.*, 2018. Performance and quality assessment of the global ocean eddy-permitting physical reanalysis GLORYS2V4, in *Proceedings of the Eight EuroGOOS International Conference*, Paper Presented at the Operational Oceanography Serving Sustainable Marine Development, EuroGOOS, Brussels, Belgium, 2018: Bergen, Norway.
- Geoffroy, O., Saint-Martin, D. & Ribes, A., 2012. Quantifying the sources of spread in climate change experiments, *Geophys. Res. Lett.*, **39**(24).
- Geruo, A., Wahr, J. & Zhong, S., 2013. Computations of the viscoelastic response of a 3-D compressible Earth to surface loading: an application to Glacial Isostatic Adjustment in Antarctica and Canada, *Geophys. J. Int.*, **192**(2), 557–572.
- Ivins, E.R., James, T.S., Wahr, J.O., Schrama, E.J., Landerer, F.W. & Simon, K.M., 2013. Antarctic contribution to sea level rise observed by GRACE with improved GIA correction, *J. geophys. Res.*, **118**(6), 3126–3141.
- Jacob, T., Wahr, J., Pfeffer, W.T. & Swenson, S., 2012. Recent contributions of glaciers and ice caps to sea level rise, *Nature*, **482**(7386), 514–518.
- Jekeli, C., 1981. Modifying Stokes' function to reduce the error of geoid undulation computations, *J. Geophys. Res.*, **86**(B8), 6985–6990, doi:10.1029/JB086iB08p06985.
- Khan, S.A. *et al.*, 2016. Geodetic measurements reveal similarities between post-Last Glacial Maximum and present-day mass loss from the Greenland ice sheet, *Sci. Adv.*, **2**(9).
- Klinger, B., Mayer-Gürr, T., Behzadpour, S., Ellmer, M., Kvas, A. & Zehentner, N., 2016. The new ITSG-Grace2016 release, in *EGU 2016 General Assembly, 2016*, Vienna, Austria.
- Kusche, J., Schmidt, R., Petrovic, S. & Rietbroek, R., 2009. Decorrelated GRACE time-variable gravity solutions by GFZ, and their validation using a hydrological model, *J. Geod.*, **83**(10), 903–913.
- Landerer, F.W. & Swenson, S.C., 2012. Accuracy of scaled GRACE terrestrial water storage estimates, *Water Resour. Res.*, **48**(4), W04531.
- Lemoine, J.-M., Bourgogne, S., Biancale, R., Bruinsma, S. & Gégout, P., 2016. CNES/GRGS solutions Focus on the inversion process, in *Paper presented at the GRACE Science Team Meeting, A1-02*, Berlin, Germany.
- Lemoine, J.-M. & Reinquin, F., 2017. Processing of SLR observations at CNES, *Newsletter EGS/EM*, October, Page 3.
- Leuliette, E.W. & Willis, J.K., 2011. Balancing the sea level budget, *Oceanography*, **24**(2), 122–129.
- Levitus, S. *et al.*, 2012. World ocean heat content and thermocline sea level change (0–2000 m), 1955–2010: World ocean heat content, *Geophys. Res. Lett.*, **39**(10).
- Llovel, W., Willis, J.K., Landerer, F.W. & Fukumori, I., 2014. Deep-ocean contribution to sea level and energy budget not detectable over the past decade, *Nature Clim. Change*, **4**(11), 1031–1035.
- Llovel, W. *et al.*, 2011. Terrestrial waters and sea level variations on inter-annual time scale, *Glob. Planet. Change*, **75**(1–2), 76–82.
- Luthcke, S.B., Sabaka, T.J., Loomis, B.D., Arendt, A.A., McCarthy, J.J. & Camp, J., 2013. Antarctica, Greenland and Gulf of Alaska land-ice evolution from an iterated GRACE global mascon solution, *J. Glaciol.*, **59**(216), 613–631.
- Martín-Español, A., King, M.A., Zammit-Mangion, A., Andrews, S.B., Moore, P. & Bamber, J.L., 2016. An assessment of forward and inverse GIA solutions for Antarctica, *J. geophys. Res.*, **121**(9).
- McMillan, M., Shepherd, A., Sundal, A., Briggs, K., Muir, A., Ridout, A., Hogg, A. & Wingham, D., 2014. Increased ice losses from Antarctica detected by CryoSat-2, *Geophys. Res. Lett.*, **41**(11), 3899–3905.
- Mémin, A., Flament, T., Rémy, F. & Llubes, M., 2014. Snow- and ice-height change in Antarctica from satellite gravimetry and altimetry data, *Earth planet. Sci. Lett.*, **404**, 344–353.
- Nilsson, J., Sandberg Sørensen, L., Barletta, V.R. & Forsberg, R., 2015. Mass changes in Arctic ice caps and glaciers: implications of regionalizing elevation changes, *Cryosphere*, **9**(1), 139–150.
- Peltier, W.R., Argus, D.F. & Drummond, R., 2017. Comment on “An Assessment of the ICE-6G_C (VM5a) Glacial Isostatic Adjustment Model” by Purcell *et al.*, *J. geophys. Res.*, **123**(2), 2019–2028.
- Pfeffer, W.T. *et al.*, 2014. The Randolph Glacier Inventory: a globally complete inventory of glaciers, *J. Glaciol.*, **60**(221), 537–552.
- Purcell, A., Tregoning, P. & Dehecq, A., 2016. An assessment of the ICE6G_C(VM5a) glacial isostatic adjustment model, *J. geophys. Res.*, **121**(5).
- Purcell, A., Tregoning, P. & Dehecq, A., 2018. Reply to Comment by W. R. Peltier, D. F. Argus, and R. Drummond on “An Assessment of the ICE6G_C (VM5a) Glacial Isostatic Adjustment Model.”, *J. geophys. Res.*, **123**(2), 2029–2032.
- Purkey, S.G., Johnson, G.C. & Chambers, D.P., 2014. Relative contributions of ocean mass and deep steric changes to sea level rise between 1993 and, 2013, *J. geophys. Res.*, **119**(11), 7509–7522.
- Quinn, K.J. & Ponte, R.M., 2010. Uncertainty in ocean mass trends from GRACE, *Geophys. J. Int.*, **181**(2), 762–768.
- Reager, J.T., Gardner, A.S., Famiglietti, J.S., Wiese, D.N., Eicker, A. & Lo, M.-H., 2016. A decade of sea level rise slowed by climate-driven hydrology, *Science*, **351**(6274), 699–703.
- Riddell, A.R., King, M.A., Watson, C.S., Sun, Y., Riva, R.E.M. & Rietbroek, R., 2017. Uncertainty in geocenter estimates in the context of ITRF2014, *J. geophys. Res.*, **122**(5), 4020–4032.

- Rietbroek, R., Brunnabend, S.-E., Kusche, J., Schröter, J. & Dahle, C., 2016. Revisiting the contemporary sea-level budget on global and regional scales, *Proc. Natl. Acad. Sci. USA*, **113**, 1504–1509.
- Rietbroek, R., Fritsche, M., Brunnabend, S.-E., Daras, I., Kusche, J., Schröter, J., Flechtner, F. & Dietrich, R., 2012. Global surface mass from a new combination of GRACE, modelled OBP and reprocessed GPS data, *J. Geodyn.*, **59–60**, 64–71.
- Roemmich, D., 2009. Argo the challenge of continuing 10 years of progress, *Oceanography*, **22**(3), 46–55.
- Sasgen, I., Martinec, Z. & Fleming, K., 2006. Wiener optimal filtering of GRACE data, *Stud. Geophys. Geod.*, **50**(4), 499–508.
- Save, H., Bettadpur, S. & Tapley, B.D., 2016. High-resolution CSR grace RL05 mascons: high-resolution CSR grace RL05 mascons, *J. geophys. Res.*, **121**(10), 7547–7569.
- Schrama, E.J.O., Wouters, B. & Lavallée, D.A., 2007. Signal and noise in Gravity Recovery and Climate Experiment (GRACE) observed surface mass variations, *J. geophys. Res.*, **112**(B8).
- Schrama, E.J.O., Wouters, B. & Rietbroek, R., 2014. A mascon approach to assess ice sheet and glacier mass balances and their uncertainties from GRACE data, *J. geophys. Res.*, **119**(7), 6048–6066.
- Shepherd, A. et al., 2012. A reconciled estimate of ice-sheet mass balance, *Science*, **338**(6111), 1183–1189.S
- Stuhne, G.R. & Peltier, W.R., 2015. Reconciling the ICE-6G.C reconstruction of glacial chronology with ice sheet dynamics: The cases of Greenland and Antarctica, *J. geophys. Res.*, **120**(9), 1841–1865.
- Swenson, S., Chambers, D. & Wahr, J., 2008. Estimating geocenter variations from a combination of GRACE and ocean model output, *J. geophys. Res.*, **113**(B8).
- Swenson, S. & Wahr, J., 2006. Post-processing removal of correlated errors in GRACE data, *Geophys. Res. Lett.*, **33**(8).
- Tapley, B.D., Bettadpur, S., Ries, J.C., Thompson, P.F. & Watkins, M.M., 2004. GRACE Measurements of mass variability in the Earth system, *Science*, **305**(5683), 503–505.
- Velicogna, I., Sutterley, T.C. & van den Broeke, M.R., 2014. Regional acceleration in ice mass loss from Greenland and Antarctica using GRACE time-variable gravity data, *Geophys. Res. Lett.*, **41**(22), 8130–8137.
- Velicogna, I. & Wahr, J., 2013. Time-variable gravity observations of ice sheet mass balance: Precision and limitations of the GRACE satellite data, *Geophys. Res. Lett.*, **40**(12), 3055–3063.
- Wahr, J., Molenaar, M. & Bryan, F., 1998. Time variability of the Earth's gravity field: hydrological and oceanic effects and their possible detection using Grace, *J. geophys. Res.*, **103**(B12), 30 205–30 229.
- Wahr, J., Nerem, R.S. & Bettadpur, S.V., 2015. The pole tide and its effect on GRACE time-variable gravity measurements: implications for estimates of surface mass variations, *J. geophys. Res.*, **120**(6).
- Wahr, J., Swenson, S. & Velicogna, I., 2006. Accuracy of GRACE mass estimates, *Geophys. Res. Lett.*, **33**(6), L06401.
- Watkins, M.M. & Eanes, R.J., 1997. Observations of tidally coherent diurnal and semidiurnal variations in the geocenter, *Geophys. Res. Lett.*, **24**(17), 2231–2234.
- Watkins, M.M., Wiese, D.N., Yuan, D.-N., Boening, C. & Landerer, F.W., 2015. Improved methods for observing Earth's time variable mass distribution with GRACE using spherical cap mascons, *J. geophys. Res.*, **120**(4).
- Whitehouse, P.L., Bentley, M.J., Milne, G.A., King, M.A. & Thomas, I.D., 2012. A new glacial isostatic adjustment model for Antarctica: calibrated and tested using observations of relative sea-level change and present-day uplift rates, *Geophys. J. Int.*, **190**(3), 1464–1482.
- Wouters, B., Bonin, J.A., Chambers, D.P., Riva, R.E.M., Sasgen, I. & Wahr, J., 2014. GRACE, time-varying gravity, Earth system dynamics and climate change, *Rep. Prog. Phys.*, **77**(11).
- Wu, X., 2010. Simultaneous Estimation of Global Present-Day Water Transport and Glacial Isostatic Adjustment, *Nature Geosci.*, **3**, 642–646.
- Wu, X., Kusche, J. & Landerer, F.W., 2017. A new unified approach to determine geocentre motion using space geodetic and GRACE gravity data, *Geophys. J. Int.*, **209**(3), 1398–1402.
- Wu, X., Ray, J. & van Dam, T., 2012. Geocenter motion and its geodetic and geophysical implications, *J. Geodyn.*, **58**, 44–61.
- Yi, S., Sun, W., Heki, K. & Qian, A., 2015. An increase in the rate of global mean sea level rise since 2010: increase in sea level rise rate, *Geophys. Res. Lett.*, **42**, 3998–4006.

SUPPORTING INFORMATION

Supplementary data are available at [GJI](#) online.

Figure S1. Filtering parameter comparison.

Figure S2. Formal error in raw solutions, *a priori* error and uncertainty of GRACE raw solutions.

Figure S3. Evaluation of the leakage correction on a synthetic field.

Figure S4. Evaluation of the leakage correction on Jan 2005 for 241st case of the ensemble.

Figure S5. Analysis of the boundary of the coastal ocean.

Figure S6. Earth mask.

Figure S7. Effect of the *Z* geocentre motion trend over the Global ocean mass.

Table S1. GIA apparent mass change expressed in mm SLE yr⁻¹.

Table S2. Unitary effect of each axis of the geocentre motion on the components of the global water budget.

Please note: Oxford University Press is not responsible for the content or functionality of any supporting materials supplied by the authors. Any queries (other than missing material) should be directed to the corresponding author for the paper.

2.3.4 Publications using the ensemble of GRACE solutions

My ensemble of GRACE solutions, called here after GRACE LEGOS, has been well received within the community because it allows users to estimate uncertainties. For this reason, I have been involved in several studies. For each study, I provided my ensemble and my expertise in how to use it and interpret it. My ensemble of GRACE solutions has been used to study the ocean mass [Carret et al., 2017; Kumar et al., 2018; Llovel et al., 2019] and ice sheet mass loss [Shepherd et al., 2018]. I summarize the articles here and detail my contribution. Abstracts are available in Annex A. I present in Table 2.3 the log of GRACE LEGOS versions which has been used in published studies.

Table 2.3: Description of the versions of the GRACE LEGOS ensemble of solution used in published articles

Version	Date	Publications	Notes
V0.4 ^a	Jul 2016	[Carret et al., 2017]	Ensemble of 30 cases including: 5 Processing centers, 1 geocenter [Swenson et al., 2008], 1 C_{20} [Cheng et al., 2013a], 2 GIA models [A et al., 2013; Stuhne and Peltier, 2015], and 3 leakage corrections based on ocean observations
V0.7 ^a	Oct 2016	[Shepherd et al., 2018] [Shepherd et al., 2019]	Ensemble of 720 cases: Inclusion of 3 geocenter [Cheng et al., 2013b; Lemoine and Reinquin, 2017; Swenson et al., 2008], 2 C_{20} [Cheng et al., 2013a; Lemoine and Reinquin, 2017], 3 GIA model [A et al., 2013; Stuhne and Peltier, 2015; Purcell et al., 2016], 4 ddk filters [Kusche et al., 2009]
V0.8 ^a	Aug 2017	[Kumar et al., 2018]	Dates extension until end of 2015
V1.0	Jul 2018	[Blazquez et al., 2018] [Llovel et al., 2019]	First version published [Blazquez et al., 2018] with 1500 cases 5 geocenter ([Cheng et al., 2013b; Lemoine and Reinquin, 2017; Swenson et al., 2008; Rietbroek et al., 2016; Wu et al., 2017], Update GIA models [A et al., 2013; Stuhne and Peltier, 2015; Purcell et al., 2016])
V1.1	Mar 2019	[In prep Blazquez et al., 2020]	Pole tide correction, 2 forward modeling runs to reduce Gibbs effect on Antarctica and Greenland. Correction of the dealiasing model to remove the degree-one. Correction on GIA model [Purcell et al., 2016] consistent with a zero degree-one and the rotational feedback. geocenter Swenson corrected with GAD instead of GAA+GAB. Land water leakage correction over south Asia.

^a Before the ensemble publication

In Carret et al. [2017], we explore the sea-level budget in the Arctic ocean, a region where data is scarce. We compare sea-level from two new regional altimetry datasets from *Collecte Localisation Satellites, France (CLS)* and from *Danmarks Tekniske Universitet,*

Denmark (DTU), steric sea-level from [Ocean ReAnalysis Pilot 5 \(ORAP5\)](#) with GRACE-based ocean mass from [JPL mascon V1.0](#), from [CSR](#) with Chambers et al. [2004] post-processing and from my GRACE LEGOS V0.4 (See [Table 2.3](#)). I analyzed all GRACE-based ocean mass solutions and participated in the explanation of the differences among the solutions. The study show regional discrepancies in the sea-level budget, especially in trends in the Beaufort Gyre and the russian coast. We find better correlation with CSR-based product and the mean value of GRACE LEGOS ensemble than JPL mascons, although the large uncertainties do not allow to further pinpoint the reasons for these differences. Abstract available in annex A1.

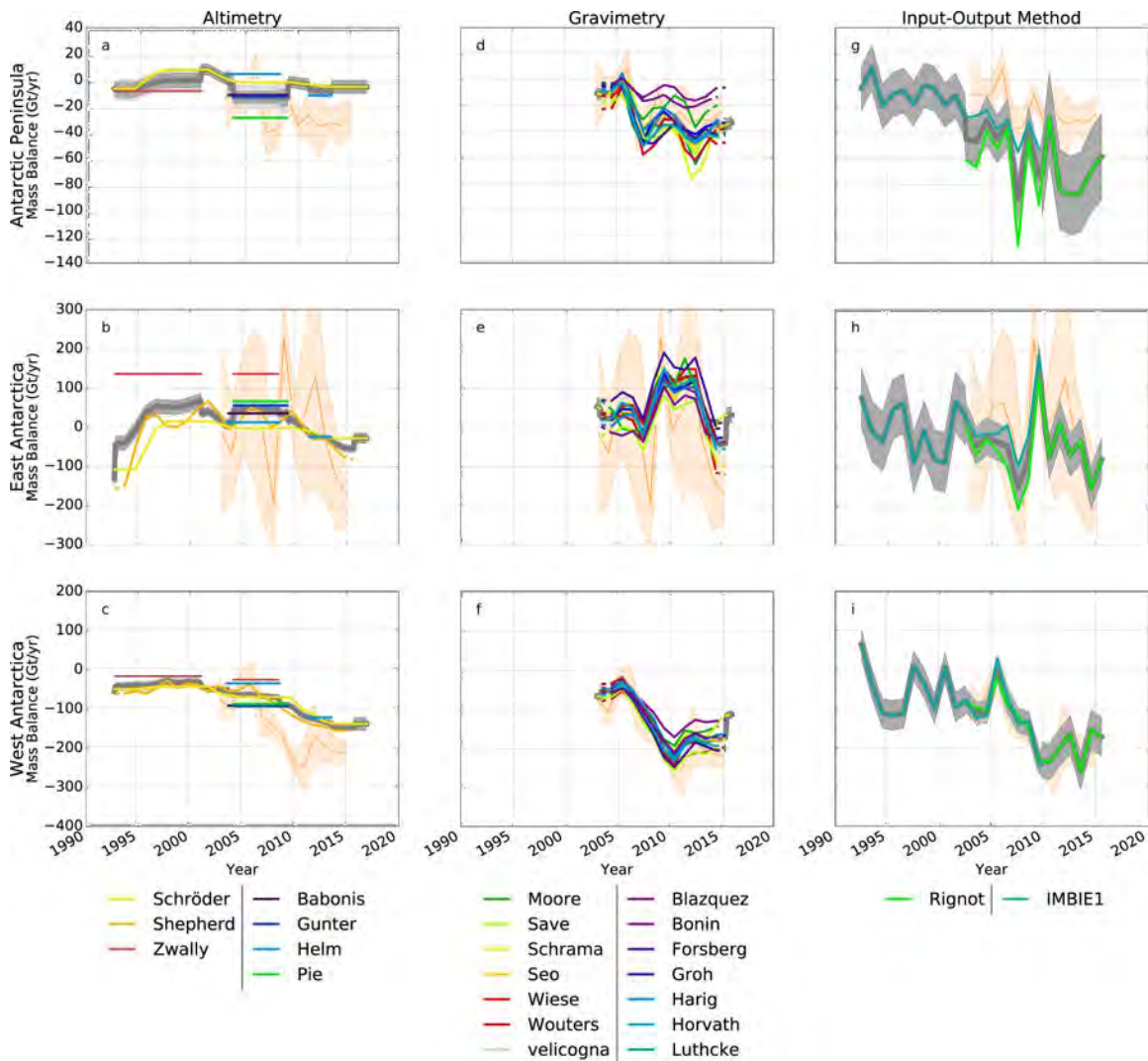


Figure 2.14: Rates of Regional ice-sheet mass balance excerpt from IMBIE 2 comparison [Shepherd et al., 2018] including altimetry, gravimetry and IOM estimates compared to GRACE LEGOS V1.1 estimates superposed in orange shaded areas.

The article Shepherd et al. [2018] consisted in a comparison of 24 independently derived estimates of Antarctica mass balance, including altimetry (7 products), gravimetry (15 products) and IOM (2 products). Due to large amount of data and different origin of the data, each group only provided one timeseries for Greenland and one for each region in Antarctica (WAIS, AP and EAIS). In my case, I provided the mean of the ensemble from

GRACE LEGOS V0.7 (See Table 2.3). My solution is within the uncertainties of the other gravimetry products except in EAIS (purple solution Fig. 2.14 e) and WAIS (Fig. 2.14 f). In AP, my solution shows discrepancies with the other gravimetry estimates upto 40 Gt/yr due to the preliminary land/ocean leakage correction we used in this version of the ensemble. Abstract available in annex A2.

I decided to take advantage of my ensemble method to compare the regional mass estimates from [Shepherd et al., 2018] with the estimates from my ensemble including this time the uncertainties derived from the ensemble. I superposed them as orange shaded areas in all panels of the figure 2.14. Our solution encompass the other gravimetry solutions (Fig. 2.14d-f), explaining the differences between the solutions. It also agrees better with IOM-based estimates than the other gravimetry products for WAIS (Fig. 2.14i) and EAIS (Fig. 2.14h). However the uncertainty in East Antarctica mass balance rate is larger than the other estimates. This uncertainty is mainly due to the uncertainty in the geocenter parameter (± 33 Gt/yr) and GIA correction (± 26 Gt/yr) and to a lesser extent C_{20} (± 11 Gt/yr).

2.4 Conclusions

I analyzed the GRACE data processing from the on board data (L1 data) to the post processing in this chapter. I found out that post-processing is responsible of most of 79% of the uncertainty in ocean mass trends estimates (Table 2.2) and only 21 % is due to the differences between the processing centers. Using my ensemble of GRACE solutions which includes a state-of-the-art of post processing parameters enables me to explore the reason for the spread in GRACE estimates of the water budget components. With this ensemble, I estimate the ocean mass trend for the period from January 2005 to December 2015 at 1.55 ± 0.33 mm/yr. This uncertainty of ± 0.33 mm/yr is mainly due to the uncertainties in geocenter trends and in GIA gravity corrections. These two post-processing parameters hamper the closure of the global water budget at an accuracy smaller than 0.1 mm SLE/yr (Scientific question 1).

Greenland is the main contributor to the global water budget with 0.80 ± 0.03 mm/yr for the period 2005-2015, followed by Antarctica with 0.61 ± 0.15 mm/yr (Fig. 2.13). Uncertainty in Antarctica mass balance comes mainly from GIA (Table 2.2). I excerpt the arctic islands contribution from the rest of the glaciers as their are not lumped with TWS. I estimated their trend at 0.27 ± 0.03 mm/yr while the rest of glaciers and TWS contribution is -0.14 ± 0.33 mm/yr. Uncertainty in the glacier and TWS mass trends is correlated with the uncertainty in ocean mass trend as their uncertainty is caused by the same post-processing parameters (geocenter and GIA from Table 2.2)(Scientific question 6).

Chapter 3

Evaluating the uncertainty in the GRACE-based estimates of land mass changes. Separating glacier and TWS changes

After analyzing the global water budget and its uncertainties in chapter 2 and in Blazquez et al. [2018], I propose in this chapter to analyze uncertainty in [Land Water Storage \(LWS\)](#). I include in [LWS](#) all emergent land with the exception of Greenland, Antarctica as detailed in 1.2.1. In the previous chapter, I extracted Arctic islands from [LWS](#) because in this region the effect of the hydrology is negligible at interannual to decennial scales and GRACE-based mass changes can accurately be retrieved [Blazquez et al., 2018]. In this chapter [LWS](#) includes glaciers and [Terrestrial Water Storage \(TWS\)](#), even in the Arctic islands.

Analyzing the uncertainty in [LWS](#) mass changes, I found a mass trend of 0.14 ± 0.36 mm/yr by summing Arctic islands and glacier & [TWS](#) mass changes from table 2.2. The uncertainty of ± 0.36 mm/yr is mainly due to the uncertainty in geocenter trends (± 0.32 mm/yr) and to a lesser extent to the uncertainties in GIA (± 0.09 mm/yr), the spread among the processing centers (± 0.06 mm/yr), and the land/ocean leakage correction (± 0.08 mm/yr) (See Table 2.2). However, at local and regional scales, land leakage from glaciers and other well located mass changes may increase the uncertainty in land mass estimates.

GRACE-based glacier mass loss trend for the period 2005-2015 from the previous studies is -0.51 ± 0.11 mm SLE/yr [Marzeion et al., 2017]. This mass loss trend is smaller than the estimates from other techniques which range from -0.72 and -0.95 mm SLE/yr (Table 1.2). GRACE-based glacier mass loss are computed from: (1) forward modeling based on GRACE only data [Chen et al., 2013; Yi et al., 2015], (2) GRACE and hydrological models estimates [Jacob et al., 2012; Gardner et al., 2013; Schrama et al., 2014; Reager et al., 2016; Wouters et al., 2019], (3) GRACE and altimetry estimates [Rietbroek et al., 2016]. They all agree within their uncertainties, although there is a large spread among these estimates from 0.38 ± 0.07 mm SLE/yr [Rietbroek et al., 2016] to 0.53 ± 0.09 mm SLE/yr [Reager et al., 2016] or 0.55 ± 0.08 mm SLE/yr [Wouters et al.,

2019].

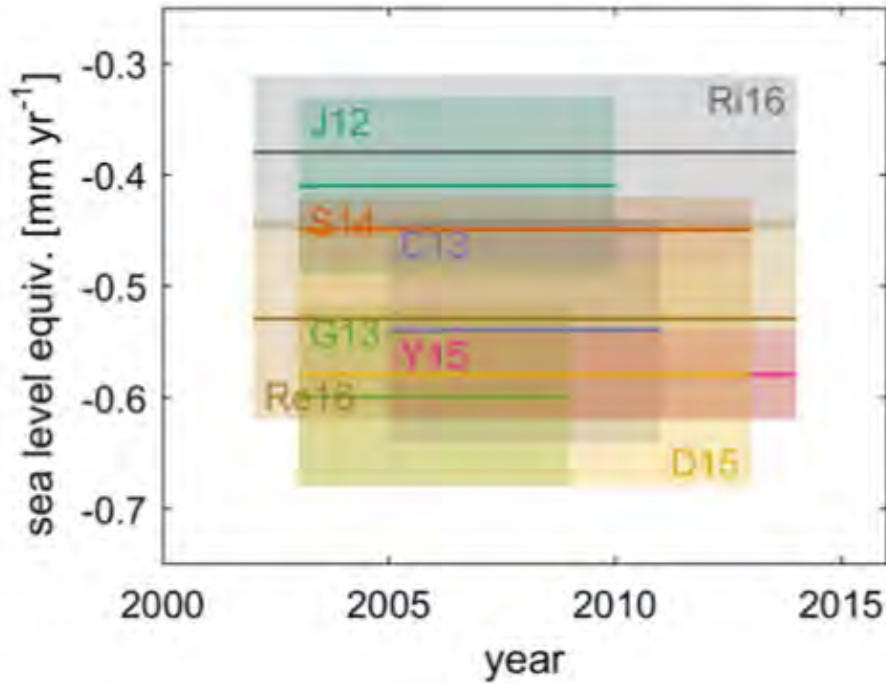


Figure 3.1: Glacier mass trend estimates based (partly) on GRACE data for the period from 2003 to 2015. Boxes indicate period covered and upper and lower confidence level of estimate. J12 is Jacob et al. [2012], G13 is Gardner et al. [2013], C13 is Chen et al. [2013], S14 is Schrama et al. [2014], D15 is Dieng et al. [2015a], Y15 is Yi et al. [2015], Re16 is Reager et al. [2016] and Ri16 is Rietbroek et al. [2016]. Figure excerpt from [Marzeion et al., 2017]. Recently, Wouters et al. [2019] estimate a trend of 0.55 ± 0.08 mm SLE/yr for the period from 2002 to 2016 (not shown in the figure).

Uncertainties in TWS mass changes from previous studies are larger than the uncertainties in glacier mass trends. There is no consensus on whether there was a mass gain of 0.32 mm SLE/yr [Reager et al., 2016] and 0.21 mm SLE/yr [Scanlon et al., 2018] or a mass loss of -0.21 mm SLE/yr [Rietbroek et al., 2016], -0.32 mm SLE/yr [Dieng et al., 2017], and 0.32 ± 0.02 mm SLE/yr [Kim et al., 2019].

In order to reduce the uncertainties in LWS mass change, I develop a land leakage correction method using independent mass change estimates spatially resolved in section 3.1. I explained the method in subsection 3.1.1, I apply this land leakage correction to the ensemble of GRACE solutions from chapter 2 in subsection 3.1.2. I attached an article where I explore the use of this land leakage method to reduce the uncertainties in TWS mass changes in south Asia [In prep Blazquez et al., 2020]. I discuss the perspectives for a global application of the method in section 3.2. I review from the bibliography, the contributions of the glaciers not included in the land leakage correction in 3.2.1. Based on these results, I present an estimate for LWS mass contribution analysing endorheic and exorheic basin and compare them to the bibliography in section 3.2.2. Then I address the scientific questions in section 3.3.

3.1 Land leakage correction

3.1.1 Land leakage correction method

Our land leakage correction is based on a forward modeling process [Chen et al., 2015] using independent observations to constraint spatially GRACE-based estimates. The forward modeling identifies the location of the sources of the mass changes and attributes the mass change signal to these locations via an iterative process to reduce the leakage. The method needs an *a priori* mass changes, known as true mass change. This true mass (M_{TRU}) is converted to predicted mass (M_{PRE}), by a conversion to spherical harmonics and a truncation at degree 60 and back to EWH. The predicted mass field is compared to the original observed mass field (M_{OBS}) and this residue is minimize via an iterative process, described in Fig. 3.2.

Forward modeling technique has been applied to retrieve Antarctica and other regions mass balance. In these regions, forward modeling has proven to be well adapted because the signal are isolated (i.e. Antarctic peninsula and the ocean [Chen et al., 2015]). However the application to other regions do not make consensus [Chen et al., 2014; Long et al., 2016].

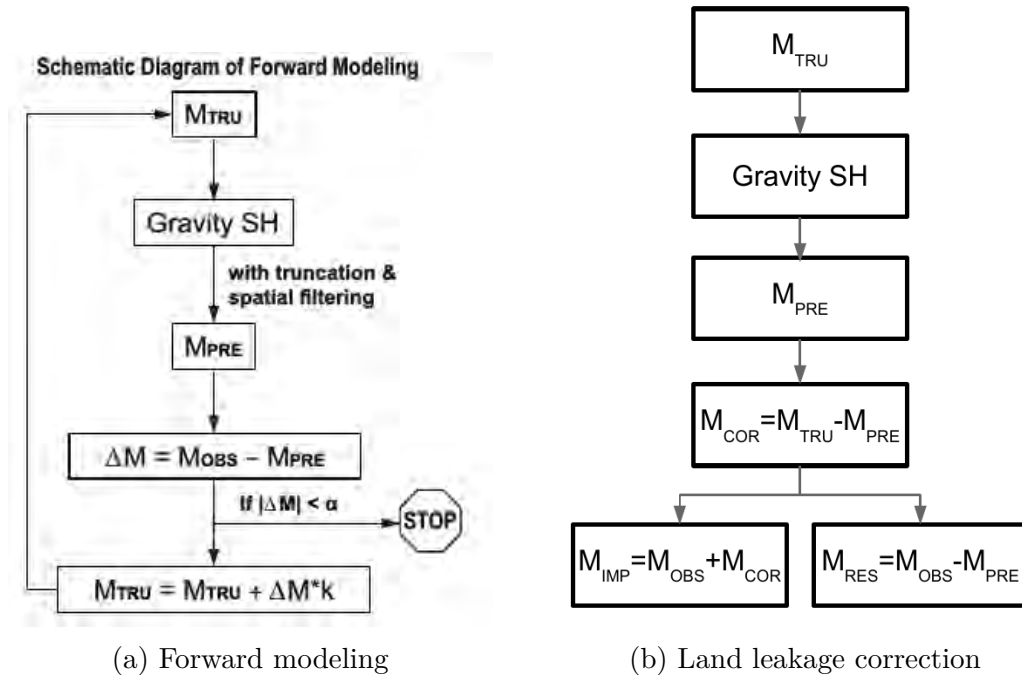


Figure 3.2: Schematic diagrams. M_{TRU} and M_{PRE} represent the true and the predicted mass fields, respectively, and M_{OBS} represents observed mass field. M_{RES} or ΔM represents the residual field. M_{COR} is the correcting field. M_{IMP} represent the improved field. In forward modeling, k is the scaling factor to speed up the convergence of the iterations, and α is the predefined threshold of minimum residuals when the iterations should stop. forward modeling figure (a) is excerpted from Chen et al. [2015]

The land leakage method I propose, consist in using independent observations where the uncertainties are smaller than the uncertainties from GRACE-based estimates (e.g.

glacier and lake mass changes). These independent observations are used as true mass to initialize a one-iteration forward-modeling (Fig. 3.2b and Fig.3.3). This true mass is convert to the predicted mass as in the forward modeling technique. Then, I define the correcting mass as the difference between the true and the predicted masses. This correcting mass corresponds to the improvement of the spatial signal. I then add this correction field to the observed field (M_{OBS}) to obtain the land leakage corrected field or improved field (M_{IMP}). As it is a one-iteration forward modeling, the land corrected field does not fit exactly the true mass. In this way, the leakage from this independent data and the corresponding uncertainties in glacier and TWS mass changes are reduced. I also analyzed the residual field (M_{RES}) as the mass changes not explained by the independent observations. This residual field illustrated the remaining leakage as well as the mass changes not observed by the independent data.

The land leakage correction method do not fully remove the leakage but reduces it drastically in regions where mass signals are well located and characterized by independent data as in the South Asia (next section).

3.1.2 Leakage correction applied to South Asia

South Asia is a region where **TWS** changes are known to be large [Babel and Wahid, 2008] and glaciers and lakes are concentrated in small locations. GRACE-only estimates based on forward modeling tend to overestimate the **TWS** mass trends [Long et al., 2016].

I decided to test and validate our land leakage correction in South Asia. Thus, I used independent mass changes based on observations for the lakes and glaciers of the regions. The lakes mass change were directly downloaded from Hydroweb [Cretaux et al., 2016] and glacier mass trends were based on Brun et al. [2017] (Fig 3.3a).

Glacier and lakes are responsible of half of the mass change trends in the region (e.g. lakes are responsible of 60% of the mass change in the Inner **Tibetan Plateau (TP)** while glaciers are responsible of 57% of the mass change in the Indus basin and 48% of the Brahmaputra basin [In prep Blazquez et al., 2020, Table 1]. However, there is still large mass changes in Northern India, near residual field (Fig.3.3f). This strong mass change is well documented as groundwater pumping [Asoka et al., 2017; Rodell et al., 2009].

Once the land leakage correction applied, I explore the water cycle at basin scale in terms of annual cycle, interannual variability and trends, through the hydrological approach (Eq. 3.1). I compared the variations of GRACE-based **LWS** ($d(LWS)/dt$) against precipitation (P), evapotranspiration (ET) and river discharge (Q) (Fig.3.4).

$$dLWS = \frac{d(LWS)}{dt} = (P - Q - ET) + errors \quad (3.1)$$

The approaches via the fluxes (P-Q-ET) and via the derivate of the **LWS** are in good agreement. I found a good correlation between both approaches in the interannual **LWS** mass change for the Indus and Ganges basins of 0.67 and 0.65. The correlation drops to 0.19 and 0.05 for Brahmaputra and the inner **TP**, respectively [In prep Blazquez et al., 2020]). Considering, the annual cycle, both techniques estimates agrees for the Ganges

3.1. LAND LEAKAGE CORRECTION

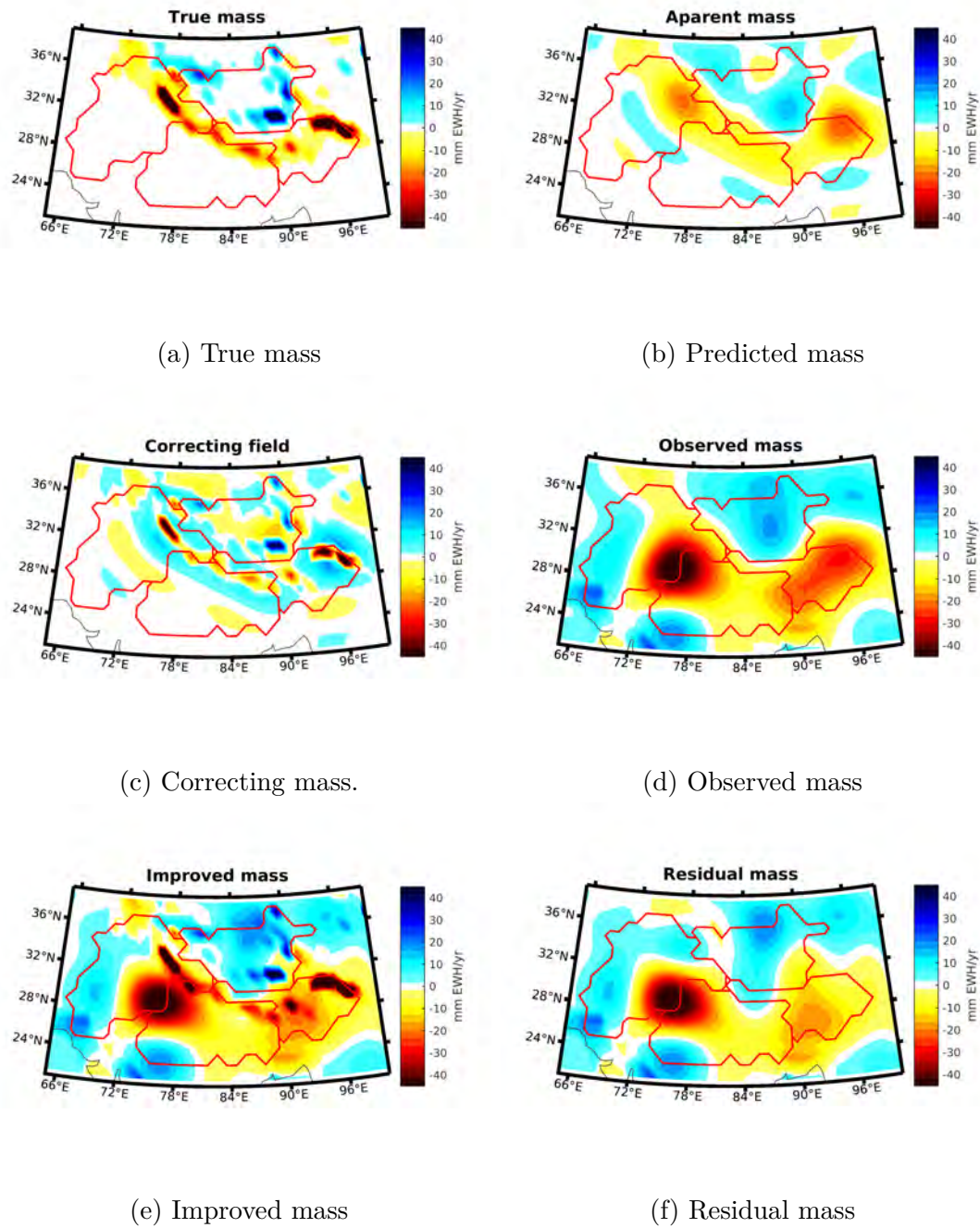


Figure 3.3: Example of the application of the land leakage correction in South Asia Field represented corresponds to the trends for the period from 2003 to 2015. (a) True mass corresponds to the independent data mass changes. (b) Predicted mass is the true mass as observed by GRACE. (c) The correcting mass corresponds to the difference between both fields. (d) Observed mass corresponds to the mass changes observed by GRACE before land leakage correction. (e) Improved mass corresponds to the mass changes after land leakage correction and (f) residual mass is the mass changes not explained by the independent observations. Note that these mass change fields are related ($c = a - b$, $e = d + c$, and $f = d - b = e - a$)

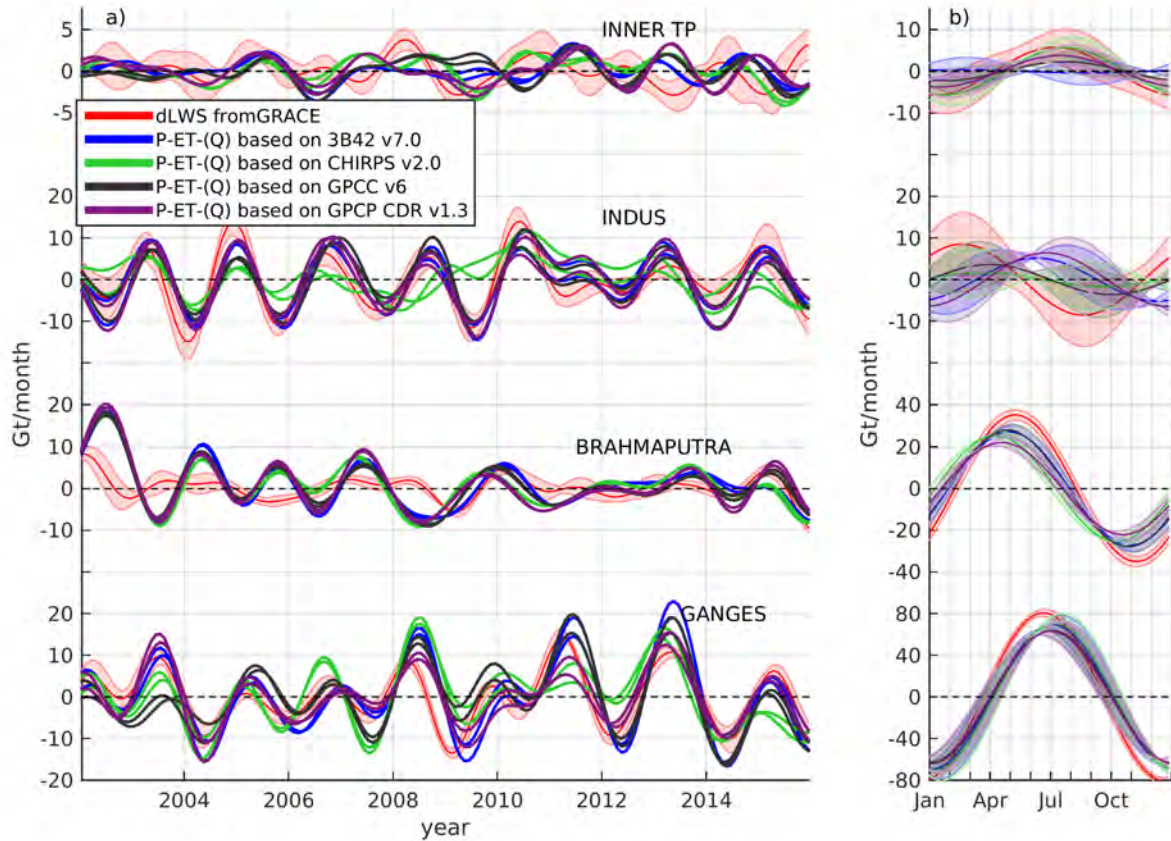


Figure 3.4: LWS GRACE-based change compared to the flux input and output analysis through the hydrological budget approach Eq 3.1. (P-ET for Inner TP and Indus; P-Q-ET for Ganges and Brahmaputra). A 13-month low-pass filter to remove sub-annual frequencies has been applied to the detrended timeseries. Annual cycles computed by fitting a sinusoid are shown in the right panel. Note that the range of values differ in the Y axis for visualization purposes.

basin while in the rest of basins, there are some precipitation products that seems to deviate a month.

This consistency analysis involved several products directly provided by colleagues from LEGOS and proved very useful to identify and correct errors. In particular, we identified anomalies in some lakes, where some years were anomalous with respect to GRACE-based LWS. We developed an uncertainty analysis for the lake mass changes with Jean François Creteaux [In prep Blazquez et al., 2020, Appendix A]. We identified three anomalous months in 2008 summer in the Brahmaputra basin, where there was an inconsistency between GRACE-based LWS and P-Q-ET (Fig. 3.5, presented in a poster at AGU 2018). In the research of possible sources for this inconsistency, we analyzed other GRACE-based products, other precipitation products from the ensemble FROGS [Roca et al., 2019]. These products helped to identify the river discharge product as responsible of the inconsistency. We found an error of missampling of ENVISat data during this period. We corrected it with the inclusion of JASON 3 data. The budget approach combining ensemble from different satellite data has proven to be an useful tool

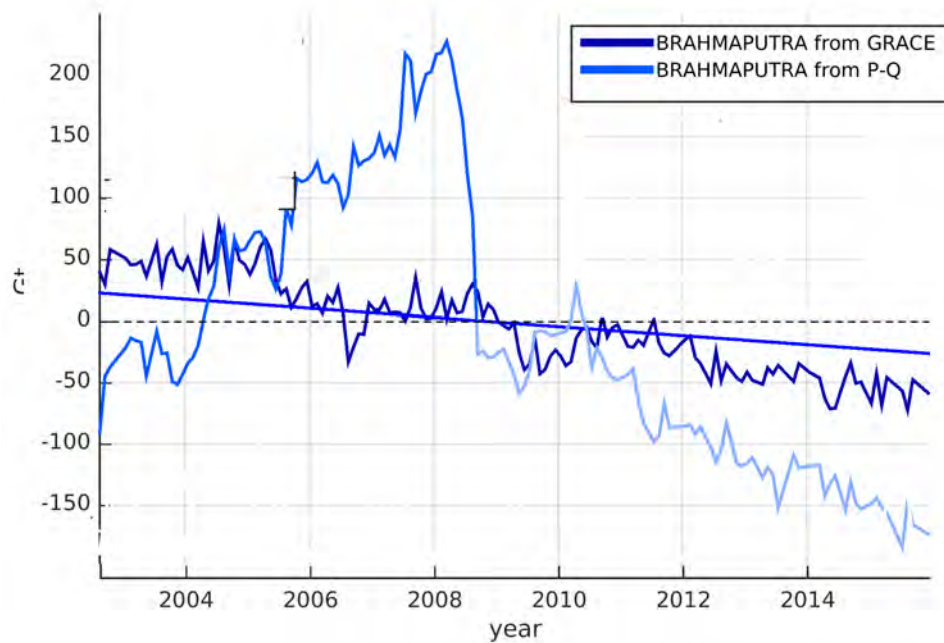


Figure 3.5: LWS GRACE-based change compared to LWS computed from fluxes analysis, showing the inconsistency in the P-Q timeseries around 2008 summer.

to verify coherence within each ensemble and consistency within each component.

This paper has been an interdisciplinary work very instructive for my PhD, as it gave me the opportunity to interact with different colleagues from different domains (hydrology, glaciology, precipitation, and lake volume estimations)

3.1.3 Article: "Monitoring the changes in terrestrial water storage in South Asia from 2003 to 2015"

This article is in preparation for a future submission to.

Monitoring the changes in terrestrial water storage in South Asia from 2003 to 2015

Blazquez Alejandro^{1,2}, Berthier Etienne¹, Papa Fabrice¹, Biencamaria Sylvain¹, Meyssignac Benoit^{1,2}, Brun Fanny^{1,3}, and Cretaux Jean François^{1,2}

¹LEGOS, Universite de Toulouse, CNES, CNRS, UPS, IRD, 31400 Toulouse, France.

²CNES, 31401 Toulouse, France.

³Univ. Grenoble Alpes, CNRS, IRD, Grenoble INP, IGE, 38000 Grenoble, France

Correspondence: Blazquez (alejandro.blazquez@legos.obs-mip.fr)

Abstract. Monitoring the spatio-temporal changes in fresh water storage of the main river basins of South Asia is key for understanding the water resource availability in one of the most densely inhabited regions of the world. Here, we analyze GRACE-based land water storage (LWS) changes jointly with independent satellite mass changes for glaciers and lakes.

From 2003 to 2015, the LWS of South Asia is characterized by a large seasonal cycle of 253.58 ± 31.0 Gt and a loss rate of 22.9 ± 6.7 Gt/yr for the four main basins in this region (Indus, Ganges, Brahmaputra and Inner Tibetan Plateau). Glaciers mass loss are responsible for 54% of this trend and the groundwater depletion in northern India for 41%. The sources of the LWS changes differ strongly compared to earlier studies when glacier mass changes are included, especially in the Brahmaputra basin.

We also analyze at basin scale the LWS against precipitation, river discharge and evapotranspiration products, finding correlations at interannual scale of 65% for Indus and Ganges basins.

Copyright statement. TEXT

1 Introduction

Understanding the regional water cycle in South Asia is fundamental to better manage freshwater availability and define adequate water policies in the area (Mathison et al., 2015; Wijngaard et al., 2018). This region comprises the inner Tibetan plateau (ITP), one of the greatest endorheic reservoirs of freshwater worldwide with more than seven thousand lakes with an area greater than 1 km^2 (Wan et al., 2016), and a large part of the Indian subcontinent, with some of the world's largest rivers (Indus, Ganges, Brahmaputra) (Fig. 1). These basins are facing both a large climate variability and strong anthropogenic pressure. Consequently, changes in the water cycle, either driven by natural variability (monsoonal precipitation, glacier or lake mass imbalance) or by human activities (irrigation, water policies in transboundary basins) might affect freshwater resource, threatening food and security for nearly a billion people Immerzeel et al. (2010); Sharma et al. (2019). Given the lack of in situ data in the region, several studies analyzed recent large-scale water mass redistributions in South Asia using satellite observations.

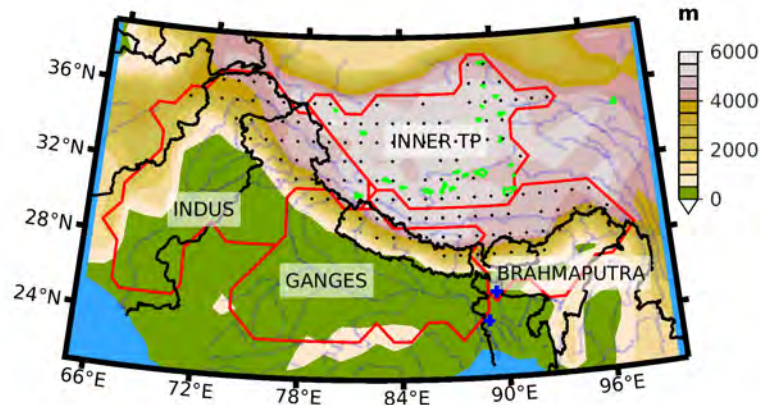


Figure 1. Our study area including: basins contours (red polygons), rivers (blue lines), river outlets (blue crosses), lakes (green polygons), glaciers (black dots) and country borders (black polygons).

Significant water depletion in northwest India has been observed with the Gravity Recovery and Climate Experiment (GRACE) data and attributed to groundwater extraction for irrigation along with precipitation changes (Rodell et al., 2009; Tiwari et al., 2009; Asoka et al., 2017; Long et al., 2016). In a recent study at the global scale, Rodell et al. (2018) analyzed recent trend
 25 in terrestrial water storage (TWS) in South Asia, using GRACE observations jointly with GPCP precipitation and irrigation products from remote sensing. They suggested that the main causes of these TWS trends are the precipitation increase for the ITP basin, precipitation decrease for the Ganges and the Brahmaputra basins and groundwater extraction for north-east India, in line with previous studies. However, these studies did not yet properly take into account the impacts of glacier and lake mass changes, which underwent important modification during this period. For example, a contrasted pattern of glacier mass
 30 change (Kääb et al., 2012), including mass gain in the Karakoram (Gardelle et al., 2012) and in the West Kunlun (Kääb et al., 2015) together with water accumulation in the ITP glaciers and lakes (Zhang et al., 2017) were observed using ICESat laser altimetry and optical or microwave imagery. There are also open questions on how the fast glacier mass loss observed in the Eastern Nyainqêntanglha Shan (Kääb et al., 2012; Brun et al., 2017) and the recent water gain in Tibetan lakes (Zhang et al., 2017) influence the TWS trend in each major water basins. It is therefore important to revisit TWS changes in light of glacier
 35 and lake mass changes, in order to determine more accurately the potential drivers of these changes.

Our study proposes to document and analyze recent land water storage (LWS) at three timescales: the trends for the period from January 2003 to December 2015, the seasonal cycle and the interannual variability. In this way, we decompose the time-series in trend, seasonal cycle, interannual variability and sub annual variability. We decompose LWS in glaciers and TWS

taking advantage of recently available independent data in South Asia related to glacier (Brun et al., 2017) and lake (Cretaux et al., 2016) mass changes. We also confront the LWS changes with precipitation products extracted from the Frequent Rainfall Observations on GridS (FROGS) database (Roca et al., 2019), evapotranspiration (Decharme et al., 2019) and river discharge (Papa et al., 2010) to understand its drivers.

2 Methodologie

2.1 Data

2.1.1 Glacier mass change derived from ASTER stereo imagery

Glacier mass change over South Asia for 2000-2016 is derived from multi-temporal ASTER digital elevation models (DEM) as detailed in Brun et al. (2017). The data cover 92% of the total glacier area and the trends are assumed similar for the remaining 8%. The total mass loss trend for all High Mountain Asia glaciers reaches 16.3 ± 3.5 Gt/yr from 2000 to 2016. Around 12.3 Gt/yr originates from our 4 basins of interest (ITP, Indus, Ganges, and Brahmaputra) and 4.0 Gt/yr from other basins, not studied here: Balkhash, Issykkul and Sasykkol (1.8 Gt/yr), Amu Darya basin (1 Gt/yr), Salween, Mekong, Syr Darya, Tarim, and Yangtze (1.4 Gt/yr). The uncertainties are computed as the quadratic sum of random and systematic errors (further details in Brun et al. (2017)). We assume trends for the period 2000-2016 to be similar to the trends in the period 2003-2015, an assumption supported by the lack of detectable changes in region-wide glacier mass loss between the periods 2000-2008 and 2008-2016 (Brun et al., 2017).

2.1.2 Lake volume change from altimetry

We consider a set of 20 lakes included in the Hydroweb database (Cretaux et al., 2016), freely available online at <http://hydroweb.theia-land.fr>. The method to estimate lake volume changes is described in Cretaux et al. (2016) and uses water level from radar and laser altimetry (Jason-1/-2, Envisat, ICESat and Saral/Altika) combined with surface area from satellite imagery (MODIS and Landsat). It is based on the determination of an hypsometric relationship, which represents the variation of lake extent with respect to lake height using a set of satellite images and their corresponding water height inferred from satellite altimetry. Once this hypsometric relationship is established, water height and extent of lakes are estimated using satellite altimetry observations only.

The estimation of the uncertainty takes into account the uncertainty in the individual altimetry measurements and in the determination of lake area (see details in Appendix A).

The lake mass change in the region shows a gain of 3.7 ± 0.1 Gt/yr between 2003 and 2015, mainly located in the ITP basin (individual lake mass change timeseries in Fig. A1). The uncertainty of ± 0.1 Gt/yr only accounts for the errors in the set of observed lakes not for the mass of the remaining non observed lakes.

Other studies focused on a shorter period (the ICESat period 2003-2009) included a larger number of lakes (59 in Zhang et al.

70 (2017)) leading to similar results. The 59 lakes were responsible of mass gain of 7.7 ± 0.6 Gt/yr in the ITP basin while our selection is responsible of 8.3 ± 0.1 Gt/yr for the same period. Recently, the combination of DEM and satellite images allowed monitoring 871 lakes in the Changtang Plateau (Yao et al., 2018), a subregion of the ITP and 1003 lakes in the whole Tibetan plateau and Quaidam basins (Treichler et al., 2019). The large uncertainty hampers the use of this data in this study.

2.1.3 GRACE Data

75 The GRACE mission (Tapley et al., 2004) sponsored by the National Aeronautics and Space Administration (NASA) and the Deutsches Zentrum für Luft-und Raumfahrt (DLR) has been providing precise, time-varying measurements of the Earth's gravitational field since April 2002 until June 2017. However, both satellites degraded over the time, some batteries were damaged provoking data gaps after 2011 and a degraded mode with the loss of one of the satellite accelerometer in November 2016. Thus, we limit our study to the period from January 2003 to December 2015.

80 We use an update of ensemble of GRACE solutions developed (Blazquez et al., 2018). This ensemble includes a wide range of post-processing parameters namely: the processing centers (CSR, GFZ, JPL, GRGS, and TUG), the 5 geocenter motion (Cheng et al., 2013b; Lemoine and Reinquin, 2017; Rietbroek et al., 2012; Swenson et al., 2008; Wu et al., 2017), the 2 C_{20} corrections (Cheng et al., 2013a; Lemoine and Reinquin, 2017), 4 filters (ddk3, ddk4, ddk5 and ddk6 from Kusche et al. (2009)), the leakage correction over a 300-km-wide zone off the coastlines based on comparison with observation-based ocean mass estimates (2 ocean reanalysis) and 3 GIA corrections (A et al., 2013; Peltier et al., 2017; Purcell et al., 2018). The pole tides are also corrected as described in Wahr et al. (2015). Each combination of the post-processing parameters leads to a solution. Combining all the solutions leads to an ensemble of 1200 monthly $1^\circ \times 1^\circ$ fields. However, GRACE-based LWS change cannot be directly used to disentangle glaciers and TWS changes. GRACE resolution of 300 km hampers to observe sharp changes in small locations. This effect is known as land leakage. There have been different approaches have been used as using hydrological models (Rodell et al., 2004), spatial location of the glaciers directly from GRACE data (Jacob et al., 2012) or via constrained forward modeling (Chen et al., 2015). We propose in the next section a new land leakage correction based on independent observation (e.g. glaciers and lakes).

2.1.4 Ancillary data: Precipitation, river discharge and evapotranspiration products

The FROGs database includes more than 19 families of precipitation products (Roca et al., 2019) on a normalized format $1^\circ \times 1^\circ$ grid at a daily resolution. We extract the flagship products for which satellite data are corrected with rain-gauge measurements available from 2003 to 2015: 3B42 V7.0 (Huffman et al., 2010), CMORPH V1.0CRT (Xie et al., 2003), CHIRPS V2.0 (Funk et al., 2015), GSMAP gauge NRT V6.0 (Kubota et al., 2007), GPCC v6.0 (Becker et al., 2013), GPCP CDR V1.3 (Huffman et al., 2001), and ERA interim (Dee et al., 2011). We discuss the coherence among these products in Appendix B.

100 The monthly river discharges from 2002 to 2016 are derived from satellite altimetry observations of river water level and calibrated with in situ discharge measurements (Papa et al., 2010). They are measured at the outlets of the Ganges (Hardinge station, blue dots in Figure 1a) and the Brahmaputra (Bahadurabad station). For these two rivers, when analyzing basin-average

timeseries (precipitation, TWS, etc), we only consider the part of the basin located upstream of the stations. Thus we exclude the Ganges-Brahmaputra-Meghna delta. For the Indus, no accurate river discharge data is available at its outlet.

We use evapotranspiration estimates from GLEAMS V3.3a (Martens et al., 2017) and from the ISBA-CTRIP model (Decharme et al., 2019). The Global Land Evaporation Amsterdam Model (GLEAM) is a set of algorithms that separately estimate the different components of terrestrial evaporation (i.e. evapotranspiration) based on satellite observations: transpiration, interception loss, baresoil evaporation, snow sublimation and open-water evaporation. ISBA-CTRIP includes the sum of the direct evaporation of the water intercepted by the canopy, the evaporation or sublimation from the bare soil, the transpiration from plants, the sublimation from snow and the direct evaporation in the floodplains. The atmospheric forcing is performed in two steps. The first one is based on NCEP-NCAR reanalysis hybridized to match the monthly values from gauge-based GPCC v6 (Becker et al., 2013) and the second one is based on ERA interim (Dee et al., 2011).

2.2 Land leakage correction

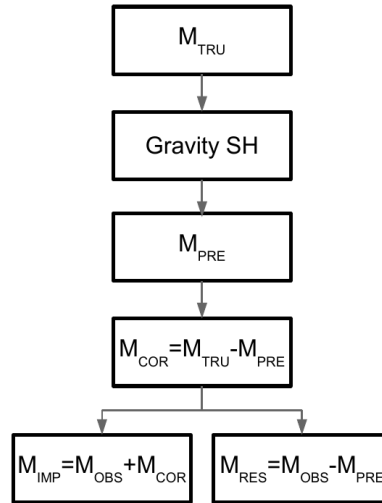


Figure 2. Schema of the land leakage correction. M_{TRU} and M_{PRE} represent the true and the predicted mass fields, respectively, and M_{OBS} represents observed mass field. gravity SH represents the equivalent in spherical harmonics of the mass fields. M_{RES} or ΔM represents the residual field. M_{COR} is the correcting field. M_{IMP} represent the improved field.

The land leakage correction we proposed is based on a forward modeling process (Chen et al., 2015) using independent observations to constraint spatially GRACE-based estimates. This land leakage correction method consist of using independent observations where the uncertainties are smaller than the uncertainties from GRACE-based estimates (e.g. glacier and lake mass changes). These independent observations are used as true mass to initialize a one-iteration forward-modeling. This true mass is convert to the predicted mass by a conversion to spherical harmonics and a truncation at degree 60 and back to EWH, as in the

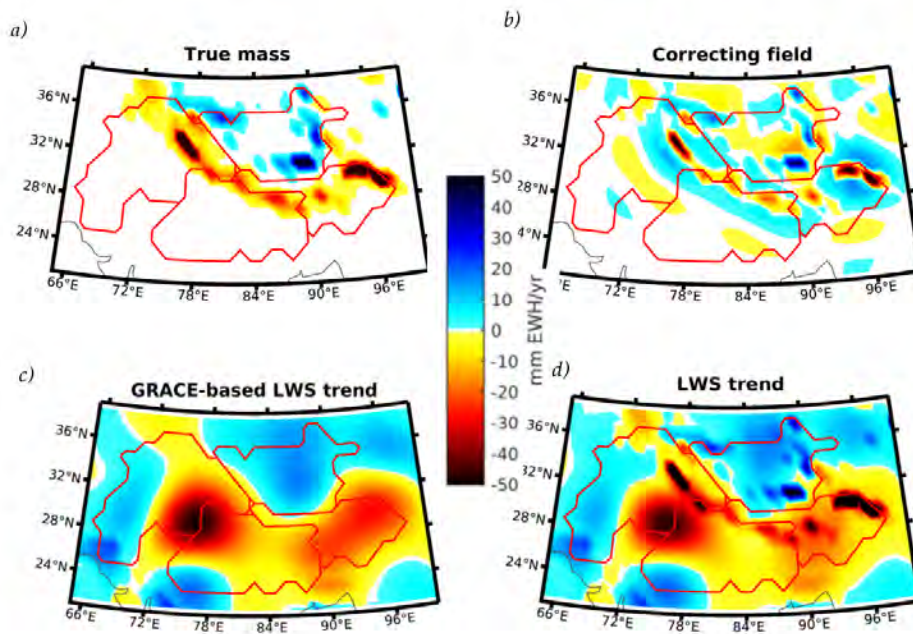


Figure 3. Land leakage correction. True mass corresponds to the independent observations mass changes (a), the correcting field computed through the land leakage correction (b), GRACE-based LWS trends before LLC (c) and LWS trend corresponds to the mass changes after LLC (d). Note that $d = c + b$

forward modeling technique. Then, we define the correcting mass as the difference between the true and the predicted masses. This correcting mass corresponds to the improvement of the spatial signal. We then add this correction field to the observed field (M_{OBS}) to obtain the land leakage corrected field or improved field (M_{IMP}) (See Fig. 2). As it is an one-iteration forward modeling, the land corrected field does not fit exactly the true mass. In this way, the leakage from this independent data and the corresponding uncertainties in glacier and TWS mass changes are reduced but not completely removed, as in the forward modeling technique. We verified that the total amount of water mass remains constant at each step of the method at regional scale.

Here we use glacier and lake mass changes from independent observations (Fig. 3a) to retrieve the land leakage correction (Fig. 3b). This land leakage correction modifies strongly the local pattern (differences between Fig. 3c and Fig. 3d) but only slightly the average trend of each basin, leading to differences below 1 Gt/yr for the period 2003-2015 (details in Table 1). The land leakage corrected LWS (LWS from here) presents an improvement near glaciers and lakes, where mass changes are redistributed and leakage reduced. We use thus this LWS in the rest of the analysis.

Once corrected for the Land leakage, the uncertainty in GRACE-based LWS trend at basin scale is dominated by the differences during the inversion method done by each processing center (uncertainty of 0.5, 1.3, 1.7 and 1.6 Gt/yr for ITP, Indus Brahmaputra, and Ganges respectively). The differences in the geocenter motion and GIA model also contribute to the uncer-

Table 1. Land leakage correction (LLC) effect on the land water storage (LWS) at basin scale. Trends are computed for the period 2003-2015.

Basin	Surface $10^6 Km^2$	LWS before LLC Gt/yr	LLC Gt/yr	LWS Gt/yr
ITP	0.71	5.82 ± 1.12	0.74	6.69 ± 0.98
INDUS	1.08	-6.03 ± 1.89	-0.25	-6.40 ± 2.01
BRAHMAPUTRA	0.52	-9.86 ± 1.93	-1.04	-11.07 ± 1.77
GANGES	1.04	-12.24 ± 2.00	-0.01	-12.15 ± 1.96
Total	3.35	-22.32 ± 6.94	-0.56	-22.92 ± 6.72

135 tainty (about 0.5, 0.8, 0.4 and 0.7 Gt/yr for ITP, Indus, Brahmaputra and Ganges respectively). More details in Appendix B. The trends for Indus, Brahmaputra and Ganges basins of -29.62 ± 5.77 Gt/yr for the period from 2003 to 2015 are smaller than the trends of -37.8 ± 8.58 Gt/yr for the period from 2003 to 2016 (Loomis et al., 2019). However, the uncertainty and the source of the uncertainties are similar.

140 The residual mass (M_{RES} in Fig. 2) includes: snow, ice, surface water (river, floodplains), groundwater, soil moisture and the water contained in biomass (Rodell and Famiglietti, 1999) as well as the uncertainties on (i) our estimates of glaciers and lakes mass changes and (ii) on GRACE-based LWS changes. The uncertainty in the groundwater mass changes estimates from historical depth-to-water measurements is too large to be included in this analysis. The measurements are only available in India, and they rely in the storage coefficients that are rarely available in this region (Loomis et al., 2019). We prefer not to separate the groundwater from the residual mass. However our results agrees in sign of the trends as in Loomis et al. (2019). This partitioning allows us to better understand the spatial distribution of the mass changes and analyze their sources.

145 2.3 Precipitation products analysis

We analyze the coherence among the precipitation products in the region in terms of trends for the period from 2002 to 2015 and seasonal cycle (Table C1) and through the consistency between the variations of LWS ($d(LWS)/dt$ or dLWS) from GRACE (GRACE-based LWS) and the variations of LWS through the fluxes analysis (fluxes-based LWS). The fluxes analysis includes: precipitation (P), evapotranspiration (ET) and river discharge (Q, when available, so here only for Brahmaputra and Ganges) following Eq. 1). P and ET are integrated at basin scale. This approach allows to assess the consistency within the different datasets, as well as, to explore the drivers of the mass changes at basin scale.

$$dLWS = \frac{d(LWS)}{dt} = (P - Q - ET) + errors \quad (1)$$

155 Among all the products, four present a good coherence in the seasonal cycle in terms of amplitude and phase (day of the year) (Table C1). These three products show also the better consistency when combined through the fluxes analysis (Fig. 4). We decided to consider these four products (3B42 V7.0, CHIRPS V2.0, GPCC v6, and GPCP CDR V1.3) in the results and

discussion. GPCC v6 and GPCP CDR V1.3 show similar results because they are based on the same rain gauges to adjust monthly bias leading to similar seasonal cycle.

The other precipitation products (CMORPH, GSMAP, ERA interim) underestimate, or overestimate the seasonal cycle, leading to inconsistencies when combined through the fluxes analysis. We decided not to include in the results and discussion but to comment them in Appendix C.

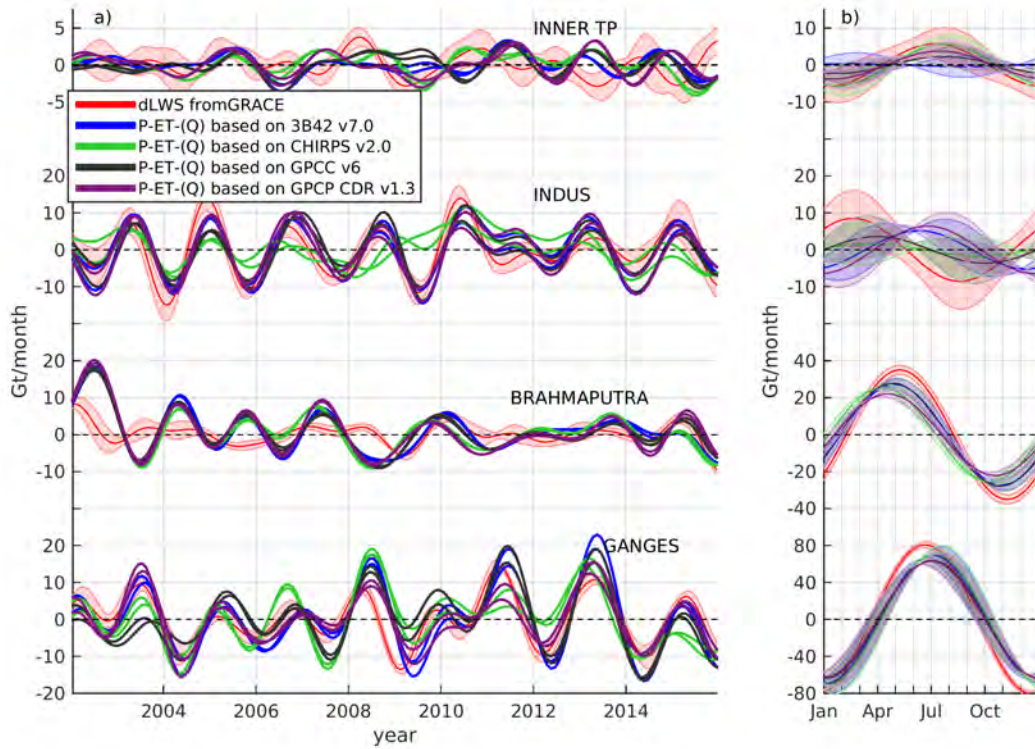


Figure 4. LWS change from GRACE and from the fluxes budget approach based on 3B42 V7.0, CHIRPS V2.0, GPCC v6, and GPCP CDR V1.3 (P-ET for ITP and Indus; P-Q-ET for Ganges and Brahmaputra). Timeseries have been decomposed in trends, seasonal scale (b) and interannual variability (a). Note that the range of values differ in the Y axis for visualization purposes.

3 Results and discussion

3.1 Inner Tibetan plateau basin

ITP experienced a LWS mass increase of 6.69 ± 0.98 Gt/yr in the period 2003-2015, whereas the increase of the lake mass accounts for 57% of the total increase in TWS (Fig 5b). Glacier mass changes impact LWS changes in this region by less than 1% (Fig.5a)

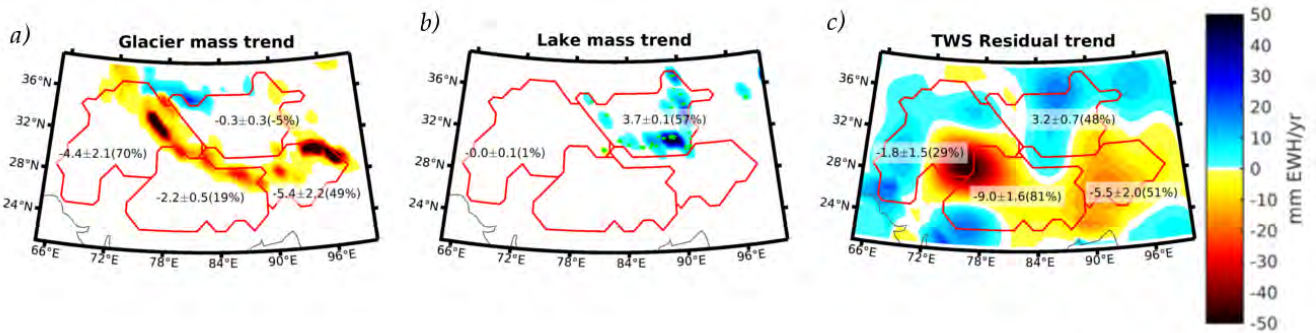


Figure 5. LWS decomposition in glaciers (a), lakes (b) and residual TWS(c) as in Eq.1. Trends are computed for the period from 2003 to 2015. The values corresponds to the basin means and their relative weight to each basin LWS mass change.

A previous study during the ICESat period from 2003 to 2009 (Zhang et al., 2017) estimated that main 59 lakes accounted for 52% in the ITP while we found 48% for the period only with 20 lakes. Two recent studies for the same period as our study (2003-2015), determined the volume changes of over 500 lakes using hydrological models or lake levels derived from Landsat
 170 images and DEM and found also that lakes account for most of the TWS change. Wang et al. (2018) found 82% for the whole Tibetan plateau while Yao et al. (2018) found 62% only for the Changtang plateau (part of the ITP).

There is a mass accumulation in groundwater in the north of the ITP (Fig.5c) . The origin of this mass accumulation remains unclear (Jiang et al., 2017). Several explanations have been proposed in previous studies (Jiang et al., 2017), one of them being a local increase in precipitation (Yao et al., 2018; Meng et al., 2019). However, the increase in precipitations for this basin is
 175 only observed in 3B42 and CMORPH (Table C1).

The LWS based on CHIRPS and GPCP and GRACE-based LWS are in good agreement at seasonal scale. This is not the case for fluxes-based LWS from 3B42, which annual amplitude is 20% smaller than CHIRPS and GPCP (Fig 4 b). The lower consistency between GRACE-based and fluxes-based LWS interannual variability may be associated with the lower signal to noise ratio of the GRACE observations in the ITP as indicated in previous studies for other basins (Longuevergne et al., 2010;
 180 Long et al., 2014, 2015). There is no significant correlation between both approaches in interannual variability.

3.2 Indus basin

The Indus basin experienced a LWS mass loss of 6.4 ± 2.0 Gt/yr for the period from 2003 to 2015 (Table 1), despite increase in precipitation registered (Table C1). Glacier mass loss accounts for 70% of it (Fig. 5).

At seasonal time scale, there is no agreement between GRACE-based LWS and fluxes-based LWS (Fig. 4b) likely because
 185 of lack of river discharge estimates at the outlet of this basin. Some authors suggest that the presence of several dams along the river might modify the natural river flow (Immerzeel et al., 2012).

Despite the unavailability of river discharge, GRACE-based LWS and fluxes-based LWS based on 3B42 and GPCP show a good agreement in the interannual variability with a positive correlation of $R^2=68\%$ for $p < 10^{-5}$ (Fig. 4a). This result suggests that river discharge may have a minor impact at interannual time scale on the basin mass change and that most of the precipitation in the basin balances out through evapotranspiration. However, this suggestion needs to be confirmed with river discharge observations. Fluxes-based LWS from ERAi show also a good agreement with a correlation of $R^2=70\%$ in the interannual variability (Fig. S.2).

3.3 Brahmaputra basin

The Brahmaputra river basin exhibits a strong negative trend in LWS (-11.07 ± 1.77 Gt/yr for the period from 2003 to 2015, Table 1). Glacier mass loss represents 49% of this trend, mainly located in the Upper Brahmaputra basin and in the northeastern part of the basin (Fig. 5c) confirming previous results (Chen et al., 2017). After removing the glacier mass change signal, the spatial pattern of residual TWS trend differs strongly with LWS trend. The remaining water loss is concentrated in the lower Brahmaputra (-5.5 ± 2.0 Gt/yr), corroborating recent studies on the impact of human activities (water pumping) in Bangladesh (Khaki et al., 2018).

GRACE-based LWS and fluxes-based LWS are in good agreement at seasonal timescale but this is not the case for the interannual variability (Fig. 4).

3.4 Ganges basin

The Ganges basin exhibits the largest water loss in the region (-12.1 ± 1.9 Gt/yr) during the period from 2003 to 2015. This result is in agreement with several earlier studies (Rodell et al., 2009; Tiwari et al., 2009; Chen et al., 2014), over similar or shorter time periods. Most of the lost is concentrated in the northern part, near the Indus basin. Glacier contribution to the LWS trend in this basin is smaller (19%) than in the Indus and Brahmaputra basins, leaving most of the observed decrease in LWS trend explained by the residual TWS terms (Eq 1). The precipitation products agree on an increase in basin-wide precipitation, except GPCP (see Table C1), while a decrease in Ganges discharge is observed (-3.1 Gt/yr). Thus precipitation and discharge trend cannot explain the strong negative trend in LWS. A slight increase in ET is observed (2.4 Gt/yr). We suggest that an increase in freshwater use for irrigation and human activities is the main cause of decreasing TWS changes, as previously reported (Rodell et al., 2009; Long et al., 2016).

GRACE-based LWS and fluxes-based LWS are in good agreement at seasonal timescale. (Fig. 4b). Fluxes-based LWS from 3B42 and GPCP show a good agreement with a correlation of $R^2=70\%$ in the interannual variability (Fig. 4a).

We analyze residual TWS changes of Northwest India including the northeast part of the Ganges basin and northwest part of the Indus basin (Green crosses in Fig. 6). The Residual TWS shows a strong negative trend for the period 2003-2009 (-14.1 ± 2.8 Gt/yr) and a less negative trend for the period 2010-2015 (-9.5 ± 2.3 Gt/yr). The overall trend from 2003 to 2015 is -9.5 ± 2.3 Gt/yr which represents 41% of the net water loss of the whole studied region.

This trend is consistent with previous results when considering the same periods. We measured -14.1 ± 2.8 Gt/yr from August 2002 to October 2008 (14.0 ± 0.4 Gt/yr in Long et al. (2016), -17.7 ± 4.5 Gt/yr in Rodell et al. (2009)). Our estimate

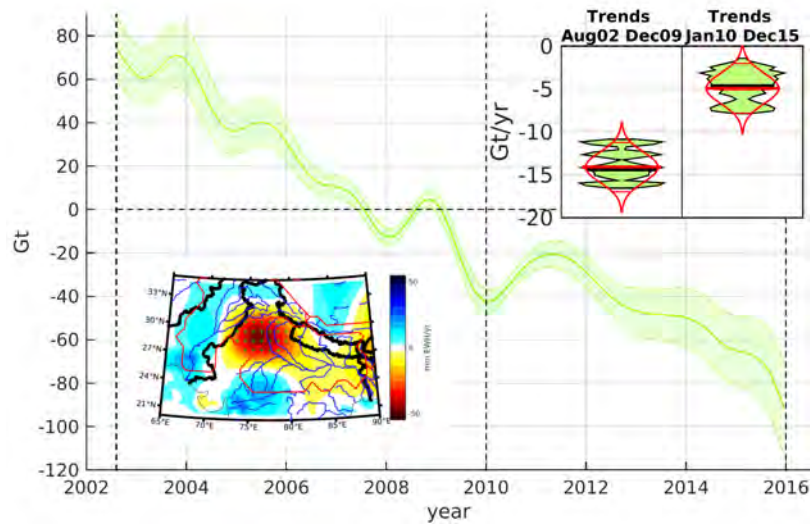


Figure 6. Residual TWS from northwest India, including parts of the Indus and Ganges basins. The area is represented by green crosses in the bottom left figure along with the rivers (blue), country borders (black) and basin contours (red) on top of the $TWS_{residual}$ trend (zoom over Fig. 1.f). In the top right box, trends for the two periods from August 2002 to December 2009 and from January 2010 to December 2015 are compared, including the trend distribution from the GRACE ensemble (shaded polygons) and the associated normal distribution (red lines).

is less negative but still consistent within the error bar with more negative values reported using constrained forward modeling on GRACE solution (Chen et al., 2014). Chen reported a trend of -20.4 ± 7.1 Gt/yr for the period from January 2003 to December 2012 and a for a slightly larger area. The use of this method leads to overestimating mass losses (Long et al., 2016). Importantly, our analysis confirms a clear decrease of the rate of water depletion in northern India between the periods of 2003-2009 and 2010-2015 (Long et al., 2016).

4 Conclusions

Glacier mass change explains a significant fraction of GRACE-based LWS trend signals from January 2003 to December 2015 in South Asia, especially in the northeastern part of the Brahmaputra basin and the eastern part of the Indus basin. They account for about half of the net water loss in these two basins. On the other hand, lake water mass increase explains up to 57% of the TWS changes in the ITP. Therefore, the inclusion of these independent observations allows to interpret the spatial distribution of LWS changes. This is particularly evident in the Indus and Brahmaputra basins where glacier mass loss explain 70% and 49% of the LWS trend, respectively. The impact of glaciers in Brahmaputra was underestimated in earlier studies (Rodell et al., 2018; Shamsudduha and Panda, 2019).

235 The use of these independent observations of mass changes to reduce the leakage in GRACE-based LWS changes is important in the South Asia region where glacier and lake mass changes are concentrated in small locations. This method improves locally the GRACE-based TWS estimates leading to a correction up to 1 Gt/yr in the basin-mean TWS change. However the accuracy of the results relies on the accuracy and the availability of these independent data (e.g., the temporal resolution of the glacier data is coarse as only trends for the period from 2000 to 2016 are available).

240 Nevertheless, after removing glacier and lake mass changes, the very peculiar pattern of TWS decrease in Northern India (Fig. 1e), spatially distributed between the eastern part of the Indus and the northwestern part of the Ganges remains. This TWS trend corresponds to -9.9 ± 2.1 Gt/yr which represents 41% of the net water loss of the region. This trend is consistent with previous results when considering the same periods (Rodell et al., 2009; Long et al., 2016; Chen et al., 2014).

Combining multiple observing systems as done here to analyse the basin-wide water budget (GRACE, altimetry, optical
245 imagery, meteorological satellites) allows assessing their consistency. In our case, it helped to identify the outliers among the precipitation products (e.g., CMORPH underestimates the precipitation seasonal cycle over the Brahmaputra while ERAi overestimates it over ITP). This result stresses the need for additional studies to understand the source of these differences, including other versions of the products (we only used rain-gauge corrected products). It would also be useful to include measurements of Indus river discharge. There have been promising attempts combining satellite altimetry and optical images
250 (Durand et al., 2016; Oubanas et al., 2018).

The land leakage correction using independent observations has proven to be an accurate method to improve the spatial distribution of GRACE-based TWS changes at basin scale. Especially in South Asia, where glaciers and lakes are concentrated in small locations. However, the lack of independent data hampers the generalization of this method to a global scale.

Data availability. The GRACE LEGOS ensemble is available in ftp.legos.obs-mip.fr/pub/soa/gravimetrie/grace_legos/

255 **Appendix A: Lake mass changes**

A1 Computation of lake volume change

Lake volume changes between two measurements (at date T_0 and T_1) is the volume difference between two pyramids (Expressed by the following equation)

$$\Delta(V) = \frac{(H_1 - H_0) \cdot (A_1 + A_0 + \sqrt{A_1 \cdot A_0})}{3} \quad (\text{A1})$$

260 Where V represents the volume variation between two consecutive measurements, H_1 , H_0 and A_1 , A_0 are levels and areal extents at date T_1/T_0 respectively.

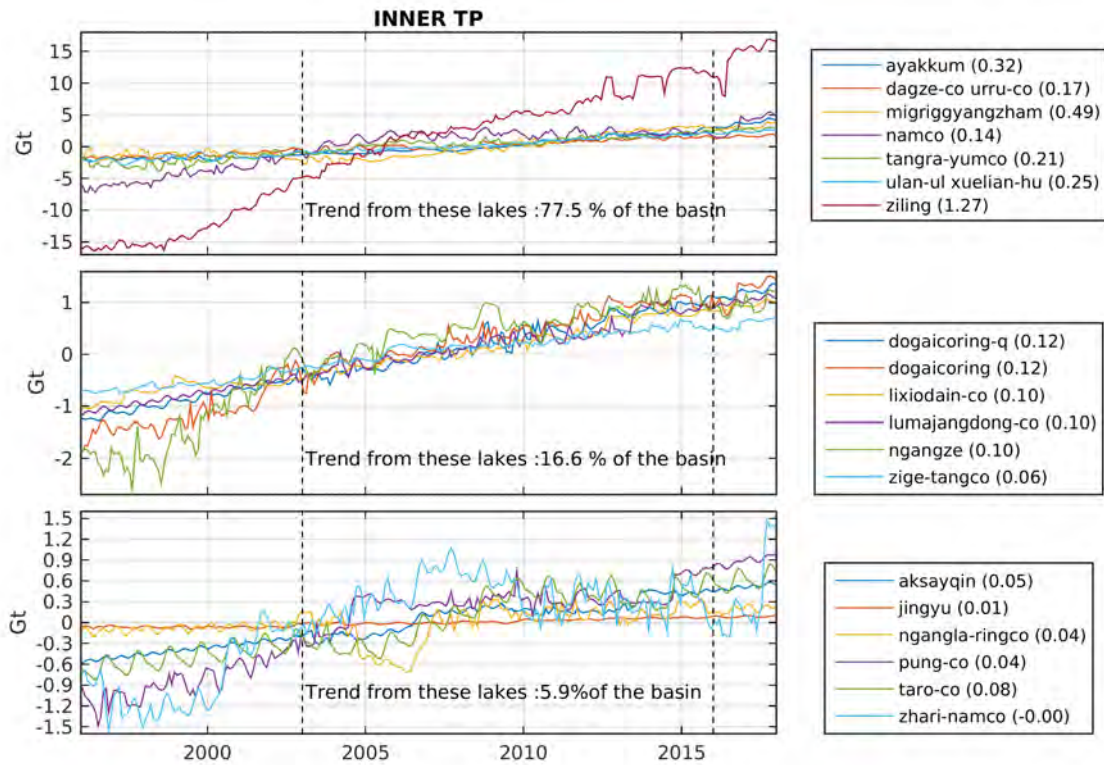


Figure A1. Lake mass change for the Inner TP basin. Lakes represented in the same line corresponds to lake in the same point of the grid at $1^\circ \times 1^\circ$. The values within parenthesis are the trend in Gt/yr for the period 2003-2015 (dot lines in the figure). The seven largest contributors are responsible of the 77.5% of the lake mass change of the 20 considered lacs.

A2 Uncertainty in the lake volume change computation

For the estimation of the uncertainty we take into account the variance of the individual altimetry measurements and the variance in the lake area determination. For altimetry, it is calculated as the standard deviation of the set of individual measurements that have been averaged to calculate the height of the lake at each pass of a satellite over the lake Cretaux et al. (2016). For the area, the standard deviation calculation is more challenging than for water height, however it is derived from the goodness-of-fit of the hypsometry curve directly. Once σ_H and σ_A (respectively standard deviations of height and area) are calculated we can derive the standard deviation of the volume change which is expressed by the following equation :

$$\sigma_V = \frac{1}{2} \cdot \sigma_H \cdot (A_1 + A_0) + \frac{\sqrt{3}}{3} \cdot \sigma_A (H_1 - H_0) \quad (\text{A2})$$

270 **Appendix B: Uncertainties in GRACE-based LWS**

The ensemble of GRACE solutions includes all solutions using the most state-of-the-art post processing parameters. Then, we analyzed the range in TWS mass changes due to the spread in these parameters. We assumed the spread in the ensemble of GRACE solutions to be representative of the uncertainty in GRACE estimates of the water budget components. On this basis, We can explore the uncertainty in GRACE estimates and find the parameters that are responsible for this uncertainty. as
 275 presented in table B1.

Table B1. Source of the uncertainties in the LWS from GRACE. Values expressed in Gt/yr at 5%-95% (1.65σ)

	ITP	Indus	Brahmaputra	Ganges
Center	0.53	1.34	1.68	1.61
Geocenter	0.56	0.85	0.40	0.81
C_{20}	0.01	0.03	0.02	0.06
Filter	0.21	0.85	0.11	0.25
GIA	0.54	0.75	0.37	0.70
Land/ocean Leakage ^a	0.	0.	0.	0.
STD	0.98	2.00	1.77	1.95

^a The land-ocean leakage correction does not affect these basins

Appendix C: Coherence and consistency in the precipitation products

The coherence between products from the same observing system and the consistency when combined with other observing systems allows to identify the outliers. We observe that the seasonal cycles CMORPH underestimates the seasonal cycle for the Brahmaputra and Ganges basins leading to inconsistent results when combined through the hydrological approach (not shown).
 280 GSMAP underestimates the seasonal cycle for every basin and particularly for the ITP (5 times smaller than the ensemble). ERA interim on the contrary overestimates the annual amplitude over ITP (17.9 Gt) and for the Brahmaputra (44.6 Gt).

When analysis spatially these differences, most of the discrepancies are located in the mountains (Minallah and Ivanov, 2019).

Table C1. Trends for the period 2003-2015 (Gt/yr), Seasonal cycle amplitude (Gt) and phase (day of the year, doy) for the precipitation products. Bold values corresponds to the outliers 5%-95% to the precipitation ensemble.

INNER TP				BRAHMAPUTRA		
source	Trend	Amplitude	Phase	Trend	Amplitude	Phase
3B42 v7.0	1.2	7.9	-162	-4.2	34.5	-172
CHIRPS v2.0	-1.1	10.9	-161	-4.0	29.9	-171
GPCC v6	-0.5	9.2	-161	-0.9	34.1	-173
GPCP CDR v1.3	-2.0	10.0	-163	-7.3	31.8	-168
CMORPH v1.0 CRT	6.8	10.5	-157	17.1	21.4	-172
GSMAP gauges NRT v6.0	-7.2	1.6	140	5.5	22.4	-167
ERAi	-4.6	17.5	-169	-20.8	44.6	-181
INDUS				GANGES		
source	Trend	Amplitude	Phase	Trend	Amplitude	Phase
3B42 v7.0	9.9	13.8	-174	2.0	63.1	-155
CHIRPS v2.0	19.3	11.3	-171	7.5	64.2	-154
GPCP CDR v1.3	11.6	14.7	-172	-2.0	59.4	-155
GPCC v6	15.1	11.3	-176	11.8	60.4	-154
CMORPH v1.0 CRT	12.5	12.2	-160	10.7	55.2	-154
GSMAP gauges NRT v6.0	3.6	5.9	172	10.1	52.0	-153
ERAi	1.2	14.2	-181	-0.5	63.6	-154

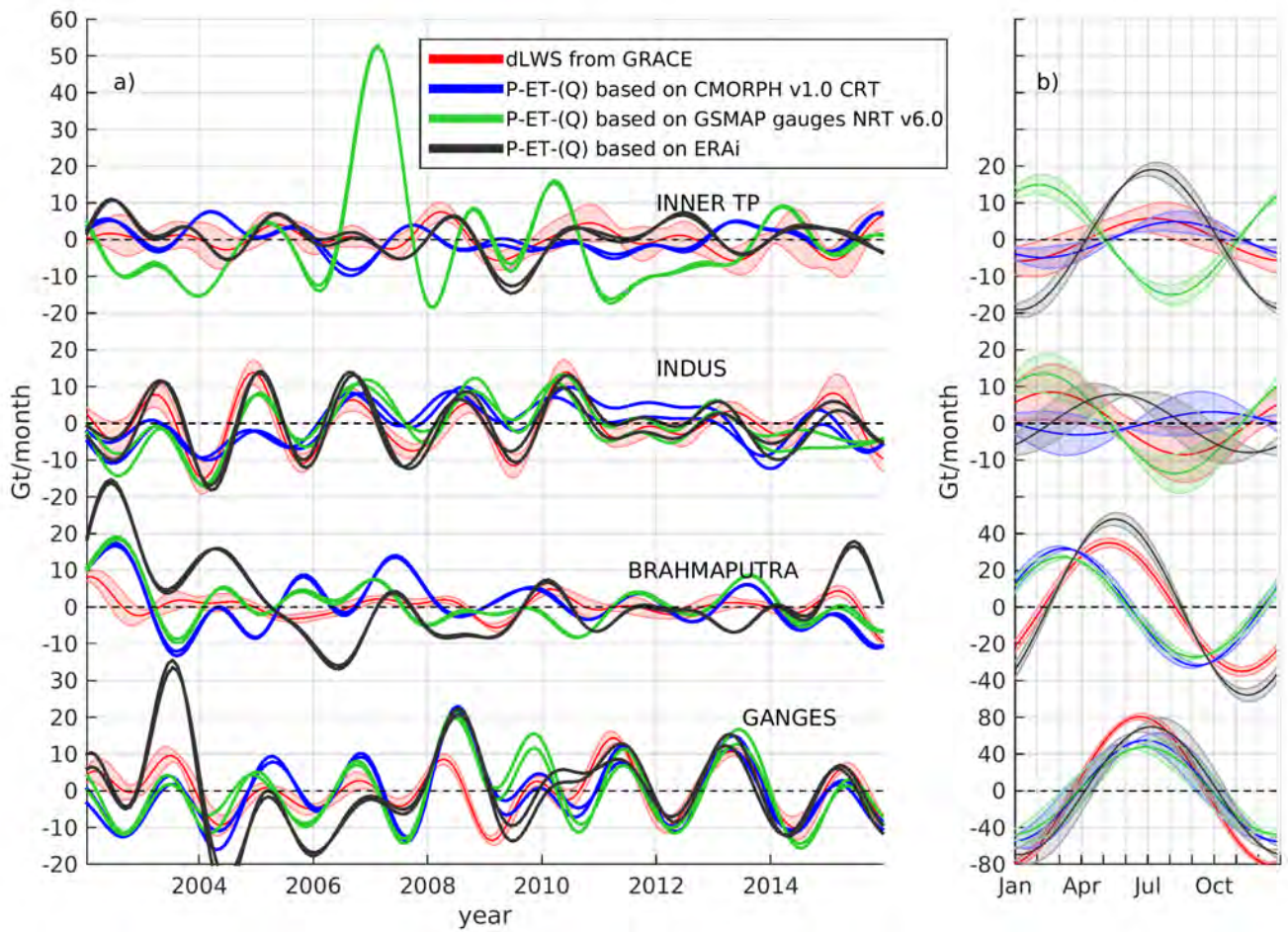


Figure C1. dLWS change from GRACE and from the fluxes budget approach Eq 2 (P-ET for ITP and Indus; P-Q-ET for Ganges and Brahmaputra). Timeseries have been decompose in trends, seasonal scale (b) and interannual variability (a). Note that the range of values differ in the Y axis for visualization purposes.

Author contributions. AB, EB, and FP designed the study. AB made the data analysis. AB, EB and FP lead the writing of the paper. Others
285 co-authors contribute to the writing and discuss the results

Competing interests. The authors declare that they have no conflict of interest

Acknowledgements. We thank Bertrand Decharme for providing the evapotranspiration from the running of ISBA-CTRIP. We also thank
Natural earth website for the national borders and rivers (www.naturalearthdata.com). We thank Valeriy Ivanov and the two anonymous
reviewers from their comments on an earlier version of the manuscript.

290 EB acknowledges support from the French espace agency (CNES).

References

- A, G., Wahr, J., and Zhong, S.: Computations of the viscoelastic response of a 3-D compressible Earth to surface loading: an application to Glacial Isostatic Adjustment in Antarctica and Canada, *Geophysical Journal International*, 192, 557–572, <https://doi.org/10.1093/gji/ggs030>, <https://academic.oup.com/gji/article/192/2/557/2889898/>
295 Computations-of-the-viscoelastic-response-of-a-3-D, 2013.
- Asoka, A., Gleeson, T., Wada, Y., and Mishra, V.: Relative contribution of monsoon precipitation and pumping to changes in groundwater storage in India, *Nature Geoscience*, 10, 109–117, <https://doi.org/10.1038/ngeo2869>, <https://www.nature.com/articles/ngeo2869>, 2017.
- Becker, A., Finger, P., Meyer-Christoffer, A., Rudolf, B., Schamm, K., Schneider, U., and Ziese, M.: A description of the global land-surface precipitation data products of the Global Precipitation Climatology Centre with sample applications including centennial (trend)
300 analysis from 1901–present, *Earth System Science Data*, 5, 71–99, <https://doi.org/https://doi.org/10.5194/essd-5-71-2013>, <https://www.earth-syst-sci-data.net/5/71/2013/>, 2013.
- Blazquez, A., Meyssignac, B., Lemoine, J. M., Berthier, E., Ribes, A., and Cazenave, A.: Exploring the uncertainty in GRACE estimates of the mass redistributions at the Earth surface: implications for the global water and sea level budgets, *Geophysical Journal International*, 215, 415–430, <https://doi.org/10.1093/gji/ggy293>, <https://academic.oup.com/gji/article/215/1/415/5056720>, 2018.
- 305 Brun, F., Berthier, E., Wagnon, P., Kääh, A., and Treichler, D.: A spatially resolved estimate of High Mountain Asia glacier mass balances from 2000 to 2016, *Nature Geoscience*, 10, 668–673, <https://doi.org/10.1038/ngeo2999>, <https://www.nature.com/articles/ngeo2999>, 2017.
- Chen, J., Li, J., Zhang, Z., and Ni, S.: Long-term groundwater variations in Northwest India from satellite gravity measurements, *Global and Planetary Change*, 116, 130–138, <https://doi.org/10.1016/j.gloplacha.2014.02.007>, <http://www.sciencedirect.com/science/article/pii/S0921818114000526>, 2014.
- 310 Chen, J., Wilson, C. R., Li, J., and Zhang, Z.: Reducing leakage error in GRACE-observed long-term ice mass change: a case study in West Antarctica, *Journal of Geodesy*, 89, 925–940, <https://doi.org/10.1007/s00190-015-0824-2>, <https://doi.org/10.1007/s00190-015-0824-2>, 2015.
- Chen, X., Long, D., Hong, Y., Zeng, C., and Yan, D.: Improved modeling of snow and glacier melting by a progressive two-stage calibration strategy with GRACE and multisource data: How snow and glacier meltwater contributes to the runoff of the Upper Brahmaputra River
315 basin?, *Water Resources Research*, 53, 2431–2466, <https://doi.org/10.1002/2016WR019656>, <https://agupubs.onlinelibrary.wiley.com/doi/abs/10.1002/2016WR019656>, 2017.
- Cheng, M., Tapley, B. D., and Ries, J. C.: Deceleration in the Earth’s oblateness, *Journal of Geophysical Research: Solid Earth*, 118, 740–747, <https://doi.org/10.1002/jgrb.50058>, <http://onlinelibrary.wiley.com.biblioplanets.gate.inist.fr/doi/10.1002/jgrb.50058/abstract>, 2013a.
- Cheng, M. K., Ries, J. C., and Tapley, B. D.: Geocenter Variations from Analysis of SLR Data, in: *Reference Frames for Applications in Geosciences*, edited by Altamimi, Z. and Collilieux, X., no. 138 in *International Association of Geodesy Symposia*, pp. 19–25, Springer Berlin Heidelberg, https://doi.org/10.1007/978-3-642-32998-2_4, http://link.springer.com.biblioplanets.gate.inist.fr/chapter/10.1007/978-3-642-32998-2_4, 2013b.
- 320 Cretaux, J.-F., Abarca-del Río, R., Berge-Nguyen, M., Arsen, A., Drolon, V., Clos, G., and Maisongrande, P.: Lake Volume Monitoring from Space, *Surveys in Geophysics*, 37, 269–305, <https://doi.org/10.1007/s10712-016-9362-6>, <https://doi.org/10.1007/s10712-016-9362-6>,
325 2016.
- Decharme, B., Delire, C., Minvielle, M., Colin, J., Vergnes, J.-P., Alias, A., Saint-Martin, D., Séférian, R., Sénési, S., and Voltaire, A.: Recent changes in the ISBA-CTRIP land surface system for use in the CNRM-CM6 climate model and in global off-line hydrological

- applications, *Journal of Advances in Modeling Earth Systems*, 0, <https://doi.org/10.1029/2018MS001545>, <http://agupubs.onlinelibrary.wiley.com/doi/abs/10.1029/2018MS001545>, 2019.
- 330 Dee, D. P., Uppala, S. M., Simmons, A. J., Berrisford, P., Poli, P., Kobayashi, S., Andrae, U., Balmaseda, M. A., Balsamo, G., Bauer, P., Bechtold, P., Beljaars, A. C. M., van de Berg, L., Bidlot, J., Bormann, N., Delsol, C., Dragani, R., Fuentes, M., Geer, A. J., Haimberger, L., Healy, S. B., Hersbach, H., Hólm, E. V., Isaksen, I., Kållberg, P., Köhler, M., Matricardi, M., McNally, A. P., Monge-Sanz, B. M., Morcrette, J.-J., Park, B.-K., Peubey, C., de Rosnay, P., Tavolato, C., Thépaut, J.-N., and Vitart, F.: The ERA-Interim reanalysis: configuration and performance of the data assimilation system, *Quarterly Journal of the Royal Meteorological Society*, 137, 553–597, 335 <https://doi.org/10.1002/qj.828>, <http://doi.wiley.com/10.1002/qj.828>, 2011.
- Durand, M., Gleason, C. J., Garambois, P. A., Bjerklie, D., Smith, L. C., Roux, H., Rodriguez, E., Bates, P. D., Pavelsky, T. M., Monnier, J., Chen, X., Baldassarre, G. D., Fiset, J.-M., Flipo, N., Frasson, R. P. d. M., Fulton, J., Goutal, N., Hossain, F., Humphries, E., Minear, J. T., Mukolwe, M. M., Neal, J. C., Ricci, S., Sanders, B. F., Schumann, G., Schubert, J. E., and Vilmin, L.: An intercomparison of remote sensing river discharge estimation algorithms from measurements of river height, width, and slope, *Water Resources Research*, 52, 340 4527–4549, <https://doi.org/10.1002/2015WR018434>, <https://agupubs.onlinelibrary.wiley.com/doi/abs/10.1002/2015WR018434>, 2016.
- Funk, C., Peterson, P., Landsfeld, M., Pedreros, D., Verdin, J., Shukla, S., Husak, G., Rowland, J., Harrison, L., Hoell, A., and Michaelsen, J.: The climate hazards infrared precipitation with stations—a new environmental record for monitoring extremes, *Scientific Data*, 2, 150 066, <https://doi.org/10.1038/sdata.2015.66>, <http://www.nature.com/articles/sdata201566>, 2015.
- Gardelle, J., Berthier, E., and Arnaud, Y.: Slight mass gain of Karakorum glaciers in the early 21st century, *Nature Geoscience*, 5, 322–325, 345 <https://doi.org/10.1038/ngeo1450>, <https://hal.archives-ouvertes.fr/hal-00743995>, 2012.
- Huffman, G. J., Adler, R. F., Morrissey, M. M., Bolvin, D. T., Curtis, S., Joyce, R., McGavock, R., and Susskind, J.: Global Precipitation at One-Degree Daily Resolution from Multisatellite Observations, *Journal of Hydrometeorology*, 2, 36–50, <https://journals-ams.org/insu.bib.cnrs.fr/doi/full/10.1175/1525-7541%282001%29002%3C0036%3AGPAODD%3E2.0.CO%3B2>, 2001.
- Huffman, G. J., Adler, R. F., Bolvin, D. T., and Nelkin, E. J.: The TRMM Multi-Satellite Precipitation Analysis (TMPA), in: *Satellite Rainfall Applications for Surface Hydrology*, edited by Gebremichael, M. and Hossain, F., pp. 3–22, Springer Netherlands, Dordrecht, 350 https://doi.org/10.1007/978-90-481-2915-7_1, http://www.springerlink.com/index/10.1007/978-90-481-2915-7_1, 2010.
- Immerzeel, W. W., Beek, L. P. H. v., and Bierkens, M. F. P.: Climate Change Will Affect the Asian Water Towers, *Science*, 328, 1382–1385, <https://doi.org/10.1126/science.1183188>, <http://science.sciencemag.org/content/328/5984/1382>, 2010.
- Immerzeel, W. W., Gobiet, A., Suklitsch, M., Pellicciotti, F., and Bierkens, M. F.: Uncertain future for the water resources of high mountain 355 Asia, *AGU Fall Meeting Abstracts*, 51, <http://adsabs.harvard.edu/abs/2012AGUFMGC51D1232I>, 2012.
- Jacob, T., Wahr, J., Pfeffer, W. T., and Swenson, S.: Recent contributions of glaciers and ice caps to sea level rise, *Nature*, 482, 514–518, <https://doi.org/10.1038/nature10847>, <http://www.nature.com/biblioplanets.gate.inist.fr/nature/journal/v482/n7386/full/nature10847.html>, 2012.
- Jiang, L., Nielsen, K., Andersen, O. B., and Bauer-Gottwein, P.: Monitoring recent lake level variations on the Tibetan Plateau using CryoSat-2 SARIn mode data, *Journal of Hydrology*, 544, 109–124, <https://doi.org/10.1016/j.jhydrol.2016.11.024>, <http://www.sciencedirect.com/science/article/pii/S0022169416307302>, 2017.
- Kääb, A., Berthier, E., Nuth, C., Gardelle, J., and Arnaud, Y.: Contrasting patterns of early twenty-first-century glacier mass change in the Himalayas, *Nature*, 488, 495–498, <https://doi.org/10.1038/nature11324>, <https://www.nature.com/articles/nature11324>, 2012.

- Kääb, A., Treichler, D., Nuth, C., and Berthier, E.: Brief Communication: Contending estimates of 2003–2008 glacier mass balance over the Pamir–Karakoram–Himalaya, *The Cryosphere*, 9, 557–564, <https://doi.org/10.5194/tc-9-557-2015>, <https://www.the-cryosphere.net/9/557/2015/tc-9-557-2015-discussion.html>, 2015.
- 365 Khaki, M., Forootan, E., Kuhn, M., Awange, J., Papa, F., and Shum, C.: A study of Bangladesh’s sub-surface water storages using satellite products and data assimilation scheme, *Science of The Total Environment*, 625, 963–977, <https://doi.org/10.1016/j.scitotenv.2017.12.289>, <https://linkinghub.elsevier.com/retrieve/pii/S0048969717337221>, 2018.
- 370 Kubota, T., Shige, S., Hashizume, H., Aonashi, K., Takahashi, N., Seto, S., Hirose, M., Takayabu, Y. N., Ushio, T., Nakagawa, K., Iwanami, K., Kachi, M., and Okamoto, K.: Global Precipitation Map Using Satellite-Borne Microwave Radiometers by the GSMaP Project: Production and Validation, *IEEE Transactions on Geoscience and Remote Sensing*, 45, 2259–2275, <https://doi.org/10.1109/TGRS.2007.895337>, <http://ieeexplore.ieee.org/document/4261062/>, 2007.
- Kusche, J., Schmidt, R., Petrovic, S., and Rietbroek, R.: Decorrelated GRACE time-variable gravity solutions by GFZ, and their validation using a hydrological model, *Journal of Geodesy*, 83, 903–913, <https://doi.org/10.1007/s00190-009-0308-3>, <http://link.springer.com/article/10.1007/s00190-009-0308-3>, 2009.
- 375 Lemoine, J.-M. and Reinquin, F.: Processing of SLR Observations at CNES, Newsletter EGSIEM, p. 3, http://www.egsiem.eu/images/Newsletters/EGSIEM_newsletter_no10.pdf, 2017.
- Long, D., Longuevergne, L., and Scanlon, B. R.: Uncertainty in evapotranspiration from land surface modeling, remote sensing, and GRACE satellites, *Water Resources Research*, 50, 1131–1151, <https://doi.org/10.1002/2013WR014581>, <https://agupubs.onlinelibrary.wiley.com/doi/abs/10.1002/2013WR014581>, 2014.
- 380 Long, D., Longuevergne, L., and Scanlon, B. R.: Global analysis of approaches for deriving total water storage changes from GRACE satellites, *Water Resources Research*, 51, 2574–2594, <https://doi.org/10.1002/2014WR016853>, <https://agupubs.onlinelibrary.wiley.com/doi/abs/10.1002/2014WR016853>, 2015.
- 385 Long, D., Chen, X., Scanlon, B. R., Wada, Y., Hong, Y., Singh, V. P., Chen, Y., Wang, C., Han, Z., and Yang, W.: Have GRACE satellites overestimated groundwater depletion in the Northwest India Aquifer?, *Scientific Reports*, 6, 24398, <https://doi.org/10.1038/srep24398>, <https://www.nature.com/articles/srep24398>, 2016.
- Longuevergne, L., Scanlon, B. R., and Wilson, C. R.: GRACE Hydrological estimates for small basins: Evaluating processing approaches on the High Plains Aquifer, USA, *Water Resources Research*, 46, <https://doi.org/10.1029/2009WR008564>, <https://agupubs.onlinelibrary.wiley.com/doi/abs/10.1029/2009WR008564>, 2010.
- 390 Loomis, B. D., Richey, A. S., Arendt, A. A., Appana, R., Deweese, Y.-J. C., Forman, B. A., Kumar, S. V., Sabaka, T. J., and Shean, D. E.: Water Storage Trends in High Mountain Asia, *Frontiers in Earth Science*, 7, <https://doi.org/10.3389/feart.2019.00235>, https://www.frontiersin.org/articles/10.3389/feart.2019.00235/full?utm_source=Email_to_relev_&utm_medium=Email&utm_content=T1_11.5e4_reviewer&utm_campaign=Email_publication&journalName=Frontiers_in_Earth_Science&id=473021, 2019.
- 395 Martens, B., Miralles, D. G., Lievens, H., van der Schalie, R., de Jeu, R. A. M., Fernández-Prieto, D., Beck, H. E., Dorigo, W. A., and Verhoest, N. E. C.: GLEAM v3: satellite-based land evaporation and root-zone soil moisture, *Geoscientific Model Development*, 10, 1903–1925, <https://doi.org/10.5194/gmd-10-1903-2017>, <https://www.geosci-model-dev.net/10/1903/2017/>, 2017.
- Mathison, C., Wiltshire, A. J., Falloon, P., and Challinor, A. J.: South Asia river-flow projections and their implications for water resources, *Hydrology and Earth System Sciences*, 19, 4783–4810, <https://doi.org/10.5194/hess-19-4783-2015>, <https://www.hydrol-earth-syst-sci.net/19/4783/2015/>, 2015.
- 400

- Meng, F., Su, F., Li, Y., and Tong, K.: Changes in terrestrial water storage during 2003–2014 and possible causes in Tibetan Plateau, *Journal of Geophysical Research: Atmospheres*, <https://doi.org/10.1029/2018JD029552>, <http://doi.wiley.com/10.1029/2018JD029552>, 2019.
- Minallah, S. and Ivanov, V. Y.: Interannual Variability and Seasonality of Precipitation in the Indus River Basin, *Journal of Hydrometeorology*, 20, 379–395, <https://doi.org/10.1175/JHM-D-18-0084.1>, <https://journals.ametsoc.org/doi/10.1175/JHM-D-18-0084.1>, 2019.
- 405 Oubanas, H., Gejadze, I., Malaterre, P.-O., Durand, M., Wei, R., Frasson, R. P. M., and Domeneghetti, A.: Discharge Estimation in Ungauged Basins Through Variational Data Assimilation: The Potential of the SWOT Mission, *Water Resources Research*, 54, 2405–2423, <https://doi.org/10.1002/2017WR021735>, <https://agupubs.onlinelibrary.wiley.com/doi/abs/10.1002/2017WR021735>, 2018.
- Papa, F., Durand, F., Rossow, W. B., Rahman, A., and Bala, S. K.: Satellite altimeter-derived monthly discharge of the Ganga-Brahmaputra River and its seasonal to interannual variations from 1993 to 2008, *Journal of Geophysical Research: Oceans*, 115, <https://doi.org/10.1029/2009JC006075>, <http://agupubs.onlinelibrary.wiley.com/doi/abs/10.1029/2009JC006075>, 2010.
- 410 Peltier, W. R., Argus, D., and Drummond, R.: Comment on "An Assessment of the ICE6G_C (VM5a) glacial isostatic adjustment Model by Purcell et al.", *Journal of Geophysical Research: Solid Earth*, 123, 2019–2028, <https://doi.org/10.1002/2016JB013844>, <http://agupubs.onlinelibrary.wiley.com/doi/abs/10.1002/2016JB013844>, 2017.
- Purcell, A., Tregoning, P., and Dehecq, A.: Reply to Comment by W. R. Peltier, D. F. Argus, and R. Drummond on "An Assessment of the ICE6G_C (VM5a) Glacial Isostatic Adjustment Model", *Journal of Geophysical Research: Solid Earth*, 123, 2029–2032, <https://doi.org/10.1002/2017JB014930>, <http://agupubs.onlinelibrary.wiley.com/doi/abs/10.1002/2017JB014930>, 2018.
- Rietbroek, R., Fritsche, M., Brunnabend, S. E., Daras, I., Kusche, J., Schröter, J., Flechtner, F., and Dietrich, R.: Global surface mass from a new combination of GRACE, modelled OBP and reprocessed GPS data, *Journal of Geodynamics*, 59–60, 64–71, <https://doi.org/10.1016/j.jog.2011.02.003>, <http://www.sciencedirect.com/science/article/pii/S0264370711000305>, 2012.
- 420 Roca, R., Alexander, L. V., Potter, G., Bador, M., Jucá, R., Contractor, S., Bosilovich, M. G., and Cloché, S.: FROGs: a daily 1° × 1° gridded precipitation database of rain gauge, satellite and reanalysis products, *Earth System Science Data Discussions*, pp. 1–36, <https://doi.org/https://doi.org/10.5194/essd-2019-51>, <https://www.earth-syst-sci-data-discuss.net/essd-2019-51/>, 2019.
- Rodell, M. and Famiglietti, J. S.: Detectability of variations in continental water storage from satellite observations of the time dependent gravity field, *Water Resources Research*, 35, 2705–2723, <https://doi.org/10.1029/1999WR900141>, <http://agupubs.onlinelibrary.wiley.com/doi/abs/10.1029/1999WR900141>, 1999.
- Rodell, M., Famiglietti, J. S., Chen, J., Seneviratne, S. I., Viterbo, P., Holl, S., and Wilson, C. R.: Basin scale estimates of evapotranspiration using GRACE and other observations, *Geophysical Research Letters*, 31, <https://doi.org/10.1029/2004GL020873>, <http://agupubs.onlinelibrary.wiley.com/doi/abs/10.1029/2004GL020873>, 2004.
- 430 Rodell, M., Velicogna, I., and Famiglietti, J. S.: Satellite-based estimates of groundwater depletion in India, *Nature*, 460, 999–1002, <https://doi.org/10.1038/nature08238>, 2009.
- Rodell, M., Famiglietti, J. S., Wiese, D. N., Reager, J. T., Beaudoin, H. K., Landerer, F. W., and Lo, M.-H.: Emerging trends in global freshwater availability, *Nature*, 557, 651–659, <https://doi.org/10.1038/s41586-018-0123-1>, <https://www-nature-com-s.docadis.ups-tlse.fr/articles/s41586-018-0123-1>, 2018.
- 435 Shamsudduha, M. and Panda, D. K.: Spatio-temporal changes in terrestrial water storage in the Himalayan river basins and risks to water security in the region: A review, *International Journal of Disaster Risk Reduction*, 35, 101 068, <https://doi.org/10.1016/j.ijdrr.2019.101068>, <http://www.sciencedirect.com/science/article/pii/S2212420919300615>, 2019.

- Sharma, E., Molden, D., Rahman, A., Khatiwada, Y. R., Zhang, L., Singh, S. P., Yao, T., and Wester, P.: Introduction to the Hindu Kush Himalaya Assessment, in: *The Hindu Kush Himalaya Assessment*, pp. 1–16, Springer International Publishing, Cham, 440 https://doi.org/10.1007/978-3-319-92288-1_1, http://link.springer.com/10.1007/978-3-319-92288-1_1, 2019.
- Swenson, S., Chambers, D., and Wahr, J.: Estimating geocenter variations from a combination of GRACE and ocean model output, *Journal of Geophysical Research: Solid Earth*, 113, B08 410, <https://doi.org/10.1029/2007JB005338>, <http://onlinelibrary.wiley.com/biblioplanets.gate.inist.fr/doi/10.1029/2007JB005338/abstract>, 2008.
- Tapley, B. D., Bettadpur, S., Ries, J. C., Thompson, P. F., and Watkins, M. M.: GRACE Measurements of Mass Variability in the Earth System, *Science*, 305, 503–505, <https://doi.org/10.1126/science.1099192>, <http://science.sciencemag.org/biblioplanets.gate.inist.fr/content/305/5683/503>, 2004. 445
- Tiwari, V., Wahr, J., and Swenson, S.: Dwindling groundwater resources in northern India, from satellite gravity observations, *Geophysical Research Letters*, 36, <https://doi.org/10.1029/2009GL039401>, <http://agupubs.onlinelibrary.wiley.com/doi/abs/10.1029/2009GL039401>, 2009.
- 450 Treichler, D., Käab, A., Salzmann, N., and Xu, C.-Y.: Recent glacier and lake changes in High Mountain Asia and their relation to precipitation changes, *The Cryosphere*, 13, 2977–3005, <https://doi.org/https://doi.org/10.5194/tc-13-2977-2019>, <https://www.the-cryosphere.net/13/2977/2019/>, 2019.
- Wahr, J., Nerem, R. S., and Bettadpur, S. V.: The pole tide and its effect on GRACE time-variable gravity measurements: Implications for estimates of surface mass variations, *Journal of Geophysical Research: Solid Earth*, 120, 2015JB011 986, 455 <https://doi.org/10.1002/2015JB011986>, <http://onlinelibrary.wiley.com/biblioplanets.gate.inist.fr/doi/10.1002/2015JB011986/abstract>, 2015.
- Wan, W., Long, D., Hong, Y., Ma, Y., Yuan, Y., Xiao, P., Duan, H., Han, Z., and Gu, X.: A lake data set for the Tibetan Plateau from the 1960s, 2005, and 2014, *Scientific Data*, 3, 160 039, <https://doi.org/10.1038/sdata.2016.39>, <http://www.nature.com/articles/sdata201639>, 2016.
- 460 Wang, J., Song, C., Reager, J. T., Yao, F., Famiglietti, J. S., Sheng, Y., MacDonald, G. M., Brun, F., Schmied, H. M., Marston, R. A., and Wada, Y.: Recent global decline in endorheic basin water storages, *Nature Geoscience*, 11, 926–932, <https://doi.org/10.1038/s41561-018-0265-7>, <https://www.nature.com/articles/s41561-018-0265-7>, 2018.
- Wijngaard, R. R., Biemans, H., Lutz, A. F., Shrestha, A. B., Wester, P., and Immerzeel, W. W.: Climate change vs. socio-economic development: understanding the future South Asian water gap, *Hydrology and Earth System Sciences*, 22, 6297–6321, 465 <https://doi.org/10.5194/hess-22-6297-2018>, <https://www.hydrol-earth-syst-sci.net/22/6297/2018/>, 2018.
- Wu, X., Kusche, J., and Landerer, F. W.: A new unified approach to determine geocentre motion using space geodetic and GRACE gravity data, *Geophysical Journal International*, 209, 1398–1402, <https://doi.org/10.1093/gji/ggx086>, <https://academic-oup-com.insu.bib.cnrs.fr/gji/article/209/3/1398/3061360/A-new-unified-approach-to-determine-geocentre>, 2017.
- Xie, P., Janowiak, J. E., Arkin, P. A., Adler, R., Gruber, A., Ferraro, R., Huffman, G. J., and Curtis, S.: GPCP Pentad Precipitation Analyses: An Experimental Dataset Based on Gauge Observations and Satellite Estimates, *Journal of Climate*, 16, 2197–2214, 470 <https://doi.org/10.1175/2769.1>, <http://journals.ametsoc.org/doi/abs/10.1175/2769.1>, 2003.
- Yao, F., Wang, J., Yang, K., Wang, C., Walter, B. A., and Cretaux, J.-F.: Lake storage variation on the endorheic Tibetan Plateau and its attribution to climate change since the new millennium, *Environmental Research Letters*, 13, 064 011, <https://doi.org/10.1088/1748-9326/aab5d3>, <https://doi.org/10.1088%2F1748-9326%2Faab5d3>, 2018.

- 475 Zhang, G., Yao, T., Shum, C. K., Yi, S., Yang, K., Xie, H., Feng, W., Bolch, T., Wang, L., Behrangi, A., Zhang, H., Wang, W., Xiang, Y., and Yu, J.: Lake volume and groundwater storage variations in Tibetan Plateau's endorheic basin, *Geophysical Research Letters*, 44, 5550–5560, <https://doi.org/10.1002/2017GL073773>, <http://agupubs.onlinelibrary.wiley.com/doi/abs/10.1002/2017GL073773>, 2017.

3.2 Perspective for global land leakage correction

In order to apply the land leakage correction in a global scale, I would need independent data for the every regions. In December 2019, the larger 156 lake volume changes are available in Hydroweb including timeseries longer than the GRACE period (2002-2016). The inclusion of this surface water in the land leakage correction method reduces the uncertainty in land mass changes at local scale as proven in South Asia. I review from the bibliography, the contributions of the glaciers not included in the land leakage correction in 3.2.1. Based on these results, I present an estimate for **LWS** mass contribution analysing endorheic and exorheic basin and compare them to the bibliography in section 3.2.2.

3.2.1 Glaciers at global scale

I review in this section the regions containing glaciers as described in **RGI6.0**. I considered as one region the Arctic islands, including: Northern and Southern Arctic Canada, Iceland, Svalbard and Russian Arctic islands (blue box in Fig.3.6). GRACE-based mass loss estimates for the Arctic islands show a very good consistency in trends with the estimates from other techniques [Blazquez et al., 2018; Bamber et al., 2018]. Therefore, I use only GRACE data to retrieve mass changes in these regions as previous studies [Reager et al., 2016; Blazquez et al., 2018; Bamber et al., 2018].

I also considered as one region **HMA** which is described as 3 regions in **RGI6.0** (blue box in Fig.3.6). In this region, GRACE-only data is not accurate enough. I use the independent mass change observations to reduce the leakage in GRACE-based **LWS** changes as described in previous section.

Land leakage correction is to be applied to the remaining regions with glaciers (Red polygons in Fig. 3.6). Considering the impact to the sea level rise, there are three regions where glacier mass loss trends are significant: Alaska, Western Canada and USA, and Southern Andes (regions 1, 2, and 17 in Fig. 3.6). These regions represent 0.12 M km² and account for 0.26 ± 0.09 mm SLE/yr for the period 2002-2016 [Hock et al., 2019]. Although there are still some differences between GRACE-based estimates and the other techniques (0.33 ± 0.10 mm SLE/yr from Zemp et al. [2019]). GRACE-based glacier mass changes need to be corrected for **Little Ice Age (LIA)** correction. **LIA** corrections considers the viscous adjustment due to on going mass changes since the end of the last cold period. **LIA** correction affects the gravity field as a linear trend [Luthcke et al., 2013; Jacob et al., 2012; Reager et al., 2016]. **LIA** correction is estimated with independent data (e.g. GPS, altimetry) which makes difficult to obtain accurate data.

The rest of glaciers are included in 6 regions detailed in figure 3.6: Scandinavia (8), North Asia (10), Central Europe (11), Caucasus and Middle East (12), Low Latitudes (16), and New Zealand (18). The glacier surface is 0.13 Mkm² and their associated mass trends are 0.02 ± 0.02 mm SLE/yr [Hock et al., 2019], although the uncertainty from GRACE is higher 0.01 ± 0.08 mm SLE/yr for the period 2002-2016 [Wouters et al., 2019]. In these regions, the hydrology beneath the glacier is not negligible. GRACE-based estimates of glacier mass change rely on hydrological models [Wouters et al., 2019; Schrama et al., 2014] which tend to have difficulties estimating trends (See chapter 1.2.3).

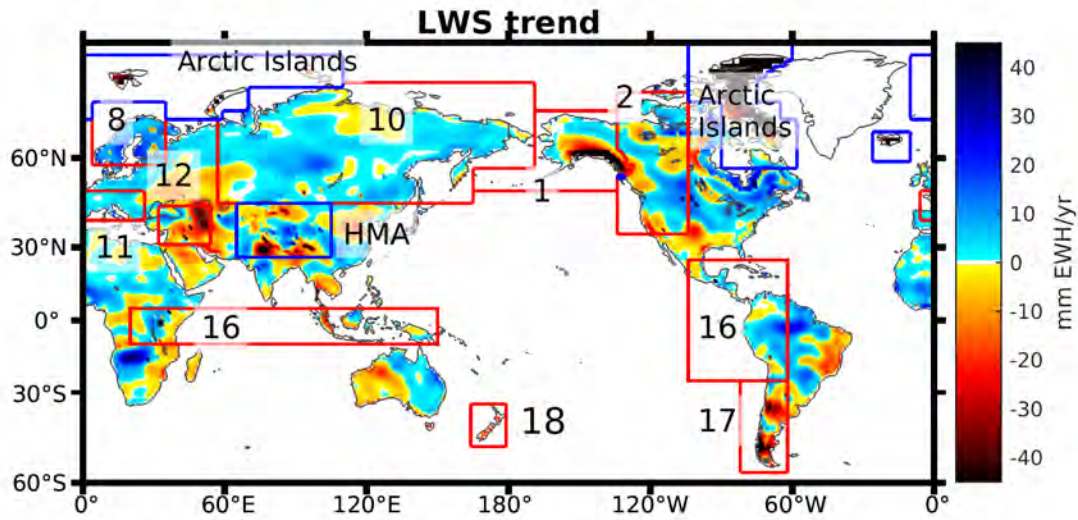


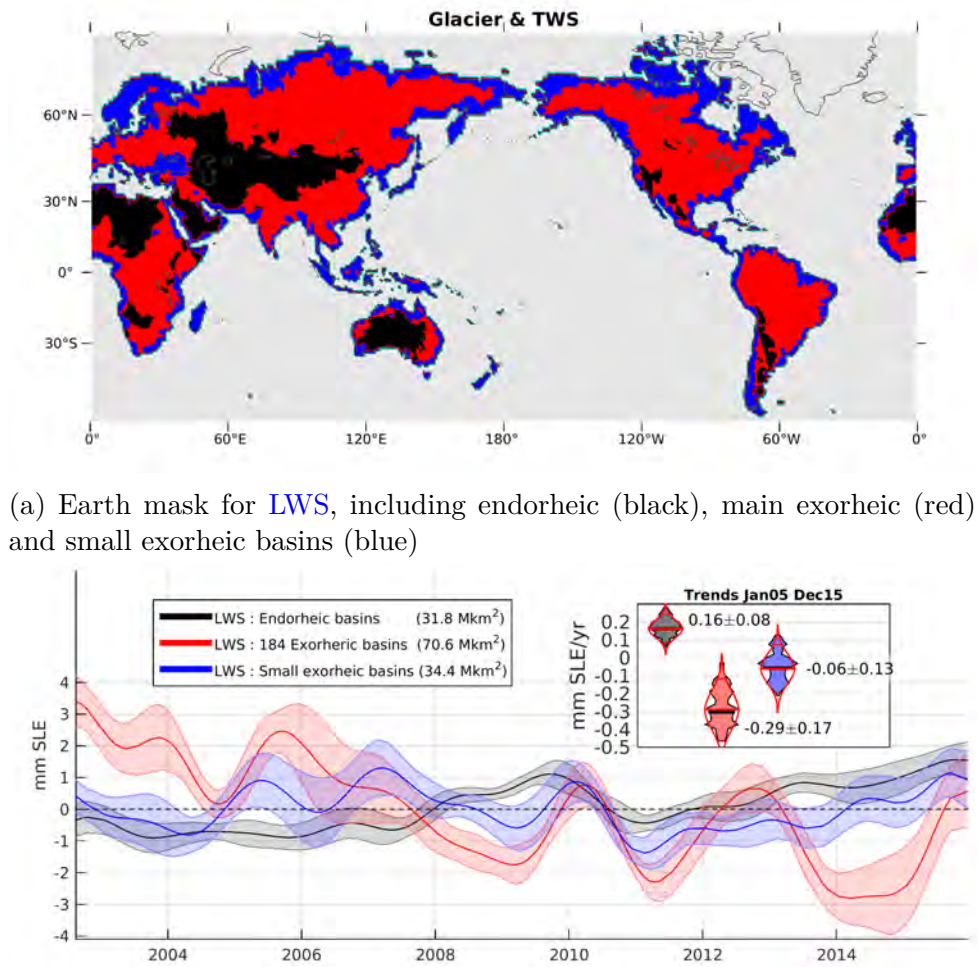
Figure 3.6: Regions containing glaciers using RGI nomenclature. Red boxes corresponds to the regions to analyse while blue boxes corresponds to arctic islands and HMA regions. The base map corresponds to the mass trends for the period 2005-2015 from GRACE.

This is one of main sources of uncertainties in GRACE-based land mass changes and the source of the differences between GRACE-based glacier mass trends and estimates from other techniques (Table 1.2).

3.2.2 LWS at global scale

I present in this section ongoing results about LWS mass changes in terms of trends for the period from 2003 to 2015 and interannual variability. Arctic islands and the glaciers from HMA have been removed from the rest of LWS. I account for the rest of the glacier by analysing LWS and not TWS. However this contribution is about 0.26 ± 0.095 mm SLE/yr or the period 2002-2016 [Wouters et al., 2019] and it mainly affects small exorheic basins in Alaska and Southern Andes. Following the global water budget from chapter 2, I focus here in the glacier & TWS component. I remove glacier mass change from HMA and the Arctic islands and I decompose the remaining glacier & TWS in (1) LWS in endorheic basins, (2) LWS in large exorheic basins, and (3) LWS in the small exorheic basins (Fig 3.7a). The endorheic basins are extracted from Wang et al. [2018]. The exorheic basins are divided in two groups depending on the basin surface: The main 184 exorheic basins with a surface larger than 50 000 km² and the small coastal basins.

I recall that my estimates of LWS are not exactly TWS as they includes glaciers. I perform a preliminary test by using a mask to remove glaciers. I remove timeseries from the LWS locations where glaciers cover more than 1% of the surface. It mainly affects small coastal basins reducing their mass loss by 0.11 mm SLE/yr and to a lesser extent endorheic basins (increase of 0.01 mm SLE/yr) and large exorheic basins (decreased of



(a) Earth mask for **LWS**, including endorheic (black), main exorheic (red) and small exorheic basins (blue)

(b) Time series after applying a low-pass filter to remove sub-annual frequencies and the associated trends for the period 2005-2015. In the trend panel, the shaded areas indicate the distribution of trends, while the red lines indicate the distribution that would be obtained under the assumption of a Gaussian distribution.

Figure 3.7: **LWS** analysis in terms of endorheic, exorheic and small exorheic basins.

0.03 mm SLE/yr). The land leakage from one basin to its neighbors is not reduced with this method. However, the differences in the filtered solutions (from ddk3 to ddk6) show very small impact in the global trends (Table 3.1)

The small impact of the filtering the basin gave **LWS** in endorheic basin are losing mass at 0.16 ± 0.08 mm SLE/yr for the period 2005-2015 mainly due to the decline of Caspian basin. This result differs with a previous study, that reported a mass loss trends of 0.30 ± 0.03 mm SLE/yr for 2002-2016 [Wang et al., 2018] while I found 0.13 ± 0.7 mm SLE/yr for the same period. I further analyze each basin and I found a good agreement in the Caspian basin mass change of 0.09 ± 0.01 . However, both studies differs in Sahara and Arabia basins, between 0.09 ± 0.01 mm SLE/yr [Wang et al., 2018] and 0.03 ± 0.02 mm SLE/yr from my ensemble. Analyzing the possible source of these discrepancies, there are known differences between the ensemble of GRACE solution I used and the JPL mascon solution used by Wang in land water mass estimates [Blazquez et al., 2018].

I further analyzed the sources of the uncertainties in **LWS** in endorheic basin from my ensemble of GRACE solution. I found that the uncertainty in geocenter motion and differences between the processing centers are the main contributions to the uncertainty in endorheic basin mass contribution to the sea level with ± 0.06 mm SLE/yr and ± 0.04 mm SLE/yr, respectively (Table 3.1).

Table 3.1: **LWS** trends and its associated uncertainties for the period from 2003 to 2015. **LWS** is excerpt from table 2.2 combining glacier & **TWS** and Arctic islands. This term is split in: (1) glaciers from Arctic islands, (2) glaciers in **HMA**, (3) **LWS** in endorheic basins, (4) **LWS** of the main exorheic basins, and (5) **LWS** in the small coastal basins.

	LWS	Arctic islands	HMA	Endorheic	Exorheic ^a	Others ^b
Trends	0.14	0.28	0.05	0.16	-0.29	-0.06
Uncertainty	0.36	0.03	< 0.01 ^c	0.08	0.17	0.13
processing center	0.06	< 0.01	^c	0.04	0.06	0.02
geocenter	0.32	0.02	^c	0.06	0.15	0.10
C ₂₀	< 0.01	< 0.01	^c	< 0.01	< 0.01	< 0.01
Filtering	0.02	< 0.01	^c	< 0.01	< 0.01	0.01
GIA	0.09	0.01	^c	0.02	0.06	0.03
Leakage correction	0.08	< 0.01	^c	< 0.01	< 0.01	0.09

^a Including 217 main exorheic basins with surface larger than 50 000 km²

^b Including small basin and the rest of emerged land

^c based on Brun et al. [2017], uncertainty of 3.5 Gt

LWS in the 184 main exorheic basins reduces the sea level rise with a trend of -0.29 ± 0.17 mm SLE/yr. This result is in agreement with previous estimates of -0.32 mm SLE/yr from Reager et al. [2016] and -0.21 ± 0.01 mm SLE/yr from Scanlon et al. [2018]. This result claims for a reevaluation of the hydrological models for the main exorheic basins, which predicted mass accumulation of 0.32 ± 0.18 mm SLE/yr [Dieng et al., 2017] and [0.03 to 1.25] mm SLE/yr [Scanlon et al., 2018] for the same periods.

Analyzing the uncertainties in the main exorheic basin with my ensemble of GRACE solution, I found that the uncertainty in geocenter motion and differences between the processing centers are the main contributions to the uncertainty in the main exorheic basin with ± 0.15 mm SLE/yr and ± 0.06 mm SLE/yr, respectively (Table 3.1). The uncertainty in the GIA correction is responsible of an uncertainty of ± 0.06 mm SLE/yr particularly important near Hudson Bay (Table 2.1 and Cazenave et al. [2018a]).

LWS in the small coastal basins (blue areas in Figure 3.7) represent about the fourth part of the total emerged land without Greenland, Antarctica and the arctic islands (34.4 M km² over 137.9 M km²). The uncertainty of ± 0.13 mm SLE/yr is mainly due to the uncertainty in the geocenter motion of ± 0.10 mm SLE/yr and in the land/ocean leakage correction of ± 0.09 mm SLE/yr. The leakage due to the Alaska and Southern Andes glaciers hampers the retrieval of accurate **TWS** mass changes. This component needs to be further analysed as it may be the key to improve the land/ocean leakage correction and the land leakage correction.

3.3 Conclusion

I explored in the chapter the use of GRACE-only and independent estimate methods to separate glacier and the local hydrological signals. The land leakage method reduces the uncertainty in GRACE-based **TWS** estimates leading to a correction up to 1 Gt/yr in the basin-mean TWS change and leakage accuracy relies on the accuracy and the availability of these independent data (e.g., the temporal resolution of the glacier data is coarse as only trends for the period from 2000 to 2016 are currently available).

GRACE-only glacier estimates are only accurate enough in regions where the hydrology beneath is negligible, e.g. the Arctic islands. In the other regions the use of independent mass change observations is crucial to retrieve accurate **TWS** estimates or the use of hydrological models to retrieve the glaciers (e.g. South Asia region). However, the question of the accuracy of GRACE-only glacier and **TWS** estimates in the remaining regions is to be addressed (Scientific Question 2).

I explore the **LWS** mass change removing glaciers from the Arctic islands and from **HMA**. The remaining glacier mass lost mainly affects the small exorheic basins. I found a **LWS** mass loss of -0.19 ± 0.33 mm SLE/yr. Uncertainties are too large to analyze if **TWS** are accumulating or losing mass in the last decades. (Scientific Question 3).

However, separating the remaining **LWS** in three groups: endorheic, main exorheic and small coastal, allows me to further analyze their influence in the global water budget. I found endorheic basins are losing mass at a rate of 0.16 ± 0.08 mm SLE/yr for the period from 2003 to 2015. The interannual variability shows small variations except for *La niña* 2011 [Fasullo et al., 2013; Cazenave et al., 2014]. This is not the case for the 184 main exorheic basins contribution. Their interannual variability varies from one year to another up to ± 3 mm SLE, making trends extremely dependent on the period. Moreover, uncertainties in the mass trend from the ensemble are ± 0.17 mm SLE/yr mainly due to the uncertainties in the geocenter and the **GIA**.

Based on these results, it is impossible to determinate if the trend of -0.29 ± 0.17 mm SLE/yr is a response to the climate change or on the contrary is due to the interannual variability of the period from 2003 to 2015. The interannual mass change variability of the exorheic basins for the first decades of the 21th century of ± 3 mm SLE hampers the attribution of this trend to climate change [Fasullo et al., 2016a]. Uncertainties of ± 0.17 mm SLE/yr and a interannual variability of ± 6 mm SLE are too large to excerpt any further conclusion for the first decades of the 21th century and analyze the changes in **TWS** (scientific question 4).

In order to reduce the uncertainties in **TWS**, I would like to apply the land leakage correction to the remaining glaciers. I will like to further investigate the uncertainties in **GIA** correction in Northern America. Once removed the glacier mass loss from the small coastal basins, I will further analyze the combination of the land leakage correction and the land/ ocean correction.

CHAPTER 3. EVALUATING THE UNCERTAINTY IN THE GRACE-BASED ESTIMATES
OF LAND MASS CHANGES. SEPARATING GLACIER AND TWS CHANGES

Chapter 4

Uncertainty in GRACE-based estimates of the ocean mass. Implications for the sea level budget and the estimation of the EEI

With my ensemble of GRACE solutions, I estimate the ocean mass trend for the period from 2005 to 2015 at 1.55 ± 0.33 mm SLE/yr. This ocean mass trend agrees, within uncertainties, with the estimates from other methods (See Table 1.3 and Fig. 2.12). The uncertainty in this estimate comes mainly from the uncertainty in geocenter correction and the uncertainty in GIA correction which cause an uncertainty of respectively ± 0.27 mm SLE/yr and ± 0.16 mm SLE/yr (Chapter 2 and Blazquez et al. [2018]). In this chapter, I propose to further analyze the geocenter correction in order to reduce the uncertainty in the ocean mass estimates from GRACE data.

The geocenter correction applied to the GRACE L2 data corresponds to a change of origin of its reference frame from a reference frame centered in the [center of mass \(CM\)](#) to a reference frame centered in the [center of figure \(CF\)](#) (See 2.2.1). I analyze the impact of this change in reference frame in the ocean mass in section 4.1.

The choice of the reference frame in which GRACE data is projected is particularly important when GRACE data is compared to or combined with other data. In such cases the reference frame of GRACE data should be consistent with the reference frame of the other data. An important example is the case of the sea level budget. In section 4.2, I revisit the sea level budget by analyzing the consistency between the reference frame of altimetry-based sea-level, gravimetry-based ocean mass and steric sea-level. I explore the impact of the reference frame in altimetry sea-level in subsection 4.2.1. In section 4.2.2, I combine altimetry data with GRACE data in different reference frames to estimate the steric sea level and I compare with the steric sea-level products. Then, I explore the consistency in the sea-level budget and analyze the implications for the characterization of the deep-ocean steric sea-level change in subsection 4.2.3 and for the [EEI](#) in section 4.3.

The content of this chapter is the result of a cooperation with [CLS](#), *Centre Nationale*

d'Études Spatiales (CNES) orbitography service, CNES geodesy service and Stellar Space Studies. These results are unpublished, and will be the topic of a future paper.

4.1 Impact of the choice of the reference frame on the ocean mass estimate from GRACE

The choice of the origin of a reference frame does not modify the gravity field of the Earth or equivalently the mass redistribution in the Earth's system. As such, the origin of the reference frame does not play any role in the estimates of the global estimate of the geoid changes or the associated mass redistributions. Now, when we focus on the mass redistribution in a subsystem of the Earth's system like the ocean, the problem is different because the ocean basin is fixed with respect to the Earth's crust, which is fixed in the frame centered in the CF. To estimate the mass redistribution in this subsystem, we need to estimate the geoid changes in a reference frame in which this subsystem is fixed. So to estimate the ocean mass we should work in the CF frame. Because GRACE, like all satellites describes orbits around the Earth's barycenter or CM, the degree-one which provide the position of the CF with the CM is not observable by GRACE instruments. In order to change the GRACE-based global water estimates from CM frame to the CF frame the main modification that we need to do is to include the degree-one or geocenter motion [Chambers et al., 2004].

We investigate the impact and choice of the reference frame in GRACE data treatment from L1 level to the ensemble of GRACE solutions in a joint effort with CNES geodesy service and Stellar Space Studies. We track down the potential influence of the reference frame in each L1 data and each treatment. We identify a possible source in the GPS data used during the inversion. Indeed during the inversion the GPS data can introduce a spurious signal in the orbits because GPS data are retrieved with ground stations fixed in the CF frame. In order to simulate this effect, we modify the orbits, considering an arbitrary spurious signal of 10 mm in the Z components of the orbits. This is equivalent to transfer the GPS ground stations towards a new frame shifted 10 mm in the Z axis and it allows to analyze the effect in the harmonic field and in equivalent water height (Fig. 4.1). We find a mean difference in the ocean mass of 0.009 mm SLE (0.09 cm in Fig. 4.1).

We assume from this synthetic study that an geocenter motion in Z of 10 mm may be responsible of 0.009 mm SLE in the ocean mass. Trends in the Z component of the geocenter motion are 200 times smaller than this 10 mm (For example ± 0.2 mm/yr from Fig. 2.4). As a consequence, not considering the orbits in the CM may provoke an error of smaller than $2 \cdot 10^{-4}$ mm SLE/yr [Bourgogne, 2019].

Another potential source is the dealiasing models used during the inversion, specially in the dealiasing models used in the RL05. The dealiasing models used by GRGS do not include the degree-one. I will need to investigate this point, for the moment I chose to fix the degree-one to zero in the monthly solutions, even if the 3hr models used may infer a degree-one in the solutions.

In conclusion, I assume that the spurious signals included during the inversion process

4.1. IMPACT OF THE CHOICE OF THE REFERENCE FRAME ON THE OCEAN MASS ESTIMATE FROM GRACE

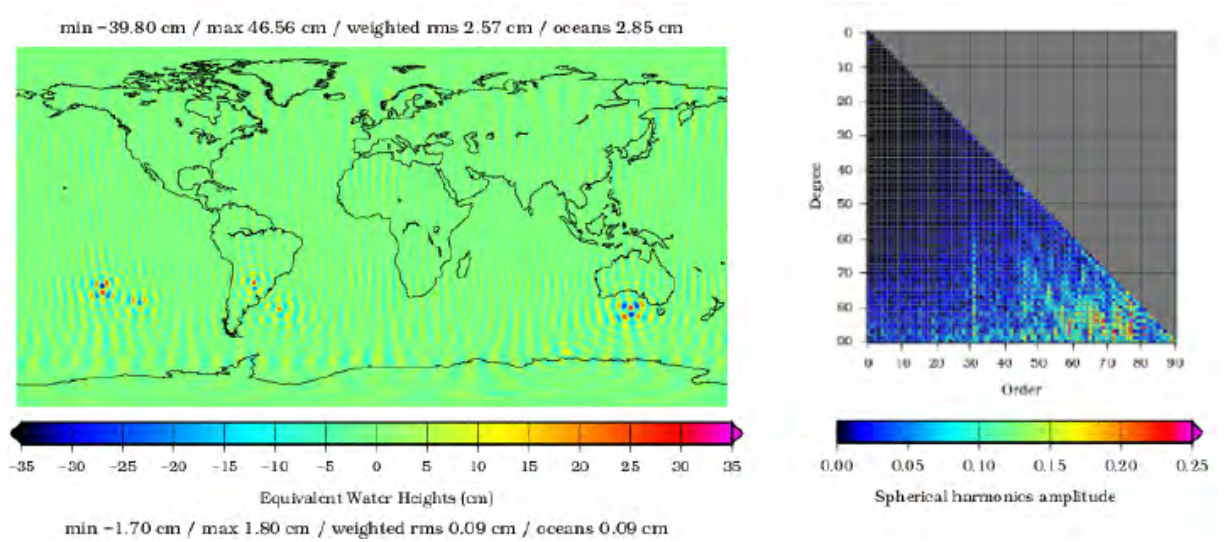


Figure 4.1: Effect of an arbitrary shift of 1 cm in Z components of the GRACE orbits in the inversion process. Left panel corresponds to the EWH differences and right panel to the differences in spherical harmonics amplitude.

are negligible compared to the inclusion of the geocenter motion. I compare here, the ocean mass in CF frame from GRACE LEGOS 1.1 which includes 5 geocenter solutions [Cheng et al., 2013b; Lemoine and Reinson, 2017; Rietbroek et al., 2016; Swenson et al., 2008; Wu et al., 2017] and the ocean mass in the CM frame from a new ensemble without including the geocenter correction (Fig 4.2).

This change of reference frame from CF frame to CM frame modifies the trends from 1.55 ± 0.33 mm SLE/yr to 1.60 ± 0.20 mm SLE/yr, the annual cycle amplitude from 10.35 ± 1.33 mm SLE to 8.87 ± 0.24 mm SLE and its phase from -94 ± 14 days to -78 ± 02 days. Changes in the interannual variability are also significant with differences upto ± 3.0 mm SLE (Fig 4.2). The gain of working in the CM frame rather than in the

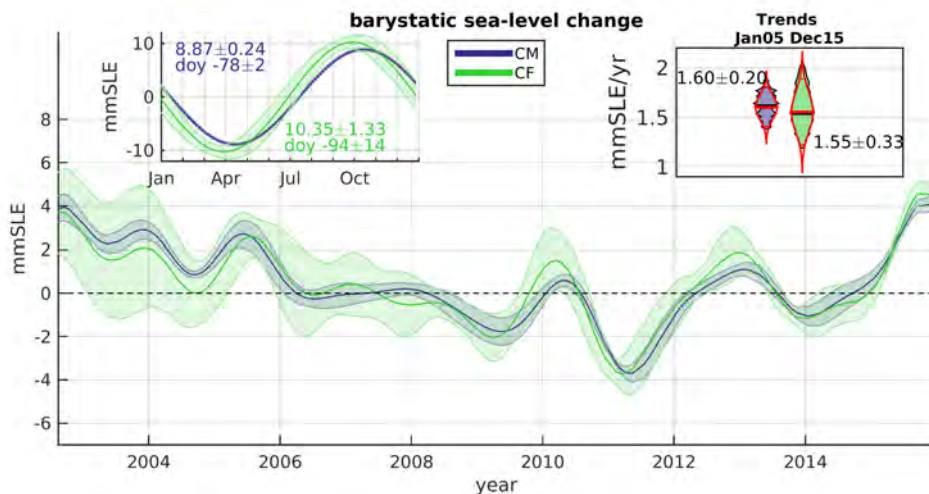


Figure 4.2: Impact of the change in the reference frame center between CM vs CF in gravimetry-based ocean mass

CF frame is that the uncertainties in trends and in the annual cycle are reduced with the change of reference frame, although we miss part of the barystatic sea-level change. The uncertainty in trend gets down to ± 0.20 mm SLE/yr in the **CM** frame and it is mainly due to the uncertainty due to the **GIA** correction of ± 0.16 mm SLE/yr.

4.2 Implications on the Sea level budget

Altimetry-based sea-level, gravimetry-based ocean mass and ARGO-based steric sea-level are related through the sea level budget (Eq. 1.5). In this section, I analyze the consistency among them in terms of trends, interannual variability and annual cycle. To combine these datasets, I work using consistent reference frames. I explore the sea-level budget in the **CM** frame (subsection 4.1) with the sea-level budget in the **CF** frame. Among the contributions of the sea level budget the steric contribution is the only data to be independent from the reference frame because it measures directly the changes in the ocean layer which due to ocean warming. There is no reference to any level datum. So I take steric sea level as my target. I estimate steric sea level as the difference between altimetry-based sea-level and gravimetry-based ocean mass. Then, I compare steric estimates in both reference frames.

4.2.1 Altimetry sea-level change

We investigated the impact and choice of reference frame in the altimetry-based geocentric sea-level. In principle, altimetry satellites measure the distance between the satellite and the sea surface and the distance between the satellite and the **CM**. The distance between the satellite and the **CM** is expressed in the **ITRF** and so, it is supposed to be in the **CM**. Thus, the sea-level is meant to be delivered in the **CM** frame [Ablain et al., 2017, 2015]. We have analyzed the influence of the reference frame center in the process of the altimetry data from the L1 level to the L4 level in a joint effort with **CNES** Orbitography team (A. Couhert, F. Mercier) and **CLS** sea-level team (M. Ablain, L. Zawadzki and A. Ollivier).

We find that all corrections applied to the L2 data are delivered in the **CM** frame, except the orbit determination. Indeed, the use of **GPS** during the orbit computation infers a small geocenter signal that need to be corrected to get the orbits truly in the **CM**. Indeed, **GPS** determines distances with respect to the satellites, but these distances are referenced to a ground network which is fixed to the Earth's crust in the **CF**. In the orbit determination process the position of the stations has not been transferred to the **CM** frame for the computation although it should have been. This leads to a small error in the position of the orbits with respect to the **CM**.

In order to quantify this effect, we tested the impact of the geocenter correction in the altimetry-based sea level using 6 different geocenter solutions [Cheng et al., 2013b; Couhert et al., 2018; Lemoine and Reinquin, 2017; Rietbroek et al., 2016; Swenson et al., 2008; Wu et al., 2017]. The impact of the geocenter motion is simulated via a variation on the **GPS** clocks which virtually shift the orbit [Couhert et al., 2018]. We reprocess the Jason 1 and 2 altimetry data with these orbits to get altimetry measurements in a

reference frame centered on the CM. The 6 different geocenter motions in the reprocessing of orbits yield to 6 gridded solutions that are compared to the global-mean geocentric sea-level changes from SL [Climate Change Initiative \(CCI\)](#) V2.0, which is supposed to be in the CM but does not include this correction [Ablain et al., 2015] (Fig. 4.3a).

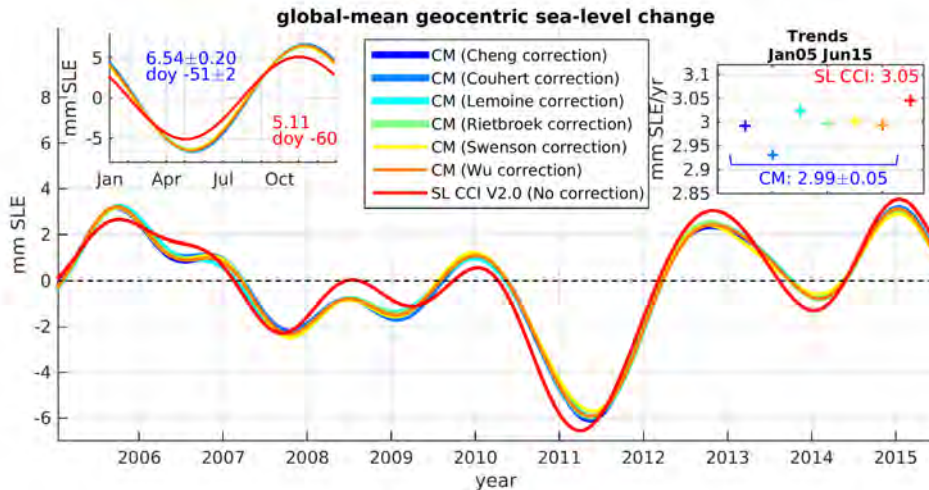


Figure 4.3: Altimetry-based global sea-level change expressed in the reference frame centered in the CM. SL CCI solution doesn't contain this correction. Trends are computed for the period 2005 to 2015. Timeseries are detrended

The spread among the solutions in the CM frame is small: ± 0.05 mm SLE/yr in trends, ± 0.20 mm SLE in the annual cycle and less than ± 0.1 mm SLE in interannual variability. On the contrary, there are significant differences between the SL CCI V2.0 solution, which is supposed to be in the CM, and the solutions that have been corrected to be in the CM frame. The latter solutions present a trend of 2.99 ± 0.05 mm SLE/yr, smaller than the trend from SL CCI of 3.05 mm SLE/yr. The difference is not significant at 90% CL as both solutions are within the uncertainties due to the orbit determination in altimetry-based global mean sea-level of ± 0.20 mm SLE/yr at 90% CL [Ablain et al., 2019]. Considering the annual cycle, the change of reference frame increase the amplitude of the annual cycle from 5.11 mm SLE to 6.54 ± 0.20 mm SLE.

In conclusion, we find that SL CCI V2.0 needs to be corrected for the geocenter motion in the orbits to be delivered in the CM frame. Our first attempt to provide such corrections shows that it lead for significant differences. A full revision of the process is needed to deliver altimetry sea-level in the CM frame properly. I found some discrepancies in previous previous studies where altimetry-based sea-level has been assumed to be in the CF frame [Chambers et al., 2004; Chambers, 2006b; Willis et al., 2008; Rietbroek et al., 2016]. This is an assumption that probably needs to be revisited.

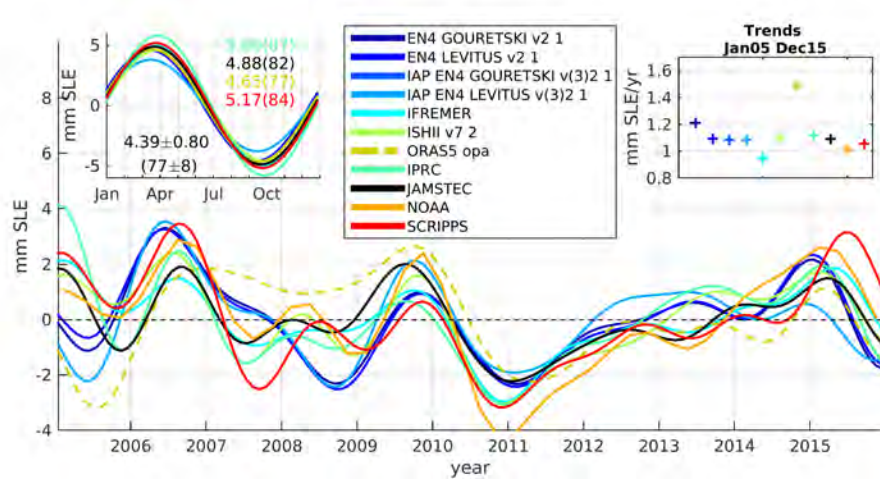
4.2.2 ARGO-based steric sea-level

Steric estimates are usually based on *in situ* temperature from XBT, CTD and ARGO floats. Steric sea-level is estimated as the dilatation of the water column under a temperature or salinity change (See 1.3.3.2). It is independent from the reference frame. In 2005,

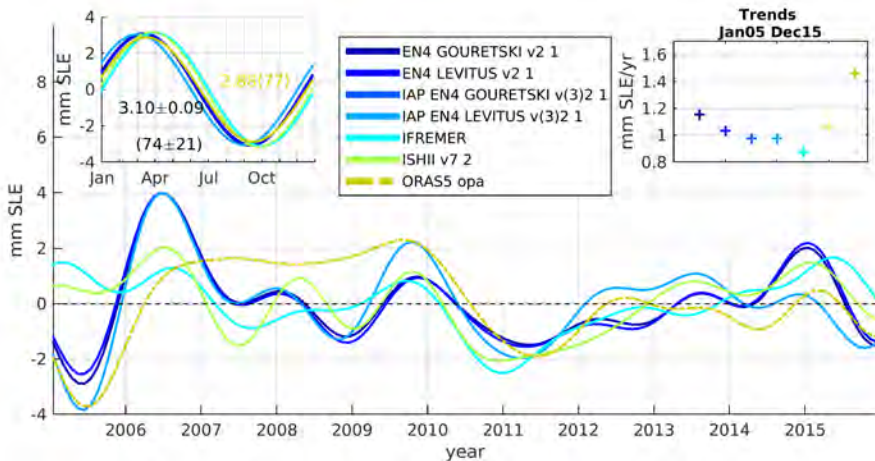
ARGO achieved a quasi global coverage (60°S - 60°N latitude), down to 2000 m depth with a monthly resolution and a spatial resolution of $3^{\circ} \times 3^{\circ}$ [Roemmich et al., 2009]. We focus here on this period from 2005 to 2015.

Several datasets of *in situ* temperature are available. I include here the products from IAP, IFREMER, IPRC, ISHII, EN4, JAMSTEC, NOAA, and SCRIPPS. Differences among these products are due to the different strategies in data editing, temporal and spatial data gap filling and instrument bias corrections [Cazenave et al., 2018a]. IPRC, JAMSTEC, and SCRIPPS are not available in the high latitudes ($|lat| > 66$) and in the marginal seas. IAP, IFREMER, ISHII, EN4, and NOAA use different techniques to extrapolate the steric estimate over these regions. In this subsection I intercompare the ARGO products and I compare them also with ORA S5. ORA S5 is an ocean reanalysis which assimilate the same *in situ* data into an ocean model.

I analyzed the annual cycle, the trends and the interannual variability for the regions of ocean where every product is available (using a mask to exclude high latitudes and marginal seas) and also for the whole ocean but this time including only the products



(a) Ocean using a a mask excluding high latitudes and without marginal seas



(b) whole ocean

Figure 4.4: Global-mean steric sea-level from ARGO

that provide global estimates.

There is a very good agreement among all products in the global-mean steric sea-level in terms of trends for the period from 2005 to 2015 of 1.01 ± 0.15 mm SLE/yr (Fig. 4.4b). Applying the ocean mask does not modify significantly this agreement in trends between products leading to 1.08 ± 0.11 mm SLE/yr (Fig. 4.4a).

Regarding the annual cycle of the steric sea-level over the masked ocean, all products show a good agreement in the amplitude of 4.49 ± 0.83 mm SLE with a phase of 80 ± 9 day of the year (doy), with the exception of IPRC estimates. IPRC steric sea-level has a larger value for the amplitude of 5.80 mm SLE and a phase shifted by +10 days (Fig. 4.4a). When considering the whole ocean, we only include the products with global coverage, leading to an amplitude of the annual cycle of 3.10 ± 0.09 mm SLE and a phase of 74 ± 21 doy instead of 4.39 ± 0.80 mm SLE and a phase of 77 ± 8 doy, using an ocean mask to remove high latitudes and marginal seas. This results suggest an important role of the high latitudes and marginal seas in the amplitude of the annual cycle. The uncertainty is 3 times larger in the global-mean estimate compared with the global-mean estimate using the ocean mask. It is puzzling to see the better agreement in the annual amplitude between global-mean compared to the mean over the masked ocean, considering the scarce data available in the masked regions. This is a point that need further investigation in the close future.

There are important differences up to 2 mm SLE in the interannual variability among the products, especially before 2009. Considering the whole ocean or using the mask do not modify significantly these differences, suggesting that ARGO products hardly resolve the interannual variability.

Based on these results, I create an ensemble with the products with a full coverage of the ocean (EN4, IAP, IFREMER, and ISHII) to be combine with the full coverage altimetry sea-level and gravimetry ocean mass.

The reanalysis ORA S5 differs considerably compare to the other products. The difference reaches 0.5 mm SLE/yr in trend, 0.22 mm SLE in amplitude of the annual cycle by and 3 mm SLE in the interannual variability (Fig. 4.4b).

4.2.3 Consistency in the sea-level budget

In this section, I compare steric from the sea-level budget (altimetry sea-level minus gravimetry ocean mass) to ARGO steric sea-level. I test different reference frame and check whether the use of a consistent reference frame improves the closure of the sea level budget. For the sea level budget in the CM frame, I use the products in the CM frame: the corrected altimetry sea-level and the GRACE ensemble of solutions 1.1 in the CM frame. While for the sea-level budget in the CF frame, I use the GRACE ensemble of solutions 1.1 and SL CCI V2.0, which is close to the CF frame (see section 4.2.1) because altimetry sea-level is not yet available in the CF frame.

Regarding the trends for the period from 2005 to 2015 (Fig. 4.5), ARGO-based steric suggests a trend of 1.01 ± 0.15 mm SLE/yr which agrees with previous published results of 1.3 ± 0.4 mm SLE/yr [Cazenave et al., 2018a], when considering a steric deep ocean

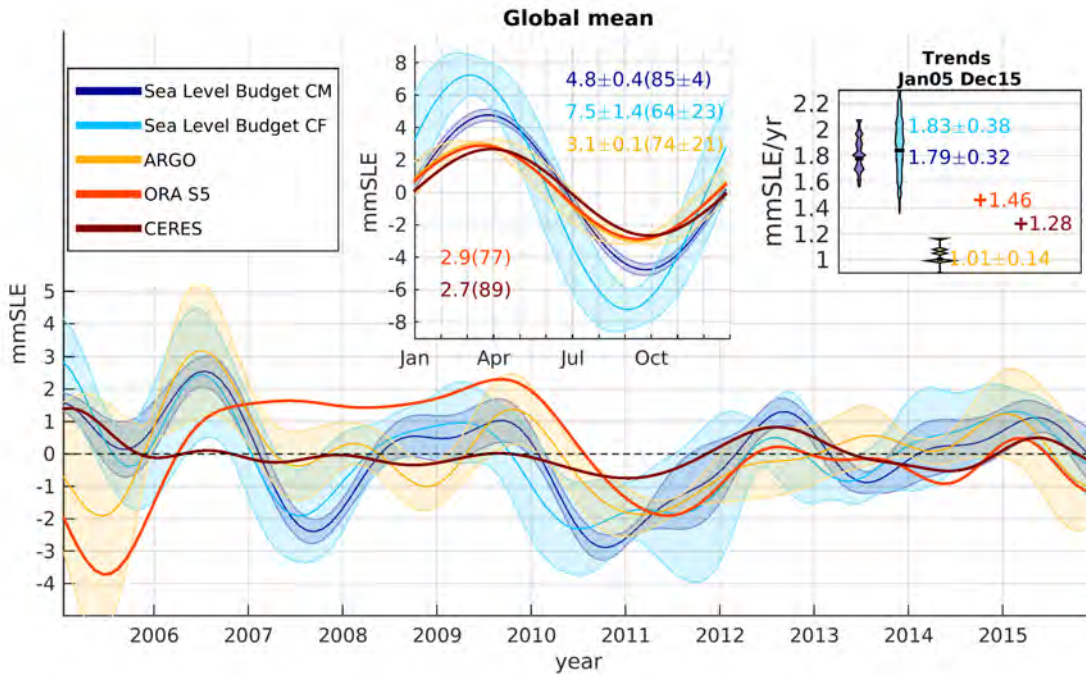


Figure 4.5: Steric sea level from sea-level budget in both frames, from ARGO, from reanalysis, and from CERES. All timeseries have been computed over the whole ocean. Note that ARGO and the reanalysis are only for the first 2000m depth

contribution of 0.15 ± 0.11 mm SLE/yr suggested by hydrographic survey [Desbruyères et al., 2016]. The steric trends computed from sea-level budget of 1.77 ± 0.32 mm SLE/yr in the **CM** frame and 1.81 ± 0.38 mm SLE/yr in the **CF** frame agree also within the uncertainties with the ARGO-based steric trend (Fig. 4.5). The change of frame present a small reduction of the trend and of the uncertainties due to the improvement of the GRACE-based ocean mass. There are important discrepancies in the interannual variability between the ARGO-based steric sea-level and both steric sea-level derived from the sea-level budget (Fig 4.5). We note the significant reduction in the uncertainty between the steric interannual variability from the **CF** frame to **CM** frame.

Regarding the annual cycle, there is no clear agreement in amplitude and phase between ARGO, the reanalysis, and steric derived from sea-level budget (Altimetry minus GRACE). This discrepancy has been recently attributed to an error in the atmospheric dealiasing model in GRACE estimates [Chen et al., 2019]. However the authors considered different masks for steric sea-level (no marginal seas), for the altimetry (no high latitudes) and for GRACE (300 or 500 km along the coasts). These different masks have an important effect of the annual cycle amplitude and phase (Fig. 4.4). So this hypothesis needs a further check.

Altimetry sea-level present large spatial variability (Fig 4.6a). Most of this spatial variability in sea level is explained by the steric sea level from the first 2000m depth (See Alti-steric in Fig. 4.6b). Correcting altimetry for steric signal estimated by ARGO leads to a residual, which is significantly more uniform (Fig. 4.6b). This is consistent to the theoretical prediction in Lorbacher et al. [2010]. Indeed deep ocean warming and

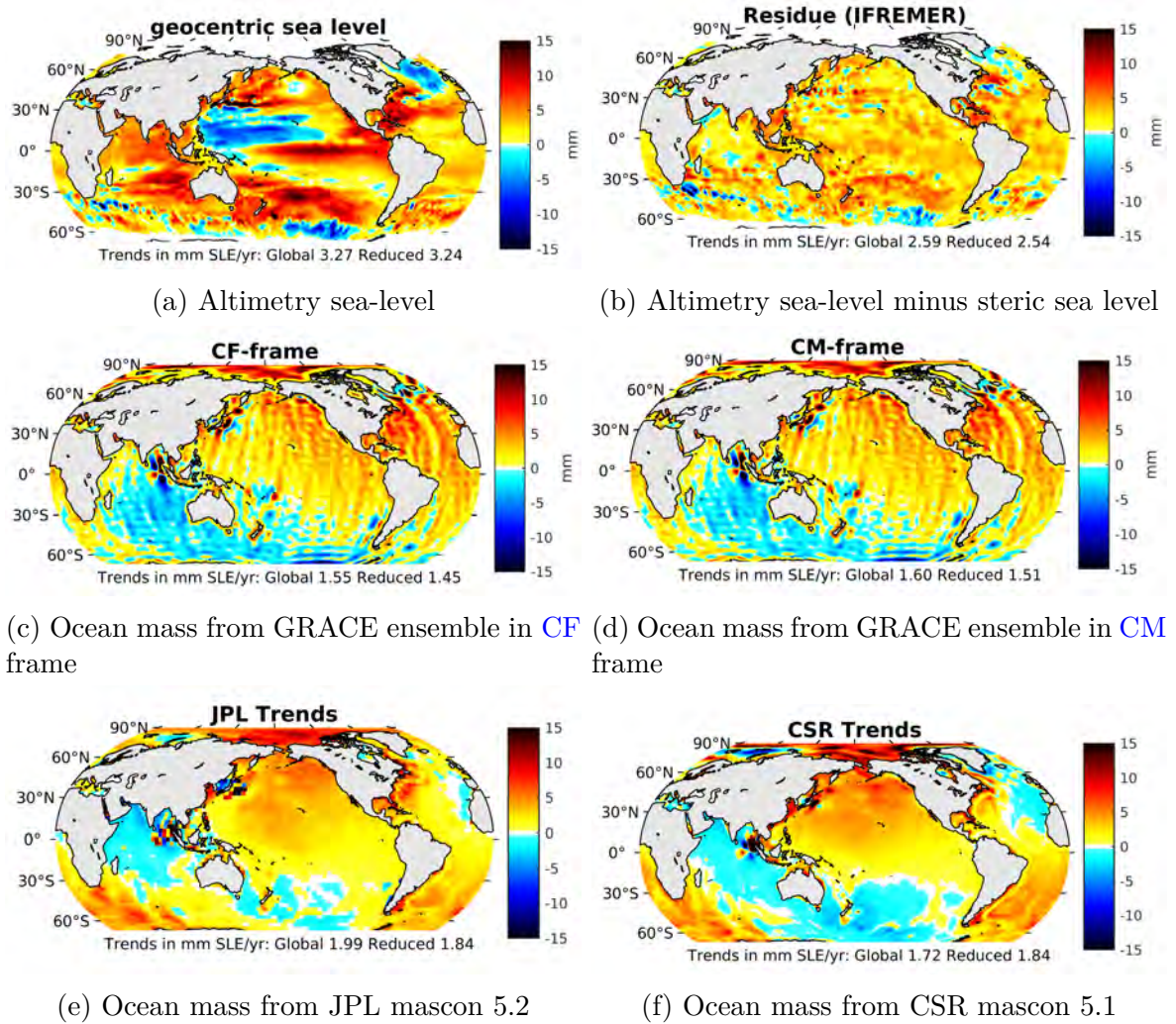


Figure 4.6: Ocean mass comparison

the barystatic sea-level are expected to have small regional variability. Note that this homogeneity is not observed in GRACE-based ocean mass in both reference frames (Fig. 4.6c,d) and it is even present in some GRACE-based mascon solutions (Fig. 4.6e,f).

This large-scale signature in GRACE signal points towards errors in the low degrees of the spherical harmonics. This discrepancy needs to be rigorously analyzed. Potential reasons for this is that we only accounted for contemporary GRD at global scale, neglecting its spatial distribution. But contemporary GRD spatial distribution is smaller than the large discrepancies between Fig. 4.6b and Fig. 4.6c-e) [Frederikse et al., 2017]. This spatial pattern could be related with the differences in global-mean trend, and explained by the differences in the pole tide correction between altimetry and gravimetry. GIA correction could also be the source of this differences as it contains an important signal C_{21}/S_{21} as it is shown in Figures (Fig. 4.6c-f).

Keeping in mind this discrepancy that is a source of errors, the deep ocean thermal expansion can be computed by removing the steric sea level for the first 2000m depth from the steric sea level computed through the sea level budget. Based on the trends computed in Fig. 4.5 and the uncertainty in ARGO-based trend of ± 0.4 mmSLE/yr [Cazenave et al.,

2018a], the deep ocean contribution is 0.76 ± 0.51 mm SLE/yr for the period from 2005 to 2015, suggesting a non negligible deep ocean heat uptake as in previous studies 0.55 ± 0.19 mm SLE/yr for the period from 2003 to 2012 [Dieng et al., 2015b]. However, this result is larger than 0.15 ± 0.11 mm SLE/yr suggested by hydrographic survey [Desbruyères et al., 2016]. Potentially the errors identified above could explain the difference with hydrographic surveys.

4.3 Implications for the EEI

In chapter 1.4, we introduced the CERES instrument which enable to estimate EEI variations. As the ocean captures 93% of the EEI, OHC is computed by integrating 93% of EEI at global scale. OHC, itself is linearly related to the global-mean steric sea-level through the expansion efficiency of heat (Eq. 1.8). So global variations in steric expansion can be estimated from CERES data presenting the advantage of a global coverage over the whole globe and the surface upto the abyssal deep ocean. These new insights in the sea-level budget are particularly accurate as the uncertainty in monthly EEI anomalies amounts $\pm 0.1 Wm^{-2}$ which is equivalent to an accuracy in steric sea-level changes of ± 0.05 mmSLE/yr [Loeb et al., 2012].

Based on this relation, I propose to compare the CERES-based estimates of the steric sea-level with ARGO-based steric sea-level and steric sea-level derived from sea-level budget (Altimetry minus grace) at seasonal and interannual scales.

The amplitude in CERES-based steric annual cycle is 2.7 ± 0.2 mm SLE and the phase is 89 ± 1 doy (Fig. 4.5), which is in agreement with ARGO and the reanalysis. However, Amplitudes computed from sea-level budget are two times (in the CM) or 3 times larger than CERES. The phase in the steric from sea level budget in the CM, of 92 ± 3 doy is in agreement with CERES-based steric annual phase. The phase of the steric from sea level budget in CF depends mainly on the geocenter motion solution used, some of them agrees with the CERES-based steric while others are 2 months shifted. This result corroborates the annual cycle in the global-mean steric from ARGO and the reanalysis pointing an error in the sea-level budget. As proposed before this result calls for more studies.

Regarding the interannual variability there was no agreement between ARGO, the reanalysis and the sea-level budget steric in Fig 4.5. I analyze the correlation with respect to CERES-based steric sea level from the different timeseries applying a 13-months filter, a 3-year filter and a 5-year filter (Table 4.1). The best correlations are found between CERES-based steric and the steric from sea-level budget, leading to values up to 0.76 ± 0.09 with altimetry minus GRACE in the CM frame and 0.65 ± 0.13 in the CF frame. Correlations with ARGO-based steric vary from small correlations (smaller than 0.1) for IAP to 0.58 for IFREMER and ISHII. This is significantly smaller than the correlation with Altimetry minus GRACE. It suggest that ARGO hardly recovers the interannual variability in global OHC unlike altimetry minus GRACE.

As for the trend, the uncertainty in CERES-based absolute EEI is about $\pm 3 Wm^{-2}$ [Meyssignac et al., 2019], which is equivalent to a steric sea-level trends of ± 1.5 mm SLE/yr. This uncertainty is too large to provide any information when compared to ARGO-based OHC or sea-level-budget based OHC.

4.4. CONCLUSIONS

Table 4.1: Correlation with respect to CERES interannual variability at different time scales after removing trend, annual and semiannual cycle. **CM** corresponds to the altimetry minus gravity in the **CM** frame, **CF** corresponds to the altimetry minus gravity in the **CF** frame, ARGO is the ensemble presented in the text

filter	CM	CF	ARGO	ORA S5
13 month	0.49 ± 0.06	0.38 ± 0.15	-0.00 ± 0.42	-0.37
3-year	0.65 ± 0.13	0.53 ± 0.16	0.06 ± 0.40	-0.48
5-year	0.75 ± 0.09	0.66 ± 0.13	0.31 ± 0.44	-0.85

ARGO-based **EEI** for the first 2000 m depth is $0.62 \pm 0.25 Wm^{-2}$. Including the deep ocean contribution from Desbruyères et al. [2016], the ARGO-based **EEI** is $0.71 \pm 0.34 Wm^{-2}$. While **EEI** inferred from the sea level budget is between $1.09 \pm 0.19 Wm^{-2}$ in the **CM**-frame and $1.11 \pm 0.23 Wm^{-2}$ in the **CF** frame.

The **EEI** from sea-level budget agrees within the errorbar with previous estimates of $0.53 \pm 0.38 m^{-2}$ for the period 2006-2015 from Meyssignac et al. [2019]. The difference between both estimated can be explained by the difference between ocean mass trend estimates [Meyssignac et al., 2019]. In Meyssignac et al. [2019], we used ocean mass based only on mascons solutions with a trend for the period from 2006 to 2016 of 2.38 ± 0.50 mm SLE/yr which is much larger than 1.55 ± 0.33 mm SLE/yr estimated for the period from 2005 to 2015 with my ensemble, although both values agrees within the uncertainties. This result highlights the need for further reduction of the uncertainty in the ocean mass.

4.4 Conclusions

The analysis of the altimetry process revealed that the present sea-level products are delivered in a frame that is close to the **CM** frame but it needs a small correction in the orbit’s computation to fully represent the altimetry in the **CM**. The effect of this correction mainly affects the sea-level annual cycle (Fig. 2.3a).

Gravimetry L2 data is already delivered in **CM** frame but with some spurious geocenter corrections can be included through the dealiasing models. A full analysis is needed to check this last point. The change of reference frame from **CM** to **CF** modifies significantly the GRACE-based ocean mass estimates and increase the uncertainties in trends from ± 0.20 mm SLE/yr to ± 0.33 mm SLE/yr, in the annual cycle amplitude from ± 0.24 mm SLE to ± 1.33 mm SLE and its phase from ± 2 days to ± 14 days.

Given the current uncertainties, the sea-level budget at global scale cannot be considered closed at ± 1 mm SLE at annual cycle (Fig 4.5). The good agreement between ARGO and CERES estimates of the steric annual signal suggests that there is an error in the altimetry sea level minus GRACE estimate of the steric annual signal. The altimetry sea-level is delivered in a daily timescale and it has been validated against tide-gauges, suggestion GRACE estimates to be responsible of this shift. Indeed we find a spread of ± 15 days among the different estimates of the ocean mass from GRACE. We suspect that the error is due to a shift in GRACE estimate of the annual phase of the ocean mass

signal. This shift in GRACE ocean mass may be a consequence of the oceanic dealiasing model for submonthly anomalies. (Scientific Question 8)

The sea level budget in terms of trends for the period from 2005 to 2015 is closed within the uncertainties at ± 0.36 mm SLE/yr. However, the discrepancies in the ocean mass at basin scale, suggest error at large scale in the ocean mass trend. (Scientific Question 9)

The good correlation between steric from sea-level budget and CERES at interannual scale gives confidence in the use of the altimetry minus grace to constrain the OHC and EEI. It allows to estimate OHC for the whole ocean including high latitudes, marginal seas and deep ocean (over 2000m depth) with a resolution of 1 degree and a timescales from monthly to multidecadal. However there are still points to be addressed as the pole tide, the GIA, the discrepancies in the spatial distribution of the ocean mass from GRACE and ocean mass from sea-level budget. (Scientific Question 11)

In this chapter, we presented the non-negligible effect of the change of the origin of the reference frame between CF and CM. We presented a consistent sea-level budget in the CM ITRF frame. However, we still need to combine the altimetry sea-level in the CF frame with GRACE ocean mass in the CF frame. The water mass transport in the Earth's surface has to be measured in the CF-centered ITRF which is fixed to the Earth's crust. In this way, we can measure the water mass transport that modifies the Earth's barycenter.

This chapter presented an on-going study, a synthesis of the results of the cooperation done in this topic with several colleagues. There are still important issues to be addressed as the origin of the differences in the annual cycles or the discrepancies in the spatial patterns. Once, these issues are solved, this work may be submit in a paper.

Chapter 5

Conclusions and outlook

We have analyzed the uncertainties in the global water budget and more specifically its closure from annual to decadal timescales using gravimetry data from GRACE. Given the spread of the state-of-the-art post-processing of GRACE data, I've developed an ensemble of GRACE solution to estimate the uncertainties in the global water budget. This approach enables the exploration of the sources of these uncertainties and at the same time it points to the research directions that should be followed to reduce these uncertainties. Here are a few of these research directives I would like to explore in the near future.

Reducing the uncertainties in GRACE-based estimates of the global water budget

With the GRACE ensemble, I have been able to estimate the mass changes and its associated uncertainties in Greenland, Antarctica, the ocean mass and the rest of the emerged lands including glaciers and TWS. Analysing the sources of these uncertainties, I find that post-processing is responsible of 79% of the uncertainty in the global water budget estimates and only 21% is due to the differences by the different processing centers (Chapter 2).

The main sources of uncertainties at annual to interannual time scales comes from the spread in the geocenter corrections and the uncertainty in GIA correction, in particular for the ocean mass and the sum of glacier and TWS mass change. Both, the ocean mass the sum of glacier and TWS show the highest level of uncertainty in trends of ± 0.33 mm SLE/yr. These uncertainties are highly correlated because it is caused by the same post-processing parameters (Chapter 2).

The consistency analysis with the altimetry-based sea level, ARGO-based steric sea-level and CERES-based OHC, highlighted the importance of the geocenter motion in the closure of the sea level budget and in the EEI estimate. These results call for more research to improve consistently the altimetry-based sea-level and the GRACE post processing in gravimetry-based ocean mass to improve the closure of the sea-level budget and get more accurate estimates of the EEI (Chapter 4). This analysis based on the comparison with independent data from ARGO and CERES also provides independent test to evaluate the geocenter motion estimates or the GIA correction used to correct GRACE data.

The second main source of uncertainty is the spread in **GIA** models. More specifically, the spread in the 2nd degree, including the trends in Earth’s oblateness (C_{20}) and the pole tide (C_{21}/S_{21}) as presented in chapter 2. This spread in the 2nd degree is responsible for large differences in the global water budget at regional scale. Further work is needed to explain such discrepancies.

With the launch of GRACE FO (June 2018), gravimetry has reached an operational status. L2 and L3 products are delivered two times per month and most of center are engaged in operational products. At the same time, all centers have delivered updates products reducing the uncertainties due to the inversion process. Note that with the previous releases, the differences within the processing centers were the third main source of uncertainty being responsible of 21% of the uncertainty in the ocean mass trend for the period from 2005 to 2015 (see Table 2.2).

GRACE mascon solutions have proven in the last years to be of great interest to resolve local mass variations. It is now a mature method to reduce land/ocean leakage and land/land leakage. In the close future, it would be interesting to develop an ensemble of mascon solutions focused on the water cycle analysis and climatic studies. This mascon solution could be based on the GRACE L2 spherical harmonics solutions for the low degrees (around 30th degree) to ensure the large scale mass conservation (which is essential in the global water cycle analysis and climate studies). We could incorporate independent constraints during the inversion process as glaciers or lake mass changes, land/ocean grid points. Similar approach with an individual GRACE solution has already provided accurate results in cryospheric studies using GRACE and **ICESat** [e.g., Sasgen et al., 2018].

Characterizing changes in GRACE-based TWS estimates

Based on the results of the Chapter 3, I plan to generalize the land leakage correction at global scale, including the use of 156 available lake volume changes from Hydroweb, South America glacier mass change [Dussaillant et al., 2019], and the future global glacier mass change estimated from multi-temporal-imagery digital elevation models derived from satellite imagery (on going Hugonnet’s PhD and SATELLITE project). This analysis will allow to accurately estimate **TWS** mass changes at global scale and separate its contribution to the global water budget from the contribution from glaciers.

Once retrieved from the GRACE gravimetry field, the solid-Earth changes and the water mass changes, the residual fields may be used to infer the state of the Earth’s interior and its evolution [Mandea et al., 2015]. Preliminary results were presented at AGU fall meeting 2018 [Mandea et al., 2018]. This magnetic signal is at very large spatial scale (continental) and it is base on theory and models.

Which constraints can observations bring to climate models?

Observations and historical runs from climate models have reached an unprecedented maturity in the past years, leading to a great numbers of analysis in different components of the Earth system as global-mean thermosteric sea-level changes [Melet and Meyssignac, 2015], **TWS** mass trends [e.g., Fasullo et al., 2016a], glacier mass change [Marzeion et al., 2017], Greenland mass balance [e.g., Meyssignac et al., 2016], etc. Observations are used

to constraint historical runs while models allow to analyze the causes of the variation in the global water budget. The anthropogenic origin of these variations can be further studied using simulations with different forcing.

I plan to analyze the global water cycle confronting GRACE-based mass exchanges and climate models. I performed some preliminary studies with the IPSL climate model runs during the year 2017. During this period, I have analyzed the closure of the water mass budget in the IPSL climate model runs (Ocean, Sea Ice, Surface, Land Ice and Atmosphere) comparing all water fluxes and stocks. I identified errors in the climate model. In particular I found leakage of mass at the interface of the ocean model and the sea ice models. I participated in the effort to reduce these errors and we manage to close the water budget in the model at the level of 0.14 mm/yr in CM610 to 0.07 mm/yr in CM612 (Fig. 5.1). This is enough to start comparison with observations.

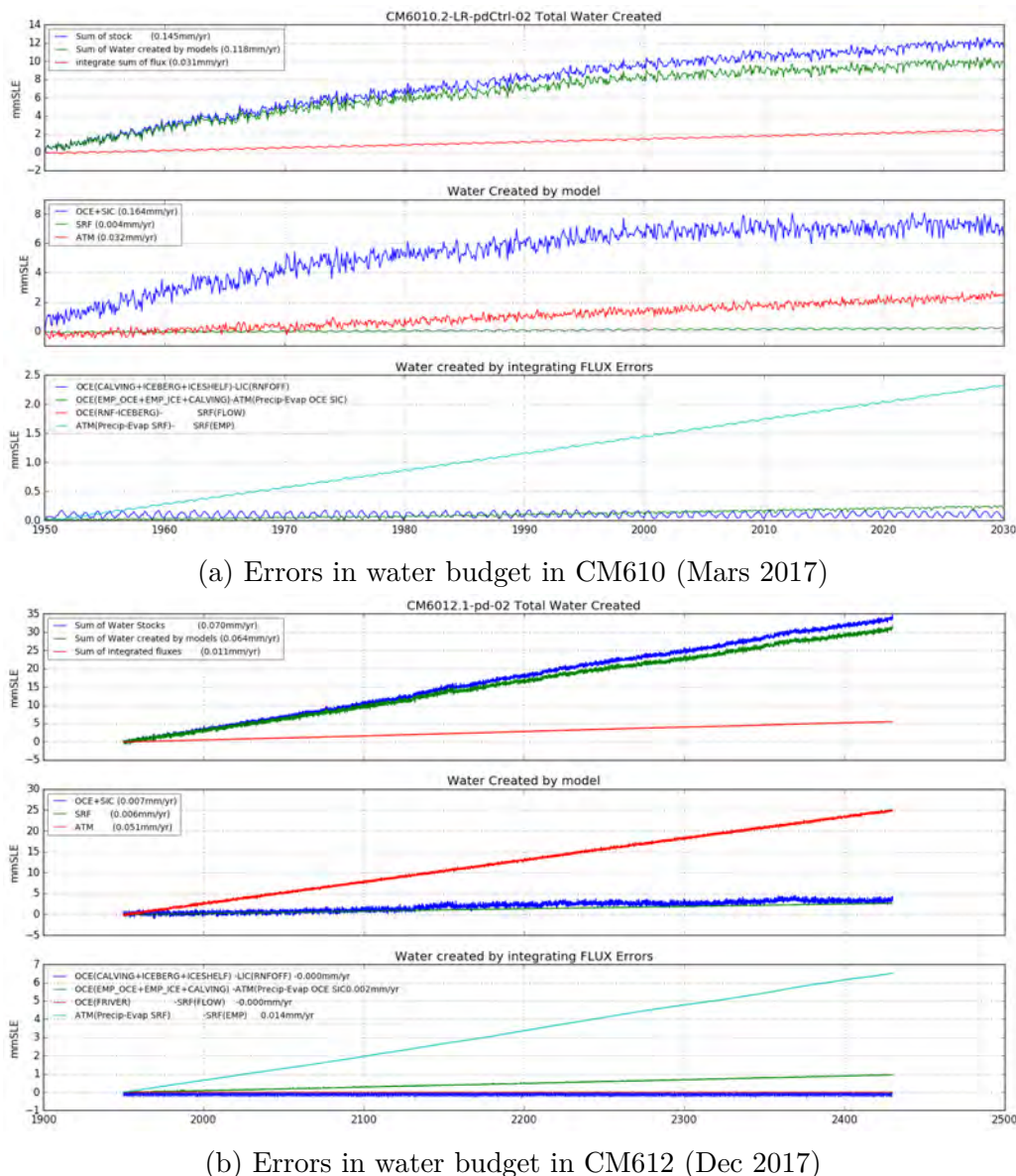


Figure 5.1: Water mass conservation in the ISPL climate models based on flux integration and stocks analysis. Analysis done in 2017.

These preliminary results were encouraging, I plan in the future to pursue this analyze with the CMIP6 models which close the water budget at least ten times better than GRACE-based water budget estimates (± 0.27 mm/yr from [Blazquez et al., 2018]).

Which constraints can geodetic techniques bring to **EEI** estimates?

As presented in the foreword, **EEI** is the key parameter to characterize the climate change. An accuracy in the absolute **EEI** of ± 0.1 Wm^{-2} is needed to monitor the **EEI** response to Greenhouse gases mitigation policies in the future [Meyssignac et al., 2019]. The uncertainty in CERES-based **EEI** is ± 3 Wm^{-2} [Meyssignac et al., 2019] and in ARGO-based **EEI** ± 0.25 Wm^{-2} for the first 2000m depth and ± 0.34 Wm^{-2} for the whole depth (Chapter 4). Based on the sea-level budget, I estimated an uncertainty in absolute **EEI** of ± 0.19 Wm^{-2} , which is still 2 times larger than the accuracy required to monitor the response to Greenhouse gases mitigation policies. But the sea-level budget approach to estimate **EEI** has the advantage of including a full depth estimate with a global coverage and at monthly basis.

When CERES-based **EEI** is converted in steric sea-level, its interannual variability correlates better with sea-level-budget based steric sea level than ARGO-based steric sea-level (Table 4.1). It suggests a non negligible influence of the deep ocean or the regions not covered by ARGO as in high latitudes, in marginal seas, and in ice-covered regions in the interannual **EEI** variability. However, there are still open issues in the sea level budget based **EEI** to correct as the annual cycle or the spatial distribution of GRACE-based ocean mass. (Chapter 4). In the future I intend to analyze further the sea-level budget approach to estimate **EEI** and try to solve this issues.

How to improve time-variable gravity observations in the next "gravimetry" missions?

GRACE mission was developed as a demonstrator to monitor the mass changes at seasonal scales. After almost 15 years, the mission demonstrates the importance of a time variable gravity monitoring. **GRACE FO** was launched with the same plateforme and instruments to ensure the continuity of the observations. The only new instrument onboard **GRACE FO** compare to **GRACE** is a laser to measure the intersatellite range and range rate with higher accuracy than the **KBR** interferometer. Although the laser improved the accuracy of the intersatellite range and range data, **GRACE FO** spatiotemporal resolution is similar to **GRACE**.

At this moment, several agencies are preparing the next gravimetry missions. On the american side, **NASA**'s Decadal Survey for Earth Science and Applications from Space for 2017-2027 has included mass change as a designated observable. In December 2019, the scientific community has finalized the Scientific and Applications Traceability Matrix

(SATM) ¹. On the european side, [European Space Agency \(ESA\)](#) is studying the Next Generation Gravity mission (NGGM) and [CNES](#) has started the phase 0 for the [Mass And Reference Variations for Earth Lookout \(MARVEL\)](#) mission.

I'm part of the scientific team which proposes this new concept MARVEL. In the near future, I intend to participate to this mission as coI and provide requirements for the technical team so that they can find a technological concept which allows the retrieval of the gravity field with higher spatiotemporal resolution so that I can improve in the future the estimates of the contributions to the global water budget.

¹https://science.nasa.gov/files/science-red/s3fs-public/atoms/files/MCDO_SATM_PublicRelease.pdf

Chapter 6

[FR] Conclusions and perspectives

Nous avons analysé les incertitudes dans le bilan global de l'eau et plus particulièrement dans sa fermeture aux échelles annuelles et décennales en utilisant les données gravimétriques de la mission [GRACE](#) lancée en 2002. Compte tenu de l'écart entre les différents post-traitements de données les plus à jour, nous avons développé un nouvel ensemble de solutions afin d'estimer les incertitudes du bilan global de l'eau. Cette approche permet d'explorer leurs origines, tout en indiquant les axes de recherche à suivre pour obtenir à terme des estimations plus précises. Voici quelques unes de ces directions de recherche que j'aimerais explorer en continuation de ce travail de thèse.

Réduire les incertitudes sur le bilan global de l'eau

Nous avons estimé, avec l'ensemble des solutions GRACE, les changements de masse ainsi que leur incertitudes au Groenland, en Antarctique, sur l'océan et sur les autres terres émergées y compris les glaciers et les eaux continentales. En analysant les sources d'incertitude, nous avons trouvé que le post-traitement est responsable de 79 % de l'incertitude dans les estimations du bilan global de l'eau et seulement 21 % est dû aux différences entre les solutions des centres de traitement ([Chapitre 2](#)).

Les principales sources d'incertitudes, aux échelles de temps annuelles à interannuelles, proviennent de l'incertitude dans les corrections du géocentre et du rebond post-glaciaire, en particulier pour l'estimation de la masse de l'océan et de la somme des changements de masse des glaciers et des eaux continentales. Leurs incertitudes sont les plus élevées dans la tendance globale de ± 0.33 mm SLE/an; elles sont fortement corrélées car elles sont causées par les mêmes paramètres de post-traitement ([Chapitre 2](#)).

L'analyse de la consistence entre les estimations du niveau de la mer basé sur l'altimétrie, du niveau de la mer stérique basé sur ARGO et du contenu en chaleur de l'océan ([OHC](#)) basé sur CERES, a souligné l'importance de la correction du mouvement du géocentre, ce au niveau de la clôture du bilan du niveau de la mer ainsi que dans les estimations du déséquilibre énergétique de la terre ([EEI](#)). Ces résultats appellent davantage de travaux de recherche dans le but d'améliorer, de manière consistente, le niveau de la mer basé sur l'altimétrie et la masse de l'océan basée sur la gravimétrie; l'objectif est d'aboutir à une meilleure fermeture du bilan du niveau de la mer ainsi qu'à une estimation plus précise du déséquilibre énergétique de la Terre ([Chapitre 4](#)). Cette analyse basée sur la comparaison avec des données indépendantes d'ARGO et de CERES fournit également un test

indépendant pour évaluer les corrections de mouvement du géocentre et du rebond post glaciaire, toutes deux utilisées pour corriger les données GRACE.

La deuxième source d'incertitude provient des écarts entre les différents modèles de rebond post glaciaire. Plus précisément, les écarts dans le degré 2, y compris les tendances de l'aplatissement de la Terre (C_{20}) et de la marée polaire (C_{21}/S_{21}) présentées dans le chapitre 2. Ces écarts sur le degré 2 sont responsables de grandes différences dans l'estimation du bilan global de l'eau à l'échelle régionale. Des travaux supplémentaires sont donc nécessaires afin d'expliquer tout cela.

Avec le lancement de GRACE FO (juin 2018), la gravimétrie spatiale a atteint un niveau opérationnel. Les produits L2 et L3 sont livrés deux fois par mois et la plupart des centres d'analyse des données sont engagés dans des produits opérationnels. Dans le même temps, tous les centres ont livré des mises à jour de leur solutions réduisant les incertitudes dues au processus d'inversion mais avec des nouvelles problématiques. Il convient de noter qu'avec les versions précédentes, les différences de solution entre les centres de traitement étaient la troisième source d'incertitude, au niveau de 21 % de l'incertitude sur la tendance de la masse de l'océan pour la période de 2005 à 2015 (voir le tableau 2.2).

Ces dernières années, les solutions de type mascon se sont avérées d'un grand intérêt afin de résoudre les variations locales de masse; c'est désormais une méthode mature pour réduire les fuites terre/océan et les fuites terre/terre. Dans un futur proche, il sera intéressant de développer un ensemble de solutions de type mascon axées sur l'analyse du cycle global de l'eau et donc les études climatiques. Cette solution en mascon pourrait être basée sur les solutions d'harmoniques sphériques GRACE L2 pour les faibles degrés (jusqu'au degré 30), afin d'assurer la conservation de masse à grande échelle; ce qui est essentiel dans l'analyse du cycle global de l'eau et les études climatiques. Nous pourrions incorporer des contraintes indépendantes pendant le processus d'inversion comme les glaciers ou les changements de masse des lacs et les points de grille terre/océan. Une approche similaire avec une solution GRACE a déjà fourni des résultats précis dans les études cryosphériques utilisant GRACE et ICESat [e.g., Sasgen et al., 2018].

Caractérisation des estimations de changement de masse dans les eaux continentales

Sur la base des résultats du chapitre 3, j'envisage de généraliser la correction des fuites au niveau des terres à l'échelle mondiale, avec l'utilisation de 156 changements de volume de lac disponibles à partir d'Hydroweb, le changement de masse des glaciers de l'Amérique du Sud [Dussaillant et al., 2019], et le produit, encore en développement, des changements de masse des glaciers à l'échelle globale estimée à partir de modèles d'élévation numériques dérivés de l'imagerie satellite multi-temporelle (thèse en cours de Hugonnet). Cette analyse permettra d'estimer avec précision les changements de masse des eaux continentales, à l'échelle mondiale, et de séparer sa contribution au bilan global de l'eau de celle des glaciers.

Les solutions de champ de gravité issues de GRACE corrigées des changements dans la Terre solide et des changements de masse d'eau, peuvent être utilisées pour en déduire l'état de l'intérieur de la Terre et de son évolution [Mandea et al., 2015]. Ce signal

magnétique peut devenir une correction pour les champs de masse d'eau basés sur GRACE; l'influence sur le bilan du niveau de la mer n'est pas encore quantifiée. Les résultats préliminaires ont été présentés lors de la réunion d'automne de l'AGU 2018 [Mandea et al., 2018].

Quelles contraintes peuvent apporter les observations aux modèles climatiques?

Les observations et les réalisations historiques des modèles de climat ont atteint une maturité sans précédent au cours des dernières années, conduisant à un grand nombre d'analyses dans différentes composantes du système terrestre comme par exemples: les changements thermostériques du niveau de la mer [Melet and Meyssignac, 2015], les changements de masse dans les eaux continentales [e.g., Fasullo et al., 2016a], le changement de masse des glaciers [Marzeion et al., 2017], bilan de masse du Groenland [e.g., Meyssignac et al., 2016], etc. Les observations sont utilisées afin de contraindre les réalisations historiques, tandis que les modèles permettent d'analyser les causes de la variation bilan global de l'eau. L'origine anthropique de ces variations peut être étudiée en utilisant des simulations avec différents forçages.

J'envisage d'analyser le cycle global de l'eau par comparaison des échanges de masse entre les modèles de climat et les observations basées sur GRACE. En 2017, j'ai effectué une étude préliminaire à partir du modèle climatique IPSL(océan, glace de mer, surface, glace terrestre et atmosphère). Pendant cette période, j'ai analysé la fermeture du bilan de masse d'eau dans plusieurs réalisations du modèle climatique IPSL en comparant tous les flux et tous les stocks d'eau. J'ai identifié des erreurs dans le modèle de climat. En particulier, j'ai trouvé une fuite de masse à l'interface du modèle océanique et des modèles de glace de mer. J'ai participé à l'effort de réduction de ces erreurs et nous sommes parvenus à clore le bilan global d'eau du modèle au niveau de 0,14 mm/yr en CM610 à 0,07 mm/yr en CM612 (Fig. 5.1).

Ces résultats préliminaires étant encourageants, je prévois à l'avenir de poursuivre cette analyse avec les modèles CMIP6 qui closent le bilan hydrique au moins dix fois mieux que les estimations du bilan global de l'eau basées sur GRACE (± 0.27 mm/yr à partir de Blazquez et al. [2018]).

Quelles contraintes peuvent apporter les techniques géodésiques aux estimations du déséquilibre énergétique de la Terre EEI?

Comme présenté dans la préface, le déséquilibre énergétique de la terre (EEI) est le paramètre clé pour caractériser le changement climatique. Une précision absolue de $\pm 0.1 \text{ Wm}^{-2}$ est nécessaire pour surveiller la réponse du déséquilibre énergétique de la terre aux politiques futures d'atténuation des gaz à effet de serre [Meyssignac et al., 2019]. L'incertitude dans EEI basée sur CERES est $\pm 3 \text{ Wm}^{-2}$ [Meyssignac et al., 2019] et dans EEI basée sur ARGO $\pm 0.25 \text{ Wm}^{-2}$ pour les premiers 2000 m de profondeur et de $\pm 0.34 \text{ Wm}^{-2}$ pour toute la profondeur (chapitre 4). Sur la base du bilan du niveau de la mer, j'ai estimé l'incertitude absolu du déséquilibre énergétique de la terre à $\pm 0.19 \text{ Wm}^{-2}$, ce qui est toujours 2 fois plus grand que la précision requise pour surveiller la réponse aux politiques d'atténuation des gaz à effet de serre. Mais l'approche du bilan du niveau de la

mer pour estimer [EEI](#) à l'avantage d'inclure une estimation complète en profondeur avec une couverture mensuelle globale.

Lorsque le déséquilibre énergétique de la terre basé sur CERES est converti en niveau stérique, sa variabilité interannuelle est mieux corrélée avec le niveau stérique de la mer basé sur le bilan du niveau de la mer que le niveau stérique de la mer basé sur ARGO (Tableau 4.1). Cela suggère une influence non négligeable des océans profonds ou des régions non couvertes par ARGO, comme les hautes latitudes, les mers marginales et les régions couvertes de glace, dans l'estimation de la variabilité interannuelle du déséquilibre énergétique de la terre. Cependant, il y a encore des problèmes à corriger dans le déséquilibre énergétique de la terre basé sur le bilan du niveau de la mer comme le déphasage du cycle annuel ou la distribution spatiale de la masse de l'océan basée sur GRACE (Chapitre 4).

À l'avenir, j'envisage d'analyser en détail l'approche du bilan du niveau de la mer afin d'estimer le déséquilibre énergétique de la terre et tenter de résoudre ces problèmes.

Comment améliorer les observations de la gravité pour les prochaines missions spatiales?

La mission [GRACE](#) a été développée comme un démonstrateur pour surveiller les changements de masse à des échelles saisonnières. Après près de 15 ans, la mission a démontré l'importance d'une surveillance des variations temporelles de la gravité. [GRACE FO](#) a été lancé avec la même plateforme et les mêmes instruments pour assurer la continuité des observations. Le seul nouvel instrument embarqué sur [GRACE FO](#) qui n'était pas [GRACE](#) est un laser pour mesurer la distance entre les satellites et la variations de cette distance avec une précision plus élevée que l'interféromètre [KBR](#). Bien que le laser ait amélioré la précision de la distance entre les satellites, la résolution spatio-temporelle de [GRACE FO](#) est similaire à celle de [GRACE](#).

En ce moment, plusieurs agences spatiales préparent les prochaines missions de gravimétrie. Du côté américain, le *Decadal Survey for Earth Science and Applications from Space for 2017-2027* de la [NASA](#) a inclus le changement de masse comme observable principale. En décembre 2019, la communauté scientifique a finalisé la matrice de traçabilité scientifique et d'applications (SATM en anglais)¹. Du côté européen, l'[ESA](#) étudie la mission gravitationnelle de prochaine génération (NGGM en anglais) et le [CNES](#) a commencé la phase 0 de la mission [gls marvel](#).

Je fais partie de l'équipe scientifique qui propose ce nouveau concept [MARVEL](#). Dans un avenir proche, j'ai l'intention de participer à cette mission en tant que CoI et de fournir des exigences à l'équipe technique afin qu'elle puisse trouver un concept technologique qui permettra la récupération du champ de gravité avec une résolution spatio-temporelle plus élevée afin que l'on puisse améliorer à l'avenir la estimations des contributions au budget mondial de l'eau.

¹https://science.nasa.gov/files/science-red/s3fs-public/atoms/files/MCDO_SATM_PublicRelease.pdf

Bibliography

- A, G., Wahr, J., and Zhong, S. (2013). Computations of the viscoelastic response of a 3-D compressible Earth to surface loading: an application to Glacial Isostatic Adjustment in Antarctica and Canada. *Geophysical Journal International*, 192(2):557–572.
- Ablain, M., Cazenave, A., Larnicol, G., Balmaseda, M., Cipollini, P., Faugère, Y., Fernandes, M. J., Henry, O., Johannessen, J. A., Knudsen, P., Andersen, O., Legeais, J., Meyssignac, B., Picot, N., Roca, M., Rudenko, S., Scharffenberg, M. G., Stammer, D., Timms, G., and Benveniste, J. (2015). Improved sea level record over the satellite altimetry era (1993–2010) from the Climate Change Initiative project. *Ocean Sci.*, 11(1):67–82.
- Ablain, M., Jugier, R., Zawadzki, L., and Picot, N. (2018). Estimating any altimeter GMSL drifts between 1993 and 2018 by comparison with Tide Gauges.
- Ablain, M., Legeais, J. F., Prandi, P., Marcos, M., Fenoglio-Marc, L., Dieng, H. B., Benveniste, J., and Cazenave, A. (2017). Satellite Altimetry-Based Sea Level at Global and Regional Scales. In Cazenave, A., Champollion, N., Paul, F., and Benveniste, J., editors, *Integrative Study of the Mean Sea Level and Its Components*, Space Sciences Series of ISSI, pages 9–33. Springer International Publishing, Cham.
- Ablain, M., Meyssignac, B., Zawadzki, L., Jugier, R., Ribes, A., Spada, G., Benveniste, J., Cazenave, A., and Picot, N. (2019). Uncertainty in satellite estimates of global mean sea-level changes, trend and acceleration. *Earth System Science Data*, 11(3):1189–1202.
- Asoka, A., Gleeson, T., Wada, Y., and Mishra, V. (2017). Relative contribution of monsoon precipitation and pumping to changes in groundwater storage in India. *Nature Geoscience*, 10(2):109–117.
- Babel, M. and Wahid, S. (2008). Freshwater Under Threat South Asia: Vulnerability Assessment of Freshwater Resources to Environmental Change.
- Balmaseda, M. A., Mogensén, K., and Weaver, A. T. (2013). Evaluation of the ECMWF ocean reanalysis system ORAS4. *Quarterly Journal of the Royal Meteorological Society*, 139(674):1132–1161.
- Bamber, J. L., Oppenheimer, M., Kopp, R. E., Aspinall, W. P., and Cooke, R. M. (2019). Ice sheet contributions to future sea-level rise from structured expert judgment. *Proceedings of the National Academy of Sciences*, 116(23):11195–11200.
- Bamber, J. L., Westaway, R. M., Marzeion, B., and Wouters, B. (2018). The land ice contribution to sea level during the satellite era. *Environmental Research Letters*, 13(6):063008.
- Bandikova, T., McCullough, C., Kruijzinga, G. L., Save, H., and Christophe, B. (2019). GRACE Accelerometer Data Transplant. *Advances in Space Research*.
- Berthier, E., Cabot, V., Vincent, C., and Six, D. (2016). Decadal Region-Wide and Glacier-Wide Mass Balances Derived from Multi-Temporal ASTER Satellite Digital Elevation Models. Validation over the Mont-Blanc Area. In *Front. Earth Sci.*

- Biancamaria, S., Cazenave, A., Mognard, N. M., Llovel, W., and Frappart, F. (2011). Satellite-based high latitude snow volume trend, variability and contribution to sea level over 1989/2006. *Global and Planetary Change*, 75(3):99–107.
- Blazquez, A., Berthier, E., and Papa, F. (2020). Monitoring the changes in terrestrial water storage in South Asia for the period 2003-2015. *Submit to HESS*.
- Blazquez, A., Meyssignac, B., Lemoine, J. M., Berthier, E., Ribes, A., and Cazenave, A. (2018). Exploring the uncertainty in GRACE estimates of the mass redistributions at the Earth surface: implications for the global water and sea level budgets. *Geophysical Journal International*, 215(1):415–430.
- Bourgogne, S. (2019). Etude de l’influence du centrage des orbites GNSS sur la restitution du champ de gravité. Technical report, Stellar Space Studies, Toulouse.
- Brun, F., Berthier, E., Wagnon, P., Kääb, A., and Treichler, D. (2017). A spatially resolved estimate of High Mountain Asia glacier mass balances from 2000 to 2016. *Nature Geoscience*, 10(9):668–673.
- Caron, L., Ivins E. R., Larour E., Adhikari S., Nilsson J., and Blewitt G. (2018). GIA Model Statistics for GRACE Hydrology, Cryosphere, and Ocean Science. *Geophysical Research Letters*, 45(5):2203–2212.
- Carret, A., Johannessen, J. A., Andersen, O. B., Ablain, M., Prandi, P., Blazquez, A., and Cazenave, A. (2017). Arctic Sea Level During the Satellite Altimetry Era. *Surveys in Geophysics*, 38(1):251–275.
- Catling, D. C. and Zahnle, K. J. (2009). The Planetary Air Leak. *Scientific American*, 300(5):36–43.
- Cazenave, A., Dieng, H.-B., Meyssignac, B., von Schuckmann, K., Decharme, B., and Berthier, E. (2014). The rate of sea-level rise. *Nature Climate Change*, 4(5):358–361.
- Cazenave, A., Meyssignac, B., Ablain, M., Balmaseda, M., Bamber, J., Barletta, V. R., Beckley, B., Benveniste, J., Berthier, E., Blazquez, A., Boyer, T., Caceres, D., Chambers, D., Champollion, N., Chao, B., Chen, J. L., Cheng, L., Church, J. A., Chuter, S., Cogley, G., Dangendorf, S., Desbruyères, D. G., Doll, P., Domingues, C. M., Falk, U., Famiglietti, J., Fenoglio-Marc, L., Galassi, G., Gardner, A., Groh, A., Hamlington, B., Hogg, A., Horwath, M., Humphrey, V., Husson, L., Ishii, M., Jaeggi, Jevrejeva, S., Johnson, G. C., Kolodziejczyk, Kusche, J., Lambeck, K., Landerer, F. W., Leclercq, P., Legrésy, B., Leuliette, E., Llovel, W., Longuevergne, L., Loomis, B. D., Luthcke, S., Marcos, M., Marzeion, B., Merchant, C. J., Merrifield, M. A., Milne, G., Mitchum, G. T., Mohajeani, Monier, Monselesan, D., Nerem, Palanisamy, H., Paul, F., Perez, B., Picuch, C. G., Ponte, R. M., Purkey, S. G., Reager, J. T., Rietbroek, R., Rignot, E., Riva, R., Roemmich, Sorensen, L. S., Sasgen, I., Schrama, Seneviratne, S., Shum, C. K., Spada, G., Stammer, D., Van De Wal, R., Velicogna, I., von Schuckmann, K., Wada, Y., Wang, J., Watson, C., Wiese, D. N., Wijffels, S., Westaway, R. M., Wopelmann, G., and Wouters, B. (2018a). Global sea-level budget 1993–present. *Earth System Science Data*, 10(3):1551–1590.
- Cazenave, A., Palanisamy, H., and Ablain, M. (2018b). Contemporary sea level changes from satellite altimetry: What have we learned? What are the new challenges? *Advances in Space Research*, 62(7):1639–1653.
- Chambers, D. (2006a). Evaluation of new GRACE time-variable gravity data over the ocean. *Geophysical Research Letters*, 33(17).
- Chambers, D. (2006b). Observing seasonal steric sea level variations with GRACE and satellite altimetry. *Journal of Geophysical Research: Oceans*, 111(C3):C03010.

BIBLIOGRAPHY

- Chambers, D., Tamisiea, M. E., Nerem, R. S., and Ries, J. C. (2007). Effects of ice melting on GRACE observations of ocean mass trends. *Geophysical Research Letters*, 34(5):L05610.
- Chambers, D., Wahr, J., and Nerem, R. S. (2004). Preliminary observations of global ocean mass variations with GRACE. *Geophysical Research Letters*, 31:L13310.
- Chambers, D. P. and Bonin, J. A. (2012). Evaluation of Release-05 GRACE time-variable gravity coefficients over the ocean. *Ocean Sci.*, 8(5):859–868.
- Chambers, D. P., Cazenave, A., Champollion, N., Dieng, H., Llovel, W., Forsberg, R., Schuckmann, K. v., and Wada, Y. (2017). Evaluation of the Global Mean Sea Level Budget between 1993 and 2014. *Surveys in Geophysics*, 38(1):309–327.
- Chen, J., Li, J., Zhang, Z., and Ni, S. (2014). Long-term groundwater variations in Northwest India from satellite gravity measurements. *Global and Planetary Change*, 116:130–138.
- Chen, J., Tapley, B., Save, H., Tamisiea, M. E., Bettadpur, S., and Ries, J. (2018). Quantification of Ocean Mass Change Using Gravity Recovery and Climate Experiment, Satellite Altimeter, and Argo Floats Observations. *Journal of Geophysical Research: Solid Earth*, 123(11):10,212–10,225.
- Chen, J., Tapley, B., Seo, K.-W., Wilson, C., and Ries, J. (2019). Improved quantification of global mean ocean mass change using GRACE satellite gravimetry measurements. *Geophysical Research Letters*, n/a(n/a).
- Chen, J., Wilson, C. R., Li, J., and Zhang, Z. (2015). Reducing leakage error in GRACE-observed long-term ice mass change: a case study in West Antarctica. *Journal of Geodesy*, 89(9):925–940.
- Chen, J. L., Wilson, C. R., and Tapley, B. D. (2013). Contribution of ice sheet and mountain glacier melt to recent sea level rise. *Nature Geoscience*, 6(7):549–552. WOS:000321002700017.
- Chen, J. L., Wilson, C. R., Tapley, B. D., and Grand, S. (2007). GRACE detects coseismic and postseismic deformation from the Sumatra-Andaman earthquake. *Geophysical Research Letters*, 34(13):L13302.
- Cheng, M. and Ries, J. (2017). The unexpected signal in GRACE estimates of C20. *Journal of Geodesy*, 91(8):897–914.
- Cheng, M., Tapley, B. D., and Ries, J. C. (2013a). Deceleration in the Earth’s oblateness. *Journal of Geophysical Research: Solid Earth*, 118(2):740–747.
- Cheng, M. K., Ries, J. C., and Tapley, B. D. (2013b). Geocenter Variations from Analysis of SLR Data. In Altamimi, Z. and Collilieux, X., editors, *Reference Frames for Applications in Geosciences*, number 138 in International Association of Geodesy Symposia, pages 19–25. Springer Berlin Heidelberg.
- Christophe, B. (2018). GRACEFO accelerometers behavior after 4 months in orbit.
- Church, J., P.U. Clark, A. Cazenave, J.M. Gregory, S. Jevrejeva, A. Levermann, M.A. Merrifield, G.A. Milne, R.S. Nerem, P.D. Nunn, A.J. Payne, W.T. Pfeffer, D. Stammer, and A.S. Unnikrishnan (2013). Sea Level Change. In *Climate Change 2013. The Physical Science Basis. Contribution of Working Group I to the Fifth Assessment Report of the Intergovernmental Panel on Climate Change*[Stocker, T.F., D. Qin, G.-K. Plattner, M. Tignor, S.K. Allen, J. Boschung, A. Nauels, Y. Xia, V. Bex and P.M. Midgley (eds.)]. Cambridge University Press, Cambridge, United Kingdom and New York, NY, USA.

- Cogley, J. (2009). A more complete version of the World Glacier Inventory. *Annals of Glaciology*, 50(53):32–38.
- Cogley, J. G., Arendt, A., Bauder, A., Braithwaite, R. J., Hock, R., Jansson, P., Kaser, G., Möller, M., Nicholson, L., Rasmussen, L. A., and Zemp, M. (2010). Glossary of glacier mass balance and related terms.
- Couhert, A., Mercier, F., Moyard, J., and Biancale, R. (2018). Systematic Error Mitigation in DORIS-Derived Geocenter Motion. *Journal of Geophysical Research: Solid Earth*, 123(11):10,142–10,161.
- Cretaux, J.-F., Abarca-del Río, R., Berge-Nguyen, M., Arsen, A., Drolon, V., Clos, G., and Maisongrande, P. (2016). Lake Volume Monitoring from Space. *Surveys in Geophysics*, 37(2):269–305.
- Cretaux, J. F., Soudarin, L., Davidson, F. J. M., Gennero, M. C., Berge-Nguyen, M., and Cazenave, A. (2002). Seasonal and interannual geocenter motion from SLR and DORIS measurements: Comparison with surface loading data. *Journal of Geophysical Research-Solid Earth*, 107(B12):2374. WOS:000181227800003.
- DeConto, R. M. and Pollard, D. (2016). Contribution of Antarctica to past and future sea-level rise. *Nature*, 531(7596):591–597.
- Desbruyères, D. G., Purkey, S. G., McDonagh, E. L., Johnson, G. C., and King, B. A. (2016). Deep and abyssal ocean warming from 35 years of repeat hydrography. *Geophysical Research Letters*, 43(19):10,356–10,365.
- Dieng, H. B., Cazenave, A., Meyssignac, B., and Ablain, M. (2017). New estimate of the current rate of sea level rise from a sea level budget approach. *Geophysical Research Letters*, 44(8):2017GL073308.
- Dieng, H. B., Champollion, N., Cazenave, A., Wada, Y., Schrama, E., and Meyssignac, B. (2015a). Total land water storage change over 2003–2013 estimated from a global mass budget approach. *Environmental Research Letters*, 10(12):124010.
- Dieng, H. B., Palanisamy, H., Cazenave, A., Meyssignac, B., and Schuckmann, K. v. (2015b). The Sea Level Budget Since 2003: Inference on the Deep Ocean Heat Content. *Surveys in Geophysics*, 36(2):209–229.
- Dussaillant, I., Berthier, E., Brun, F., Masiokas, M., Hugonnet, R., Favier, V., Rabatel, A., Pitte, P., and Ruiz, L. (2019). Two decades of glacier mass loss along the Andes. *Nature Geoscience*, 12(10):802–808.
- Edwards, T., Holden, P., Edwards, N., and Wernecke, A. (2017). Reconciling projections of the Antarctic contribution to sea level rise. volume 19, page 17489.
- Escudier, P., Couhert, A., Mercier, F., Mallet, A., Thibaut, P., Tran, N., Amarouche, L., Picard, B., Carrere, L., Dibarboure, G., Ablain, M., Richard, J., Steunou, N., Dubois, P., Rio, M.-H., Dorandeu, J., Couhert, A., Mercier, F., Mallet, A., Thibaut, P., Tran, N., Amarouche, L., Picard, B., Carrere, L., Dibarboure, G., Ablain, M., Richard, J., Steunou, N., Dubois, P., Rio, M.-H., and Dorandeu, J. (2017). Satellite Radar Altimetry : Principle, Accuracy, and Precision.
- Farinotti, D., Huss, M., Fürst, J. J., Landmann, J., Machguth, H., Maussion, F., and Pandit, A. (2019). A consensus estimate for the ice thickness distribution of all glaciers on Earth. *Nature Geoscience*, 12(3):168–173.
- Farrell, W. (1972). Deformation of the Earth by surface loads. *Reviews of Geophysics*.

BIBLIOGRAPHY

- Fasullo, J. T., Boening, C., Landerer, F. W., and Nerem, R. S. (2013). Australia’s unique influence on global sea level in 2010–2011. *Geophysical Research Letters*, 40(16):4368–4373.
- Fasullo, J. T., Lawrence, D. M., and Swenson, S. C. (2016a). Are GRACE-era Terrestrial Water Trends Driven by Anthropogenic Climate Change? *Advances in Meteorology*, 2016:e4830603.
- Fasullo, J. T., Nerem, R. S., and Hamlington, B. (2016b). Is the detection of accelerated sea level rise imminent? *Scientific Reports*, 6:31245.
- Frappart, F., Ramillien, G., and Seoane, L. (2016). Monitoring Water Mass Redistributions on Land and Polar Ice Sheets Using the GRACE Gravimetry from Space Mission. In Baghdadi, N. and Zribi, M., editors, *Land Surface Remote Sensing in Continental Hydrology*, pages 255–279. Elsevier.
- Frederikse, T., Jevrejeva, S., Riva, R. E. M., and Dangendorf, S. (2017). A Consistent Sea-Level Reconstruction and Its Budget on Basin and Global Scales over 1958–2014. *Journal of Climate*, 31(3):1267–1280.
- Gardner, A. S., Moholdt, G., Cogley, J. G., Wouters, B., Arendt, A. A., Wahr, J., Berthier, E., Hock, R., Pfeffer, W. T., Kaser, G., Ligtenberg, S. R. M., Bolch, T., Sharp, M. J., Hagen, J. O., van den Broeke, M. R., and Paul, F. (2013). A Reconciled Estimate of Glacier Contributions to Sea Level Rise: 2003 to 2009. *Science*, 340(6134):852–857.
- Garric, G., Parent, L., Greiner, E., Drévilion, M., Hamon, M., Lellouche, J., Régnier, C., Desportes, C., Le Galloudec, O., Bricaud, C., Drillet, Y., Hernandez, F., Dubois, C., Hernandez, O., and Le Traon, P. (2018). Performance and quality assessment of the global ocean eddy-permitting physical reanalysis GLORYS2v4. In *Proceedings of the Eight EuroGOOS International Conference*, Bergen, Norway. EuroGOOS. Brussels, Belgium. 2018.
- Gregory, J. M. and Lowe, J. A. (2000). Predictions of global and regional sea-level rise using AOGCMs with and without flux adjustment. *Geophysical Research Letters*, 27(19):3069–3072. WOS:000089711900011.
- Gross, R. S. (2007). Earth Rotation Variations – Long Period, in *Physical Geodesy. Treatise on Geophysics*.
- Guerreiro, K., Fleury, S., Zakharova, E., Rémy, F., and Kouraev, A. (2016). Potential for estimation of snow depth on Arctic sea ice from CryoSat-2 and SARAL/AltiKa missions. *Remote Sensing of Environment*, 186:339–349.
- Han, S.-C., Riva, R., Sauber, J., and Okal, E. (2013). Source parameter inversion for recent great earthquakes from a decade-long observation of global gravity fields. *Journal of Geophysical Research: Solid Earth*, 118(3):1240–1267.
- Hartmann, D., A.M.G. Klein Tank, M. Rusticucci, L.V. Alexander, S. Brönniman, Y. Charabi, F.J. Dentener, E.J. Dlugokencky, D.R. Easterling, A. Kaplan, B.J. Soden, P.W. Thorne, M. Wild, and P.M. Zhai (2013). Atmosphere and Surface. In *Climate Change 2013. The Physical Science Basis. Contribution of Working Group I to the Fifth Assessment Report of the Intergovernmental Panel on Climate Change*[Stocker, T.F., D. Qin, G.-K. Plattner, M. Tignor, S.K. Allen, J. Boschung, A. Nauels, Y. Xia, V. Bex and P.M. Midgley (eds.)]. Cambridge University Press, Cambridge, United Kingdom and New York, NY, USA.
- Helm, V., Humbert, A., and Miller, H. (2014). Elevation and elevation change of Greenland and Antarctica derived from CryoSat-2. *The Cryosphere*, 8(4):1539–1559.

- Hock, R., Rasul, G., Adler, C., Cáceres, B., Gruber, S., Hirabayashi, Y., Jackson, M., Kääb, A., Kang, S., Kutuzov, S., Milner, A., Molau, U., Morin, S., Orlove, B., Steltzer, H., Allen, S., Arenson, L., Baneerjee, S., Barr, I., Bórquez, R., Brown, L., Cao, B., Carey, M., Cogley, G., Fischlin, A., de Sherbinin, A., Eckert, N., Geertsema, M., Hagenstad, M., Honsberg, M., Hood, E., Huss, M., Jimenez Zamora, E., Kotlarski, S., Lefeuvre, P.-M., Ignacio López Moreno, J., Lundquist, J., McDowell, G., Mills, S., Mou, C., Nepal, S., Noetzli, J., Palazzi, E., Pepin, N., Rixen, C., Shahgedanova, M., McKenzie Skiles, S., Vincent, C., Viviroli, D., Weyhenmeyer, G., Yangjee Sherpa, P., Weyer, N., Wouters, B., Yasunari, T., You, Q., and Zhang, Y. (2019). High Mountain Areas. In Kaser, G. and Mukherji, A., editors, *IPCC Special Report on the Ocean and Cryosphere in a Changing Climate*. The Intergovernmental Panel on Climate Change (IPCC).
- Jacob, T., Wahr, J., Pfeffer, W. T., and Swenson, S. (2012). Recent contributions of glaciers and ice caps to sea level rise. *Nature*, 482(7386):514–518.
- Jekeli, C. (1981). Alternative methods to smooth the Earth’s gravity field,. *report, Dep. of Geod. Sci. and Surv., Ohio State Univ., Columbus*.
- Khaki, M., Forootan, E., Kuhn, M., Awange, J., Longuevergne, L., and Wada, Y. (2018). Efficient basin scale filtering of GRACE satellite products. *Remote Sensing of Environment*, 204:76–93.
- Khan, S. A., Sasgen, I., Bevis, M., van Dam, T., Bamber, J. L., Wahr, J., Willis, M., Kjaer, K. H., Wouters, B., Helm, V., Csatho, B., Fleming, K., Bjork, A. A., Aschwanden, A., Knudsen, P., and Munneke, P. K. (2016). Geodetic measurements reveal similarities between post-Last Glacial Maximum and present-day mass loss from the Greenland ice sheet. *Science Advances*, 2(9):e1600931. WOS:000383734400020.
- Kim, J.-S., Seo, K.-W., Jeon, T., Chen, J., and Wilson, C. R. (2019). Missing Hydrological Contribution to Sea Level Rise. *Geophysical Research Letters*, n/a(n/a).
- Klinger, B, Mayer-Gürr, T, Behzadpour, S, Ellmer, M, Kvas, A, and Zehentner, N (2016). The new ITSG-Grace2016 release. *EGU 2016 General Assembly 2016*.
- Kopp, R. E., DeConto, R. M., Bader, D. A., Hay, C. C., Horton, R. M., Kulp, S., Oppenheimer, M., Pollard, D., and Strauss, B. H. (2017). Evolving Understanding of Antarctic Ice-Sheet Physics and Ambiguity in Probabilistic Sea-Level Projections. *Earth’s Future*, 5(12):1217–1233.
- Kumar, V., Melet, A., Meyssignac, B., Ganachaud, A., Kessler, W. S., Singh, A., and Aucan, J. (2018). Reconstruction of Local Sea-Levels At South West Pacific Islands: A Multiple Linear Regression Approach (1988-2014). *Journal of Geophysical Research: Oceans*, pages n/a–n/a.
- Kusche, J., Eicker, A., Forootan, E., Springer, A., and Longuevergne, L. (2016). Mapping probabilities of extreme continental water storage changes from space gravimetry. *Geophysical Research Letters*, 43(15):8026–8034.
- Kusche, J., Schmidt, R., Petrovic, S., and Rietbroek, R. (2009). Decorrelated GRACE time-variable gravity solutions by GFZ, and their validation using a hydrological model. *Journal of Geodesy*, 83(10):903–913.
- Landerer, F. W. and Swenson, S. C. (2012). Accuracy of scaled GRACE terrestrial water storage estimates. *Water Resources Research*, 48(4):W04531.
- Leclercq, P. W., Oerlemans, J., Basagic, H. J., Bushueva, I., Cook, A. J., and Le Bris, R. (2014). A data set of worldwide glacier length fluctuations. *The Cryosphere*, 8(2):659–672.

BIBLIOGRAPHY

- Legeais, J. F., Ablain, M., Zawadzki, L., Zuo, H., Johannessen, J. A., Scharffenberg, M. G., Fenoglio-Marc, L., Fernandes, M. J., Andersen, O., Rudenko, S., Cipollini, P., Quartly, G. D., Passaro, M., Cazenave, A., and Benveniste, J. (2018). An Improved and Homogeneous Altimeter Sea Level Record from the ESA Climate Change Initiative. *Earth System Science Data*, 10:281–301.
- Lemoine, J.-M., Bourgoigne, S., Biancale, R., Bruinsma, S., and Gégout, P. (2016). CNES/GRGS solutions Focus on the inversion process. volume A1-02, Berlin, Germany.
- Lemoine, J.-M. and Reinquin, F. (2017). Processing of SLR Observations at CNES. *Newsletter EGSIM*, page 3.
- Levitus, S., Antonov, J. I., Boyer, T. P., Baranova, O. K., Garcia, H. E., Locarnini, R. A., Mishonov, A. V., Reagan, J. R., Seidov, D., Yarosh, E. S., and Zweng, M. M. (2012). World ocean heat content and thermosteric sea level change (0-2000 m), 1955-2010. *Geophysical Research Letters*, 39(10):5 PP.
- Llovel, W., Purkey, S., Meyssignac, B., Blazquez, A., Kolodziejczyk, N., and Bamber, J. (2019). Global ocean freshening, ocean mass increase and global mean sea level rise over 2005–2015. *Scientific Reports*, 9(1):1–10.
- Llovel, W., Willis, J. K., Landerer, F. W., and Fukumori, I. (2014). Deep-ocean contribution to sea level and energy budget not detectable over the past decade. *Nature Climate Change*, 4(11):1031–1035.
- Loeb, N. G., Lyman, J. M., Johnson, G. C., Allan, R. P., Doelling, D. R., Wong, T., Soden, B. J., and Stephens, G. L. (2012). Observed changes in top-of-the-atmosphere radiation and upper-ocean heating consistent within uncertainty. *Nature Geoscience*, 5(2):110–113.
- Long, D., Chen, X., Scanlon, B. R., Wada, Y., Hong, Y., Singh, V. P., Chen, Y., Wang, C., Han, Z., and Yang, W. (2016). Have GRACE satellites overestimated groundwater depletion in the Northwest India Aquifer? *Scientific Reports*, 6:24398.
- Longuevergne, L., Scanlon, B. R., and Wilson, C. R. (2010). GRACE Hydrological estimates for small basins: Evaluating processing approaches on the High Plains Aquifer, USA. *Water Resources Research*, 46(11).
- Loomis, B. D., Rachlin, K. E., and Luthcke, S. B. (2019). Improved Earth oblateness rate reveals increased ice sheet losses and mass-driven sea level rise. *Geophysical Research Letters*, 0(ja).
- Lorbacher, K., Dengg, J., Boning, C., and Biastoch, A. (2010). Regional patterns of sea level change related to interannual variability and multidecadal trends in the Atlantic meridional overturning circulation. *Journal of Climate*, 23(15):4243–4254.
- Luthcke, S. B., Sabaka, T. J., Loomis, B. D., Arendt, A. A., McCarthy, J. J., and Camp, J. (2013). Antarctica, Greenland and Gulf of Alaska land-ice evolution from an iterated GRACE global mascon solution. *Journal of Glaciology*, 59(216):613–631. WOS:000324153800002.
- Mandea, M., Cazenave, A. A., Dehant, V. M. A., de Viron, O., Blazquez, A., Laguerre, R., Zhu, P., and Wardinski, I. (2018). Magnetic and gravimetric signals in relation with the core flow.
- Mandea, M., Narteau, C., Panet, I., and Le Mouél, J.-L. (2015). Gravimetric and magnetic anomalies produced by dissolution-crystallization at the core-mantle boundary. *Journal of Geophysical Research-Solid Earth*, 120(9):5983–6000. WOS:000363420000002.

- Martin-Español, A., King, M. A., Zammit-Mangion, A., Andrews, S. B., Moore, P., and Bamber, J. L. (2016). An assessment of forward and inverse GIA solutions for Antarctica. *Journal of Geophysical Research: Solid Earth*, 121(9):2016JB013154.
- Marzeion, B., Champollion, N., Haeberli, W., Langley, K., Leclercq, P., and Paul, F. (2017). Observation-Based Estimates of Global Glacier Mass Change and Its Contribution to Sea-Level Change. In Cazenave, A., Champollion, N., Paul, F., and Benveniste, J., editors, *Integrative Study of the Mean Sea Level and Its Components*, Space Sciences Series of ISSI, pages 107–132. Springer International Publishing, Cham.
- Marzeion, B., Leclercq, P. W., Cogley, J. G., and Jarosch, A. H. (2015). Brief Communication: Global reconstructions of glacier mass change during the 20th century are consistent. *The Cryosphere*, 9(6):2399–2404.
- Melet, A. and Meyssignac, B. (2015). Explaining the Spread in Global Mean Thermosteric Sea Level Rise in CMIP5 Climate Models. *Journal of Climate*, 28(24):9918–9940.
- Meyssignac, B., Boyer, T., Zhao, Z., Hakuba, M. Z., Landerer, F. W., Stammer, D., Köhl, A., Kato, S., L’Ecuyer, T., Ablain, M., Abraham, J. P., Blazquez, A., Cazenave, A., Church, J. A., Cowley, R., Cheng, L., Domingues, C. M., Giglio, D., Gouretski, V., Ishii, M., Johnson, G. C., Killick, R. E., Legler, D., Llovel, W., Lyman, J., Palmer, M. D., Piotrowicz, S., Purkey, S. G., Roemmich, D., Roca, R., Savita, A., Schuckmann, K. v., Speich, S., Stephens, G., Wang, G., Wijffels, S. E., and Zilberman, N. (2019). Measuring Global Ocean Heat Content to Estimate the Earth Energy Imbalance. *Frontiers in Marine Science*, 6.
- Meyssignac, B., Fettweis, X., Chevrier, R., and Spada, G. (2016). Regional Sea Level Changes for the Twentieth and the Twenty-First Centuries Induced by the Regional Variability in Greenland Ice Sheet Surface Mass Loss. *Journal of Climate*, 30(6):2011–2028.
- Mignucci, A. and Blazquez, A. (2016). L’influence du changement climatique sur le champ de gravité de la Terre.
- Mitchum, G. T., Nerem, R. S., Merrifield, M. A., and Gehrels, W. R. (2010). Modern Sea Level Change Estimates. In Church, J. A., Woodworth, P. L., Aarup, T., and Wilson, W. S., editors, *Understanding Sea-Level Rise and Variability*, pages 122–142. Wiley-Blackwell.
- Mouginot, J., Rignot, E., Bjørk, A. A., Broeke, M. v. d., Millan, R., Morlighem, M., Noël, B., Scheuchl, B., and Wood, M. (2019). Forty-six years of Greenland Ice Sheet mass balance from 1972 to 2018. *Proceedings of the National Academy of Sciences*, 116(19):9239–9244.
- Munk, W. (2003). Ocean Freshening, Sea Level Rising. *Science*, 300(5628):2041–2043.
- Nerem, R. S., Beckley, B. D., Fasullo, J. T., Hamlington, B. D., Masters, D., and Mitchum, G. T. (2018). Climate-change-driven accelerated sea-level rise detected in the altimeter era. *Proceedings of the National Academy of Sciences*, 115(9):2022–2025.
- Panet, I., Bonvalot, S., Narteau, C., Remy, D., and Lemoine, J.-M. (2018). Migrating pattern of deformation prior to the Tohoku-Oki earthquake revealed by GRACE data. *Nature Geoscience*, 11(5):367–373.
- Panet, I., Mikhailov, V., Diament, M., Pollitz, F., King, G., De Viron, O., Holschneider, M., Biancale, R., and Lemoine, J.-M. (2007). Coseismic and post-seismic signatures of the Sumatra 2004 December and 2005 March earthquakes in GRACE satellite gravity. *Geophysical Journal International*, 171(1):177–190.

BIBLIOGRAPHY

- Peltier, W. (2004). Global glacial isostasy and the surface of the ice-age earth: the ICE-5G (VM2) model and GRACE. *Annual Review of Earth and Planetary Sciences*, 32:111–149.
- Peltier, W. R., Argus, D., and Drummond, R. (2017). Comment on "An Assessment of the ICE6g_c (VM5a) glacial isostatic adjustment Model by Purcell et al.". *Journal of Geophysical Research: Solid Earth*, 123(2):2019–2028.
- Purcell, A., Tregoning, P., and Dehecq, A. (2016). An assessment of the ICE6g_c(VM5a) glacial isostatic adjustment model. *Journal of Geophysical Research: Solid Earth*, 121(5):2015JB012742.
- Purcell, A., Tregoning, P., and Dehecq, A. (2018). Reply to Comment by W. R. Peltier, D. F. Argus, and R. Drummond on "An Assessment of the ICE6g_c (VM5a) Glacial Isostatic Adjustment Model". *Journal of Geophysical Research: Solid Earth*, 123(2):2029–2032.
- Reager, J. T., Gardner, A. S., Famiglietti, J. S., Wiese, D. N., Eicker, A., and Lo, M.-H. (2016). A decade of sea level rise slowed by climate-driven hydrology. *Science*, 351(6274):699–703.
- RGI Consortium (2017). Randolph Glacier Inventory – A Dataset of Global Glacier Outlines: Version 6.0. Technical Report, Global Land Ice Measurements from Space, Colorado, USA. type: dataset.
- Riddell, A. R., King, M. A., Watson, C. S., Sun, Y., Riva, R. E. M., and Rietbroek, R. (2017). Uncertainty in geocenter estimates in the context of ITRF2014. *Journal of Geophysical Research: Solid Earth*, 122(5):2016JB013698.
- Rietbroek, R., Brunnabend, S.-E., Kusche, J., Schröter, J., and Dahle, C. (2016). Revisiting the contemporary sea-level budget on global and regional scales. *Proceedings of the National Academy of Sciences*, page 201519132.
- Rignot, E., Mouginot, J., Scheuchl, B., Broeke, M. v. d., Wessem, M. J. v., and Morlighem, M. (2019). Four decades of Antarctic Ice Sheet mass balance from 1979–2017. *Proceedings of the National Academy of Sciences*, 116(4):1095–1103.
- Roca, R., Alexander, L. V., Potter, G., Bador, M., Jucá, R., Contractor, S., Bosilovich, M. G., and Cloché, S. (2019). FROGS: a daily 1° × 1° gridded precipitation database of rain gauge, satellite and reanalysis products. *Earth System Science Data Discussions*, pages 1–36.
- Rodell, M., Beaudoin, H. K., L’Ecuyer, T. S., Olson, W. S., Famiglietti, J. S., Houser, P. R., Adler, R., Bosilovich, M. G., Clayson, C. A., Chambers, D., Clark, E., Fetzer, E. J., Gao, X., Gu, G., Hilburn, K., Huffman, G. J., Lettenmaier, D. P., Liu, W. T., Robertson, F. R., Schlosser, C. A., Sheffield, J., and Wood, E. F. (2015). The Observed State of the Water Cycle in the Early Twenty-First Century. *Journal of Climate*, 28(21):8289–8318.
- Rodell, M., Famiglietti, J. S., Chen, J., Seneviratne, S. I., Viterbo, P., Holl, S., and Wilson, C. R. (2004). Basin scale estimates of evapotranspiration using GRACE and other observations. *Geophysical Research Letters*, 31(20).
- Rodell, M., Velicogna, I., and Famiglietti, J. S. (2009). Satellite-based estimates of groundwater depletion in India. *Nature*, 460(7258):999–1002.
- Roemmich, D., Johnson, G. C., Riser, S., Davis, R., Gilson, J., Owens, W. B., Garzoli, S. L., Schmid, C., and Ignaszewski, M. (2009). The Argo Program Observing the Global Ocean with Profiling Floats RID A-3556-2010. *Oceanography*, 22(2):34–43.

- Sasgen, I., Martín-Español, A., Horwath, A., Klemann, V., Petrie, E. J., Wouters, B., Horwath, M., Pail, R., Bamber, J. L., Clarke, P. J., Konrad, H., Wilson, T., and Drinkwater, M. R. (2018). Altimetry, gravimetry, GPS and viscoelastic modeling data for the joint inversion for glacial isostatic adjustment in Antarctica (ESA STSE Project REGINA). *Earth System Science Data*, 10(1):493–523.
- Sasgen, I., Martinec, Z., and Fleming, K. (2006). Wiener optimal filtering of GRACE data. *Studia Geophysica et Geodaetica*, 50(4):499–508.
- Save, H., Bettadpur, S., and Tapley, B. D. (2016). High-resolution CSR GRACE RL05 mascons: HIGH-RESOLUTION CSR GRACE RL05 MASCONS. *Journal of Geophysical Research: Solid Earth*, 121(10):7547–7569.
- Scanlon, B. R., Zhang, Z., Rateb, A., Sun, A., Wiese, D., Save, H., Beaudoin, H., Lo, M. H., Müller-Schmied, H., Döll, P., Beek, R. v., Swenson, S., Lawrence, D., Croteau, M., and Reedy, R. C. (2019). Tracking Seasonal Fluctuations in Land Water Storage Using Global Models and GRACE Satellites. *Geophysical Research Letters*, 46(10):5254–5264.
- Scanlon, B. R., Zhang, Z., Save, H., Sun, A. Y., Müller Schmied, H., van Beek, L. P. H., Wiese, D. N., Wada, Y., Long, D., Reedy, R. C., Longuevergne, L., Döll, P., and Bierkens, M. F. P. (2018). Global models underestimate large decadal declining and rising water storage trends relative to GRACE satellite data. *Proceedings of the National Academy of Sciences*, 115(6):E1080–E1089.
- Schrama, E. J. O., Wouters, B., and Lavallée, D. A. (2007). Signal and noise in Gravity Recovery and Climate Experiment (GRACE) observed surface mass variations. *Journal of Geophysical Research: Solid Earth*, 112(B8):B08407.
- Schrama, E. J. O., Wouters, B., and Rietbroek, R. (2014). A mascon approach to assess ice sheet and glacier mass balances and their uncertainties from GRACE data. *Journal of Geophysical Research: Solid Earth*, 119(7):6048–6066.
- Schröder, L., Horwath, M., Dietrich, R., Helm, V., Broeke, M. R. v. d., and Ligtenberg, S. R. M. (2019). Four decades of Antarctic surface elevation changes from multi-mission satellite altimetry. *The Cryosphere*, 13(2):427–449.
- Schweiger, A., Lindsay, R., Zhang, J., Steele, M., Stern, H., and Kwok, R. (2011). Uncertainty in modeled Arctic sea ice volume. *Journal of Geophysical Research*, 116:C00D06.
- Shepherd, A., Ivins, E., Rignot, E., Smith, B., van der Broeke, M., Velicogna, I., Whitehouse, P. L., Briggs, K., Joughin, I., Krinner, G., Nowicki, S., Payne, A., Scambos, T., Schlegel, N., A, G., Agosta, C., Ahlstrom, A., Babonis, G., Barletta, V. R., Blazquez, A., Boning, J., Csatho, B., Cullather, R., Felikson, D., Fettweis, X., Forsberg, R., Gallee, H., Gardner, A., Gilbert, L., Groh, A., Gunther, H., Hanna, E., Harig, C., Helm, V., Horwath, A., Horwath, M., Khan, S. A., Kjeldsen, K., Konrad, H., Langen, P., Lecavalier, Loomis, B. D., Luthcke, S., McMillan, M., Melini, D., Mernild, S. H., Mohajerani, Y., Moore, P., Mouginot, J., Moyano, G., Muir, A., Nagler, T., Nield, G., Nilsson, J., Noel, B., Otosaka, P., Pattle, M., Peltier, W. R., Pie, N., Rietbroek, R., Rott, H., Sandberg, L., Sasgen, I., Save, H., Scheuchl, B., Schrama, E., Schroder, L., Seo, K., Simonsen, S., Slater, T., Spada, G., Sutterley, T. C., Talpe, M., Tarasov, L., van de Berg, W. J., van der Wal, W., van Wessel, M., vishwakarma, Wiese, D. N., and Wouters, B. (2018). Mass balance of the Antarctic Ice Sheet from 1992 to 2017. *Nature*, 558(7709):219–222.
- Shepherd, A., Ivins, E. R., A, G., Barletta, V. R., Bentley, M. J., Bettadpur, S., Briggs, K. H., Bromwich, D. H., Forsberg, R., Galin, N., Horwath, M., Jacobs, S., Joughin, I., King, M. A., Lenaerts, J. T. M., Li, J., Ligtenberg, S. R. M., Luckman, A., Luthcke, S. B., McMillan, M., Meister, R., Milne, G., Mouginot, J., Muir, A., Nicolas, J. P.,

BIBLIOGRAPHY

- Paden, J., Payne, A. J., Pritchard, H., Rignot, E., Rott, H., Sørensen, L. S., Scambos, T. A., Scheuchl, B., Schrama, E. J. O., Smith, B., Sundal, A. V., Angelen, J. H. v., Berg, W. J. v. d., Broeke, M. R. v. d., Vaughan, D. G., Velicogna, I., Wahr, J., Whitehouse, P. L., Wingham, D. J., Yi, D., Young, D., and Zwally, H. J. (2012). A Reconciled Estimate of Ice-Sheet Mass Balance. *Science*, 338(6111):1183–1189.
- Shepherd, A., Ivins, E. R., Rignot, E., Blazquez, A., and TEAM, I. (2019). Mass balance of the Greenland Ice Sheet from 1992 to 2018. *Nature*, pages 1–1.
- Spada, G. (2017). Glacial Isostatic Adjustment and Contemporary Sea Level Rise: An Overview. In Cazenave, A., Champollion, N., Paul, F., and Benveniste, J., editors, *Integrative Study of the Mean Sea Level and Its Components*, Space Sciences Series of ISSI, pages 155–187. Springer International Publishing, Cham.
- Stephens, G. L. and L’Ecuyer, T. (2015). The Earth’s energy balance. *Atmospheric Research*, 166:195–203.
- Stuhne, G. R. and Peltier, W. R. (2015). Reconciling the ICE-6g_c reconstruction of glacial chronology with ice sheet dynamics: The cases of Greenland and Antarctica. *Journal of Geophysical Research: Earth Surface*, 120(9):2015JF003580.
- Swenson, S. (2012). GRACE monthly land water mass grids NETCDF RELEASE 5.0. Ver. 5.0.
- Swenson, S., Chambers, D., and Wahr, J. (2008). Estimating geocenter variations from a combination of GRACE and ocean model output. *Journal of Geophysical Research: Solid Earth*, 113(B8):B08410.
- Swenson, S. and Wahr, J. (2006). Post-processing removal of correlated errors in GRACE data. *Geophysical Research Letters*, 33(8):L08402.
- Tamisiea, M. E. (2011). Ongoing glacial isostatic contributions to observations of sea level change. *Geophysical Journal International*, 186(3):1036–1044.
- Tapley, B. D., Bettadpur, S., Ries, J. C., Thompson, P. F., and Watkins, M. M. (2004). GRACE Measurements of Mass Variability in the Earth System. *Science*, 305(5683):503–505.
- Tapley, B. D., Watkins, M. M., Flechtner, F., Reigber, C., Bettadpur, S., Rodell, M., Sasgen, I., Famiglietti, J. S., Landerer, F. W., Chambers, D. P., Reager, J. T., Gardner, A. S., Save, H., Ivins, E. R., Swenson, S. C., Boening, C., Dahle, C., Wiese, D. N., Dobslaw, H., Tamisiea, M. E., and Velicogna, I. (2019). Contributions of GRACE to understanding climate change. *Nature Climate Change*, 9(5):358–369.
- Trenberth, K. E. (2014). Challenges for Observing and Modeling the Global Water Cycle. In *Remote Sensing of the Terrestrial Water Cycle*, pages 511–519. American Geophysical Union (AGU).
- Uebbing, B., Kusche, J., Rietbroek, R., and Landerer, F. W. (2019). Processing Choices Affect Ocean Mass Estimates From GRACE. *Journal of Geophysical Research: Oceans*, 124(2):1029–1044.
- van den Broeke, M., Enderlin, E., Howat, I., Kuipers Munneke, P., Noël, B., van de Berg, W. J., van Meijgaard, E., and Wouters, B. (2016). On the recent contribution of the Greenland ice sheet to sea level change. *The Cryosphere Discussions*, pages 1–26.
- Vaughan, D. G., Comiso, J., Allison, I., Carrasco, J., Kaser, G., Kwok, R., Mote, P., Murray, T., Paul, F., Ren, E., Rignot, E., Solomina, O., Steffen, K., and Zhang, T. (2013). Cryosphere. In *Climate Change 2013. The Physical Science Basis. Contribution of Working Group I to the Fifth Assessment Report of the Intergovernmental Panel on*

- Climate Change*[Stocker, T.F., D. Qin, G.-K. Plattner, M. Tignor, S.K. Allen, J. Boschung, A. Nauels, Y. Xia, V. Bex and P.M. Midgley (eds.)]. Cambridge University Press, Cambridge, United Kingdom and New York, NY, USA.
- Velicogna, I. and Wahr, J. (2006). Measurements of Time-Variable Gravity Show Mass Loss in Antarctica. *Science*, 311(5768):1754–1756.
- Wada, Y., Lo, M.-H., Yeh, P. J.-F., Reager, J. T., Famiglietti, J. S., Wu, R.-J., and Tseng, Y.-H. (2016). Fate of water pumped from underground and contributions to sea-level rise. *Nature Climate Change*, 6(8):777–780.
- Wahr, J., Molenaar, M., and Bryan, F. (1998). Time variability of the Earth’s gravity field: Hydrological and oceanic effects and their possible detection using GRACE. *Journal of Geophysical Research: Solid Earth*, 103(B12):30205–30229.
- Wahr, J., Nerem, R. S., and Bettadpur, S. V. (2015). The pole tide and its effect on GRACE time-variable gravity measurements: Implications for estimates of surface mass variations. *Journal of Geophysical Research: Solid Earth*, 120(6):2015JB011986.
- Wahr, J., Swenson, S., and Velicogna, I. (2006). Accuracy of GRACE mass estimates. *Geophysical Research Letters*, 33(6):L06401.
- Wang, J., Song, C., Reager, J. T., Yao, F., Famiglietti, J. S., Sheng, Y., MacDonald, G. M., Brun, F., Schmied, H. M., Marston, R. A., and Wada, Y. (2018). Recent global decline in endorheic basin water storages. *Nature Geoscience*, 11(12):926–932.
- Watkins, M. M., Wiese, D. N., Yuan, D.-N., Boening, C., and Landerer, F. W. (2015). Improved methods for observing Earth’s time variable mass distribution with GRACE using spherical cap mascons. *Journal of Geophysical Research: Solid Earth*, 120(4):2648–2671.
- Watson, C. S., White, N. J., Church, J. A., King, M. A., Burgette, R. J., and Legresy, B. (2015). Unabated global mean sea-level rise over the satellite altimeter era. *Nature Climate Change*, 5(6):565–568.
- Whitehouse, P. L., Bentley, M. J., Milne, G. A., King, M. A., and Thomas, I. D. (2012). A new glacial isostatic adjustment model for Antarctica: calibrated and tested using observations of relative sea-level change and present-day uplift rates. *Geophysical Journal International*, 190(3):1464–1482.
- Wild, M., Folini, D., Hakuba, M. Z., Schär, C., Seneviratne, S. I., Kato, S., Rutan, D., Ammann, C., Wood, E. F., and König-Langlo, G. (2015). The energy balance over land and oceans: an assessment based on direct observations and CMIP5 climate models. *Climate Dynamics*, 44(11):3393–3429.
- Willis, J. K., Chambers, D. P., and Nerem, R. S. (2008). Assessing the globally averaged sea level budget on seasonal to interannual timescales. *Journal of Geophysical Research: Oceans*, 113(C6).
- Wouters, B., Bonin, J. A., Chambers, D. P., Riva, R. E. M., Sasgen, I., and Wahr, J. (2014). GRACE, time-varying gravity, Earth system dynamics and climate change. *Reports on Progress in Physics*, 77(11):116801.
- Wouters, B., Gardner, A. S., and Moholdt, G. (2019). Global glacier mass loss during the GRACE satellite mission (2002-2016). *Frontiers in Earth Science*, 7.
- Wu, X., Kusche, J., and Landerer, F. W. (2017). A new unified approach to determine geocentre motion using space geodetic and GRACE gravity data. *Geophysical Journal International*, 209(3):1398–1402.

- Wu, X., Ray, J., and van Dam, T. (2012). Geocenter motion and its geodetic and geophysical implications. *Journal of Geodynamics*, 58:44–61.
- Yi, S., Sun, W., Heki, K., and Qian, A. (2015). An increase in the rate of global mean sea level rise since 2010: increase in sea level rise rate. *Geophysical Research Letters*, pages n/a–n/a.
- Zemp, M., Huss, M., Thibert, E., Eckert, N., McNabb, R., Huber, J., Barandun, M., Machguth, H., Nussbaumer, S. U., Gärtner-Roer, I., Thomson, L., Paul, F., Maussion, F., Kutuzov, S., and Cogley, J. G. (2019). Global glacier mass changes and their contributions to sea-level rise from 1961 to 2016. *Nature*, page 1.

Acronyms

AIUB	Astronomical Institute of the University of Bern, Switzerland	25
AP	Antarctic Peninsula	4, 5, 60, 61
CCI	Climate Change Initiative	103, 105, 141
CE	center of solid Earth	26
CERES	Clouds and the Earth's Radiant Energy System	16
CF	center of figure	26, 27, 99–103, 105–110, 141, 143
CL	Confidence Level	4, 11, 28, 40–42, 140, 143
CLS	<i>Collecte Localisation Satellites</i> , France	59, 99, 102
CM	center of mass	26, 27, 99–103, 105–110, 141, 143
CNES	<i>Centre Nationale d'Études Spatiales</i>	99, 100, 102, 115, 120
CSR	Center for Spatial Research, USA	25, 26, 60
DLR	<i>Deutsches Zentrum für Luft und Raumfahrt</i> , Germany	22
doy	day of the year	105, 108
DTU	<i>Danmarks Tekniske Universitet</i> , Denmark	59
EAIS	East-Antarctica Ice Sheet	4, 5, 60, 61

EEI	Earth's Energy Imbalance	i, iii–v, viii, 16–18, 99, 108–111, 114, 117, 119, 120, 139
EGSIEM	European Gravity Service for Improved Emergency Management	25
ESA	European Space Agency	115, 120
EWH	Equivalent Water Height	29, 34, 38, 65, 101, 140, 141
GCFC	Goddard Space Flight Center, USA	26
GFZ	<i>GeoForschungsZentrum</i> , Germany	22, 25
GIA	Glacial Isostatic Adjustment	i, iv, vi, 4, 11–13, 19, 25, 33, 35–37, 39, 61, 97, 99, 102, 107, 110–112, 143
GMGSLR	Global-mean geocentric sea-level rise	12–14
GMSLR	Global-mean sea-level rise	12–17
GPS	Global Positioning System	23, 24, 27, 100, 102
GRACE	Gravity Recovery and Climate Experiment	i–iv, vi, 4, 9, 10, 19, 21, 22, 28, 39, 68, 114, 117, 120
GRACE FO	Gravity Recovery and Climate Experiment Follow On	4, 21–23, 114, 120
GRD	Earth G ravity, Earth R otation and viscoelastic solid-Earth D eformation	13, 107
GRGS	<i>Groupe de Recherche de Géodésie Spatiale</i> , France	25, 30, 36, 100

HMA	High Mountain Asia	7, 31, 93, 94, 96, 97, 141, 143
ICESat	Ice, Cloud, and land Elevation SATellite	3, 112, 118
IERS	International Earth rotation and Reference system	35, 36, 140
IOM	Input-Output Method	3–6, 60, 61, 140
IPCC	International Panel for Climate Change	iii, v, 3
ITRF	International Terrestrial Reference Frame	12, 102
JPL	Jet Propulsion Laboratory, USA	25, 26, 60
KBR	K-Band Range	22–24, 114, 120
LGM	Last glacial maximum	13, 33, 34
LIA	Little Ice Age	93
LWS	Land Water Storage	viii, 63, 64, 66, 68, 93– 97, 141, 143
MARVEL	Mass And Reference Variations for Earth Lookout	115
NAO	North Atlantic Oscillation	8
NASA	National Aeronautics and Space Administration, USA	22, 114, 120
OHC	Ocean Heat Content	16, 17, 108, 110, 111, 117
ORAP5	Ocean ReAnalysis Pilot 5	60
RGI	Randolph’s Glacier Inventory	7, 93, 94, 139, 141
SAR	Synthetic Aperture Radar	3, 4
SLE	Sea-Level Equivalent	3, 6, 8
SLR	Satellite Laser Ranging	28
SMB	Surface Mass Balance	5
TP	Tibetan Plateau	66, 68, 141
TUG	<i>Technische Universität Graz</i> , Austria	25

TWS	Terrestrial Water Storage	i, 3, 8–11, 14, 18, 39, 40, 61, 63, 64, 66, 94, 96, 97, 111, 112, 139, 143
WAIS	West-Antarctica Ice Sheet	4, 5, 60, 61

List of Figures

1.1	Observations (black numbers) and reanalysis (color numbers in the boxes) estimates of the water cycle fluxes in 10^3Gt/yr and storages in 10^3Gt . Excerpt from [Trenberth, 2014].	2
1.2	Cumulative mass balance for Greenland (a) and Antarctica (b) from different techniques	4
1.3	Regional glacier contributions to sea-level rise from 1961 to 2016. The cumulative regional and global mass changes (in Gt, represented by the volume of the bubbles) are shown for the 19 regions (outlined with bold black lines from RGI 6.0). Specific mass-change rates (m water equivalent yr^{-1}) are indicated by the colors of the bubbles. Excerpt from Zemp et al. [2019].	7
1.4	GRACE-based TWS contribution to the sea-level (black lines), global hydrological and water resources models (PCR-GLOBWB and WGHM) and land surface models (MOSAIC, VIC, NOAH-3.3, CLSM-F2.5, and CLM-4.0). Numbers in the figure corresponds to trends for the period from 2002 to 2015. Note that in the figure positive numbers means positive contribution to sea-level and negative mass balance for the TWS. Excerpt from [Scanlon et al., 2018]	9
1.5	global-mean sea-level rise (Total SSH, Altimetry in the figure), barystatic sea-level rise (Ocean mass in the figure), global-mean thermosteric rise (Thermosteric, ARGO in the figure) and GMSLR (the sum of GRACE + Argo in the figure). Figure excerpt from IPCC AR5 Fig 13-6 [Church et al., 2013]	12
1.6	Schematic representations of the flow and storage of energy in the Earth's climate system (top), and main consequences of the EEI in the Earth's climate system (bottom)	17
2.1	GRACE monthly data. Colors corresponds to the reliability and the availability of the data. Numbers expressed the missing days in the months. Asterisks corresponds to the month with repeat cycles.	23
2.2	GRACE and GRACE-FO measurement is implemented by two identical satellites (GRACE A/B and GRACE C/D respectively) orbiting one behind the other in a near-polar orbit plane. The figure shows the effect on the intersatellite range and inter satellite range rate as a synthetic mass affect their orbits. Excerpt from Tapley et al. [2019]	24
2.3	Excerpt from Wu et al. [2012]. Simplified illustration of the Center of mass (CM) and center of the figure (CF), including the solid-Earth plus the surface mass system in the fluid envelope (FE).	27

2.4	Geocenter motion in the X,Y,Z. Time-series in mm (a), associated trends over the period January 2005–December 2015 in mm/yr (b) and annual cycle in mm (c) [Swenson et al., 2008; Rietbroek et al., 2016; Cheng et al., 2013b; Lemoine and Reinquin, 2017; Wu et al., 2017; Couhert et al., 2018] A low-pass filter to remove sub-annual frequencies have been applied to the time-series. The trends are represented by error bars at 90 %CL from the individual errors. Update from Blazquez et al. [2018, Fig.1]	28
2.5	Timeseries of the C_{20} coefficient from Cheng et al. [2013a] and Lemoine and Reinquin [2017] expressed in the tide-free convention. Timeseries are centered around $-4841653.22 \cdot 10^{-10}$. Trends are computed for the period from 2002 to 2016. We also include C_{20} trends from GIA models (AG13, Caron18, ICE6G D, ICE6G ANU D) for information. Note that the sign of the trend due to the GIA is opposite to the current sign of the C_{20} trend.	29
2.6	Filter comparison excerpt from [Blazquez et al., 2018, Fig S1]. The figures represents the trends for the period from 2005 to 2015	30
2.7	Examples of Leakage and Gibbs effect	32
2.8	Rates of gravitational GIA correction in mm EWH/yr. Mean field (a) and difference between each product and the mean field (b). Note that there is a scale factor of 2 between bottom and top panels.	34
2.9	X mean pole and Y mean pole extracted from 115 years of observations after removing the Chandler period and annual cycle. IERS 2003 standards, IERS 2010 standards and C_{21}/S_{21} from GRACE GRGS RL03 v1. All values are expressed in mas (milliarcsecond)	35
2.10	Timeseries for C_{21} S_{21} from CSR, GFZ, GRGS, JPL and TUG. Values in the legend and in the box corresponds to the trends for the period 2003-2015	36
2.11	Impact of the Earthquake correction on the Water mass timeseries and trends. Extract from Mignucci’s internal report [Mignucci and Blazquez, 2016]	38
2.12	Comparison of GRACE LEGOS ensemble V1.1 with previous estimates of some of the water budget components trends. Vertical lines represent 90% CL around the mean values and the grey shaded areas the distribution of trends from GRACE LEGOS V1.1.	40
2.13	Time-series of the global water budget components after applying a low-pass filter to remove sub-annual frequencies (left) and their trends distributions for 2005–2015 (right). In the left panel, the shaded areas correspond to the distribution of the timeseries while the lines correspond to the mean values at each month. In the right-hand panel, the shaded areas indicate the distribution of trends, while the red lines indicate the distribution that would be obtained under the assumption of a Gaussian distribution. Uncertainties are expressed at 90 % CL. For comparison, estimates have been offset in the left-hand panel. Updated from Blazquez et al. [2018, Figure 5] using GRACE LEGOS ensemble 1.1	41
2.14	Rates of Regional ice-sheet mass balance excerpt from IMBIE 2 comparison [Shepherd et al., 2018] including altimetry, gravimetry and IOM estimates compared to GRACE LEGOS V1.1 estimates superposed in orange shaded areas.	60
3.1	Glacier mass trend estimates based (partly) on GRACE data for the period from 2003 to 2015. Boxes indicate period covered and upper and lower confidence level of estimate. J12 is Jacob et al. [2012], G13 is Gardner et al. [2013], C13 is Chen et al. [2013], S14 is Schrama et al. [2014], D15 is Dieng et al. [2015a], Y15 is Yi et al. [2015], Re16 is Reager et al. [2016] and Ri16 is Rietbroek et al. [2016]. Figure excerpt from [Marzeion et al., 2017]. Recently, Wouters et al. [2019] estimate a trend of 0.55 ± 0.08 mm SLE/yr for the period from 2002 to 2016 (not shown in the figure).	64

3.2	Schematic diagrams. M_{TRU} and M_{PRE} represent the true and the predicted mass fields, respectively, and M_{OBS} represents observed mass field. M_{RES} or ΔM represents the residual field. M_{COR} is the correcting field. M_{IMP} represent the improved field. In forward modeling, k is the scaling factor to speed up the convergence of the iterations, and α is the predefined threshold of minimum residuals when the iterations should stop. forward modeling figure (a) is excerpted from Chen et al. [2015]	65
3.3	Example of the application of the land leakage correction in South Asia Field represented corresponds to the trends for the period from 2003 to 2015. (a) True mass corresponds to the independent data mass changes. (b) Predicted mass is the true mass as observed by GRACE. (c) The correcting mass corresponds to the difference between both fields. (d) Observed mass corresponds to the mass changes observed by GRACE before land leakage correction. (e) Improved mass corresponds to the mass changes after land leakage correction and (f) residual mass is the mass changes not explained by the independent observations. Note that these mass change fields are related ($c = a - b$, $e = d + c$, and $f = d - b = e - a$)	67
3.4	LWS GRACE-based change compared to the flux input and output analysis through the hydrological budget approach Eq 3.1. (P-ET for Inner TP and Indus; P-Q-ET for Ganges and Brahmaputra). A 13-month low-pass filter to remove sub-annual frequencies has been applied to the detrended timeseries. Annual cycles computed by fitting a sinusoid are shown in the right panel. Note that the range of values differ in the Y axis for visualization purposes.	68
3.5	LWS GRACE-based change compared to LWS computed from fluxes analysis, showing the inconsistency in the P-Q timeseries around 2008 summer.	69
3.6	Regions containing glaciers using RGI nomenclature. Red boxes corresponds to the regions to analyse while blue boxes corresponds to arctic islands and HMA regions. The base map corresponds to the mass trends for the period 2005-2015 from GRACE.	94
3.7	LWS analysis in terms of endorheic, exorheic and small exorheic basins.	95
4.1	Effect of an arbitrary shift of 1 cm in Z components of the GRACE orbits in the inversion process. Left panel corresponds to the EWH differences and right panel to the differences in spherical harmonics amplitude.	101
4.2	Impact of the change in the reference frame center between CM vs CF in gravimetry-based ocean mass	101
4.3	Altimetry-based global sea-level change expressed in the reference frame centered in the CM. SL CCI solution doesn't contain this correction. Trends are computed for the period 2005 to 2015. Timeseries are detrended	103
4.4	Global-mean steric sea-level from ARGO	104
4.5	Steric sea level from sea-level budget in both frames, from ARGO, from reanalysis, and from CERES. All timeseries have been computed over the whole ocean. Note that ARGO and the reanalysis are only for the first 2000m depth	106
4.6	Ocean mass comparison	107
5.1	Water mass conservation in the ISPL climate models based on flux integration and stocks analysis. Analysis done in 2017.	113

List of Tables

1.1	Ice sheet mass trends in Gt/yr estimated using the input-output method (IOM), laser altimetry (LA), and gravimetry.	6
1.2	Global glacier mass trends estimated from different techniques. Values are expressed in Gt/yr. Excerpt from Marzeion et al. [2017] with the addition of estimates from Zemp et al. [2019]	7
1.3	Published trends of the global water budget (Eq 1.3) in mm SLE/yr. Ocean mass and land contributions from Greenland , Antarctica, glaciers and TWS. Note that the periods are slightly different for each publication and all uncertainties are expressed at 90 %CL.	11
2.1	GIA corrections for the gravity and altimetry fields. values are expressed as apparent mass in mm SLE/yr. Red values corresponds to the extreme values. First 4 models are compared in Fig 2.8, the rest are listed for comparison.	33
2.2	Trends and uncertainties of GRACE estimates of the global water budget for the period from 2005 to 2015. First two lines correspond to the mean trends and the uncertainty at 90 % CL. The next lines are the uncertainties associated to each post-processing parameters. All numbers are expressed in mm SLE /yr. Updated from Blazquez et al. [2018, Table 1]	42
2.3	Description of the versions of the GRACE LEGOS ensemble of solution used in published articles	59
3.1	LWS trends and its associated uncertainties for the period from 2003 to 2015. LWS is excerpt from table 2.2 combining glacier & TWS and Arctic islands. This term is split in: (1) glaciers from Arctic islands, (2) glaciers in HMA, (3) LWS in endorheic basins, (4) LWS of the main exorheic basins, and (5) LWS in the small coastal basins.	96
4.1	Correlation with respect to CERES interannual variability at different time scales after removing trend, annual and semiannual cycle. CM corresponds to the altimetry minus gravity in the CM frame, CF corresponds to the altimetry minus gravity in the CF frame, ARGO is the ensemble presented in the text	109

Annex A: Abstracts of the articles not included in the main text

I present in this annex the articles where I've participated as coauthor and the results have been discussed in the main text.

Annex A.1: Arctic Sea Level During the Satellite Altimetry Era


Carret, A., Johannessen J. A., Andersen O. B., Ablain M., Prandi P., Blazquez A., and Cazenave A. . "Arctic Sea Level During the Satellite Altimetry Era." *Surveys in Geophysics* 38, no. 1 (January 1, 2017): 251–75. <https://doi.org/10.1007/s10712-016-9390-2>.

Surv Geophys

DOI 10.1007/s10712-016-9390-2



Arctic Sea Level During the Satellite Altimetry Era

A. Carret¹  · J. A. Johannessen² · O. B. Andersen³ · M. Ablain⁴ · P. Prandi⁴ · A. Blazquez¹ · A. Cazenave¹

Received: 2 May 2016 / Accepted: 17 October 2016

© Springer Science+Business Media Dordrecht 2016

Abstract Results of the sea-level budget in the high latitudes (up to 80°N) and the Arctic Ocean during the satellite altimetry era. We investigate the closure of the sea-level budget since 2002 using two altimetry sea-level datasets based on the Envisat waveform retracking: temperature and salinity data from the ORAP5 reanalysis, and Gravity Recovery And Climate Experiment (GRACE) space gravimetry data to estimate the steric and mass components. Regional sea-level trends seen in the altimetry map, in particular over the Beaufort Gyre and along the eastern coast of Greenland, are of halosteric origin. However, in terms of regional average over the region ranging from 66°N to 80°N, the steric component contributes little to the observed sea-level trend, suggesting a dominant mass contribution in the Arctic region. This is confirmed by GRACE-based ocean mass time series that agree well with the altimetry-based sea-level time series. Direct estimate of the mass component is not possible prior to GRACE. Thus, we estimated the mass contribution from the difference between the altimetry-based sea level and the steric component. We also investigate the coastal sea level with tide gauge records. Twenty coupled climate models from the CMIP5 project are also used. The models lead us to the same conclusions concerning the halosteric origin of the trend patterns.

Abstract of [Carret et al., 2017] available in <https://link.springer.com/article/10.1007/s10712-016-9390-2>

Annex A.2: Mass Balance of the Antarctic Ice Sheet from 1992 to 2017

Shepherd, A., Ivins E., Rignot E., Smith B., van der Broeke M., Velicogna I., Whitehouse P., Briggs K., Joughin I., Krinner I., Nowicki S., Payne A.J., Scambos T. A., Schlegel N., [...], **Blazquez A.**, [...]. 2018. “Mass Balance of the Antarctic Ice Sheet from 1992 to 2017.” *Nature* 558(7709):219–22.

ANALYSIS

<https://doi.org/10.1038/s41586-018-0179-y>

Mass balance of the Antarctic Ice Sheet from 1992 to 2017

The IMBIE team*

The Antarctic Ice Sheet is an important indicator of climate change and driver of sea-level rise. Here we combine satellite observations of its changing volume, flow and gravitational attraction with modelling of its surface mass balance to show that it lost $2,720 \pm 1,390$ billion tonnes of ice between 1992 and 2017, which corresponds to an increase in mean sea level of 7.6 ± 3.9 millimetres (errors are one standard deviation). Over this period, ocean-driven melting has caused rates of ice loss from West Antarctica to increase from 53 ± 29 billion to 159 ± 26 billion tonnes per year; ice-shelf collapse has increased the rate of ice loss from the Antarctic Peninsula from 7 ± 13 billion to 33 ± 16 billion tonnes per year. We find large variations in and among model estimates of surface mass balance and glacial isostatic adjustment for East Antarctica, with its average rate of mass gain over the period 1992–2017 (5 ± 46 billion tonnes per year) being the least certain.

Abstract of [Shepherd et al., 2018] available in <https://www.nature.com/articles/s41586-018-0179-y>

Annex A.3: Global Sea-Level Budget 1993–Present

Cazenave, A., Meyssignac B., [...], **Blazquez A.**,[...]. 2018. “Global Sea-Level Budget 1993–Present.” *Earth System Science Data* 10(3):1551–90.

Global sea-level budget 1993–present

WCRP Global Sea Level Budget Group

A full list of authors and their affiliations appears at the end of the paper.

Correspondence: Anny Cazenave (anny.cazenave@legos.obs-mip.fr)

Received: 13 April 2018 – Discussion started: 15 May 2018

Revised: 31 July 2018 – Accepted: 1 August 2018 – Published: 28 August 2018

Open Access
Earth System
Science
Data

Abstract. Global mean sea level is an integral of changes occurring in the climate system in response to unforced climate variability as well as natural and anthropogenic forcing factors. Its temporal evolution allows changes (e.g., acceleration) to be detected in one or more components. Study of the sea-level budget provides constraints on missing or poorly known contributions, such as the unsurveyed deep ocean or the still uncertain land water component. In the context of the World Climate Research Programme Grand Challenge entitled “Regional Sea Level and Coastal Impacts”, an international effort involving the sea-level community worldwide has been recently initiated with the objective of assessing the various datasets used to estimate components of the sea-level budget during the altimetry era (1993 to present). These datasets are based on the combination of a broad range of space-based and in situ observations, model estimates, and algorithms. Evaluating their quality, quantifying uncertainties and identifying sources of discrepancies between component estimates is extremely useful for various applications in climate research. This effort involves several tens of scientists from about 50 research teams/institutions worldwide (www.wcrp-climate.org/grand-challenges/gc-sea-level, last access: 22 August 2018). The results presented in this paper are a synthesis of the first assessment performed during 2017–2018. We present estimates of the altimetry-based global mean sea level (average rate of $3.1 \pm 0.3 \text{ mm yr}^{-1}$ and acceleration of 0.1 mm yr^{-2} over 1993–present), as well as of the different components of the sea-level budget (<http://doi.org/10.17882/54854>, last access: 22 August 2018). We further examine closure of the sea-level budget, comparing the observed global mean sea level with the sum of components. Ocean thermal expansion, glaciers, Greenland and Antarctica contribute 42 %, 21 %, 15 % and 8 % to the global mean sea level over the 1993–present period. We also study the sea-level budget over 2005–present, using GRACE-based ocean mass estimates instead of the sum of individual mass components. Our results demonstrate that the global mean sea level can be closed to within 0.3 mm yr^{-1} (1σ). Substantial uncertainty remains for the land water storage component, as shown when examining individual mass contributions to sea level.

Abstract of [Cazenave et al., 2018a] available in <https://doi.org/10.5194/essd-10-1551-2018>

Annex A.4: Measuring Global Ocean Heat Content to Estimate the Earth Energy Imbalance

Meyssignac, Benoit, Boyer T., Zhao Z., Hakuba M., Landerer F., Stammer D., Köhl A., Kato S., L'Ecuyer T., [...], **Blazquez A.**, [...]. " Measuring Global Ocean Heat Content to Estimate the Earth Energy Imbalance ". *Frontiers in Marine Science* 6 (2019). <https://doi.org/10.3389/fmars.2019.00432>.

Measuring Global Ocean Heat Content to Estimate the Earth Energy Imbalance

Benoit Meyssignac^{1*}, Tim Boyer², Zhongxiang Zhao³, Maria Z. Hakuba^{4,5}, Felix W. Landerer⁴, Detlef Stammer⁶, Armin Köhl⁶, Seiji Kato⁷, Tristan L'Ecuyer⁸, Michael Ablain⁹, John Patrick Abraham¹⁰, Alejandro Blazquez¹, Anny Cazenave¹, John A. Church¹¹, Rebecca Cowley¹², Lijing Cheng¹³, Catia M. Domingues^{14,15,16}, Donata Giglio¹⁷, Viktor Gouretski¹⁸, Masayoshi Ishii¹⁹, Gregory C. Johnson²⁰, Rachel E. Killick²¹, David Legler²², William Llovel¹, John Lyman^{20,23}, Matthew Dudley Palmer²¹, Steve Piotrowicz²², Sarah G. Purkey²⁴, Dean Roemmich¹⁷, Rémy Roca¹, Abhishek Savita^{14,16}, Karina von Schuckmann²⁵, Sabrina Speich²⁶, Graeme Stephens⁴, Gongjie Wang²⁷, Susan Elisabeth Wijffels²⁸ and Nathalie Zilberman¹⁷

The energy radiated by the Earth toward space does not compensate the incoming radiation from the Sun leading to a small positive energy imbalance at the top of the atmosphere (0.4–1 Wm⁻²). This imbalance is coined Earth's Energy Imbalance (EEI). It is mostly caused by anthropogenic greenhouse gas emissions and is driving the current warming of the planet. Precise monitoring of EEI is critical to assess the current status of climate change and the future evolution of climate. But the monitoring of EEI is challenging as EEI is two orders of magnitude smaller than the radiation fluxes in and out of the Earth system. Over 93% of the excess energy that is gained by the Earth in response to the positive EEI accumulates into the ocean in the form of heat. This accumulation of heat can be tracked with the ocean observing system such that today, the monitoring of Ocean Heat Content (OHC) and its long-term change provide the most efficient approach to estimate EEI. In this community paper we review the current four state-of-the-art methods to estimate global OHC changes and evaluate their relevance to derive EEI estimates on different time scales. These four methods make use of: (1) direct observations of *in situ* temperature; (2) satellite-based measurements of the ocean surface net heat fluxes; (3) satellite-based estimates of the thermal expansion of the ocean and (4) ocean reanalyses that assimilate observations from both satellite and *in situ* instruments. For each method we review the potential and the uncertainty of the method to estimate global OHC changes. We also analyze gaps in the current capability of each method and identify ways of progress for the future to fulfill the requirements of EEI monitoring. Achieving the observation of EEI with sufficient accuracy will depend on merging the remote sensing techniques with *in situ* measurements of key variables as an integral part of the Ocean Observing System.

OPEN ACCESS

Edited by:

Maria Snoussi,
Mohammed V University, Morocco

Reviewed by:

Patrick Heimbach,
University of Texas at Austin,
United States
Ru Chen,
University of California, Los Angeles,
United States

*Correspondence:

Benoit Meyssignac
benoit.meyssignac@
legos.obs-mip.fr

Specialty section:

This article was submitted to
Ocean Observation,
a section of the journal
Frontiers in Marine Science

Received: 08 November 2018

Accepted: 05 July 2019

Published: 20 August 2019







Abstract of [Meyssignac et al., 2019] available in <https://doi.org/10.3389/fmars.2019.00432>

Annex A.5: Global Ocean Freshening, Ocean Mass Increase and Global Mean Sea Level Rise over 2005–2015

Llovel, William, Purkey S., Meyssignac B., Blazquez A., Kolodziejczyk N., and Bamber J.. "Global Ocean Freshening, Ocean Mass Increase and Global Mean Sea Level Rise over 2005–2015". Scientific Reports 9, n1 (27 November 2019): 1–10. <https://doi.org/10.1038/s41598-019-54239-2>.

**SCIENTIFIC
REPORTS**
nature research

OPEN Global ocean freshening, ocean mass increase and global mean sea level rise over 2005–2015

William Llovel ^{1,3*}, S. Purkey ², B. Meyssignac ¹, A. Blazquez ¹, N. Kolodziejczyk ³ & J. Bamber ⁴

Global mean sea level has experienced an unabated rise over the 20th century. This observed rise is due to both ocean warming and increasing continental freshwater discharge. We estimate the net ocean mass contribution to sea level by assessing the global ocean salt budget based on the unprecedented amount of *in situ* data over 2005–2015. We obtain the ocean mass trends of $1.30 \pm 1.13 \text{ mm} \cdot \text{yr}^{-1}$ (0–2000 m) and $1.55 \pm 1.20 \text{ mm} \cdot \text{yr}^{-1}$ (full depth). These new ocean mass trends are smaller by 0.63–0.88 $\text{mm} \cdot \text{yr}^{-1}$ compared to the ocean mass trend estimated through the sea level budget approach. Our result provides an independent validation of Gravity Recovery And Climate Experiment (GRACE)-based ocean mass trend and, in addition, places an independent constraint on the combined Glacial Isostatic Adjustment – the Earth's delayed viscoelastic response to the redistribution of mass that accompanied the last deglaciation – and geocenter variations needed to directly infer the ocean mass trend based on GRACE data.

Abstract of [Llovel et al., 2019] available in <https://doi.org/10.1038/s41598-019-54239-2>

Annex A.6: Mass Balance of the Greenland Ice Sheet from 1992 to 2017

Shepherd, A., Ivins E., Rignot E., Smith B., van der Broeke M., Velicogna I., Whitehouse P., Briggs K., Joughin I., Krinner I., Nowicki S., Payne A.J., Scambos T. A., Schlegel N., [...], **Blazquez A.**, [...]. 2019. "Mass Balance of the Greenland Ice Sheet from 1992 to 2017." Nature accepted.

Article

Mass balance of the Greenland Ice Sheet from 1992 to 2018

<https://doi.org/10.1038/s41586-019-1855-2>

The IMBIE Team*

Received: 15 August 2019

Accepted: 25 November 2019

Published online: 10 December 2019

In recent decades, the Greenland Ice Sheet has been a major contributor to global sea-level rise^{1,2}, and it is expected to be so in the future³. Although increases in glacier flow^{4–6} and surface melting^{7–9} have been driven by oceanic^{10–12} and atmospheric^{13,14} warming, the degree and trajectory of today's imbalance remain uncertain. Here we compare and combine 26 individual satellite measurements of changes in the ice sheet's volume, flow and gravitational potential to produce a reconciled estimate of its mass balance. Although the ice sheet was close to a state of balance in the 1990s, annual losses have risen since then, peaking at 335 ± 62 billion tonnes per year in 2011. In all, Greenland lost $3,800 \pm 339$ billion tonnes of ice between 1992 and 2018, causing the mean sea level to rise by 10.6 ± 0.9 millimetres. Using three regional climate models, we show that reduced surface mass balance has driven $1,971 \pm 555$ billion tonnes (52%) of the ice loss owing to increased meltwater runoff. The remaining $1,827 \pm 538$ billion tonnes (48%) of ice loss was due to increased glacier discharge, which rose from 41 ± 37 billion tonnes per year in the 1990s to 87 ± 25 billion tonnes per year since then. Between 2013 and 2017, the total rate of ice loss slowed to 217 ± 32 billion tonnes per year, on average, as atmospheric circulation favoured cooler conditions¹⁵ and as ocean temperatures fell at the terminus of Jakobshavn Isbræ¹⁶. Cumulative ice losses from Greenland as a whole have been close to the IPCC's predicted rates for their high-end climate warming scenario¹⁷, which forecast an additional 50 to 120 millimetres of global sea-level rise by 2100 when compared to their central estimate.

Abstract of [Shepherd et al., 2019] available in <https://www.nature.com/articles/TBD>

Annex B: Stokes coefficients

Annex B1: Stokes coefficients description

The Earth's gravitational field is described by the geopotential V . At a point above the Earth's surface, with spherical coordinates radius r , co-latitude θ and longitude λ , it can be expressed as a sum of Legendre functions:

$$V(r, \theta, \lambda, t) = \frac{GM}{r_e} \left\{ \sum_{l=0}^{\infty} \sum_{m=0}^l (r_e/r)^{l+1} P_{lm}(\cos\theta) \times (C_{lm}(t)\cos m\lambda + S_{lm}(t)\sin m\lambda) \right\} \quad (6.1)$$

where GM is the product of gravitational constant and mass of the planet and r_e is the mean equatorial radius. P_{lm} are the Legendre polynomials of degree l and order m , and $C_{lm}(t)$ and $S_{lm}(t)$ are the spherical harmonic coefficients. From equation 6.1 and defining a reference ellipsoid, we can express the gravity field as the geoid height N with respect this reference ellipsoid (Eq. 6.2). This geoid height only depends on the colatitude and longitude.

$$N(\theta, \lambda, t) = r_e \left\{ \sum_{l=0}^{\infty} \sum_{m=0}^l P_{lm}(\cos\theta) \times (C_{lm}(t)\cos m\lambda + S_{lm}(t)\sin m\lambda) \right\} \quad (6.2)$$

Another possibility is to represent this gravity field by the surface density in the equivalent water height (EWH). To do that we assume the thin layer hypothesis which assumes that mass redistribution occurs in a thin layer compare to Earth radius. In this case, $(r_e/r)^{l+1}$ from Eq. 6.1 is equals to 1 and the gravity is expressed as anomaly in surface density $\sigma(\theta, \lambda, t)$ expressed in mEWH:

$$\sigma(\theta, \lambda, t) = \frac{r_e \rho_e}{3\rho_w} \left\{ \sum_{l=0}^{\infty} \sum_{m=0}^l P_{lm} \frac{2l+1}{1+k_i} (\cos\theta) \times (C_{lm}(t)\cos m\lambda + S_{lm}(t)\sin m\lambda) \right\} \quad (6.3)$$

where ρ_e is the average density of the Earth ($5517\text{kg}/\text{m}^3$), ρ_w is the density of the fresh water ($1000\text{kg}/\text{m}^3$) and k_i are the load Love numbers Farrell [1972] which account for deformation of the solid Earth due to the loading of the mass anomaly on its surface.

Annex B2: Use of Stokes coefficients in GIA models

C_0 is only used in the sea-floor VLM, it accounts for the change of isopotential due to the past global sea-level rise [Tamisiea, 2011]. In fact, during the computation of GIA, the sea level equation assumes at each timestep the amount of water to remain constant but from one step to the next there is a change of isopotential. To express this change of isopotential, Tamisiea [2011] proposed to use C_0 , although C_0 usually accounts for the change in the Earth's mass of water.

The effect of GIA in the gravity field does not need this change of isopotential (C_0 equal to 0) and it is delivered in a reference frame in the center of masses (See 2.2.1) (C_{10} , C_{11} , and S_{11} equal to 0). It differs on the polar motion trend (Coefficients C_{21} , S_{21}) because VLM is measured in the rotation frame while gravity GIA is not. We need to removed the rotational feedback which reduces C_{21} and S_{21} by a factor of 2.06 [Tamisiea, 2011].

Caractérisation par satellite des échanges d'eau entre l'océan et les continents aux échelles interannuelles à décennales

Auteur : Alejandro BLAZQUEZ

Directeurs de thèse : Benoit Meyssignac et Etienne Berthier

Lieu et date de soutenance : Observatoire Midi-Pyrénées, le 2 Octobre 2020

Résumé:

Depuis 2002, GRACE fournit des estimations des échanges d'eau entre l'océan et les continents. Cependant, ces estimations sont incertaines car elles montrent des écarts lorsque différentes approches et différents paramètres sont utilisés pour traiter les données GRACE. Je revois le traitement des données GRACE, en accordant une attention particulière aux différentes sources d'erreurs et d'incertitudes. L'incertitude dans le bilan global de l'eau, à des échelles annuelles à interannuelles est due à la correction du mouvement du géocentre ainsi qu'à l'incertitude dans la correction du GIA. Cela est particulièrement vrai pour l'estimation de la masse de l'océan et les eaux continentales dont l'incertitude liée à la tendance pour la période 2005 à 2015 est de $\pm 0.33 \text{ mm SLE/yr}$.

Discipline : Océan, Atmosphère, Climat

Mots clés: Bilan global de l'eau, masse de l'océan, gravimétrie spatiale, changement climatique; Géodésie Spatiale

Laboratoire : LEGOS, Observatoire Midi-Pyrénées

14, Avenue Edouard Belin, 31400 Toulouse